COLLECTIVE ELEMENTARY EXCITATIONS OF BOSE-EINSTEIN CONDENSED TWO-DIMENSIONAL MAGNETOEXCITONS STRONGLY INTERACTING WITH ELECTRON-HOLE PLASMA

S.A. Moskalenko[1], M.A. Liberman[2], V.V. Botan[2], E.V. Dumanov[1] and Ig.V. Podlesny[1]

[1]Institute of Applied Physics of the Academy of Sciences of Moldova, Academiei Street 5, Kishinev, MD2028, Republic of Moldova
[2]Department of Physics, Uppsala University, Box 530, SE-751 21, Uppsala, Sweden

Abstract

The collective elementary excitations of a system of Bose-Einstein condensed two-dimensional magnetoexcitons interacting with electron-hole(e-h) plasma in a strong perpendicular magnetic field are studied. The breaking of the gauge symmetry is introduced into the Hamiltonian following the Bogoliubov`s theory of quasiaverages.

The motion equations for the summary operators describing the creation and annihilation of magnetoexcitons as well as the density fluctuations of the electron-hole(e-h) plasma were derived. They suggest the existence of magneto-exciton-plasmon complexes, the energies of which differ by the energies of one or two plasmon quanta.

Starting with these motion equations one can study the Bose-Einstein Condensation (BEC) of different magneto-exciton-plasmon complexes introducing different constants of the broken symmetry correlated with their energies. The Green`s functions constructed from these summary operators are two-particle Green`s functions. They obey the chains of equations expressing the two-particle Green`s functions through the four-particle and six-particle Green`s functions. These chains were truncated in such a way that the six-particle Green`s functions, were expressed through the two-particle ones. At the same time the elementary excitations with different wave vectors were decoupled. As a result of these simplifications the Dyson-type equation in a matrix form for the two-particle Green`s functions was obtained.

The 4×4 determinant constructed from the self-energy part $\sum_{ij}(\vec{P},\omega)$ gives rise to dispersion equation. The dispersion relations were obtained in analytical form, when in the self-energy parts $\sum_{ij}(\vec{P},\omega)$ only the terms linear in Coulomb interaction were kept. Taking into account also the terms quadratic in Coulomb interaction the dispersion equation becomes cumbersome and it can be solved only numerically.

1.Introduction.

In previous papers [1-5] the coherent pairing of two-dimensional electrons and holes in a strong perpendicular magnetic field was studied. In last papers [4,5] it was shown, that the Bose-Einstein Condensation (BEC) of magnetoexcitons with different from zero wave vector $\vec{k}$ and motional dipole moments essentially differs from the case $k=0$. The supplementary attraction between the parallel aligned in-plane motional dipole moments gives rise to the metastable dielectric liquid phase. Its chemical potential reaches the minimal value at some filling factor of the lowest Landau level (LLL) and lies on the energy scale below or in the vicinity of the chemical potential of the degenerate Bose gas of magnetoexcitons with $k=0$. In these conditions the drops of the dielectric liquid phase are surrounded by the degenerate

Bose gas and the coexistence of two BEC-tes is possible. The correlation energy due to coherent excited states of BEC-ed magnetoexcitons becomes important at significant values of wave vectors and vanishes in the point $k = 0$. On the contrary the influence of the excited Landau levels is especially efficient on the BECed magnetoexcitons with the wave vector $k = 0$ and rapidly decreases with the increasing of k. In difference on the chemical potential the collective elementary excitations of the BEC-ed magnetoexcitons practically were not studied. Some preliminary remarks were made in [3]. This question happens to be unusual and our paper completely is devoted to it. We realized that in two-dimensional electron-hole system in a strong perpendicular magnetic field the role of plasmon oscillations is similar with the role of magnetic flux quanta in the case of 2D electron gas in the condition of the fractional quantum Hall effect (FQHE) [6]. The magnetic flux quanta induce the vortices formation in the electron gas. The electron being accompanied by a few vortices forms a composite particle of a fermion or boson types.

One can also remember the case of electron gas in the field of laser radiation. The electron state accompanied by a photon gives rise to quasi – energy states [7]. Returning to the case of collective elementary excitations in the system of BEC-ed two-dimensional magnetoexcitons we must remark that they are inseparable from the plasma oscillations. They are strongly interconnected and must be considered simultaneously. The same happens with the exciton gas interacting with phonons in deformable lattices. But there are some more unusual properties. The motion equations for the exciton creation and annihilation operators as well for the density fluctuation operators, as we will see below contain free terms and terms describing the nonlinearity in the system due to the Coulomb interaction in the two-dimensional e-h system. The dispersion relation for the free excitons looks as $E_{ex}(\vec{P}) = -I_l + E(\vec{P})$ where I_l is the ionization potential of the magnetoexciton with two-dimensional wave vector $\vec{P} = 0$ and $E(\vec{P})$ is the proper dispersion relation, which changes quadratically in the range of small wave vectors $\vec{P}$ and tends to the finite value I_l when P tends to infinite, so as $E_{ex}(P)$ tend to zero.

The free energy for the plasmon looks as $E(\vec{P})$ and coincide exactly with the second term in the dispersion relation of magneto-exciton. The magneto-exciton with wave vector $\vec{P}$ can be regarded as magnetoexciton with wave vector $\vec{P} = 0$ and a plasmon with wave vector $\vec{P}$. The magnetoexciton can be regarded as a simple quasiparticle and at the same time as a complex consisting of an exciton and a plasmon, when the part depending on the wave vector $\vec{P}$ is determined by the plasmon. Such interpretation follows from the properties of the motion equations. They will be analyzed in detail below. In contrast to the 2D e-h gas the 3D electron plasma has plasmon oscillations with a energy gap [8], whereas the collective elementary excitations of a 3D Bose-gas have gapless energy spectrum. By this reason the interconnection of the exciton and plasmon elementary excitation in 3D system does not appear.

Below we will study this interconnection in 2D-e-h system in a strong magnetic field in detail. But for the beginning a short review of the papers dedicated to the study of the collective elementary excitations in the system of 2D two-component electron-electron and electron-hole gases is presented.

As one remember [8] the plasma oscillations in three-dimensional (3D) crystals are determined by the frequency ω_p satisfying the relation

$$\omega_p^2 = \frac{4\pi e^2 n_v}{\varepsilon_o m}; \qquad n_v = \frac{N_e}{V} \tag{1}$$

Where N_e is the number of electrons, V is the volume of the crystal, n_e is the bulk electron density, m is the effective electron mass and ε_0 is the dielectric constant of the crystal. In the two-dimensional ideal monolayer with the surface area S in the similar way one can derive the dispersion relation

$$\omega_p^2(q) = \frac{2\pi e^2 n_s q}{\varepsilon_0 m}; \qquad \omega_p(q) \sim \sqrt{q}; \qquad n_s = \frac{N_e}{S}; \tag{2}$$

Here n_S is the surface electron density. The differentce between two expressions (1) and (2) is due to the change of the role of Coulomb interaction in two different dimensionalities. Two Fourier transforms V_K of the Coulomb potential and the kinetic energy T_K of the electron have the forms

$$V_K^{3D} = \frac{4\pi e^2}{V\varepsilon_0 k^2}; \qquad V_K^{2D} = \frac{2\pi e^2}{\varepsilon_0 Sk}; \qquad T_K = \frac{\hbar^2 k^2}{2m} \tag{3}$$

It is recognized in literature that the role of Coulomb interaction is enhanced in 2D structure in comparison with the bulk crystals, whereas the kinetic energy remains with the same quadratic dependence on wave vector $\vec{k}$ in the absence of the strong magnetic field.
The both expressions (1) and (2) can be join by a formula

$$\hbar^2 \omega_p^2(k) = 2N_e T_K V_K \tag{4}$$

Das Sarma and Madhukar [9] have investigated theoretically the longitudinal collective modes of spatially separated two-component two-dimensional plasma in solids using the generalized random phase approximation. It can be realized in semiconductor heterojunctions and superlattices. The two-layer structure with two-component plasma is discussed below. It has long been known that two-component plasma has two branches to its longitudinal oscillations. The higher frequency branch is named as optical plasmon (OP). Here the two carrier densities of the same signs oscillate in-phase and their density fluctuation operators $\hat{\rho}_{e,1}(\vec{Q})$ and $\hat{\rho}_{e,2}(\vec{Q})$ form an in-phase superposition

$$\hat{\rho}_{OP}(\vec{Q}) = \hat{\rho}_{e,1}(\vec{Q}) + \hat{\rho}_{e,2}(\vec{Q}) \tag{5}$$

In the case of opposite signs electron and hole charges they oscillate out-of-phase and their charge density fluctuation operators $\hat{\rho}_e(\vec{Q})$ and $\hat{\rho}_h(\vec{Q})$ combine in out-of-phase manner

$$\hat{\rho}_{OP}(\vec{Q}) = \hat{\rho}_e(\vec{Q}) - \hat{\rho}_h(-\vec{Q}) \tag{6}$$

The lower frequency branch is named as acoustical plasmon (AP). Now the carriers of different signs oscillate in-phase, whereas the carriers of the same signs oscillate out-of-phase. Their charge density fluctuation operators combine in the form

$$\hat{\rho}_{AP}(\vec{Q}) = \hat{\rho}_{e,1}(\vec{Q}) - \hat{\rho}_{e,2}(\vec{Q}); \qquad \hat{\rho}_{AP}(\vec{Q}) = \hat{\rho}_e(\vec{Q}) + \hat{\rho}_h(-\vec{Q}) \tag{7}$$

The optical and acoustical branches have the dispersion relations in the long wavelength region as follows

$$\omega_{OP}(q) \sim \sqrt{q}; \qquad \omega_{AP}(q) \sim q; \qquad q \to 0 \tag{8}$$

By virtue of spatial separation z between the two components of the 2D plasma the AP branch becomes with a greater slope of the linear q dependence, because this slope is proportional to z, when z is of the order of Bohr radius a_B. At small $z \to 0$ the AP branch

lies inside the single-particle excitation spectrum of the faster moving charged carriers. They leave the corresponding Fermi seas crossing the Fermi energies of the degenerate Fermi gases. This single-particle spectrum is severely Landau damped. At larges values $z > a_B$ the Coulomb interaction between charges in different layers can be neglected and each layer supports an ordinary 2D plasma oscillations with a dispersion $\omega_P(q) \sim q^{1/2}$ [9].

They have been thoroughly studied experimentally In the absence of a magnetic field, but have not so far been addressed in the presence of an external magnetic field. The transformation of the optical and acoustical plasma excitations under the influence of an external perpendicular to the layer magnetic field was studied experimentally by the authors of paper [10], using the AlGaAs/GaAs double quantum well (DQW) and magnetic fields up till 10T.

As was mentioned in this paper in a perpendicular magnetic field many –body interactions become relevant as the electron kinetic energy is completely quenched and the strong Coulomb interaction drives the two-dimensional electron system (2DES) into new phases of matter such as incompressible fractional quantum Hall liquid or Wigner crystal.

In paper [10] the acoustical and optical plasmons at zero field were investigated first. The dispersion relation of the AP was measured in the whole range of accessible in-plane momenta and it was found to be a nearly linear dependence in agreement with the theory.

The entire H field range covered was cut into two parts. In one range the influence of the Bernstein modes (BM) on to the principal plasmons AP and OP can be neglected. The Bernstein modes are charge-density magnetoexcitons having energies $n\hbar\omega_c$, $n \geq 2$ at $ql \to 0$, where ω_c is the cyclotron frequency and l is the magnetic length

$$\omega_c = \frac{eH}{mc}; \qquad l^2 = \frac{\hbar c}{eH} \tag{9}$$

In another range of magnetic field the AP_S and OP_S resonate with BM_S.

When the BM_S can be neglected the energies of the principal plasmons are monotonically increasing functions of H field, slowly covering to the cyclotron energy. In the limit $H \to 0$ the both plasmon excitations can be approximated

$$\omega^2(q \mid H \neq 0) = \omega^2(q \mid H = 0) + \omega_c^2 \tag{10}$$

The complex anticrossing behavior close to the resonances between AP and OP with BM_S was observed.

The plasmon oscillations in one-component system on the monolayer in a strong perpendicular magnetic field were studied by Girvin, MacDonald and Platzman [11], who proposed the magnetoroton theory of collective excitations in the conditions of the fractional quantum Hall effect (FQHE). The FQHE occurs in low-disorder, high-mobility samples with partially filled Landau levels with filling factor of the form $\nu = \frac{1}{m}$, where m is an integer, for which there is no single-particle gap. In this case the excitation is a collective effect arising from many-body correlations due to the Coulomb interaction. Considerable progress has recently been achieved toward understanding the nature of the many-body ground state well described by Laughlin variational wave function [12]. The theory of the collective excitation spectrum proposed by [11] is closely analogous to Feynman`s theory of superfluid helium [13]. The main Feynman`s arguments lead to the conclusions that on general grounds the low lying excitations of any system will include density waves. As regards the 2D system the perpendicular magnetic field quenches the single particle continuum of kinetic energy leaving a series of discrete highly degenerate Landau levels spaced in energy at intervals $\hbar\omega_c$. In the

case of filled Landau level $\nu = 1$ because of Pauli exclusion principle the lowest excitation is necessarily the cyclotron mode in which particles are excited into the next Landau level. In the case of FQHE the lowest Landau level (LLL) is fractionally filled. The Pauli principle no longer excludes low-energy intra-Landau-level excitations. For the FQHE case the low-lying excitations have the primary importance rather than the high-energy inter-Landau-level cyclotron modes [11]. The spectrum has a relatively large excitation gap at zero wave vector $kl = 0$ and in addition it exhibits a deep magneto-roton minimum at $kl \sim 1$ quite analogous to the roton minimum in helium. The magneto-roton minimum becomes deeper and deeper at the decreasing of the filling factor ν in the row $1/3, 1/5, 1/7$ and is the precursor to the gap collapse associated with the Wigner crystallization which occurs at $\nu = \frac{1}{7}$. For larges wave vectors the low lying mode crosses over from being a density wave to becoming a quasiparticle excitation [11]. The Wigner crystal transition occurs slightly before the roton mode goes completely soft. The magnitude of the primitive reciprocal lattice vector for the crystal lies close to the position of the magneto-roton minimum. The authors of [11] suggested also the possibility of pairing of two rotons of opposite momenta leading to the bound two-roton state with small total momentum, as it is known to occur in helium. In contrast to the case of fractional filling factor, the excitations from a filled Landau level in the 2DEG were studied by Kallin and Halperin [14]. They considered an interacting two-dimensional electron system with a uniform positive background in a strong perpendicular magnetic field at zero temperatures. It was supposed that an integral number of Landau levels is filled and the Coulomb energy $\frac{e^2}{\varepsilon_0 l}$ is smaller than the cyclotron energy $\hbar\omega_c$.

The elementary neutral excitations may be described alternatively as magnetoplasma modes or as magnetoexcitons formed by a hole in a filled Landau level and an electron in an empty level. In contrast to the hole in the valence band, which takes part in the formation of the usual magnetoexciton, we deal with the hole in the conduction band, namely in its filled Landau level. It can be denoted as (c,n,h). Its bound state with the electron in the empty Landau level with number n' in the same conduction band denoted as (c, n', e) gives rise to the magnetoexciton named as integer quantum Hall exciton. It is characterized by a conserved wave vector $\vec{k}$ in Landau gauge. The dispersion relation may be calculated exactly to first order in $I_l / \hbar\omega_c$, where I_l is the ionization potential of magnetoexciton with $k = 0$ and equals to $\frac{e^2}{\varepsilon_0 l}\sqrt{\frac{\pi}{2}}$.

The lowest magnetoplasmon band comes in to the cyclotron frequency $m\hbar\omega_c$ at $k = 0$, where $m = n' - n$, if the Coulomb electron-electron interaction is neglected. If the Coulomb interaction is included, then the energy of neutral plasmon will come to the value $m\hbar\omega_c - I_l$. Excitation modes with $m = 0$ do not exist if the initial state has an integer occupation numbers of the Landau levels of both spins. In the ferromagnetic ground state the $m = 0$ excitations are spin waves.

Apal'kov and Rashba[15] considered a case of an electron-hole pair in the presence of an incompressible liquid formed by electrons in the condition of the fractional quantum Hall effect (FQHE). The magnetoplasmons have a dispersion law similar to the rotons in liquid

helium and are named as magnerotons. They play the role of phonons in the incompressible liquid and influence on the state of exciton interacting with plasmons. This influence is analogous with the influence of the phonons on the states of electrons or excitons interacting with crystal lattice oscillations in bulk semiconductors and is named as polaron effect. The authors of [15] arrived to the conclusion that the influence of magnetorotons, leads to a giant suppression of the magnetoexciton dispersion in symmetric case. There is a region in the momentum space, where the elementary excitations are interpreted as bound states of a phonon (magnetoroton) with a slow magnetoexciton. As was mentioned the interaction of the exciton with the fluid can be treated as a polaron effect resulting from a dressing by magnetorotons. The polaron shift is zero at $k = 0$ in symmetric systems. When the confinement planes for electrons and hole have a distance z different from zero (asymmetric case), the polaron shift of the exciton level is positive, what is determined in an asymmetric system by the influence of the Pauli exclusion principle which is not compensated by the ordinary polaron effect.

Fertig [16] investigated the excitation spectrum of two-layer and three-layer electron systems. In particular case the two-layer system in a strong perpendicular magnetic field with filling factor $\nu = \frac{1}{2}$ of the lowest Landau level (LLL) in the conduction band of each layer was considered. Inter-layer separation z was introduced. The spontaneous coherence of two-component two-dimensional (2D) electron gas was introduced constructing the function

$$\left|\Psi\right\rangle = \prod_k (n a_k^{+} + \mathrm{v} b_k^{+}) \left|0\right\rangle \quad ; \qquad u^2 = \mathrm{v}^2 = 1/2 \quad , \tag{11}$$

where a_k^{+}, a_k are the creation and annihilation operators of spin polarized electrons on the LLL of the layer **a** and b_k^{+}, b_k play the same role for the electrons resided on the layer **b**.

Here the vacuum state $\left|0\right\rangle$ was introduced

$$a_k \left|0\right\rangle = b_k \left|0\right\rangle = 0 \tag{12}$$

Both half filled layers **a** and **b** are accompanied by a substrate with positive charge guaranteeing the electrical neutrality of the system. The half filled layer **a** can be considered as a full filled with electrons in the LLL of the conduction band and a half filled by holes in the LLL of the same conduction band. The wave function of the full filled LLL of the layer **a** can be written as

$$\left|\Psi_0\right\rangle = \prod_k a_k^{+} \left|0\right\rangle \tag{13}$$

The hole creation operator in the conduction band of the layer **a** can be introduced

$$d_k^{+} = a_{-k} \tag{14}$$

The electrons of the full filled conduction band are compensated by the charge of the substrate and we can only consider the electrons on the layer **b** and the holes on the layer **a**.

Then the wave function (11) of the coherent two-layer electron system can be rewritten in the form

$$\left|\Psi\right\rangle = \prod_k (u + \mathrm{v} b_k^{+} d_{-k}^{+}) \left|\Psi_0\right\rangle \quad , \tag{15}$$

which coincides with the BCS-type wave function of the superconductor. It represents the coherent pairing of the conduction electrons on the LLL of the layer **b** with the holes in the LLL of the conduction band of the layer **a** and describes the BEC of such unusual excitons named as FQHE excitons, because they appear in the conditions proper to the observation of

the fractional quantum Hall effect. Here only the BEC on the single exciton state with wave vector $\vec{k} = 0$ is considered.

Fertig has determined the energy spectrum of the elementary excitations in the frame of this ground state. In the case of z=0 the lowest-lying excitations of the system are the higher energy excitons.

Because of the neutral nature of the $\vec{k} = 0$ excitons the dispersion relation of these excitations is given in a good approximation by

$$\hbar\omega(k) = E_{ex}(k) - E_{ex}(0), \tag{16}$$

where $E_{ex}(k)$ is the energy of exciton with wave vector $\vec{k}$. This result was first obtained by Paquet, Rice and Ueda [3,17] using a random phase approximation [RPA]. In the case z=0 the dispersion relation $\omega(k)$ vanishes as k^2 for $k \to 0$, as one expect for Goldstone modes.

For z>0 $\omega(k)$ behaves as an acoustical mode $\omega(k) \sim k$ in the range of small k, whereas in the limit $k \to \infty$ $\omega(k)$ tends to the ionization potential $\Delta(z)$ in the form

$$\hbar\omega(k) = \Delta(z) - \frac{e^2}{\varepsilon_0 k l^2} \tag{17}$$

In the region of intermediate values of k, when $kl \sim 1$, the dispersion relation develops the dips as z is increased. At certain critical value of $z=z_{er}$ the modes in the vicinity of the minima become equal to zero and are named as soft modes. Their appearance testifies that the two-layer system undergo a phase transition to the Wigner crystal state.

The similar results concerning the linear and quadratic dependences of the dispersion relations in the range of small wave vectors q were obtained by Kuramoto and Horie [18], who studied the coherent pairing of electrons and holes spatially separated by the insulator barrier in the structure of the type coupled double quantum wells (CDQW).

The magnetic field is sufficiently strong, so that the carriers populate only their lowest Landau levels (LLL) in the conduction and valence bands. Apparently the electron-hole interaction becomes less important than the repulsive electron-electron and hole-hole interactions as the separation d increases. However at low densities the ground state of the system will be the excitonic phase, instead of the Wigner lattice, for which the repulsive interaction is responsible. The reason is that the energy per electron-hole pair in the excitonic phase is lower than in Wigner crystal. The BEC of magnetoexcitons in the state with zero total momentum was considered and the dispersion relation of the collective excitation modes was derived. In the case $d \neq 0$ the lowest excitation branch has a linear dispersion relation in the region of small wave vectors q $\omega(q) \sim ql$; whereas at d=0 it transforms in the quadratic dependence $\omega(q) \sim (ql)^2$; Kuramoto and Horie mentioned that the linear dispersion relation originates in the fact that at $d \neq 0$ the repulsive Coulomb interaction prevails and the carriers feel this resulting repulsive long-range force [18]. As in the Bogoliubov theory of weakly interacting Bose gas the repulsive interaction leads to the transformation of the quadratic dispersion relation into another one with the linear dependence at small wave vectors.

Spontaneous Coherence in a two-component electron gas created in bilayer quantum well structure in a strong perpendicular magnetic field was recently studied experimentally by Eisenstein [19] and theoretically by MacDonald [20].

The bilayer electron-electron system is much easy to realize in experiment than e-h bilayer, when the holes are created in the valence band and are spatially separated from the electrons in the conduction band. The experimental indications of spontaneous coherence have been seen first in e-e bilayer, which is analogous to Josephson junction. When the two

2D electron layers each at half-filling of the lowest Landau level (LLL) are sufficiently close together, then the ground state of the system possesses interlayer phase coherence. The ground state can be considered as an equilibrium Bose-Einstein condensate of excitons formed by the electrons on the LLL in the conduction band with the residence on one layer and the holes on the LLL of the conduction band with the residence on another layer. This collective state exhibits the quantum Hall effect when electrical currents are driven in parallel through two layers [19]. Counterflow transport experiments were realized. The oppositely directed currents were driven through the two layers. The counterflow proceeds via the collective transport of neutral particles, i.e. interlayer excitons. The Hall resistance of the individual layer vanishes at $T \to 0$ in the collective phase. A weak dissipation is present at finite temperatures. The free vortices are present at all temperatures being induced by the disorders. The existence of the anticipated Goldstone mode linearly dispersing was confirmed experimentally [19]. This mode is the consequence of a spontaneously broken $U(1)$ symmetry in the bilayer system. Measurements of the tunneling conductance between the layers have shown that the tunneling conductance at zero bias grows explosively, when the separation between the layers is brought below a critical value [19].

The counterflow conductivity and inter-layer tunneling experiments both suggest that the system does not have long range order because of the presence of the unbound vortices nucleated by disorder. The finite phase coherence length appears [20].

The appearance of the soft modes in the spectrum of the collective elementary excitations may signalize not only about the possible phase transition of the two-layer system to the Wigner crystal state or to the charge-density-wave (CDW) of a 2D electron system, but also to another variant of the excitonic charge-density-wave (ECDW) state. This new state was revealed theoretically by Chen and Quinn [21,22], who studied the ground state and the collective elementary excitations of a system consisting of spatially separated electron and hole layers in strong magnetic field. When the interlayer Coulomb attraction in strong electrons and holes pair together to form excitons. Excitonically condensed state of e-h pairs is the preferable ground state. If the layer separation is larger than a critical value, a novel excitonic-density-wave state is found to have a lower energy than either a homogeneous exciton fluid or a double charge-density-wave state in 2D electron system.

All these details and information will permit to better understand the results of our paper, which is organized as follows.

In section two the breaking of the gauge symmetry of the initial Hamiltonian is introduced by an alternative method following the idea proposed by Bogoliubov in his theory of quasiaverages [23]. The equivalence with another Bogoliubov u-v transformation method is revealed.

In section three the motion equations for the operators were obtained, whereas in section four on their base the main equations determining the many-particle Green`s functions were deduced.

Section five is devoted to the discussion of the used approximations. One of them corresponds to the Hartree-Fock-Bogoliubov approximation (HFBA) and the second one to the calculations of the correlation energy [4,5]. The energy spectrum in HFBA is represented in section six. The more complete results are discussed in the seventh section.

2. The breaking of the gauge symmetry of the initial Hamiltonian. Two equivalent representations

For the very beginning we will introduce the operators describing the magneto-excitons and plasmons, and their commutation relations.

The creation and annihilation operators of magnetoexcitons are two-particle operators reflecting the electron-hole (e-h) structure of the excitons. They are denoted below as $d^{\dagger}(\vec{p})$ and $d(\vec{p})$, where $\vec{p}(p_x, p_y)$ is the two-dimensional wave vector. There are also the density fluctuation operators for electrons $\hat{\rho}_e(\vec{Q})$ and for holes $\hat{\rho}_h(\vec{Q})$ as well as their linear combinations $\hat{\rho}(\vec{Q})$ and $\hat{D}(\vec{Q})$. They are determined below

$$\begin{aligned}
&\hat{\rho}_e(\vec{Q}) = \sum_t e^{iQ_y t l^2} a^{\dagger}_{t-\frac{Q_x}{2}} a_{t+\frac{Q_x}{2}};\\
&\hat{\rho}_h(\vec{Q}) = \sum_t e^{iQ_y t l^2} b^{\dagger}_{t+\frac{Q_x}{2}} b_{t-\frac{Q_x}{2}};\\
&\hat{\rho}(\vec{Q}) = \hat{\rho}_e(\vec{Q}) - \hat{\rho}_h(-\vec{Q});\\
&\hat{D}(\vec{Q}) = \hat{\rho}_e(\vec{Q}) + \hat{\rho}_h(-\vec{Q});\\
&d^{\dagger}(\vec{P}) = \frac{1}{\sqrt{N}} \sum_t e^{-iP_y t l^2} a^{\dagger}_{t+\frac{P_x}{2}} b^{\dagger}_{-t+\frac{P_x}{2}};\\
&d(\vec{P}) = \frac{1}{\sqrt{N}} \sum_t e^{iP_y t l^2} b_{-t+\frac{P_x}{2}} a_{t+\frac{P_x}{2}};\\
&\hat{N}_e = \hat{\rho}_e(0);\\
&\hat{N}_h = \hat{\rho}_h(0);\\
&\hat{\rho}(0) = \hat{N}_e - \hat{N}_h;\\
&\hat{D}(0) = \hat{N}_e + \hat{N}_h;
\end{aligned} \tag{18}$$

and are expressed through the Fermi creation and annihilation operators $a_p^{\dagger}, a_p$ for electrons and $b_p^{\dagger}, b_p$ for holes. The e-h Fermi operators depend on two quantum numbers. In Landau gauge one of them is the wave number p and the second one is the quantum number n of the Landau level. In the lowest Landau level (LLL) approximation n has only the value zero and its notation is dropped. The wave number p enumerates the N-fold degenerate states of the 2D electrons in a strong magnetic field. N can be expressed through the layer surface area S and the magnetic length l as follows

$$N = \frac{S}{2\pi l^2}; \quad l^2 = \frac{\hbar c}{eH} \quad , \tag{19}$$

where H is the magnetic field strength. The operators (18) obey the following commutation relations, most of which being for the first time established by Apal`kov and Rashba [15]

$$\left[\hat{\rho}(\vec{Q}),\hat{\rho}(\vec{P})\right]=-2iSin\left(\frac{\left[\vec{P}\times\vec{Q}\right]_z l^2}{2}\right)\hat{\rho}(\vec{P}+\vec{Q})$$

$$\left[\hat{D}(\vec{Q}),\hat{D}(\vec{P})\right]=-2iSin\left(\frac{\left[\vec{P}\times\vec{Q}\right]_z l^2}{2}\right)\hat{\rho}(\vec{P}+\vec{Q}) \qquad (20)$$

$$\left[\hat{\rho}(\vec{Q}),\hat{D}(\vec{P})\right]=-2iSin\left(\frac{\left[\vec{P}\times\vec{Q}\right]_z l^2}{2}\right)\hat{D}(\vec{P}+\vec{Q})$$

$$\left[d(p),d^{+}(Q)\right]=\delta_{kr}(\vec{P},\vec{Q})-$$

$$-\frac{1}{N}\left[i\sin\left(\frac{\left[\vec{P}\times\vec{Q}\right]_z l^2}{2}\right)\hat{\rho}\left(\vec{P}-\vec{Q}\right)+\cos\left(\frac{\left[\vec{P}\times\vec{Q}\right]_z l^2}{2}\right)\hat{D}\left(\vec{P}-\vec{Q}\right)\right]$$

$$\left[\hat{\rho}\left(\vec{P}\right),d\left(\vec{Q}\right)\right]=2i\sin\left(\frac{\left[\vec{P}\times\vec{Q}\right]_z l^2}{2}\right)d\left(\vec{P}+\vec{Q}\right)$$

$$\left[\hat{\rho}\left(\vec{P}\right),d^{+}\left(\vec{Q}\right)\right]=-2i\sin\left(\frac{\left[\vec{P}\times\vec{Q}\right]_z l^2}{2}\right)d^{+}\left(-\vec{P}+\vec{Q}\right)$$

$$\left[\hat{D}\left(\vec{P}\right),d^{+}\left(\vec{Q}\right)\right]=2\cos\left(\frac{\left[\vec{P}\times\vec{Q}\right]_z l^2}{2}\right)d^{+}\left(\vec{Q}-\vec{P}\right)$$

$$\left[\hat{D}\left(\vec{P}\right),d\left(\vec{Q}\right)\right]=-2\cos\left(\frac{\left[\vec{P}\times\vec{Q}\right]_z l^2}{2}\right)d\left(\vec{P}+\vec{Q}\right)$$

One can observe that the density fluctuation operators (18) with different wave vectors $\vec{P}$ and $\vec{Q}$ do not commute. Their non-commutativity is related with the vorticity which accompanies the presence of the strong magnetic field and depends on the vector-product of two wave vectors $\vec{P}$ and $\vec{Q}$ and its projection on the direction of the magnetic field $[\vec{P}\times\vec{Q}]_z$. These properties considerably influence the structure of the motion equations for the operators (1) and determine new aspect of the magneto-exciton-plasmon physics. Indeed in the case of 3D e-h plasma in the absence of the external magnetic field the density fluctuation operators do commute [8]. The magneto-exciton creation and annihilation operators $d^{\dagger}(\vec{p})$ and $d(\vec{Q})$ as in general case do not obey exactly the Bose commutation rule. Their deviation from it is proportional to the density fluctuation operators $\hat{\rho}(\vec{P}-\vec{Q})$ and $\hat{D}(\vec{P}-\vec{Q})$. The discussed above operators determine the structure of the 2D e-h system Hamiltonian in the LLL approximation. In previous papers [1,2,3,4,5] the initial Hamiltonian was gauge-invariant.

It has the form

$$\hat{H} = \frac{1}{2}\sum_{\vec{Q}} W_{\vec{Q}}\left[\hat{\rho}(\vec{Q})\hat{\rho}(-\vec{Q}) - \hat{N}_e - \hat{N}_h\right] - \mu_e\hat{N}_e - \mu_h\hat{N}_h \ , \tag{21}$$

where

$$W_{\vec{Q}} = \frac{2\pi e^2}{\varepsilon_0 S\left|\vec{Q}\right|} Exp\left[-\frac{Q^2 l^2}{2}\right]; \quad \mu = \mu_e + \mu_h \tag{22}$$

The energy of the two-dimensional magnetoexciton $E_{ex}(P)$ depends on the two-dimensional wave vector $\vec{P}$ and forms a band with the dependence

$$E_{ex}(\vec{P}) = -I_{ex}(\vec{P}) = -I_l + E(\vec{P});$$
$$I_{ex}(\vec{P}) = I_l e^{-\frac{P^2 l^2}{2}} I_0\left(\frac{P^2 l^2}{2}\right); \qquad I_l = \frac{e^2}{\varepsilon_0 l}\sqrt{\frac{\pi}{2}}; \tag{23}$$

The ionization potential $I_{ex}(P)$ is expressed through the modified Bessel function $I_0(z)$, which has the limiting expressions [10].

$$\underset{z\to 0}{I_0(z)} = 1 + \frac{z^2}{4} + \ldots; \ \underset{z\to\infty}{I_0(z)} = \frac{e^z}{\sqrt{2\pi z}} \tag{24}$$

It means that the function $E(P)$ can be approximated as follows

$$\underset{P\to 0}{E(\vec{P})} = \frac{\hbar^2 P^2}{2M}; \qquad M = M(0) = 2\sqrt{\frac{2}{\pi}}\frac{\hbar^2\varepsilon_0}{e^2 l}; \tag{25}$$

$$\underset{P\to\infty}{E(P)} = I_l\left(1 - \frac{\sqrt{\frac{2}{\pi}}}{Pl}\right); \quad l^2 = \frac{\hbar c}{eH};$$

Instead of the chemical potential μ (22) we will use the value $\bar{\mu}$ accounted from the bottom of the exciton band

$$\bar{\mu} = \mu - E_{ex}(0) = \mu + I_l; \tag{26}$$

In the case of BEC of the magnetoexcitons on the state with $k \neq 0$ the chemical potential accounted from the exciton level $E_{ex}(k)$ will lead to the expression

$$\mu - E_{ex}(\vec{K}) = \bar{\mu} - E(\vec{K}); \tag{27}$$

For introduction of the phenomenon of Bose-Einstein condensation (BEC) of excitons the gauge symmetry of the initial Hamiltonian was broken by the help of the unitary transformation $\hat{D}(\sqrt{N_{ex}})$ following the Keldysh-Kozlov-Kopaev method [24]. We can shortly remember the main outlines of the Keldysh-Kozlov-Kopaev method [24], [25] as it was realized in papers [4,5]. The unitary transformation $\hat{D}(\sqrt{N_{ex}})$ was determined by the formula (25) [4]. Here N_{ex} is the number of condensed excitons. It transforms the operators a_p, b_p to another ones α_p, β_p, as is shown in formulas (30), (31) [4], and gives rise to the BCS-type wave function $\left|\psi_g(\bar{k})\right\rangle$ of the new coherent macroscopic state represented by expression (27) [4]. These results are summarized below

$$\hat{D}(\sqrt{N_{ex}}) = \exp[\sqrt{N_{ex}}(d^{\dagger}(\bar{k}) - d(\bar{k}))]$$
$$\left|\psi_g(\bar{k})\right\rangle = \hat{D}(\sqrt{N_{ex}})\left|0\right\rangle$$
$$\alpha_p = \hat{D}a_p\hat{D}^{\dagger} = ua_p - \mathrm{v}(p - \frac{k_x}{2})b^{\dagger}_{k_x - p}$$
$$\beta_p = \hat{D}b_p\hat{D}^{\dagger} = ub_p + \mathrm{v}(\frac{k_x}{2} - p)a^{\dagger}_{k_x - p} \qquad (28)$$
$$a_p = u\alpha_p + \mathrm{v}(p - \frac{k_x}{2})\beta^{\dagger}_{k_x - p}$$
$$b_p = u\beta_p - \mathrm{v}(\frac{k_x}{2} - p)\alpha^{\dagger}_{k_x - p}$$

$$a_p\left|0\right\rangle = b_p\left|0\right\rangle = 0; \qquad \alpha_p\left|\psi_g(\bar{k})\right\rangle = \beta_p\left|\psi_g(\bar{k})\right\rangle = 0$$
$$u = \cos g; \quad \mathrm{v} = \sin g; \qquad \mathrm{v}(t) = \mathrm{v}e^{-ik_y tl^2} \qquad (29)$$
$$g = \sqrt{2\pi l^2 n_{ex}}; \quad n_{ex} = \frac{N_{ex}}{S} = \frac{\mathrm{v}^2}{2\pi l^2} \quad g = \mathrm{v}; \quad \mathrm{v}=\mathrm{Sin}\mathrm{v};$$

The developed theory [4,5] is true in the limit $\mathrm{v}^2 \approx Sin^2\mathrm{v}$, what means the restriction $\mathrm{v}^2 < 1$. In the frame of this approach the collective elementary excitations can be studied constructing the Green's functions on the base of operators α_p, β_p and dealing with the transformed cumbersome Hamiltonian $\hat{\tilde{\mathcal{H}}} = D(\sqrt{N_{ex}})\hat{H}D^{\dagger}(\sqrt{N_{ex}})$.

We propose another way, which is supplementary but completely equivalent to the previous one and is based on the idea suggested by Bogoliubov in his theory of quasiaverages [23]. Considering the case of a 3D ideal Bose gas with the Hamiltonian

$$H = \sum_{\vec{p}}(\frac{\hbar^2 p^2}{2m} - \mu)a^{\dagger}_{\vec{p}}a_{\vec{p}} \qquad , \qquad (30)$$

where a_p^{+}, a_p are Bose operators and μ is the chemical potential, Bogoliubov added a term

$$-\nu\sqrt{V}(a_0 e^{i\varphi} + a_0 e^{-i\varphi}) \qquad (31)$$

breaking the gauge symmetry and proposed to consider the BEC on the state with p=0 in the frame of the Hamiltonian

$$\hat{\mathcal{H}} = \sum_p \left(\frac{\hbar^2 p^2}{2m} - \mu\right)a^{\dagger}_p a_p - \nu\sqrt{V}(a^{\dagger}_0 e^{i\varphi} + a_0 e^{-i\varphi}) \quad , \qquad (32)$$

where

$$\nu = -\mu\sqrt{\frac{N_0}{V}} = -\mu\sqrt{n_0}; \qquad -\frac{\nu}{\mu} = \sqrt{n_0}; \qquad (33)$$

We will name the Hamiltonian of the type (32) as the Hamiltonian of the theory of quasiaverages. It is written in the frame of the operators a_p^{+}, a_p of the initial Hamiltonian (30).

Our intention is to apply this idea to the case of BEC of interacting 2D magnetoexcitons and to deduce explicitly the Hamiltonian of the type (32) with the finite parameters μ and ν

but with the relation of the type (33). We intend to formulate the new Hamiltonian with broken symmetry in the terms of the operators a_p, b_p avoiding the obligatory crossing to the operators α_p, β_p (28) at least at some stages of the investigation where the representation in the a_p, b_p operators remains preferential.

Of course the two representations are completely equivalent and complimentary each other. We will follow the quasiaverage variant (32) instead of u,v variant (29), because it opens some new possibilities, which were not studied up till now to the best of our knowledge. For example the Hamiltonian of the type (32) is simpler than the Hamiltonian $\hat{\tilde{\mathcal{H}}} = D(\sqrt{N_{ex}})\hat{H}D^{\dagger}(\sqrt{N_{ex}})$ in the α_p, β_p representation and the deduction of the motion equation for the operators (18) and for the many-particle Green's functions constructed on their base is also much simple. We will profit by this advantage at some stages of investigation. On the contrary, when we will deal with the calculations of the average values of different operators on the base of the ground coherent macroscopic state (28) or using the coherent excited states, as we have done in papers [4,5], the most convenient way is to use the α_p, β_p representation. We will use in the wide manner the both representations. The new variant in the style of the theory of quasiaverages can be realized rewriting the transformed Hamiltonian $D(\sqrt{N_{ex}})\hat{H}D^{\dagger}(\sqrt{N_{ex}})$ in the a_p, b_p representation as follows below. To demonstrate it we will represent the unitary transformation

$$\hat{D}(\sqrt{N_{ex}}) = e^{\hat{X}} = \sum_{n=0}^{\infty} \frac{\hat{X}^n}{n!}; \quad , \qquad (34)$$
$$D^{\dagger}(\sqrt{N_{ex}}) = e^{-\hat{X}}$$

where

$$\hat{X} = \sqrt{N_{ex}}(e^{i\varphi}d^{\dagger}(K) - e^{-i\varphi}d(K)); \qquad (35)$$
$$\hat{X}^{\dagger} = -\hat{X};$$

The creation and annihilation operators $d^{+}(k), d(k)$ (18) are written in the Landau gauge when the electrons and holes forming the magnetoexcitons are situated on their lowest Landau levels (LLL). Only this variant is considered here without taking into account the excited Landau levels (ELL) , as it was done in [4]. The BEC of 2D magnetoexcitons is considered on the single-exciton state characterized by two-dimensional wave vector $\vec{k}$. Expanding in series the unitary operators $D(\sqrt{N_{ex}}), D^{\dagger}(\sqrt{N_{ex}})$ we will find the transformed operator $\hat{\tilde{\mathcal{H}}}$ in the form

$$\hat{\tilde{\mathcal{H}}} = e^{\hat{X}}\hat{H}e^{-\hat{X}} = \hat{H} + \frac{1}{1!}\left[\hat{X}, \hat{H}\right] + \frac{1}{2!}\left[\hat{X}, \left[\hat{X}, \hat{H}\right]\right] + \frac{1}{3!}\left[\hat{X}, \left[\hat{X}, \left[\hat{X}, \hat{H}\right]\right]\right] + ... = \hat{\mathcal{H}} + \hat{\mathcal{H}}' \qquad (36)$$

Here the Hamiltonian $\hat{\mathcal{H}}$ contains the main contributions of the first three terms in the series expansion (36), whereas the operator $\hat{\mathcal{H}}'$ gathers the all remaining terms.

As one can see looking at formulas (35) operator $\hat{X}$ is proportional to the square root of the exciton concentration $\sqrt{N_{ex}}$, which is proportional to the filling number ν. One can see that the contributions arising from the first commutator $\left[\hat{X}, \hat{H}\right]$ are proportional to ν, the contributions arising from the second commutator $\left[\hat{X}, \left[\hat{X}, \hat{H}\right]\right]$ are proportional to ν^2 and so

on. Following the Bogoliubov's theory of quasiaverages only the linear terms of the type $\left(d^{+}(k)e^{i\varphi}+e^{-i\varphi}d(k)\right)\nu$ arising from the first commutator $\left[\hat{X},\hat{H}\right]$ must be included into $\hat{\mathcal{H}}$. But taking into account the deviation of the exciton creation and annihilation operators from the pure Bose statistics, we will take into account also the term proportional to $N_{ex}D(0)$ from the second commutator.

We will show below, that such foresight permits to obtain a Hamiltonian $\hat{\mathcal{H}}$ which will generate the motion equation of the exciton creation and annihilation operators in concordance with the basic suppositions concerning their BEC. Such supplimentary term in the Hamiltonian $\hat{\mathcal{H}}$ introduces the needed corrections related with the deviation of the exciton operators from the true Bose statistics. The commutations were effectuated using the commutation relations (20).

The Hamiltonian $\hat{\mathcal{H}}$ with the broken gauge symmetry describing the BEC of 2D magnetoexcitons on the state with wave vector $k\neq 0$ being written in the style of the Bogoliubov's theory of quasiaverages has the form

$$\hat{\mathcal{H}}=\hat{H}+\sqrt{N_{ex}}(\bar{\mu}-E(\vec{K}))(e^{i\varphi}d^{\dagger}(\vec{K})+e^{-i\varphi}d(\vec{K}))+N_{ex}(E(\vec{K})-\bar{\mu})(1-\frac{\hat{D}(0)}{N});$$
$$\hat{D}(0)=\hat{N}_{e}+\hat{N}_{h}; \qquad (37)$$

For the case of an ideal 2D Bose gas we can rewrite the coefficient $-\nu\sqrt{V}$ in the Hamiltonian (32), in the form $-\nu\sqrt{N}$ and comparing it with the deduced expression (37), we will find

$$\nu=\left(E(k)-\bar{\mu}\right)\mathrm{v}, \qquad (38)$$

where N and the filling number v are determined by expressions (19) and (23). Relation (38) coincides exactly with relation (33) of the Bogoliubov's theory of quasiaverages. In the case of ideal Bose gas ν and $\left(E(k)-\bar{\mu}\right)$ both tend to zero, whereas the filling number is real and different from zero. In the interacting exciton gas the parameter ν and $\left(E(k)-\bar{\mu}\right)$ are both different from zero. But we kept in the expression for $\hat{\mathcal{H}}$ else the last term proportional to $N_{ex}\left(E(k)-\bar{\mu}\right)=N\mathrm{v}^{2}\left(E(k)-\bar{\mu}\right)$, which was absent in the theory of quasiaverages for the ideal Bose gas. It reflects, as was mentioned above, the deviation of the exciton creation and annihilation operators from the true Bose operators. The influence of the last term will be discussed below writing the motion equations for the exciton operators.

Now the remaining terms gathered in $\hat{\mathcal{H}}'$ will be written. They contain the contributions proportional to $\mathrm{v}^{2},\mathrm{v}^{3}$ and so on. There is also one term proportional to v, but it is nonlinear containing the products of the exciton and plasmon operators. We suppose that their influence on the BEC of magnetoexcitons is less in comparison with the second term in expression (37). The first terms included in $\hat{\mathcal{H}}'$ are

$$\hat{\mathcal{H}}'=-(2i)\sqrt{N_{ex}}\sum_{\vec{Q}}W_{\vec{Q}}Sin\left(\frac{\left[\vec{K}\times\vec{Q}\right]_{z}l^{2}}{2}\right)\left(e^{i\varphi}d^{\dagger}(\vec{K}-\vec{Q})\hat{\rho}(-\vec{Q})-e^{-i\varphi}\hat{\rho}(\vec{Q})d(\vec{K}-\vec{Q})\right)+$$

$$+2N_{ex}\sum_{\vec{Q}}W_{\vec{Q}}Sin^2\left(\frac{\left[\vec{K}\times\vec{Q}\right]_z l^2}{2}\right)(e^{2i\varphi}d^\dagger(\vec{K}-\vec{Q})d^\dagger(\vec{K}+\vec{Q})+e^{-2i\varphi}d(\vec{K}+\vec{Q})d(\vec{K}-\vec{Q})+$$

$$+2d^\dagger(\vec{K}-\vec{Q})d(\vec{K}-\vec{Q})-\frac{1}{N}\hat{\rho}(\vec{Q})\hat{\rho}(-\vec{Q}))- \qquad (39)$$

$$-i\frac{N_{ex}}{N}\sum_{\vec{Q}}W_{\vec{Q}}Sin\left(\frac{\left[\vec{K}\times\vec{Q}\right]_z l^2}{2}\right)Cos\left(\frac{\left[\vec{K}\times\vec{Q}\right]_z l^2}{2}\right)(\hat{D}(\vec{Q})\hat{\rho}(-\vec{Q})-\hat{\rho}(\vec{Q})\hat{D}(-\vec{Q}))+...$$

Below we will construct the motion equations for the operators (18) on the base of the Hamiltonian (37) in the quasiaverages theory approximation (QTA).

3. The motion equations for operators. Magneto-exciton-plasmon complexes.

The starting Hamiltonian $\hat{\mathcal{H}}$ of the variant developed below has the form

$$\hat{\mathcal{H}}=\frac{1}{2}\sum_{\vec{Q}}W_{\vec{Q}}\left[\hat{\rho}(\vec{Q})\hat{\rho}(-\vec{Q})-\hat{N}_e-\hat{N}_h\right]-\mu_e\hat{N}_e-\mu_h\hat{N}_h+$$

$$+\sqrt{N_{ex}}(\bar{\mu}-E(\vec{k}))(e^{i\varphi}d^\dagger(\vec{k})+e^{-i\varphi}d(\vec{k}))-N_{ex}(\bar{\mu}-E(\vec{k}))\left(1-\frac{\hat{D}(0)}{N}\right) \qquad (40)$$

The motion equations for the operators (18) are obtained using the commutation relations (20). They are

$$i\hbar\frac{d}{dt}d(P)=\left[d(P),\hat{\mathcal{H}}\right]=(E(p)-\tilde{\mu})d(\vec{P})-$$

$$-\nu\sqrt{N}e^{i\varphi}\delta_{kr}(\vec{P},\vec{K})-2i\sum_{\vec{Q}}W_{\vec{Q}}Sin\left(\frac{\left[\vec{P}\times\vec{Q}\right]_z l^2}{2}\right)\hat{\rho}(\vec{Q})d(\vec{P}-\vec{Q})+$$

$$+\nu e^{i\varphi}\left[iSin\left(\frac{\left[\vec{P}\times\vec{K}\right]_z l^2}{2}\right)\frac{\hat{\rho}(\vec{P}-\vec{K})}{\sqrt{N}}+Cos\left(\frac{\left[\vec{P}\times\vec{K}\right]_z l^2}{2}\right)\frac{\hat{D}(\vec{P}-\vec{K})}{\sqrt{N}}\right];$$

$$i\hbar\frac{d}{dt}d^\dagger(\vec{P})=[d^\dagger(\vec{P}),\hat{\mathcal{H}}]=(\tilde{\mu}-E(\vec{P}))d^\dagger(\vec{P})+\nu\sqrt{N}e^{-i\varphi}\delta_{kr}(\vec{P},\vec{K})-2i\sum_{\vec{Q}}W_{\vec{Q}}Sin\left(\frac{\left[\vec{P}\times\vec{K}\right]_z l^2}{2}\right)\times$$

$$\times d^\dagger(\vec{P}-\vec{Q})\hat{\rho}(-\vec{Q})+$$

$$+\nu e^{-i\varphi}\left[iSin\left(\frac{\left[\vec{P}\times\vec{K}\right]_z l^2}{2}\right)\frac{\hat{\rho}(\vec{K}-\vec{P})}{\sqrt{N}}-Cos\left(\frac{\left[\vec{P}\times\vec{K}\right]_z l^2}{2}\right)\frac{\hat{D}(\vec{K}-\vec{P})}{\sqrt{N}}\right];$$

$$i\hbar\frac{d}{dt}\hat{\rho}(\vec{P})=[\hat{\rho}(\vec{P}),\hat{\mathcal{H}}]=E(\vec{P})\hat{\rho}(\vec{P})-2i\sum_{\vec{Q}}W_{\vec{Q}}Sin\left(\frac{\left[\vec{P}\times\vec{Q}\right]_z l^2}{2}\right)\times \qquad (41)$$

$$\times\hat{\rho}(\vec{Q})\hat{\rho}(\vec{P}-\vec{Q})+2i\nu\sqrt{N}Sin\left(\frac{\left[\vec{P}\times\vec{K}\right]_z l^2}{2}\right)\left[e^{i\varphi}d^\dagger(\vec{K}-\vec{P})-e^{-i\varphi}d(\vec{P}+\vec{K})\right];$$

$$i\hbar\frac{d}{dt}\hat{D}(\vec{P})=[\hat{D}(\vec{P}),\hat{\mathcal{H}}]=E(\vec{P})\hat{D}(\vec{P})-2i\sum_{\vec{Q}}W_{\vec{Q}}Sin\left(\frac{\left[\vec{P}\times\vec{Q}\right]_z l^2}{2}\right)\times$$

$$\times\hat{\rho}(\vec{Q})\hat{D}(\vec{P}-\vec{Q})-2\nu\sqrt{N}Cos\left(\frac{\left[\vec{P}\times\vec{K}\right]_z l^2}{2}\right)\left[e^{i\varphi}d^{\dagger}(\vec{K}-\vec{P})-e^{-i\varphi}d(\vec{K}+\vec{P})\right].$$

Here ν and $\widetilde{\mu}$ are determined by the expressions

$$\widetilde{\mu}=\bar{\mu}(1-\frac{2N_{ex}}{N})+\frac{2N_{ex}}{N}E(\vec{k});$$

$$(\widetilde{\mu}-E(\vec{k}))=(\bar{\mu}-E(\vec{k}))(1-2\mathrm{v}^2);\qquad \frac{N_{ex}}{N}=\mathrm{v}^2; \tag{42}$$

$$\nu=\sqrt{\frac{N_{ex}}{N}}(E(\vec{k})-\bar{\mu})=(E(\vec{k})-\bar{\mu})\mathrm{v};$$

The expression for ν was deduced in the previous section. The last term in the Hamiltonian $\hat{\mathcal{H}}$ (37) gives rise to the shift of the all exiton levels in the motion equations by the same value, what leads to the difference between $\bar{\mu}$ and $\widetilde{\mu}$.

Now we must pay attention to one important aspect of the derived motion equations, which is closely related with the noncommutativity of the operators (18) expressed by formulas (20). Applying them one can prove, for example, the equalities

$$(E(\vec{P})-\widetilde{\mu})d(\vec{P})-2i\sum_{\vec{Q}}W_{\vec{Q}}Sin\left(\frac{\left[\vec{P}\times\vec{Q}\right]_z l^2}{2}\right)\hat{\rho}(\vec{Q})d(\vec{P}-\vec{Q})=$$

$$=-(E(\vec{P})+\widetilde{\mu})d(\vec{P})-2i\sum_{\vec{Q}}W_{\vec{Q}}Sin\left(\frac{\left[\vec{P}\times\vec{Q}\right]_z l^2}{2}\right)d(\vec{P}-\vec{Q})\hat{\rho}(\vec{Q})=$$

$$=-\widetilde{\mu}\,d(P)-i\sum_{\vec{Q}}W_{\vec{Q}}Sin\left(\frac{\left[\vec{P}\times\vec{Q}\right]_z l^2}{2}\right)(\hat{\rho}(\vec{Q})d(\vec{P}-\vec{Q})+d(\vec{P}-\vec{Q})\hat{\rho}(\vec{Q})).$$

$$E(\vec{P})\hat{\rho}(\vec{P})-2i\sum_{\vec{Q}}W_{\vec{Q}}Sin\left(\frac{\left[\vec{P}\times\vec{Q}\right]_z l^2}{2}\right)\hat{\rho}(\vec{Q})\hat{\rho}(\vec{P}-\vec{Q})=$$

$$=-E(\vec{P})\hat{\rho}(\vec{P})-2i\sum_{\vec{Q}}W_{\vec{Q}}Sin\left(\frac{\left[\vec{P}\times\vec{Q}\right]_z l^2}{2}\right)\hat{\rho}(\vec{P}-\vec{Q})\hat{\rho}(\vec{Q})= \tag{43}$$

$$=-i\sum_{\vec{Q}}W_{\vec{Q}}Sin\left(\frac{\left[\vec{P}\times\vec{Q}\right]_z l^2}{2}\right)\left[\hat{\rho}(\vec{Q})\hat{\rho}(\vec{P}-\vec{Q})+\hat{\rho}(\vec{P}-\vec{Q})\hat{\rho}(\vec{Q})\right]$$

They can be verified taking into account that

$$2\sum_{\vec{Q}} W_{\vec{Q}} Sin^2\left(\frac{\left[\vec{P}\times\vec{Q}\right]_z l^2}{2}\right) = E(P) \tag{44}$$

The quantum energy $E(P)$ is related with the vorticity of the strong magnetic field. These quanta can be added in different combinations to the free energies of the exciton or of the plasmon, which in their turn themselves also are determined by these quanta.

The quantum energy $E(P)$ is due to Coulomb interaction of electrons in the presence of a strong magnetic field and can be named as a plasmon quantum.

The possibility to add or to subtract a photon quantum from the electron energy in the presence of laser radiation gives rise to the notion of quasi – energy [7], which reflects the possibility of formation of electron – photon replicas.

In the same way one can understand the appearance of the different "free" magneto-exciton energies in three variants of the motion equations (43) as a result of formation of three different magneto-exciton-plasmon complexes: one with the "free" energy $(E(P)-\widetilde{\mu})$, the second with the "free" energy - $(E(P)+\widetilde{\mu})$ and the third with the "free" energy - $\widetilde{\mu}$. Starting with different "free" energies we will deal with the BEC of different magneto-exciton-plasmon complexes. In these three variants the constant ν of the broken gauge symmetry as well as $\widetilde{\mu}$ will be also different being conjugated with different "free" energies of the condensed particles. One can conclude that in the case of 2D e-h system in a strong perpendicular magnetic field the plasmon quanta (44) can accompany and influence the exciton quantum – statistical phenomena. In the case of the fractional quantum Hall effect (FQHE) discussed in [6], there are N magnetic flux quanta $\phi_0 = \frac{\hbar c}{e}$ accompanying the transport phenomena. The flux quanta enforce the formation of vortices in the 2D electron gas. The electrons and the vortices form composite particles and determine the properties of the electron liquid [6].

Instead of photons in the case of laser radiation and instead of magnetic flux quanta ϕ_0 and vortices in the electron medium, which appear in the case of FQHE, in our case of 2D–e-h system in a strong magnetic field we deal with plasmon quanta $E(P)$. Instead of electron – vortex composite particles we meet with the magneto-exciton-plasmon complexes. Equations (41) for four concrete interconnected operators $d^+(P), d(2\vec{K}-\vec{P}), \hat{\rho}(\vec{K}-\vec{P})$ and $\hat{D}(\vec{K}-\vec{P})$ have the forms

$$i\hbar\frac{d}{dt}d^\dagger(\vec{P}) = -(E(\vec{P})-\widetilde{\mu})d^\dagger(\vec{P}) + \nu\sqrt{N}e^{-i\varphi}\delta_{kr}(\vec{P},\vec{K}) - 2i\sum_{\vec{Q}} W_{\vec{Q}} Sin\left(\frac{\left[\vec{P}\times\vec{Q}\right]_z l^2}{2}\right)\times$$

$$\times d^\dagger(\vec{P}-\vec{Q})\hat{\rho}(-\vec{Q}) +$$

$$+\nu e^{-i\varphi}\left[iSin\left(\frac{\left[\vec{P}\times\vec{K}\right]_z l^2}{2}\right)\frac{\hat{\rho}(\vec{K}-\vec{P})}{\sqrt{N}} - Cos\left(\frac{\left[\vec{P}\times\vec{K}\right]_z l^2}{2}\right)\frac{\hat{D}(\vec{K}-\vec{P})}{\sqrt{N}}\right];$$

$$
\begin{aligned}
&i\hbar\frac{d}{dt}d(2\vec{K}-\vec{P}) = (E(2\vec{K}-\vec{P})-\tilde{\mu})d(2\vec{K}-\vec{P}) - \nu\sqrt{N}e^{i\varphi}\delta_{kr}(\vec{P},\vec{K}) - \\
&-2i\sum_{\vec{Q}}W_{\vec{Q}}Sin\left(\frac{\left[(2\vec{K}-\vec{P})\times\vec{Q}\right]_z l^2}{2}\right)\times\hat{\rho}(\vec{Q})d(2\vec{K}-\vec{P}-\vec{Q}) + \\
&+\nu e^{i\varphi}\left[-iSin\left(\frac{\left[\vec{P}\times\vec{K}\right]_z l^2}{2}\right)\frac{\hat{\rho}(\vec{K}-\vec{P})}{\sqrt{N}} + Cos\left(\frac{\left[\vec{P}\times\vec{K}\right]_z l^2}{2}\right)\frac{\hat{D}(\vec{K}-\vec{P})}{\sqrt{N}}\right]; \\
&i\hbar\frac{d}{dt}\hat{\rho}(\vec{K}-\vec{P}) = E(\vec{K}-\vec{P})\hat{\rho}(\vec{K}-\vec{P}) - 2i\sum_{\vec{Q}}W_{\vec{Q}}Sin\left(\frac{\left[(\vec{K}-\vec{P})\times\vec{Q}\right]_z l^2}{2}\right)\times \\
&\times\hat{\rho}(\vec{Q})\hat{\rho}(\vec{K}-\vec{P}-\vec{Q}) - 2i\nu\sqrt{N}Sin\left(\frac{\left[\vec{P}\times\vec{K}\right]_z l^2}{2}\right)\left[e^{i\varphi}d^{\dagger}(\vec{P}) - e^{-i\varphi}d(2\vec{K}-\vec{P})\right]; \\
&i\hbar\frac{d}{dt}\hat{D}(\vec{K}-\vec{P}) = E(\vec{K}-\vec{P})\hat{D}(\vec{K}-\vec{P}) - 2i\sum_{\vec{Q}}W_{\vec{Q}}Sin\left(\frac{\left[(\vec{K}-\vec{P})\times\vec{Q}\right]_z l^2}{2}\right)\times \\
&\times\hat{\rho}(\vec{Q})\hat{D}(\vec{K}-\vec{P}-\vec{Q}) - 2\nu\sqrt{N}Cos\left(\frac{\left[\vec{P}\times\vec{K}\right]_z l^2}{2}\right)\left[e^{i\varphi}d^{\dagger}(\vec{P}) - e^{-i\varphi}d(2\vec{K}-\vec{P})\right].
\end{aligned}
\tag{45}
$$

On the base of these equations the Green's functions will be introduced and the chains of equations will be developed. Only one variant between many ones reflected by equations (43) will be considered.

4. Many – operator many – particle Green's functions.

Following the motion equations (45) we will introduce four interconnected retarded Green's functions at T=0 [26, 27]

$$
\begin{aligned}
&\langle\langle d^{\dagger}(\vec{P},t); d(\vec{P},0)\rangle\rangle; \qquad && \langle\langle d(2\vec{K}-\vec{P},t); d(\vec{P},0)\rangle\rangle; \\
&\langle\langle\frac{\hat{\rho}(\vec{K}-\vec{P},t)}{\sqrt{N}}; d(\vec{P},0)\rangle\rangle; \qquad && \langle\langle\frac{\hat{D}(\vec{K}-\vec{P},t)}{\sqrt{N}}; d(\vec{P},0)\rangle\rangle,
\end{aligned}
\tag{46}
$$

and their Fourier – transforms

$$
\begin{aligned}
&G_{11}(\vec{P},\omega) = \langle\langle d^{\dagger}(\vec{P})\Big| d(\vec{P})\rangle\rangle_{\omega}; \qquad && G_{12}(\vec{P},\omega) = \langle\langle d(2\vec{K}-\vec{P})\Big| d(\vec{P})\rangle\rangle_{\omega}; \\
&G_{13}(\vec{P},\omega) = \langle\langle\frac{\hat{\rho}(\vec{K}-\vec{P}))}{\sqrt{N}}\Big| d(\vec{P})\rangle\rangle_{\omega}; \qquad && G_{14}(\vec{P},\omega) = \langle\langle\frac{\hat{D}(\vec{K}-\vec{P}))}{\sqrt{N}}\Big| d(\vec{P})\rangle\rangle_{\omega};
\end{aligned}
\tag{47}
$$

They are determined by the relations

$$
\langle\langle\hat{A}(t);\hat{B}(0)\rangle\rangle = -i\Theta(t)\langle\left[\hat{A}(t),\hat{B}(0)\right]\rangle; \quad A(t) = e^{\frac{i\hat{\mathcal{H}}t}{\hbar}}Ae^{-\frac{i\hat{\mathcal{H}}t}{\hbar}}; \quad \left[\hat{A},\hat{B}\right] = \hat{A}\hat{B} - \hat{B}\hat{A}, \tag{48}
$$

where $\hat{\mathcal{H}}$ is the Hamiltonian (40).

The average $\langle\rangle$ is calculated at T=0 using the ground state wave function $\left|\psi_g(\vec{K})\right\rangle$ (28) as well as, if needed, the coherent excited states (46)-(56) [4,5].

The time derivative of the Green's function is calculated as follows

$$i\hbar\frac{d}{dt}\langle\langle\hat{A}(t);\hat{B}(0)\rangle\rangle=\hbar\delta(t)\langle\left[\hat{A},\hat{B}\right]\rangle+\langle\langle i\hbar\frac{d}{dt}\hat{A}(t);\hat{B}(0)\rangle\rangle;$$
$$i\hbar\frac{d\hat{A}(t)}{dt}=\left[\hat{A}(t),\hat{\mathcal{H}}\right]=e^{\frac{i\hat{\mathcal{H}}t}{\hbar}}\left[\hat{A},\hat{\mathcal{H}}\right]e^{-\frac{i\hat{\mathcal{H}}t}{\hbar}} \tag{49}$$

The term $\langle\left[\hat{A},\hat{B}\right]\rangle$ and other similar ones will be denoted by constant C. The Fourier representation is introduced by

$$\langle\langle\hat{A}(t);\hat{B}(0)\rangle\rangle=\int_{-\infty}^{\infty}d\omega e^{-i\omega t}\langle\langle\hat{A}\left|\hat{B}\right\rangle\rangle_{\omega}$$

$$\delta(t)=\frac{1}{2\pi}\int_{-\infty}^{\infty}e^{-i\omega t}d\omega \tag{50}$$

$$i\hbar\frac{d}{dt}\langle\langle\hat{A}(t);\hat{B}(0)\rangle\rangle=\int_{-\infty}^{\infty}d\omega e^{-i\omega t}\hbar\omega\langle\langle\hat{A}\left|\hat{B}\right\rangle\rangle_{\omega}$$

Calculating the Fourier transform of the retarded Green's function one needs to guarantee the convergence of the time integral. It is achieved by introducing an infinitesimal value $\delta\to+0$ in the form

$$\langle\langle\hat{A}\left|\hat{B}\right\rangle\rangle_{\omega}=\int_{-\infty}^{\infty}dte^{i\omega t}\langle\langle\hat{A}(t);\hat{B}(0)\rangle\rangle=\int_{0}^{\infty}dte^{i\omega t-\delta t}\langle\langle\hat{A}(t);\hat{B}(0)\rangle\rangle \tag{51}$$

By this reason in the resonance denominators containing ω we will substitute $\hbar\omega$ by $(\hbar\omega+i\delta)$.

The Green's function (47) as well as (46) will be named as one – operator Green's functions because they contain in the left hand side of the vertical line only one summary operator of the type $d^{\dagger}(\vec{P}),d(2\vec{K}-\vec{P}),\frac{\hat{\rho}(\vec{K}-\vec{P})}{\sqrt{N}}$ and $\frac{\hat{D}(\vec{K}-\vec{P})}{\sqrt{N}}$. At the same time these Green's functions are two – particle Green's functions because the summary operators (18) are expressed through the products of two Fermi operators.

In this sense the Green's functions (47) are equivalent to the two – particle Green's functions introduced by Keldysh-Kozlov in their theory of the collective elementary excitations in bulk crystals in the absence of the external magnetic field [24].

The exact equations determining the one operator, two – particle Green's functions (47) in the frame of the quasi-average variant of the theory of BEC of magnetoexcitons follow directly from the motion equations (45)

$$\langle\langle d^{\dagger}(\vec{P})\left|d(\vec{P})\right\rangle\rangle_{\omega}\left[\hbar\omega+E(P)-\widetilde{\mu}\right]+$$

$$+2i\sum_{\vec{Q}}W_{\vec{Q}}Sin\left(\frac{\left[\vec{P}\times\vec{Q}\right]_z l^2}{2}\right)\langle\langle d^{\dagger}(\vec{P}-\vec{Q})\hat{\rho}(-\vec{Q})\left|d(\vec{P})\right\rangle\rangle_{\omega}-$$

$$-ive^{-i\varphi}Sin\left(\frac{\left[\vec{P}\times\vec{K}\right]_z l^2}{2}\right)\langle\langle\frac{\hat{\rho}(\vec{K}-\vec{P})}{\sqrt{N}}\left|d(\vec{P})\right\rangle\rangle_{\omega}+\nu e^{-i\varphi}Cos\left(\frac{\left[\vec{P}\times\vec{K}\right]_z l^2}{2}\right)\langle\langle\frac{\hat{D}(\vec{K}-\vec{P})}{\sqrt{N}}\left|d(\vec{P})\right\rangle\rangle_{\omega}=C_{11};$$

$$\langle\langle d(2\vec{K}-\vec{P})\Big|d(\vec{P})\rangle\rangle_{\omega}\left[\hbar\omega-E(2\vec{K}-\vec{P})+\widetilde{\mu}\right]+$$

$$+2i\sum_{\vec{Q}}W_{\vec{Q}}Sin\left(\frac{\left[(2\vec{K}-\vec{P})\times\vec{Q}\right]_z l^2}{2}\right)\langle\langle\hat{\rho}(\vec{Q})d(2\vec{K}-\vec{P}-\vec{Q})\Big|d(\vec{P})\rangle\rangle_{\omega}+$$

$$+i\nu e^{i\varphi}Sin\left(\frac{\left[\vec{P}\times\vec{K}\right]_z l^2}{2}\right)\langle\langle\frac{\hat{\rho}(\vec{K}-\vec{P})}{\sqrt{N}}\Big|d(\vec{P})\rangle\rangle_{\omega}-\nu e^{i\varphi}Cos\left(\frac{\left[\vec{P}\times\vec{K}\right]_z l^2}{2}\right)\langle\langle\frac{\hat{D}(\vec{K}-\vec{P})}{\sqrt{N}}\Big|d(\vec{P})\rangle\rangle_{\omega}=C_{12}$$

$$\langle\langle\frac{\hat{\rho}(\vec{K}-\vec{P})}{\sqrt{N}}\Big|d(\vec{P})\rangle\rangle_{\omega}\left[\hbar\omega-E(\vec{K}-\vec{P})\right]+$$

$$+2i\sum_{\vec{Q}}W_{\vec{Q}}Sin\left(\frac{\left[(\vec{K}-\vec{P})\times\vec{Q}\right]_z l^2}{2}\right)\langle\langle\hat{\rho}(\vec{Q})\frac{\hat{\rho}(\vec{K}-\vec{P}-\vec{Q})}{\sqrt{N}}\Big|d(\vec{P})\rangle\rangle_{\omega}+ \qquad (52)$$

$$+2i\nu e^{i\varphi}Sin\left(\frac{\left[\vec{P}\times\vec{K}\right]_z l^2}{2}\right)\langle\langle d^{\dagger}(\vec{P})\Big|d(\vec{P})\rangle\rangle_{\omega}-2i\nu e^{-i\varphi}Sin\left(\frac{\left[\vec{P}\times\vec{K}\right]_z l^2}{2}\right)\langle\langle d(2\vec{K}-\vec{P})\Big|d(\vec{P})\rangle\rangle_{\omega}=C_{13}$$

$$\langle\langle\frac{\hat{D}(\vec{K}-\vec{P})}{\sqrt{N}}\Big|d(\vec{P})\rangle\rangle_{\omega}\left[\hbar\omega-E(\vec{K}-\vec{P})\right]+$$

$$+2i\sum_{\vec{Q}}W_{\vec{Q}}Sin\left(\frac{\left[(\vec{K}-\vec{P})\times\vec{Q}\right]_z l^2}{2}\right)\langle\langle\hat{\rho}(\vec{Q})\frac{\hat{D}(\vec{K}-\vec{P}-\vec{Q})}{\sqrt{N}}\Big|d(\vec{P})\rangle\rangle_{\omega}+$$

$$+2\nu e^{i\varphi}Cos\left(\frac{\left[\vec{P}\times\vec{K}\right]_z l^2}{2}\right)\langle\langle d^{\dagger}(\vec{P})\Big|d(\vec{P})\rangle\rangle_{\omega}-2\nu e^{-i\varphi}Cos\left(\frac{\left[\vec{P}\times\vec{K}\right]_z l^2}{2}\right)\langle\langle d(2\vec{K}-\vec{P})\Big|d(\vec{P})\rangle\rangle_{\omega}=C_{14}$$

The constants C_{1i}, where $i=1,2,3,4$ depend on $\vec{P}$ and ω. But they are not needed in an explicit form, because we are interested only in the energy spectrum of the collective elementary excitations and it is determined only by the self – energy parts of the Green's functions. All constants, which will appear in the equations for any Green's functions will be denoted by C capital, without detalization.

Equations (52) for one-operator Green`s functions (47) contain in their componence the two-operator (four-particle) Green`s functions generated by the nonlinear terms in motion equations (41), (45) for the operators (18). These two-operator (four-particle) Green`s function will be determined below. They will obey to new exact equations in the frame of Hamiltonian (40) containing new three-operator (six-particle) Green`s functions. And this process is infinite giving rise to infinite chains of equations with n-operator (2n-particle) Green`s functions, where n increases by one at each new step in the chains evolution. As usual such chains are truncated, what leads to concrete approximate solutions [27]. Below we will obtain the exact equations in the frame of Hamiltonian (40) for four two-operator Green`s functions appeared in the first-step equations (35). These second step equations will contain new three-operators (six-particle) Grenn`s functions. They are

$$\left\langle\left\langle d^{\dagger}(\vec{P}-\vec{Q})\hat{\rho}(-\vec{Q})\,|\,d(\vec{P})\right\rangle\right\rangle_{\omega}\left[\hbar\omega-\tilde{\mu}+E(\vec{P}-\vec{Q})-E(-\vec{Q})\right]=C+\nu Ne^{-i\varphi}\delta_{kr}(\vec{Q},\vec{P}-\vec{K})\left\langle\left\langle\frac{\hat{\rho}(\vec{K}-\vec{P})}{\sqrt{N}}\,|\,d(\vec{P})\right\rangle\right\rangle_{\omega}-$$

$$-2i\sum_{\vec{R}}W_{\vec{R}}Sin\left(\frac{[(\vec{P}-\vec{Q})\times\vec{R}]_z l^2}{2}\right)\left\langle\left\langle d^{\dagger}(\vec{P}-\vec{Q}-\vec{R})\hat{\rho}(-\vec{R})\hat{\rho}(-\vec{Q})\,|\,d(\vec{P})\right\rangle\right\rangle_{\omega}+$$

$$+2i\sum_{\vec{R}}W_{\vec{R}}Sin\left(\frac{[\vec{Q}\times\vec{R}]_z l^2}{2}\right)\left\langle\left\langle d^{\dagger}(\vec{P}-\vec{Q})\hat{\rho}(\vec{R})\hat{\rho}(-\vec{Q}-\vec{R})\,|\,d(\vec{P})\right\rangle\right\rangle_{\omega}-$$

$$-2i\nu\sqrt{N}e^{i\varphi}Sin\left(\frac{[\vec{Q}\times\vec{K}]_z l^2}{2}\right)\left\langle\left\langle d^{\dagger}(\vec{P}-\vec{Q})d^{\dagger}(\vec{K}+\vec{Q})\,|\,d(\vec{P})\right\rangle\right\rangle_{\omega}+$$

$$+2i\nu\sqrt{N}e^{-i\varphi}Sin\left(\frac{[\vec{Q}\times\vec{K}]_z l^2}{2}\right)\left\langle\left\langle d^{\dagger}(\vec{P}-\vec{Q})d(\vec{K}-\vec{Q})\,|\,d(\vec{P})\right\rangle\right\rangle_{\omega}+$$

$$+i\nu e^{-i\varphi}Sin\left(\frac{[(\vec{P}-\vec{Q})\times\vec{K}]_z l^2}{2}\right)\left\langle\left\langle\frac{\hat{\rho}(\vec{K}-\vec{P}+\vec{Q})}{\sqrt{N}}\hat{\rho}(-\vec{Q})\,|\,d(\vec{P})\right\rangle\right\rangle_{\omega}-$$

$$-\nu e^{-i\varphi}Cos\left(\frac{[(\vec{P}-\vec{Q})\times\vec{K}]_z l^2}{2}\right)\left\langle\left\langle\frac{\hat{D}(\vec{K}-\vec{P}+\vec{Q})}{\sqrt{N}}\hat{\rho}(-\vec{Q})\,|\,d(\vec{P})\right\rangle\right\rangle_{\omega};\qquad(53)$$

$$\left\langle\left\langle\hat{\rho}(\vec{Q})d(2\vec{K}-\vec{P}-\vec{Q})\,|\,d(\vec{P})\right\rangle\right\rangle_{\omega}\left[\hbar\omega+\tilde{\mu}-E(2\vec{K}-\vec{P}-\vec{Q})-\vec{E}(\vec{Q})\right]=C-\nu Ne^{i\varphi}\delta_{kr}(\vec{Q},\vec{K}-\vec{P})\left\langle\left\langle\frac{\hat{\rho}(\vec{K}-\vec{P})}{\sqrt{N}}\,|\,d(\vec{P})\right\rangle\right\rangle_{\omega}-$$

$$-2i\sum_{\vec{R}}W_{\vec{R}}Sin\left(\frac{[(2\vec{K}-\vec{P}-\vec{Q})\times\vec{R}]_z l^2}{2}\right)\left\langle\left\langle\hat{\rho}(\vec{Q})\hat{\rho}(\vec{R})d(2\vec{K}-\vec{P}-\vec{Q}-\vec{R})\,|\,d(\vec{P})\right\rangle\right\rangle_{\omega}-$$

$$-2i\sum_{\vec{R}}W_{\vec{R}}Sin\left(\frac{[\vec{Q}\times\vec{R}]_z l^2}{2}\right)\left\langle\left\langle\hat{\rho}(\vec{R})\hat{\rho}(\vec{Q}-\vec{R})d(2\vec{K}-\vec{P}-\vec{Q})\,|\,d(\vec{P})\right\rangle\right\rangle_{\omega}+$$

$$+2ive^{i\varphi}\sqrt{N}Sin\left(\frac{[\vec{Q}\times\vec{K}]_z l^2}{2}\right)\left\langle\left\langle d^{\dagger}(\vec{K}-\vec{Q})d(2\vec{K}-\vec{P}-\vec{Q})\,|\,d(\vec{P})\right\rangle\right\rangle_{\omega}-$$

$$-2ive^{-i\varphi}\sqrt{N}Sin\left(\frac{[\vec{Q}\times\vec{K}]_z l^2}{2}\right)\left\langle\left\langle d(\vec{K}+\vec{Q})d(2\vec{K}-\vec{P}-\vec{Q})\,|\,d(\vec{P})\right\rangle\right\rangle_{\omega}-$$

$$-ive^{i\varphi}Sin\left(\frac{[(\vec{P}+\vec{Q})\times\vec{K}]_z l^2}{2}\right)\left\langle\left\langle\frac{\hat{\rho}(\vec{Q})\hat{\rho}(\vec{K}-\vec{P}-\vec{Q})}{\sqrt{N}}\,|\,d(\vec{P})\right\rangle\right\rangle_{\omega}+$$

$$+\nu e^{i\varphi}Cos\left(\frac{[(\vec{P}+\vec{Q})\times\vec{K}]_z l^2}{2}\right)\left\langle\left\langle\frac{\hat{\rho}(\vec{Q})\hat{D}(\vec{K}-\vec{P}-\vec{Q})}{\sqrt{N}}\,|\,d(\vec{P})\right\rangle\right\rangle_{\omega};\qquad(54)$$

$$\left\langle\left\langle\frac{\hat{\rho}(\vec{Q})\hat{\rho}(\vec{K}-\vec{P}-\vec{Q})}{\sqrt{N}}\,|\,d(\vec{P})\right\rangle\right\rangle_{\omega}\left[\hbar\omega-E(\vec{K}-\vec{P}-\vec{Q})-E(\vec{Q})\right]=C-$$

$$-2i\sum_{\vec{R}}W_{\vec{R}}Sin\left(\frac{[(\vec{K}-\vec{P}-\vec{Q})\times\vec{R}]_z l^2}{2}\right)\left\langle\left\langle\frac{\hat{\rho}(\vec{Q})\hat{\rho}(\vec{R})\hat{\rho}(\vec{K}-\vec{P}-\vec{Q}-\vec{R})}{\sqrt{N}}\,|\,d(\vec{P})\right\rangle\right\rangle_{\omega}-$$

$$-2i\sum_{\vec{R}}W_{\vec{R}}Sin\left(\frac{[\vec{Q}\times\vec{R}]_z l^2}{2}\right)\left\langle\left\langle\frac{\hat{\rho}(\vec{R})\hat{\rho}(\vec{Q}-\vec{R})\hat{\rho}(\vec{K}-\vec{P}-\vec{Q})}{\sqrt{N}}\,|\,d(\vec{P})\right\rangle\right\rangle_{\omega}+$$

$$
\begin{aligned}
&+2i\nu Sin\left(\frac{[\vec{Q}\times\vec{K}]_z l^2}{2}\right)\Big[e^{i\varphi}\left\langle\left\langle d^{\dagger}(\vec{K}-\vec{Q})\hat{\rho}(\vec{K}-\vec{P}-\vec{Q})\,|\,d(\vec{P})\right\rangle\right\rangle_{\omega}-\\
&-e^{-i\varphi}\left\langle\left\langle d(\vec{Q}+\vec{K})\hat{\rho}(\vec{K}-\vec{P}-\vec{Q})\,|\,d(\vec{P})\right\rangle\right\rangle_{\omega}\Big]-\\
&-2i\nu Sin\left(\frac{[(\vec{P}+\vec{Q})\times\vec{K}]_z l^2}{2}\right)\Big[e^{i\varphi}\left\langle\left\langle \hat{\rho}(\vec{Q})d^{\dagger}(\vec{P}+\vec{Q})\,|\,d(\vec{P})\right\rangle\right\rangle_{\omega}-\\
&-e^{-i\varphi}\left\langle\left\langle \hat{\rho}(\vec{Q})d(2\vec{K}-\vec{P}-\vec{Q})\,|\,d(\vec{P})\right\rangle\right\rangle_{\omega}\Big];
\end{aligned}
\tag{55}
$$

$$
\begin{aligned}
&\left\langle\left\langle \frac{\hat{\rho}(\vec{Q})\hat{D}(\vec{K}-\vec{P}-\vec{Q})}{\sqrt{N}}\,|\,d(\vec{P})\right\rangle\right\rangle_{\omega}\Big[\hbar\omega-E(\vec{K}-\vec{P}-\vec{Q})-E(\vec{Q})\Big]=C-\\
&-2i\sum_{\vec{R}}W_{\vec{R}}Sin\left(\frac{[(\vec{K}-\vec{P}-\vec{Q})\times\vec{R}]_z l^2}{2}\right)\left\langle\left\langle \frac{\hat{\rho}(\vec{Q})\hat{\rho}(\vec{R})\hat{D}(\vec{K}-\vec{P}-\vec{Q}-\vec{R})}{\sqrt{N}}\,|\,d(\vec{P})\right\rangle\right\rangle_{\omega}-\\
&-2i\sum_{\vec{R}}W_{\vec{R}}Sin\left(\frac{[\vec{Q}\times\vec{R}]_z l^2}{2}\right)\left\langle\left\langle \frac{\hat{\rho}(\vec{R})\hat{\rho}(\vec{Q}-\vec{R})\hat{D}(\vec{K}-\vec{P}-\vec{Q})}{\sqrt{N}}\,|\,d(\vec{P})\right\rangle\right\rangle_{\omega}+\\
&+2i\nu Sin\left(\frac{[\vec{Q}\times\vec{K}]_z l^2}{2}\right)\Big[e^{i\varphi}\left\langle\left\langle d^{\dagger}(\vec{K}-\vec{Q})\hat{D}(\vec{K}-\vec{P}-\vec{Q})\,|\,d(\vec{P})\right\rangle\right\rangle_{\omega}-\\
&-e^{-i\varphi}\left\langle\left\langle d(\vec{K}+\vec{Q})\hat{D}(\vec{K}-\vec{P}-\vec{Q})\,|\,d(\vec{P})\right\rangle\right\rangle_{\omega}\Big]-\\
&-2\nu Cos\left(\frac{[(\vec{P}+\vec{Q})\times\vec{K}]_z l^2}{2}\right)\Big[e^{i\varphi}\left\langle\left\langle \hat{\rho}(\vec{Q})d^{\dagger}(\vec{P}+\vec{Q})\,|\,d(\vec{P})\right\rangle\right\rangle_{\omega}-\\
&-e^{-i\varphi}\left\langle\left\langle \hat{\rho}(\vec{Q})d(2\vec{K}-\vec{P}-\vec{Q})\,|\,d(\vec{P})\right\rangle\right\rangle_{\omega}\Big].
\end{aligned}
\tag{56}
$$

As one can see, the second step equations (53)-(56) for the two-operator (four-particle) Green`s functions are exact what is the advantage of this method. They contain side by side with the three-operator Green`s functions other two-operator Greeen`s functions, for which in their turn the new equations must be deduced. It is one usual situation in the case of Green`s function method [13]. If one substitutes, for example, expression (53) for the two-operator Green`s function $\left\langle\left\langle d^{\dagger}(\vec{P}-\vec{Q})\hat{\rho}(-\vec{Q})\,|\,d(\vec{P})\right\rangle\right\rangle_{\omega}$ into the first equation (52) its contribution will be equal to

$$
\begin{aligned}
&2i\sum_{\vec{Q}}W_{\vec{Q}}Sin\left(\frac{[\vec{P}\times\vec{Q}]_z l^2}{2}\right)\left\langle\left\langle d^{\dagger}(\vec{P}-\vec{Q})\hat{\rho}(-\vec{Q})\,|\,d(\vec{P})\right\rangle\right\rangle_{\omega}=\\
&C-\frac{2i\nu e^{-i\varphi}NW_{\vec{P}-\vec{K}}Sin\left(\dfrac{[\vec{P}\times\vec{K}]_z l^2}{2}\right)}{[\hbar\omega-\tilde{\mu}+E(\vec{K})-E(\vec{K}-\vec{P})+i\delta]}\left\langle\left\langle \frac{\hat{\rho}(\vec{K}-\vec{P})}{\sqrt{N}}\,|\,d(\vec{P})\right\rangle\right\rangle_{\omega}+
\end{aligned}
$$

$$+4\sum_{\vec{Q}}\sum_{\vec{R}}W_{\vec{Q}}W_{\vec{R}}Sin\left(\frac{[\vec{P}\times\vec{Q}]_z l^2}{2}\right)Sin\left(\frac{[(\vec{P}-\vec{Q})\times\vec{R}]_z l^2}{2}\right)\frac{\left\langle\left\langle d^{\dagger}(\vec{P}-\vec{Q}-\vec{R})\hat{\rho}(-\vec{R})\hat{\rho}(-\vec{Q})\,|\,d(\vec{P})\right\rangle\right\rangle_{\omega}}{[\hbar\omega-\widetilde{\mu}+E(\vec{P}-\vec{Q})-E(-\vec{Q})+i\delta]}-$$

$$-4\sum_{\vec{Q}}\sum_{\vec{R}}W_{\vec{Q}}W_{\vec{R}}Sin\left(\frac{[\vec{P}\times\vec{Q}]_z l^2}{2}\right)Sin\left(\frac{[\vec{Q}\times\vec{R}]_z l^2}{2}\right)\frac{\left\langle\left\langle d^{\dagger}(\vec{P}-\vec{Q})\hat{\rho}(\vec{R})\hat{\rho}(-\vec{Q}-\vec{R})\,|\,d(\vec{P})\right\rangle\right\rangle_{\omega}}{[\hbar\omega-\widetilde{\mu}+E(\vec{P}-\vec{Q})-E(-\vec{Q})+i\delta]}+$$

$$+4\nu e^{i\varphi}\sqrt{N}\sum_{\vec{Q}}W_{\vec{Q}}Sin\left(\frac{[\vec{P}\times\vec{Q}]_z l^2}{2}\right)Sin\left(\frac{[\vec{Q}\times\vec{K}]_z l^2}{2}\right)\frac{\left\langle\left\langle d^{\dagger}(\vec{P}-\vec{Q})d^{\dagger}(\vec{K}+\vec{Q})\,|\,d(\vec{P})\right\rangle\right\rangle_{\omega}}{[\hbar\omega-\widetilde{\mu}+E(\vec{P}-\vec{Q})-E(-\vec{Q})+i\delta]}-$$

$$-4\nu e^{-i\varphi}\sqrt{N}\sum_{\vec{Q}}W_{\vec{Q}}Sin\left(\frac{[\vec{P}\times\vec{Q}]_z l^2}{2}\right)Sin\left(\frac{[\vec{Q}\times\vec{K}]_z l^2}{2}\right)\frac{\left\langle\left\langle d^{\dagger}(\vec{P}-\vec{Q})d(\vec{K}-\vec{Q})\,|\,d(\vec{P})\right\rangle\right\rangle_{\omega}}{[\hbar\omega-\widetilde{\mu}+E(\vec{P}-\vec{Q})-E(-\vec{Q})+i\delta]}-$$

$$-2\nu e^{-i\varphi}\sum_{\vec{Q}}W_{\vec{Q}}Sin\left(\frac{[\vec{P}\times\vec{Q}]_z l^2}{2}\right)Sin\left(\frac{[(\vec{P}-\vec{Q})\times\vec{K}]_z l^2}{2}\right)\frac{\left\langle\left\langle\frac{\hat{\rho}(\vec{K}-\vec{P}+\vec{Q})\hat{\rho}(-\vec{Q})}{\sqrt{N}}\,|\,d(\vec{P})\right\rangle\right\rangle_{\omega}}{[\hbar\omega-\widetilde{\mu}+E(\vec{P}-\vec{Q})-E(-\vec{Q})+i\delta]}-$$

$$-2i\nu e^{-i\varphi}\sum_{\vec{Q}}W_{\vec{Q}}Sin\left(\frac{[\vec{P}\times\vec{Q}]_z l^2}{2}\right)Cos\left(\frac{[(\vec{P}-\vec{Q})\times\vec{K}]_z l^2}{2}\right)\frac{\left\langle\left\langle\frac{\hat{D}(\vec{K}-\vec{P}+\vec{Q})\hat{\rho}(-\vec{Q})}{\sqrt{N}}\,|\,d(\vec{P})\right\rangle\right\rangle_{\omega}}{[\hbar\omega-\widetilde{\mu}+E(\vec{P}-\vec{Q})-E(-\vec{Q})+i\delta]}. \qquad (57)$$

The-two operator Green's function (54) gives rise to the contribution to the second equation (52) in the form

$$2i\sum_{\vec{Q}}W_{\vec{Q}}Sin\left(\frac{\left[(2\vec{K}-\vec{P})\times\vec{Q}\right]_z l^2}{2}\right)\langle\langle\hat{\rho}(\vec{Q})d(2\vec{K}-\vec{P}-\vec{Q})\Big|d(\vec{P})\rangle\rangle_{\omega}=C-$$

$$-\frac{2i\nu e^{i\varphi}NW_{\vec{K}-\vec{P}}Sin\left(\frac{\left[\vec{P}\times\vec{K}\right]_z l^2}{2}\right)}{\left[\hbar\omega+\widetilde{\mu}-E(\vec{K})-E(\vec{K}-\vec{P})+i\delta\right]}\langle\langle\frac{\hat{\rho}(\vec{K}-\vec{P})}{\sqrt{N}}\Big|d(\vec{P})\rangle\rangle_{\omega}+$$

$$+4\sum_{\vec{Q}}\sum_{\vec{R}}W_{\vec{Q}}W_{\vec{R}}Sin\left(\frac{\left[(2\vec{K}-\vec{P})\times\vec{Q}\right]_z l^2}{2}\right)Sin\left(\frac{\left[\vec{Q}\times\vec{R}\right]_z l^2}{2}\right)\times$$

$$\times\frac{\langle\langle\hat{\rho}(\vec{R})\hat{\rho}(\vec{Q}-\vec{R})d(2\vec{K}-\vec{P}-\vec{Q})\Big|d(\vec{P})\rangle\rangle_{\omega}}{\left[\hbar\omega+\widetilde{\mu}-E(2\vec{K}-\vec{P}-\vec{Q})-E(\vec{Q})+i\delta\right]}+$$

$$+4\sum_{\vec{Q}}\sum_{\vec{R}}W_{\vec{Q}}W_{\vec{R}}Sin\left(\frac{\left[(2\vec{K}-\vec{P})\times\vec{Q}\right]_z l^2}{2}\right)Sin\left(\frac{\left[(2\vec{K}-\vec{P}-\vec{Q})\times\vec{R}\right]_z l^2}{2}\right)\times$$

$$\times\frac{\langle\langle\hat{\rho}(\vec{Q})\hat{\rho}(\vec{R})d(2\vec{K}-\vec{P}-\vec{Q}-\vec{R})\Big|d(\vec{P})\rangle\rangle_{\omega}}{\left[\hbar\omega+\widetilde{\mu}-E(2\vec{K}-\vec{P}-\vec{Q})-E(\vec{Q})+i\delta\right]}-$$

$$-4\nu\sqrt{N}e^{i\varphi}\sum_{\vec{Q}}W_{\vec{Q}}Sin\left(\frac{\left[(2\vec{K}-\vec{P})\times\vec{Q}\right]_z l^2}{2}\right)Sin\left(\frac{\left[\vec{Q}\times\vec{K}\right]_z l^2}{2}\right)\times$$

$$\times\frac{\langle\langle d^{\dagger}(\vec{K}-\vec{Q})d(2\vec{K}-\vec{P}-\vec{Q})\Big|d(\vec{P})\rangle\rangle_{\omega}}{\left[\hbar\omega+\widetilde{\mu}-E(2\vec{K}-\vec{P}-\vec{Q})-E(\vec{Q})+i\delta\right]}+$$

$$+4\nu\sqrt{N}e^{-i\varphi}\sum_{\vec{Q}}W_{\vec{Q}}Sin\left(\frac{\left[(2\vec{K}-\vec{P})\times\vec{Q}\right]_z l^2}{2}\right)Sin\left(\frac{\left[\vec{Q}\times\vec{K}\right]_z l^2}{2}\right)\times$$

$$\times\frac{\langle\langle d^{\dagger}(\vec{Q}+\vec{K})d(2\vec{K}-\vec{P}-\vec{Q})\Big|d(\vec{P})\rangle\rangle_{\omega}}{\left[\hbar\omega+\widetilde{\mu}-E(2\vec{K}-\vec{P}-\vec{Q})-E(\vec{Q})+i\delta\right]}+$$

$$+2\nu e^{i\varphi}\sum_{\vec{Q}}W_{\vec{Q}}Sin\left(\frac{\left[(2\vec{K}-\vec{P})\times\vec{Q}\right]_z l^2}{2}\right)Sin\left(\frac{\left[(\vec{P}+\vec{Q})\times\vec{K}\right]_z l^2}{2}\right)\times$$

$$\times\frac{\langle\langle\hat{\rho}(\vec{Q})\dfrac{\hat{\rho}(\vec{K}-\vec{P}-\vec{Q})}{\sqrt{N}}\Big|d(\vec{P})\rangle\rangle_{\omega}}{\left[\hbar\omega+\widetilde{\mu}-E(2\vec{K}-\vec{P}-\vec{Q})-E(\vec{Q})+i\delta\right]}+$$

$$+2i\nu e^{i\varphi}\sum_{\vec{Q}}W_{\vec{Q}}Sin\left(\frac{\left[(2\vec{K}-\vec{P})\times\vec{Q}\right]_z l^2}{2}\right)Cos\left(\frac{\left[(\vec{P}+\vec{Q})\times\vec{K}\right]_z l^2}{2}\right)\times \tag{58}$$

$$\times\frac{\langle\langle\hat{\rho}(\vec{Q})\dfrac{\hat{D}(\vec{K}-\vec{P}-\vec{Q})}{\sqrt{N}}\Big|d(\vec{P})\rangle\rangle_{\omega}}{\left[\hbar\omega+\widetilde{\mu}-E(2\vec{K}-\vec{P}-\vec{Q})-E(\vec{Q})+i\delta\right]}.$$

The contribution of the Green`s functions (55) and (56) to the third and fourth equations (52) are correspondingly

$$2i\sum_{\vec{Q}} W_{\vec{Q}} Sin\left(\frac{[(\vec{K}-\vec{P})\times\vec{Q}]_z l^2}{2}\right)\left\langle\left\langle \hat{\rho}(\vec{Q})\frac{\hat{\rho}(\vec{K}-\vec{P}-\vec{Q})}{\sqrt{N}} \mid d(\vec{P})\right\rangle\right\rangle_\omega =$$

$$C+4\sum_{\vec{Q}}\sum_{\vec{R}} W_{\vec{Q}} W_{\vec{R}} Sin\left(\frac{[(\vec{K}-\vec{P})\times\vec{Q}]_z l^2}{2}\right) Sin\left(\frac{[(\vec{K}-\vec{P}-\vec{Q})\times\vec{R}]_z l^2}{2}\right)\frac{\left\langle\left\langle \hat{\rho}(\vec{Q})\hat{\rho}(\vec{R})\frac{\hat{\rho}(\vec{K}-\vec{P}-\vec{Q}-\vec{R})}{\sqrt{N}} \mid d(\vec{P})\right\rangle\right\rangle_\omega}{[\hbar\omega - E(\vec{Q}) - E(\vec{K}-\vec{P}-\vec{Q}) + i\delta]} +$$

$$+4\sum_{\vec{Q}}\sum_{\vec{R}} W_{\vec{Q}} W_{\vec{R}} Sin\left(\frac{[(\vec{K}-\vec{P})\times\vec{Q}]_z l^2}{2}\right) Sin\left(\frac{[\vec{Q}\times\vec{R}]_z l^2}{2}\right)\frac{\left\langle\left\langle \hat{\rho}(\vec{R})\hat{\rho}(\vec{Q}-\vec{R})\frac{\hat{\rho}(\vec{K}-\vec{P}-\vec{Q})}{\sqrt{N}} \mid d(\vec{P})\right\rangle\right\rangle_\omega}{[\hbar\omega - E(\vec{Q}) - E(\vec{K}-\vec{P}-\vec{Q}) + i\delta]} -$$

$$-4\nu\sum_{\vec{Q}} W_{\vec{Q}} Sin\left(\frac{[(\vec{K}-\vec{P})\times\vec{Q}]_z l^2}{2}\right) Sin\left(\frac{[\vec{Q}\times\vec{K}]_z l^2}{2}\right)\times$$

$$\times\frac{[e^{i\varphi}\left\langle\left\langle d^\dagger(\vec{K}-\vec{Q})\hat{\rho}(\vec{K}-\vec{P}-\vec{Q}) \mid d(\vec{P})\right\rangle\right\rangle_\omega - e^{-i\varphi}\left\langle\left\langle d(\vec{Q}+\vec{K})\hat{\rho}(\vec{K}-\vec{P}-\vec{Q}) \mid d(\vec{P})\right\rangle\right\rangle_\omega]}{[\hbar\omega - E(\vec{Q}) - E(\vec{K}-\vec{P}-\vec{Q}) + i\delta]} +$$

$$+4\nu\sum_{\vec{Q}} W_{\vec{Q}} Sin\left(\frac{[(\vec{K}-\vec{P})\times\vec{Q}]_z l^2}{2}\right) Sin\left(\frac{[(\vec{P}+\vec{Q})\times\vec{K}]_z l^2}{2}\right)\times$$

$$\times\frac{[e^{i\varphi}\left\langle\left\langle \hat{\rho}(\vec{Q})d^\dagger(\vec{P}+\vec{Q}) \mid d(\vec{P})\right\rangle\right\rangle_\omega - e^{-i\varphi}\left\langle\left\langle \hat{\rho}(\vec{Q})d(2\vec{K}-\vec{P}-\vec{Q}) \mid d(\vec{P})\right\rangle\right\rangle_\omega]}{[\hbar\omega - E(\vec{Q}) - E(\vec{K}-\vec{P}-\vec{Q}) + i\delta]}; \qquad (59)$$

$$2i\sum_{\vec{Q}} W_{\vec{Q}} Sin\left(\frac{[(\vec{K}-\vec{P})\times\vec{Q}]_z l^2}{2}\right)\left\langle\left\langle \hat{\rho}(\vec{Q})\frac{\hat{D}(\vec{K}-\vec{P}-\vec{Q})}{\sqrt{N}} \mid d(\vec{P})\right\rangle\right\rangle_\omega =$$

$$C+4\sum_{\vec{Q}}\sum_{\vec{R}} W_{\vec{Q}} W_{\vec{R}} Sin\left(\frac{[(\vec{K}-\vec{P})\times\vec{Q}]_z l^2}{2}\right) Sin\left(\frac{[\vec{Q}\times\vec{R}]_z l^2}{2}\right)\frac{\left\langle\left\langle \frac{\hat{\rho}(\vec{R})\hat{\rho}(\vec{Q}-\vec{R})\hat{D}(\vec{K}-\vec{P}-\vec{Q})}{\sqrt{N}} \mid d(\vec{P})\right\rangle\right\rangle_\omega}{[\hbar\omega - E(\vec{K}-\vec{P}-\vec{Q}) - E(\vec{Q}) + i\delta]} +$$

$$+4\sum_{\vec{Q}}\sum_{\vec{R}} W_{\vec{Q}} W_{\vec{R}} Sin\left(\frac{[(\vec{K}-\vec{P})\times\vec{Q}]_z l^2}{2}\right) Sin\left(\frac{[(\vec{K}-\vec{P}-\vec{Q})\times\vec{R}]_z l^2}{2}\right)\frac{\left\langle\left\langle \frac{\hat{\rho}(\vec{Q})\hat{\rho}(\vec{R})\hat{D}(\vec{K}-\vec{P}-\vec{Q}-\vec{R})}{\sqrt{N}} \mid d(\vec{P})\right\rangle\right\rangle_\omega}{[\hbar\omega - E(\vec{Q}) - E(\vec{K}-\vec{P}-\vec{Q}) + i\delta]} -$$

$$-4\nu\sum_{\vec{Q}} W_{\vec{Q}} Sin\left(\frac{[(\vec{K}-\vec{P})\times\vec{Q}]_z l^2}{2}\right) Sin\left(\frac{[\vec{Q}\times\vec{K}]_z l^2}{2}\right)\times$$

$$\times\frac{[e^{i\varphi}\left\langle\left\langle d^\dagger(\vec{K}-\vec{Q})\hat{D}(\vec{K}-\vec{P}-\vec{Q}) \mid d(\vec{P})\right\rangle\right\rangle_\omega - e^{-i\varphi}\left\langle\left\langle d(\vec{Q}+\vec{K})\hat{D}(\vec{K}-\vec{P}-\vec{Q}) \mid d(\vec{P})\right\rangle\right\rangle_\omega]}{[\hbar\omega - E(\vec{Q}) - E(\vec{K}-\vec{P}-\vec{Q}) + i\delta]} -$$

$$-4i\nu\sum_{\vec{Q}} W_{\vec{Q}} Sin\left(\frac{[(\vec{K}-\vec{P})\times\vec{Q}]_z l^2}{2}\right) Cos\left(\frac{[(\vec{P}+\vec{Q})\times\vec{K}]_z l^2}{2}\right)\times$$

$$\times\frac{[e^{i\varphi}\left\langle\left\langle \hat{\rho}(\vec{Q})d^\dagger(\vec{P}+\vec{Q}) \mid d(\vec{P})\right\rangle\right\rangle_\omega - e^{-i\varphi}\left\langle\left\langle \hat{\rho}(\vec{Q})d(2\vec{K}-\vec{P}-\vec{Q}) \mid d(\vec{P})\right\rangle\right\rangle_\omega]}{[\hbar\omega - E(\vec{Q}) - E(\vec{K}-\vec{P}-\vec{Q}) + i\delta]}. \qquad (60)$$

5. Decoupling of the elementary excitations. Shrinkage of the six-particle Green`s functions.

Expressions (57),(58),(59),(60) are too cumbersome to be prolonged in the same way because the three-operator Green`s functions will be expressed through the four-operator Green`s functions and so on. The shrinkage of the chains of Green`s functions can be achieved, if one will express the three operators, six-particle Green`s functions through the one-operator, two-particle Green`s functions as will be demonstrated below following the method of factorization elaborated in [27]. Another important simplification is the separation or the decoupling of the elementary excitations with different wave vectors as was proposed in [27, 28]. In the equations for the Green`s functions (30) only the terms containing the same Green`s functions are kept. The one-operator Green`s functions with other wave vectors different from $\vec{P},(2\vec{K}-\vec{P})$ and $(\vec{K}-\vec{P})$ are neglected. The two-operator Green`s functions will be expressed through the three-operator Green`s functions and the last will be approximatively expressed through the one-operator Green`s function multiplied by the average values of the remaining two operators. These approximations lead to the expressions:

$$\langle\langle d^{\dagger}(\vec{P}-\vec{Q}-\vec{R})\hat{\rho}(-\vec{R})\hat{\rho}(-\vec{Q})\Big|d(\vec{P})\rangle\rangle_{\omega}\approx\delta_{kr}(\vec{R},-\vec{Q})\times$$

$$\times\langle\langle d^{\dagger}(\vec{P})\Big|d(\vec{P})\rangle\rangle_{\omega}\left\langle\hat{\rho}(\vec{Q})\hat{\rho}(-\vec{Q})\right\rangle+\langle\langle\frac{\hat{\rho}(\vec{K}-\vec{P})}{\sqrt{N}}\Big|d(\vec{P})\rangle\rangle_{\omega}\times$$

$$\times\Big[\delta_{kr}(\vec{R},\vec{P}-\vec{K})\left\langle d^{\dagger}(\vec{K}-\vec{Q})\hat{\rho}(-\vec{Q})\right\rangle+\delta_{kr}(\vec{Q},\vec{P}-\vec{K})\left\langle d^{\dagger}(\vec{K}-\vec{R})\hat{\rho}(-\vec{R})\right\rangle\Big]\sqrt{N};$$

$$\langle\langle d^{\dagger}(\vec{P}-\vec{Q})\hat{\rho}(\vec{R})\hat{\rho}(-\vec{Q}-\vec{R})\Big|d(\vec{P})\rangle\rangle_{\omega}\approx\delta_{kr}(\vec{Q},0)\langle\langle d^{\dagger}(\vec{P})\Big|d(\vec{P})\rangle\rangle_{\omega}\times$$

$$\times\left\langle\hat{\rho}(\vec{R})\hat{\rho}(-\vec{R})\right\rangle+\langle\langle\frac{\hat{\rho}(\vec{K}-\vec{P})}{\sqrt{N}}\Big|d(\vec{P})\rangle\rangle_{\omega}\times$$

$$\times\Big[\delta_{kr}(\vec{R},\vec{K}-\vec{P})+\delta_{kr}(\vec{R},\vec{P}-\vec{K}-\vec{Q})\Big]\left\langle d^{\dagger}(\vec{P}-\vec{Q})\hat{\rho}(\vec{P}-\vec{K}-\vec{Q})\right\rangle\sqrt{N};$$

$$\langle\langle\hat{\rho}(\vec{R})\hat{\rho}(\vec{Q}-\vec{R})d(2\vec{K}-\vec{P}-\vec{Q})\Big|d(\vec{P})\rangle\rangle_{\omega}\approx\delta_{kr}(\vec{Q},0)\langle\langle d^{\dagger}(2\vec{K}-\vec{P})\Big|d(\vec{P})\rangle\rangle_{\omega}\times$$

$$\times\left\langle\hat{\rho}(\vec{R})\hat{\rho}(-\vec{R})\right\rangle+\langle\langle\frac{\hat{\rho}(\vec{K}-\vec{P})}{\sqrt{N}}\Big|d(\vec{P})\rangle\rangle_{\omega}\times$$

$$\times\Big[\delta_{kr}(\vec{R},\vec{K}-\vec{P})+\delta_{kr}(\vec{R},\vec{P}+\vec{Q}-\vec{K})\Big]\left\langle\hat{\rho}(\vec{P}+\vec{Q}-\vec{K})d(2\vec{K}-\vec{P}-\vec{Q})\right\rangle\sqrt{N};$$

$$\langle\langle\hat{\rho}(\vec{Q})\hat{\rho}(\vec{R})d(2\vec{K}-\vec{P}-\vec{Q}-\vec{R})\Big|d(\vec{P})\rangle\rangle_{\omega}\approx\delta_{kr}(\vec{R},-\vec{Q})\langle\langle d^{\dagger}(2\vec{K}-\vec{P})\Big|d(\vec{P})\rangle\rangle_{\omega}\times$$

$$\times\left\langle\hat{\rho}(\vec{Q})\hat{\rho}(-\vec{Q})\right\rangle+\langle\langle\frac{\hat{\rho}(\vec{K}-\vec{P})}{\sqrt{N}}\Big|d(\vec{P})\rangle\rangle_{\omega}\Big[\delta_{kr}(\vec{Q},\vec{K}-\vec{P})\left\langle\hat{\rho}(\vec{R})d(\vec{K}-\vec{R})\right\rangle+ \tag{61}$$

$$+\delta_{kr}(\vec{R},\vec{K}-\vec{P})\left\langle\hat{\rho}(\vec{Q})d(\vec{K}-\vec{Q})\right\rangle\Big]\sqrt{N}.$$

The decoupled and shrinked three-operator Green`s functions (61) being substituted into expressions (57) and (58) correspondingly will generate the following contributions to the desirable closed equations

$$4\sum_{\vec{Q}}\sum_{\vec{R}} W_{\vec{Q}} W_{\vec{R}} Sin\left(\frac{\left[\vec{P}\times\vec{Q}\right]_z l^2}{2}\right) Sin\left(\frac{\left[(\vec{P}-\vec{Q})\times\vec{R}\right]_z l^2}{2}\right)\times$$

$$\times\frac{\langle\langle d^{\dagger}(\vec{P}-\vec{Q}-\vec{R})\hat{\rho}(-\vec{R})\hat{\rho}(-\vec{Q})\left|d(\vec{P})\right\rangle\rangle_{\omega}}{\left[\hbar\omega-\tilde{\mu}+E(\vec{P}-\vec{Q})-E(-\vec{Q})+i\delta\right]}\approx$$

$$\approx -4\sum_{\vec{Q}} W_{\vec{Q}}{}^2 Sin^2\left(\frac{\left[\vec{P}\times\vec{Q}\right]_z l^2}{2}\right)\frac{\left\langle\hat{\rho}(\vec{Q})\hat{\rho}(-\vec{Q})\right\rangle}{\left[\hbar\omega-\tilde{\mu}+E(\vec{P}-\vec{Q})-E(-\vec{Q})+i\delta\right]} G_{11}(\vec{P},\omega)+$$

$$+G_{13}(\vec{P},\omega)\left\{4\sum_{\vec{Q}} W_{\vec{Q}} W_{\vec{P}-\vec{K}} Sin\left(\frac{\left[\vec{P}\times\vec{Q}\right]_z l^2}{2}\right) Sin\left(\frac{\left[(\vec{P}-\vec{Q})\times(\vec{P}-\vec{K})\right]_z l^2}{2}\right)\times\right.$$

$$\times\frac{\left\langle d^{\dagger}(\vec{K}-\vec{Q})\hat{\rho}(-\vec{Q})\right\rangle\sqrt{N}}{\left[\hbar\omega-\tilde{\mu}+E(\vec{P}-\vec{Q})-E(-\vec{Q})+i\delta\right]}-$$

$$\left.-\frac{4W_{\vec{P}-\vec{K}} Sin\left(\frac{\left[\vec{P}\times\vec{K}\right]_z l^2}{2}\right)}{\left[\hbar\omega-\tilde{\mu}+E(\vec{K})-E(\vec{K}-\vec{P})+i\delta\right]}\sum_{\vec{Q}} W_{\vec{R}} Sin\left(\frac{\left[\vec{K}\times\vec{R}\right]_z l^2}{2}\right)\left\langle d^{\dagger}(\vec{K}-\vec{R})\hat{\rho}(-\vec{R})\right\rangle\sqrt{N}\right\}; \tag{62}$$

$$-4\sum_{\vec{Q}}\sum_{\vec{R}} W_{\vec{Q}} W_{\vec{R}} Sin\left(\frac{\left[\vec{P}\times\vec{Q}\right]_z l^2}{2}\right) Sin\left(\frac{\left[\vec{Q}\times\vec{R}\right]_z l^2}{2}\right)\frac{\langle\langle d^{\dagger}(\vec{P}-\vec{Q})\hat{\rho}(\vec{R})\hat{\rho}(-\vec{Q}-\vec{R})\left|d(\vec{P})\right\rangle\rangle_{\omega}}{\left[\hbar\omega-\tilde{\mu}+E(\vec{P}-\vec{Q})-E(-\vec{Q})+i\delta\right]}\approx$$

$$\approx -4\sum_{\vec{Q}} W_{\vec{Q}}(W_{\vec{K}-\vec{P}}-W_{\vec{P}-\vec{K}-\vec{Q}}) Sin\left(\frac{\left[\vec{P}\times\vec{Q}\right]_z l^2}{2}\right)\times \tag{63}$$

$$\times Sin\left(\frac{\left[\vec{Q}\times(\vec{K}-\vec{P})\right]_z l^2}{2}\right)\frac{\left\langle d^{\dagger}(\vec{P}-\vec{Q})\hat{\rho}(\vec{P}-\vec{Q}-\vec{K})\right\rangle\sqrt{N}}{\left[\hbar\omega-\tilde{\mu}+E(\vec{P}-\vec{Q})-E(-\vec{Q})+i\delta\right]} G_{13}(\vec{P},\omega);$$

$$4\sum_{\vec{Q}}\sum_{\vec{R}} W_{\vec{Q}} W_{\vec{R}} Sin\left(\frac{\left[(2\vec{K}-\vec{P})\times\vec{Q}\right]_z l^2}{2}\right) Sin\left(\frac{\left[\vec{Q}\times\vec{R}\right]_z l^2}{2}\right)\times$$

$$\times\frac{\langle\langle\hat{\rho}(\vec{R})\hat{\rho}(\vec{Q}-\vec{R})d(2\vec{K}-\vec{P}-\vec{Q})\left|d(\vec{P})\right\rangle\rangle_{\omega}}{\left[\hbar\omega+\tilde{\mu}+E(2\vec{K}-\vec{P}-\vec{Q})-E(\vec{Q})+i\delta\right]}\approx G_{13}(\vec{P},\omega)\times$$

$$\times 4\sum_{\vec{Q}} W_{\vec{Q}}(W_{\vec{K}-\vec{P}} - W_{\vec{P}+\vec{Q}-\vec{K}}) Sin\left(\frac{\left[(2\vec{K}-\vec{P})\times\vec{Q}\right]_z l^2}{2}\right) Sin\left(\frac{\left[\vec{Q}\times(\vec{K}-\vec{P})\right]_z l^2}{2}\right)\times$$

$$\times\frac{\left\langle\hat{\rho}(\vec{P}+\vec{Q}-\vec{K})d(2\vec{K}-\vec{P}-\vec{Q})\right\rangle\sqrt{N}}{\left[\hbar\omega+\tilde{\mu}-E(2\vec{K}-\vec{P}-\vec{Q})-E(\vec{Q})+i\delta\right]}; \tag{64}$$

$$4\sum_{\vec{Q}}\sum_{\vec{R}} W_{\vec{Q}}W_{\vec{R}} Sin\left(\frac{\left[(2\vec{K}-\vec{P})\times\vec{Q}\right]_z l^2}{2}\right) Sin\left(\frac{\left[(2\vec{K}-\vec{P}-\vec{Q})\times\vec{R}\right]_z l^2}{2}\right)\times$$

$$\times\frac{\langle\langle\hat{\rho}(\vec{Q})\hat{\rho}(\vec{R})d(2\vec{K}-\vec{P}-\vec{Q}-\vec{R})\big|d(\vec{P})\rangle\rangle_\omega}{\left[\hbar\omega+\tilde{\mu}-E(2\vec{K}-\vec{P}-\vec{Q})-E(\vec{Q})+i\delta\right]}\approx$$

$$\approx -4\sum_{\vec{Q}} W_{\vec{Q}}{}^2 Sin^2\left(\frac{\left[(2\vec{K}-\vec{P})\times\vec{Q}\right]_z l^2}{2}\right)\frac{\left\langle\hat{\rho}(\vec{Q})\hat{\rho}(-\vec{Q})\right\rangle}{\left[\hbar\omega+\tilde{\mu}-E(2\vec{K}-\vec{P}-\vec{Q})-E(\vec{Q})+i\delta\right]} G_{12}(\vec{P},\omega)+$$

$$+G_{13}(\vec{P},\omega)\left\{\frac{4W_{\vec{K}-\vec{P}} Sin\left(\frac{\left[\vec{P}\times\vec{K}\right]_z l^2}{2}\right)}{\left[\hbar\omega+\tilde{\mu}-E(\vec{K})-E(\vec{K}-\vec{P})+i\delta\right]}\sum_{\vec{R}} W_{\vec{R}} Sin\left(\frac{\left[\vec{K}\times\vec{R}\right]_z l^2}{2}\right)\left\langle\hat{\rho}(\vec{R})d(\vec{K}-\vec{R})\right\rangle\sqrt{N}+\right.$$

$$+4\sum_{\vec{Q}} W_{\vec{Q}}W_{\vec{K}-\vec{P}} Sin\left(\frac{\left[(2\vec{K}-\vec{P})\times\vec{Q}\right]_z l^2}{2}\right) Sin\left(\frac{\left[(\vec{K}-\vec{Q})\times(\vec{K}-\vec{P})\right]_z l^2}{2}\right)\times$$

$$\left.\times\frac{\left\langle\hat{\rho}(\vec{Q})d(\vec{K}-\vec{P})\right\rangle\sqrt{N}}{\left[\hbar\omega+\tilde{\mu}-E(2\vec{K}-\vec{P}-\vec{Q})-E(\vec{Q})+i\delta\right]}\right\}. \tag{65}$$

The contributions (62)-(65) are proportional to Coulomb interaction in power two of the type $W_{\vec{Q}}W_{\vec{R}}$. Formulas (57) and (58) contain side by side with the three-operator Green`s functions also the two-operator Green`s functions. The latter are incorporated into the terms proportional to $\nu W_{\vec{Q}}$. After their expression through the three-operator Green`s functions and the following transformation into the one-operator Green`s functions their contribution will be proportional to $\nu W_{\vec{Q}}{}^2$.

The constant ν and its dependence on μ in our case was determined above. It is of the same type as (33) and its dependence on the Coulomb interaction originates from the dependence of μ, which was determined in [4]. In the Hartree-Fock-Bogoliubov approximation the chemical potential has the value [4]

$$\bar{\mu}^{HF} - E(K) = 2\nu^2 E(K)$$

and depends linearly on the constant of the Coulomb interaction, whereas its correlation corrections are quadratic on this interaction. In all our next calculations we will confine ourselves to the self-energy parts linear and quadratic in Coulomb interaction. In these restrictions one can neglect all the terms containing two-operator Green`s functions in formulas (57)-(60) because their investements will be of the order $\nu W_{\vec{Q}}{}^2$. By the same reason we will neglect the terms proportional to $\nu^2 W_{\vec{Q}}$.

As a result in our present variant of the paper we will take into account the terms proportional to $\nu, W_{\vec{Q}}, \nu W_{\vec{Q}}$ and $W_{\vec{Q}}{}^2$ and will neglect the terms proportional to $W_{\vec{Q}}{}^3, \nu W_{\vec{Q}}{}^2$ and $\nu^2 W_{\vec{Q}}$. In this approximation the nonlinear terms of the first and second equations (52) are

$$2i\sum_{\vec{Q}} W_{\vec{Q}} Sin\left(\frac{\left[\vec{P}\times\vec{Q}\right]_z l^2}{2}\right)\langle\langle d^\dagger(\vec{P}-\vec{Q})\hat{\rho}(-\vec{Q})\Big|d(\vec{P})\rangle\rangle_\omega \approx$$

$$\approx C - 4\sum_{\vec{Q}} W_{\vec{Q}}{}^2 Sin^2\left(\frac{\left[\vec{P}\times\vec{Q}\right]_z l^2}{2}\right)\frac{\left\langle\hat{\rho}(\vec{Q})\hat{\rho}(-\vec{Q})\right\rangle}{\left[\hbar\omega - \tilde{\mu} + E(\vec{P}-\vec{Q}) - E(-\vec{Q}) + i\delta\right]} G_{11}(\vec{P},\omega) +$$

$$+G_{13}(\vec{P},\omega)\left\{-\frac{2i\nu e^{-i\varphi}(W_{\vec{P}-\vec{K}}N)Sin\left(\frac{\left[\vec{P}\times\vec{K}\right]_z l^2}{2}\right)}{\left[\hbar\omega - \tilde{\mu} + E(\vec{K}) - E(\vec{K}-\vec{P}) + i\delta\right]} + \right.$$

$$+4\sum_{\vec{Q}} W_{\vec{Q}} W_{\vec{P}-\vec{K}} Sin\left(\frac{\left[\vec{P}\times\vec{Q}\right]_z l^2}{2}\right) Sin\left(\frac{\left[(\vec{P}-\vec{Q})\times(\vec{P}-\vec{K})\right]_z l^2}{2}\right)\frac{\left\langle d^\dagger(\vec{K}-\vec{Q})\hat{\rho}(-\vec{Q})\right\rangle\sqrt{N}}{\left[\hbar\omega - \tilde{\mu} + E(\vec{P}-\vec{Q}) - E(-\vec{Q}) + i\delta\right]} -$$

$$\left. -\frac{4W_{\vec{P}-\vec{K}} Sin\left(\frac{\left[\vec{P}\times\vec{K}\right]_z l^2}{2}\right)}{\left[\hbar\omega - \tilde{\mu} + E(\vec{K}) - E(\vec{K}-\vec{P}) + i\delta\right]}\sum_{\vec{R}} W_{\vec{R}} Sin\left(\frac{\left[\vec{K}\times\vec{R}\right]_z l^2}{2}\right)\left\langle d^\dagger(\vec{K}-\vec{R})\hat{\rho}(-\vec{R})\right\rangle\sqrt{N} -\right.$$

$$-4\sum_{\vec{Q}} W_{\vec{Q}}(W_{\vec{K}-\vec{P}} - W_{\vec{P}-\vec{K}-\vec{Q}}) Sin\left(\frac{\left[\vec{P}\times\vec{Q}\right]_z l^2}{2}\right) Sin\left(\frac{\left[\vec{Q}\times(\vec{K}-\vec{P})\right]_z l^2}{2}\right)\times$$

$$\times\frac{\left\langle d^{\dagger}(\vec{P}-\vec{Q})\hat{\rho}(\vec{P}-\vec{Q}-\vec{K})\right\rangle\sqrt{N}}{\left[\hbar\omega-\widetilde{\mu}+E(\vec{P}-\vec{Q})-E(-\vec{Q})+i\delta\right]}\Bigg\}; \tag{66}$$

$$2i\sum_{\vec{Q}} W_{\vec{Q}} Sin\left(\frac{\left[(2\vec{K}-\vec{P})\times\vec{Q}\right]_z l^2}{2}\right)\langle\langle\hat{\rho}(\vec{Q})d(2\vec{K}-\vec{P}-\vec{Q})\Big|d(\vec{P})\rangle\rangle_{\omega}\approx$$

$$\approx C-4\sum_{\vec{Q}} W_{\vec{Q}}{}^2 Sin^2\left(\frac{\left[(2\vec{K}-\vec{P})\times\vec{Q}\right]_z l^2}{2}\right)\frac{\left\langle\hat{\rho}(\vec{Q})\hat{\rho}(-\vec{Q})\right\rangle}{\left[\hbar\omega+\widetilde{\mu}-E(2\vec{K}-\vec{P}-\vec{Q})-E(\vec{Q})+i\delta\right]}G_{12}(\vec{P},\omega)+$$

$$+G_{13}(\vec{P},\omega)\Bigg\{-\frac{2iv e^{i\varphi}(W_{\vec{K}-\vec{P}}N)Sin\left(\frac{\left[\vec{P}\times\vec{K}\right]_z l^2}{2}\right)}{\left[\hbar\omega+\widetilde{\mu}-E(\vec{K})-E(\vec{K}-\vec{P})+i\delta\right]}+$$

$$+4\sum_{\vec{Q}} W_{\vec{Q}}(W_{\vec{K}-\vec{P}} - W_{\vec{P}+\vec{Q}-\vec{K}})\frac{Sin\left(\frac{\left[(2\vec{K}-\vec{P})\times\vec{Q}\right]_z l^2}{2}\right)Sin\left(\frac{\left[\vec{Q}\times(\vec{K}-\vec{P})\right]_z l^2}{2}\right)}{\left[\hbar\omega+\widetilde{\mu}-E(2\vec{K}-\vec{P}-\vec{Q})-E(\vec{Q})+i\delta\right]}\times$$

$$\times\left\langle\hat{\rho}(\vec{P}+\vec{Q}-\vec{K})d(2\vec{K}-\vec{P}-\vec{Q})\right\rangle\sqrt{N}+$$

$$+\frac{4W_{\vec{K}-\vec{P}}Sin\left(\frac{\left[\vec{P}\times\vec{K}\right]_z l^2}{2}\right)}{\left[\hbar\omega+\widetilde{\mu}-E(\vec{K})-E(\vec{K}-\vec{P})+i\delta\right]}\sum_{\vec{R}} W_{\vec{R}} Sin\left(\frac{\left[\vec{K}\times\vec{R}\right]_z l^2}{2}\right)\left\langle\hat{\rho}(\vec{R})d(\vec{K}-\vec{R})\right\rangle\sqrt{N}+ \tag{67}$$

$$+4\sum_{\vec{Q}} W_{\vec{Q}}W_{\vec{K}-\vec{P}}\frac{Sin\left(\frac{\left[(2\vec{K}-\vec{P})\times\vec{Q}\right]_z l^2}{2}\right)Sin\left(\frac{\left[(\vec{K}-\vec{Q})\times(\vec{K}-\vec{P})\right]_z l^2}{2}\right)}{\left[\hbar\omega+\widetilde{\mu}-E(2\vec{K}-\vec{P}-\vec{Q})-E(\vec{Q})+i\delta\right]}\left\langle\hat{\rho}(\vec{Q})d(\vec{K}-\vec{Q})\right\rangle\sqrt{N}\Bigg\}$$

Now the two first equations (52) can be written in the forms

$$G_{11}(\vec{P},\omega)\sum\nolimits_{11}(P,\omega)+G_{12}(\vec{P},\omega)\sum\nolimits_{21}(P,\omega)+G_{13}(\vec{P},\omega)\sum\nolimits_{31}(P,\omega)+$$

$$+G_{14}(\vec{P},\omega)\sum\nolimits_{41}(P,\omega)=C_{11}$$

$$G_{11}\Sigma_{12}(\vec{P},\omega)+G_{12}\Sigma_{22}(\vec{P},\omega)+G_{13}\Sigma_{32}(\vec{P},\omega)+G_{14}\Sigma_{42}(\vec{P},\omega)=C_{12} \tag{68}$$

Their self-energy parts are determined by the following expressions:

$$\Sigma_{11}(\vec{P},\omega)=\hbar\omega-\widetilde{\mu}+E(\vec{P})-4\sum_{\vec{Q}}W_{\vec{Q}}^2\frac{Sin^2\left(\frac{[\vec{P}\times\vec{Q}]_z l^2}{2}\right)}{[\hbar\omega-\widetilde{\mu}+E(\vec{P}-\vec{Q})-E(-\vec{Q})+i\delta]}\left\langle\hat{\rho}(\vec{Q})\hat{\rho}(-\vec{Q})\right\rangle;$$

$$\Sigma_{21}(\vec{P},\omega)=0;$$

$$\Sigma_{31}(\vec{P},\omega)=-i\nu e^{-i\varphi}Sin\left(\frac{[\vec{P}\times\vec{K}]_z l^2}{2}\right)\left[1+\frac{2W_{\vec{P}-\vec{K}}N}{[\hbar\omega-\widetilde{\mu}+E(\vec{K})-E(\vec{K}-\vec{P})+i\delta]}\right]+$$

$$+4\sum_{\vec{Q}}W_{\vec{Q}}W_{\vec{P}-\vec{K}}\frac{Sin\left(\frac{[\vec{P}\times\vec{Q}]_z l^2}{2}\right)Sin\left(\frac{[(\vec{P}-\vec{Q})\times(\vec{P}-\vec{K})]_z l^2}{2}\right)}{[\hbar\omega-\widetilde{\mu}+E(\vec{P}-\vec{Q})-E(-\vec{Q})+i\delta]}\left\langle d^{\dagger}(\vec{K}-\vec{Q})\hat{\rho}(-\vec{Q})\right\rangle\sqrt{N}- \tag{69}$$

$$-4W_{\vec{P}-\vec{K}}\frac{Sin\left(\frac{[\vec{P}\times\vec{K}]_z l^2}{2}\right)}{[\hbar\omega-\widetilde{\mu}+E(\vec{K})-E(\vec{K}-\vec{P})+i\delta]}\sum_{\vec{R}}W_{\vec{R}}Sin\left(\frac{[\vec{K}\times\vec{R}]_z l^2}{2}\right)\left\langle d^{\dagger}(\vec{K}-\vec{R})\hat{\rho}(-\vec{R})\right\rangle\sqrt{N}-$$

$$-4\sum_{\vec{Q}}W_{\vec{Q}}\frac{\left(W_{\vec{K}-\vec{P}}-W_{\vec{P}-\vec{K}-\vec{Q}}\right)Sin\left(\frac{[\vec{P}\times\vec{Q}]_z l^2}{2}\right)Sin\left(\frac{[\vec{Q}\times(\vec{K}-\vec{P})]_z l^2}{2}\right)}{[\hbar\omega-\widetilde{\mu}+E(\vec{P}-\vec{Q})-E(-\vec{Q})+i\delta]}\left\langle d^{\dagger}(\vec{P}-\vec{Q})\hat{\rho}(\vec{P}-\vec{Q}-\vec{K})\right\rangle\sqrt{N};$$

$$\Sigma_{41}(\vec{P},\omega)=\nu e^{-i\varphi}Cos\left(\frac{[\vec{P}\times\vec{K}]_z l^2}{2}\right).$$

The self-energy parts $\Sigma_{i1}(\vec{P},\omega)$ determine the coefficients of the first equation (68). The self-energy parts $\Sigma_{i2}(\vec{P},\omega)$ of the second equation (68) are

$$\Sigma_{12}(\vec{P},\omega)=0;$$

$$\Sigma_{22}(\vec{P},\omega)=\hbar\omega+\widetilde{\mu}-E(2\vec{K}-\vec{P})-$$

$$-4\sum_{\vec{Q}}W_{\vec{Q}}^2\frac{Sin^2\left(\frac{[(2\vec{K}-\vec{P})\times\vec{Q}]_z l^2}{2}\right)\left\langle\hat{\rho}(\vec{Q})\hat{\rho}(-\vec{Q})\right\rangle}{[\hbar\omega+\widetilde{\mu}-E(2\vec{K}-\vec{P}-\vec{Q})-E(\vec{Q})+i\delta]};$$

$$\Sigma_{32}(\vec{P},\omega)=ive^{i\varphi}Sin\left(\frac{[\vec{P}\times\vec{K}]_z l^2}{2}\right)\left[1-\frac{2W_{\vec{K}-\vec{P}}N}{[\hbar\omega+\tilde{\mu}-E(\vec{K})-E(\vec{K}-\vec{P})+i\delta]}\right]+$$

$$+4\sum_{\vec{Q}}W_{\vec{Q}}(W_{\vec{K}-\vec{P}}-W_{\vec{P}+\vec{Q}-\vec{K}})Sin\left(\frac{[(2\vec{K}-\vec{P})\times\vec{Q}]_z l^2}{2}\right)\frac{Sin\left(\frac{[\vec{Q}\times(\vec{K}-\vec{P})]_z l^2}{2}\right)\left\langle\hat{\rho}(\vec{P}+\vec{Q}-\vec{K})d(2\vec{K}-\vec{P}-\vec{Q})\right\rangle\sqrt{N}}{[\hbar\omega+\tilde{\mu}-E(2\vec{K}-\vec{P}-\vec{Q})-E(\vec{Q})+i\delta]}+$$

$$+4\sum_{\vec{Q}}W_{\vec{Q}}\frac{W_{\vec{K}-\vec{P}}Sin\left(\frac{[(2\vec{K}-\vec{P})\times\vec{Q}]_z l^2}{2}\right)Sin\left(\frac{[(\vec{K}-\vec{Q})\times(\vec{K}-\vec{P})]_z l^2}{2}\right)\left\langle\hat{\rho}(\vec{Q})d(\vec{K}-\vec{Q})\right\rangle\sqrt{N}}{[\hbar\omega+\tilde{\mu}-E(2\vec{K}-\vec{P}-\vec{Q})-E(\vec{Q})+i\delta]}+ \quad (70)$$

$$+4W_{\vec{K}-\vec{P}}\frac{Sin\left(\frac{[\vec{P}\times\vec{K}]_z l^2}{2}\right)}{[\hbar\omega+\tilde{\mu}-E(\vec{K})-E(\vec{K}-\vec{P})+i\delta]}\sum_{\vec{R}}W_{\vec{R}}Sin\left(\frac{[\vec{K}\times\vec{R}]_z l^2}{2}\right)\left\langle\hat{\rho}(\vec{R})d(\vec{K}-\vec{R})\right\rangle\sqrt{N};$$

$$\Sigma_{42}(\vec{P},\omega)=-\nu e^{i\varphi}Cos\left(\frac{[\vec{P}\times\vec{K}]_z l^2}{2}\right).$$

Now the remaining two equations (52) will be considered. The reduction of three-operator Green`s functions encountered in the nonlinear terms (59) and (60) is made as follows

$$\left\langle\left\langle\hat{\rho}(\vec{R})\hat{\rho}(\vec{Q}-\vec{R})\frac{\hat{\rho}(\vec{K}-\vec{P}-\vec{Q})}{\sqrt{N}}\,|\,d(\vec{P})\right\rangle\right\rangle_\omega\simeq G_{13}(\vec{P},\omega)[(\delta_{kr}(\vec{R},\vec{K}-\vec{P})+$$

$$+\delta_{kr}(\vec{R},\vec{Q}+\vec{P}-\vec{K}))\left\langle\hat{\rho}(\vec{Q}+\vec{P}-\vec{K})\hat{\rho}(\vec{K}-\vec{P}-\vec{Q})\right\rangle+\delta_{kr}(\vec{Q},0)\left\langle\hat{\rho}(\vec{R})\hat{\rho}(-\vec{R})\right\rangle];$$

$$\left\langle\left\langle\hat{\rho}(\vec{Q})\hat{\rho}(\vec{R})\hat{\rho}(\vec{K}-\vec{P}-\vec{Q}-\vec{R})\,|\,d(\vec{P})\right\rangle\right\rangle_\omega\simeq G_{13}(\vec{P},\omega)[(\delta_{kr}(\vec{R},\vec{K}-\vec{P})+$$

$$+\delta_{kr}(\vec{R},-\vec{Q}))\left\langle\hat{\rho}(\vec{Q})\hat{\rho}(-\vec{Q})\right\rangle+\delta_{kr}(\vec{Q},\vec{K}-\vec{P})\left\langle\hat{\rho}(\vec{R})\hat{\rho}(-\vec{R})\right\rangle];$$

$$\left\langle\left\langle\hat{\rho}(\vec{R})\hat{\rho}(\vec{Q}-\vec{R})\frac{\hat{D}(\vec{K}-\vec{P}-\vec{Q})}{\sqrt{N}}\,|\,d(\vec{P})\right\rangle\right\rangle_\omega\simeq G_{13}(\vec{P},\omega)(\delta_{kr}(\vec{R},\vec{K}-\vec{P})+$$

$$+\delta_{kr}(\vec{R},\vec{Q}+\vec{P}-\vec{K}))\left\langle\hat{\rho}(\vec{Q}+\vec{P}-\vec{K})\hat{D}(\vec{K}-\vec{P}-\vec{Q})\right\rangle+G_{14}(\vec{P},\omega)\delta_{kr}(\vec{Q},0)\left\langle\hat{\rho}(\vec{R})\hat{\rho}(-\vec{R})\right\rangle \quad (71)$$

$$\left\langle\left\langle\hat{\rho}(\vec{Q})\hat{\rho}(\vec{R})\frac{\hat{D}(\vec{K}-\vec{P}-\vec{Q})}{\sqrt{N}}\,|\,d(\vec{P})\right\rangle\right\rangle_\omega\simeq G_{13}(\vec{P},\omega)[(\delta_{kr}(\vec{Q},\vec{K}-\vec{P})\left\langle\hat{\rho}(\vec{R})\hat{D}(-\vec{R})\right\rangle+$$

$$+\delta_{kr}(\vec{R},\vec{K}-\vec{P}))\left\langle\hat{\rho}(\vec{Q})\hat{D}(-\vec{Q})\right\rangle]+G_{14}(\vec{P},\omega)\delta_{kr}(\vec{R},-\vec{Q})\left\langle\hat{\rho}(\vec{Q})\hat{\rho}(-\vec{Q})\right\rangle.$$

They lead to approximate expression of two main components of (42)

$$4\sum_{\vec{Q}}\sum_{\vec{R}} W_{\vec{Q}}W_{\vec{R}}Sin\left(\frac{[(\vec{K}-\vec{P})\times\vec{Q}]_z l^2}{2}\right)Sin\left(\frac{[\vec{Q}\times\vec{R}]_z l^2}{2}\right)\frac{\left\langle\left\langle\hat{\rho}(\vec{R})\hat{\rho}(\vec{Q}-\vec{R})\hat{\rho}(\vec{K}-\vec{P}-\vec{Q})\,|\,d(\vec{P})\right\rangle\right\rangle}{[\hbar\omega-E(\vec{Q})-E(\vec{K}-\vec{P}-\vec{Q})+i\delta]\sqrt{N}}\approx$$

$$\approx G_{13}(\vec{P},\omega)4\sum_{\vec{Q}}W_{\vec{Q}}\frac{(W_{\vec{Q}+\vec{P}-\vec{K}}-W_{\vec{K}-\vec{P}})Sin^2\left(\frac{[(\vec{K}-\vec{P})\times\vec{Q}]_z l^2}{2}\right)\left\langle\hat{\rho}(\vec{Q}+\vec{P}-\vec{K})\hat{\rho}(\vec{K}-\vec{P}-\vec{Q})\right\rangle}{[\hbar\omega-E(\vec{Q})-E(\vec{K}-\vec{P}-\vec{Q})+i\delta]}; \tag{72}$$

$$4\sum_{\vec{Q}}\sum_{\vec{R}} W_{\vec{Q}}W_{\vec{R}}Sin\left(\frac{[(\vec{K}-\vec{P})\times\vec{Q}]_z l^2}{2}\right)Sin\left(\frac{[(\vec{K}-\vec{P}-\vec{Q})\times\vec{R}]_z l^2}{2}\right)\frac{\left\langle\left\langle\hat{\rho}(\vec{Q})\hat{\rho}(\vec{R})\hat{\rho}(\vec{K}-\vec{P}-\vec{Q}-\vec{R})\,|\,d(\vec{P})\right\rangle\right\rangle}{[\hbar\omega-E(\vec{Q})-E(\vec{K}-\vec{P}-\vec{Q})+i\delta]\sqrt{N}}\approx$$

$$\approx G_{13}(\vec{P},\omega)4\sum_{\vec{Q}}W_{\vec{Q}}(W_{\vec{K}-\vec{P}}-W_{-\vec{Q}})Sin^2\left(\frac{[(\vec{K}-\vec{P})\times\vec{Q}]_z l^2}{2}\right)\left\langle\hat{\rho}(\vec{Q})\hat{\rho}(-\vec{Q})\right\rangle.$$

Taking into account only the terms proportional to $W_{\vec{Q}}W_{\vec{R}}$ and neglecting the last two terms in (59) because they give the contributions to the one-operator Green`s functions $G_{i1}(\vec{P},\omega)$ proportional to $\nu W_{\vec{Q}}^2$ one will obtain

$$2i\sum_{\vec{Q}}W_{\vec{Q}}Sin\left(\frac{[(\vec{K}-\vec{P})\times\vec{Q}]_z l^2}{2}\right)\left\langle\left\langle\hat{\rho}(\vec{Q})\frac{\hat{\rho}(\vec{K}-\vec{P}-\vec{Q})}{\sqrt{N}}\,|\,d(\vec{P})\right\rangle\right\rangle_{\omega}\approx$$

$$\approx C+G_{13}(\vec{P},\omega)4\sum_{\vec{Q}}W_{\vec{Q}}Sin^2\left(\frac{[(\vec{K}-\vec{P})\times\vec{Q}]_z l^2}{2}\right)\times \tag{73}$$

$$\times\frac{[(W_{\vec{K}-\vec{P}}-W_{-\vec{Q}})\left\langle\hat{\rho}(\vec{Q})\hat{\rho}(-\vec{Q})\right\rangle+(W_{\vec{Q}+\vec{P}-\vec{K}}-W_{\vec{K}-\vec{P}})\left\langle\hat{\rho}(\vec{Q}+\vec{P}-\vec{K})\hat{\rho}(\vec{K}-\vec{P}-\vec{Q})\right\rangle]}{[\hbar\omega-E(\vec{Q})-E(\vec{K}-\vec{P}-\vec{Q})+i\delta]}.$$

The same processing will be made with the contribution (60). Here we have obtained

$$4\sum_{\vec{Q}}\sum_{\vec{R}} W_{\vec{Q}}W_{\vec{R}}Sin\left(\frac{[(\vec{K}-\vec{P})\times\vec{Q}]_z l^2}{2}\right)Sin\left(\frac{[\vec{Q}\times\vec{R}]_z l^2}{2}\right)\frac{\left\langle\left\langle\hat{\rho}(\vec{R})\hat{\rho}(\vec{Q}-\vec{R})\hat{D}(\vec{K}-\vec{P}-\vec{Q})\,|\,d(\vec{P})\right\rangle\right\rangle_{\omega}}{[\hbar\omega-E(\vec{K}-\vec{P}-\vec{Q})-E(\vec{Q})+i\delta]\sqrt{N}}\approx$$

$$\approx G_{13}(\vec{P},\omega)4\sum_{\vec{Q}}W_{\vec{Q}}(W_{\vec{Q}+\vec{P}-\vec{K}}-W_{\vec{K}-\vec{P}})Sin^2\left(\frac{[(\vec{K}-\vec{P})\times\vec{Q}]_z l^2}{2}\right)\times$$

$$\times\frac{\left\langle\hat{\rho}(\vec{Q}+\vec{P}-\vec{K})\hat{D}(\vec{K}-\vec{P}-\vec{Q})\right\rangle}{[\hbar\omega-E(\vec{K}-\vec{P}-\vec{Q})-E(\vec{Q})+i\delta]};$$

$$4\sum_{\vec{Q}}\sum_{\vec{R}} W_{\vec{Q}}W_{\vec{R}}Sin\left(\frac{[(\vec{K}-\vec{P})\times\vec{Q}]_z l^2}{2}\right)Sin\left(\frac{[(\vec{K}-\vec{P}-\vec{Q})\times\vec{R}]_z l^2}{2}\right)\frac{\left\langle\left\langle\hat{\rho}(\vec{Q})\hat{\rho}(\vec{R})\hat{D}(\vec{K}-\vec{P}-\vec{Q}-\vec{R})\,|\,d(\vec{P})\right\rangle\right\rangle_{\omega}}{[\hbar\omega-E(\vec{Q})-E(\vec{K}-\vec{P}-\vec{Q})+i\delta]\sqrt{N}}\approx$$

$$\approx G_{13}(\vec{P},\omega)4\sum_{\vec{Q}}W_{\vec{Q}}^2Sin^2\left(\frac{[(\vec{K}-\vec{P})\times\vec{Q}]_z l^2}{2}\right)\frac{\left\langle\hat{\rho}(\vec{Q})\hat{D}(-\vec{Q})\right\rangle}{[\hbar\omega-E(\vec{Q})-E(\vec{K}-\vec{P}-\vec{Q})+i\delta]}- \tag{74}$$

$$-G_{14}(\vec{P},\omega)4\sum_{\vec{Q}}W_{\vec{Q}}^2Sin^2\left(\frac{[(\vec{K}-\vec{P})\times\vec{Q}]_z l^2}{2}\right)\frac{\left\langle\hat{\rho}(\vec{Q})\hat{\rho}(-\vec{Q})\right\rangle}{[\hbar\omega-E(\vec{Q})-E(\vec{K}-\vec{P}-\vec{Q})+i\delta]}.$$

In the same approximation as was applied to (59), the nonlinear term will be determined as equal to

$$2i\sum_{\vec{Q}} W_{\vec{Q}} Sin\left(\frac{[(\vec{K}-\vec{P})\times\vec{Q}]_z l^2}{2}\right)\left\langle\left\langle \hat{\rho}(\vec{Q})\frac{\hat{D}(\vec{K}-\vec{P}-\vec{Q})}{\sqrt{N}} \mid d(\vec{P})\right\rangle\right\rangle_{\omega} \approx$$

$$\approx C(\omega) + G_{13}(\vec{P},\omega) 4\sum_{\vec{Q}} W_{\vec{Q}} Sin^2\left(\frac{[(\vec{K}-\vec{P})\times\vec{Q}]_z l^2}{2}\right)\times$$

$$\times\frac{[(W_{\vec{Q}+\vec{P}-\vec{K}} - W_{\vec{K}-\vec{P}})\left\langle\hat{\rho}(\vec{Q}+\vec{P}-\vec{K})\hat{D}(\vec{K}-\vec{P}-\vec{Q})\right\rangle + W_{\vec{Q}}\left\langle\hat{\rho}(\vec{Q})\hat{D}(-\vec{Q})\right\rangle]}{[\hbar\omega - E(\vec{Q}) - E(\vec{K}-\vec{P}-\vec{Q}) + i\delta]} - \tag{75}$$

$$G_{14}(\vec{P},\omega) 4\sum_{\vec{Q}} W_{\vec{Q}}^2 Sin^2\left(\frac{[(\vec{K}-\vec{P})\times\vec{Q}]_z l^2}{2}\right)\frac{\left\langle\hat{\rho}(\vec{Q})\hat{\rho}(-\vec{Q})\right\rangle}{[\hbar\omega - E(\vec{Q}) - E(\vec{K}-\vec{P}-\vec{Q}) + i\delta]}.$$

Now we will substitute the nonlinear terms (74) and (75) into the third and fourth equations (52) correspondingly. These two equations can be written in the forms

$$G_{11}(\vec{P},\omega)\Sigma_{13}(\vec{P},\omega) + G_{12}(\vec{P},\omega)\Sigma_{23}(\vec{P},\omega) + G_{13}(\vec{P},\omega)\Sigma_{33}(\vec{P},\omega) +$$
$$+G_{14}(\vec{P},\omega)\Sigma_{43}(\vec{P},\omega) = C_{13} \tag{76}$$
$$G_{11}(\vec{P},\omega)\Sigma_{14}(\vec{P},\omega) + G_{12}(\vec{P},\omega)\Sigma_{24}(\vec{P},\omega) + G_{13}(\vec{P},\omega)\Sigma_{34}(\vec{P},\omega) +$$
$$+G_{14}(\vec{P},\omega)\Sigma_{44}(\vec{P},\omega) = C_{14}$$

Their self-energy parts are:

$$\Sigma_{13}(\vec{P},\omega) = 2ive^{i\varphi} Sin\left(\frac{[\vec{P}\times\vec{K}]_z l^2}{2}\right);$$

$$\Sigma_{23}(\vec{P},\omega) = -2ive^{-i\varphi} Sin\left(\frac{[\vec{P}\times\vec{K}]_z l^2}{2}\right);$$

$$\Sigma_{33}(\vec{P},\omega) = \hbar\omega - E(\vec{K}-\vec{P}) + 4\sum_{\vec{Q}} W_{\vec{Q}} Sin^2\left(\frac{[(\vec{K}-\vec{P})\times\vec{Q}]_z l^2}{2}\right)\times$$

$$\times\frac{[(W_{\vec{K}-\vec{P}} - W_{-\vec{Q}})\left\langle\hat{\rho}(\vec{Q})\hat{\rho}(-\vec{Q})\right\rangle + (W_{\vec{Q}+\vec{P}-\vec{K}} - W_{\vec{K}-\vec{P}})\left\langle\hat{\rho}(\vec{Q}+\vec{P}-\vec{K})\hat{\rho}(\vec{K}-\vec{P}-\vec{Q})\right\rangle]}{[\hbar\omega - E(\vec{Q}) - E(\vec{K}-\vec{P}-\vec{Q}) + i\delta]};$$

$$\Sigma_{43}(0) = 0;$$

$$\Sigma_{14}(\vec{P},\omega) = 2ve^{i\varphi} Cos\left(\frac{[\vec{P}\times\vec{K}]_z l^2}{2}\right); \tag{77}$$

$$\Sigma_{24}(\vec{P},\omega) = -2ve^{-i\varphi} Cos\left(\frac{[\vec{P}\times\vec{K}]_z l^2}{2}\right);$$

$$\Sigma_{34}(\vec{P},\omega)=4\sum_{\vec{Q}}\ W_{\vec{Q}}Sin^2\left(\frac{[(\vec{K}-\vec{P})\times\vec{Q}]_z l^2}{2}\right)\times$$

$$\times\frac{[(W_{\vec{Q}+\vec{P}-\vec{K}}-W_{\vec{K}-\vec{P}})\left\langle\hat{\rho}(\vec{Q}+\vec{P}-\vec{K})\hat{D}(\vec{K}-\vec{P}-\vec{Q})\right\rangle+W_{\vec{Q}}\left\langle\hat{\rho}(\vec{Q})\hat{D}(-\vec{Q})\right\rangle]}{[\hbar\omega-E(\vec{Q})-E(\vec{K}-\vec{P}-\vec{Q})+i\delta]};$$

$$\Sigma_{44}(\vec{P},\omega)=\hbar\omega-E(\vec{K}-\vec{P})-4\sum_{\vec{Q}}\ W_{\vec{Q}}^2Sin^2\left(\frac{[(\vec{K}-\vec{P})\times\vec{Q}]_z l^2}{2}\right)\times$$

$$\times\frac{\left\langle\hat{\rho}(\vec{Q})\hat{\rho}(-\vec{Q})\right\rangle}{[\hbar\omega-E(\vec{Q})-E(\vec{K}-\vec{P}-\vec{Q})+i\delta]}.$$

The self-energy part (69) and (77) determine the full set of self-energy parts in the approximation which is equivalent to the taking into account of the correlation energy in the frame of coherent excited states discussed in [4,5] beyond the Hartree-Fock-Bogoliubov (HFB) approximation. But before we will study the energy spectrum in a simpler approach.

6. Energy spectrum in the Hartree-Fock-Bogoliubov approximation.

The exact equations for the Green`s functions (47) following expressions (52), (57)-(60) contains terms of type $E(p)$ linear in the Coulomb interaction $W_{\vec{Q}}$, the terms of the type $W_{\vec{Q}}W_{\vec{R}}$ quadratic in the Coulomb interaction as well as the mixed terms $\nu W_{\vec{Q}}$, where the constant ν characterizing the broken symmetry is proportional to $(E(k)-\bar{\mu})$, if the BEC of magnetoexcitons takes place on the state with $\vec{k}\neq 0$. The last relation was established in (42). The chemical potential μ was deduced in [4,5] and it also contains terms proportional to $W_{\vec{Q}}$ and $W_{\vec{Q}}{}^2$. In the Hartree-Fock-Bogoliubov (HFB) approximation we will confine ourselves only with the terms linear in Coulomb interaction $W_{\vec{Q}}$. The possibility of such approach must be verified posteriory. If so, equation (52) for the Green`s functions (47) will take the simple forms of Dyson equations with zeroth-order, or (HFB) self-energy parts $\sum_{ij}^{HF}(P,\omega)$ as follows

$$G_{11}^{(P,\omega)}\sum_{1i}^{HF}(P,\omega)+G_{12}^{(P,\omega)}\sum_{2i}^{HF}(P,\omega)+G_{13}^{(P,\omega)}\sum_{3i}^{HF}(P,\omega)+$$
$$G_{14}^{(P,\omega)}\sum_{4i}^{HF}(P,\omega)=C_{1i};\qquad (78)$$
$$i=1,2,3,4$$

If one will introduce the Green`s functions and self-energy parts in the matrix forms and if we will add a matrix formed by the coefficients C_{ij}

$$\hat{G}(\vec{P},\omega)=\left\|G_{ij}(\vec{P},\omega)\right\|;\qquad \hat{\Sigma}^{HF}(\vec{P},\omega)=\left\|\sum_{ij}^{HF}(\vec{P},\omega)\right\|\qquad \hat{C}=\left\|C_{ij}\right\| \qquad (79)$$

it will permit to write the Dyson equation in a matrix form

$$\hat{G}(\vec{P},\omega)\hat{\Sigma}^{HF}(\vec{P},\omega)=\hat{C} \qquad (80)$$

Equations (68) coincide with one part of equations (80). The other part is not needed because they lead to the same dispersion equation as equations (52) do. The self-energy parts $\sum_{ij}^{HF}(\vec{P},\omega)$ introduced into formulas (54), (55), (56) are listed below

$$\sum\nolimits_{11}^{HF}(\vec{P},\omega)=\hbar\omega+E(\vec{P})-\tilde{\mu}^{HF};\qquad \sum\nolimits_{21}^{HF}(\vec{P},\omega)=0;$$

$$\sum\nolimits_{31}^{HF}(\vec{P},\omega)=-i\nu^{HF}e^{-i\varphi}Sin\left(\frac{[\vec{P}\times\vec{K}]_z l^2}{2}\right);\qquad \sum\nolimits_{41}^{HF}(\vec{P},\omega)=\nu^{HF}e^{-i\varphi}Cos\left(\frac{[\vec{P}\times\vec{K}]_z l^2}{2}\right);$$

$$\sum\nolimits_{12}^{HF}(\vec{P},\omega)=0;\qquad \sum\nolimits_{22}^{HF}(\vec{P},\omega)=\hbar\omega+\tilde{\mu}^{HF}-E(2\vec{K}-\vec{P});\qquad (81)$$

$$\sum\nolimits_{32}^{HF}(\vec{P},\omega)=i\nu^{HF}e^{i\varphi}Sin\left(\frac{[\vec{P}\times\vec{K}]_z l^2}{2}\right);\qquad \sum\nolimits_{42}^{HF}(\vec{P},\omega)=-\nu^{HF}e^{i\varphi}Cos\left(\frac{[\vec{P}\times\vec{K}]_z l^2}{2}\right);$$

$$\sum\nolimits_{13}^{HF}(\vec{P},\omega)=2i\nu^{HF}e^{i\varphi}Sin\left(\frac{[\vec{P}\times\vec{K}]_z l^2}{2}\right);\qquad \sum\nolimits_{23}^{HF}(\vec{P},\omega)=-2i\nu^{HF}e^{-i\varphi}Sin\left(\frac{[\vec{P}\times\vec{K}]_z l^2}{2}\right);$$

$$\sum\nolimits_{33}^{HF}(\vec{P},\omega)=\hbar\omega-E(\vec{K}-\vec{P});\qquad \sum\nolimits_{43}^{HF}(\vec{P},\omega)=0;$$

$$\sum\nolimits_{14}^{HF}(\vec{P},\omega)=2\nu^{HF}e^{i\varphi}Cos\left(\frac{[\vec{P}\times\vec{K}]_z l^2}{2}\right);\qquad \sum\nolimits_{24}^{HF}(\vec{P},\omega)=-2\nu^{HF}e^{-i\varphi}Cos\left(\frac{[\vec{P}\times\vec{K}]_z l^2}{2}\right);$$

$$\sum\nolimits_{44}^{HF}(\vec{P},\omega)=\hbar\omega-E(\vec{K}-\vec{P});\qquad \sum\nolimits_{34}^{HF}(\vec{P},\omega)=0.$$

The values $\tilde{\mu}$ and ν of the zeroth order are denoted by $\tilde{\mu}^{HF}$ and ν^{HF}. It corresponds to the Hartree-Fock-Bogoliubov (HFB) approximation. Following formula (42) [4]

$$\bar{\mu}^{HF}-E(k)=-2\nu^2E(k)$$

The energy spectrum is determined by the solution of the determinant equation

$$\det\left\|\sum\nolimits_{ij}^{HF}(P,\omega)\right\|=0 \qquad (82)$$

which has the form

$$\begin{vmatrix} \sum_{11}^{HF}(P,\omega) & 0 & \sum_{31}^{HF}(P,\omega) & \sum_{41}^{HF}(P,\omega) \\ 0 & \sum_{22}^{HF}(P,\omega) & \sum_{32}^{HF}(P,\omega) & \sum_{42}^{HF}(P,\omega) \\ \sum_{13}^{HF}(P,\omega) & \sum_{23}^{HF}(P,\omega) & \sum_{33}^{HF}(P,\omega) & 0 \\ \sum_{14}^{HF}(P,\omega) & \sum_{24}^{HF}(P,\omega) & 0 & \sum_{44}^{HF}(P,\omega) \end{vmatrix}=0 \qquad (83)$$

The expressions $\sum_{ij}^{HF}(\vec{P},\omega)$ obey one exact relation

$$\sum\nolimits_{31}^{HF}(P,\omega)\sum\nolimits_{13}^{HF}(P,\omega)\sum\nolimits_{42}^{HF}(P,\omega)\sum\nolimits_{24}^{HF}(P,\omega)+\sum\nolimits_{32}^{HF}(P,\omega)\sum\nolimits_{23}^{HF}(P,\omega)\sum\nolimits_{41}^{HF}(P,\omega)\sum\nolimits_{14}^{HF}(P,\omega)-$$
$$-\sum\nolimits_{31}^{HF}(P,\omega)\sum\nolimits_{23}^{HF}(P,\omega)\sum\nolimits_{42}^{HF}(P,\omega)\sum\nolimits_{14}^{HF}(P,\omega)-\sum\nolimits_{32}^{HF}(P,\omega)\sum\nolimits_{13}^{HF}(P,\omega)\sum\nolimits_{41}^{HF}(P,\omega)\sum\nolimits_{24}^{HF}(P,\omega)=0 \qquad (84)$$

It leads to simplification of the dispersion relation (83), which will take the form

$$\sum_{11}^{HF}(P,\omega)\sum_{22}^{HF}(P,\omega)\sum_{33}^{HF}(P,\omega)\sum_{44}^{HF}(P,\omega)- \\ -2(\nu^{HF})^2\left(\sum_{11}^{HF}(P,\omega)\sum_{33}^{HF}(P,\omega)+\sum_{22}^{HF}(P,\omega)\sum_{44}^{HF}(P,\omega)\right)=0 \tag{85}$$

Due to the equality $\sum_{33}^{HF}(P,\omega)=\sum_{44}^{HF}(P,\omega)$, this dispersion relation can be factorized and two relations can be written. One of them describes the simple plasmon solution

$$\sum_{33}^{HF}(P)=0; \quad \hbar\omega=E(\vec{K}-\vec{P}) \tag{86}$$

The other one is the third order equation

$$\sum_{11}^{HF}(P,\omega)\sum_{22}^{HF}(P,\omega)\sum_{44}^{HF}(P,\omega)-2(\nu^{HF})^2\left(\sum_{11}^{HF}(P,\omega)+\sum_{22}^{HF}(P,\omega)\right)=0 \tag{87}$$

which takes the form

$$\left[(\hbar\omega)^2-(\tilde{\mu}^{HF})^2-E(\vec{P})E(2\vec{K}-\vec{P})+\hbar\omega(E(\vec{P})-E(2\vec{K}-\vec{P}))+\tilde{\mu}^{HF}(E(\vec{P})+E(2\vec{K}-\vec{P}))\right]\times \\ \times(\hbar\omega-E(\vec{K}-\vec{P}))-2(\nu^{HF})^2(2\hbar\omega+E(\vec{P})-E(2\vec{K}-\vec{P}))=0 \tag{88}$$

In the special case $\vec{P}=\vec{K}$ it looks as

$$(\hbar\omega)^3-\hbar\omega\left[(E(\vec{K})-\tilde{\mu}^{HF})^2+4(\nu^{HF})^2\right]=0$$

and has three solutions

$$\hbar\omega_1(\vec{P}=\vec{K})=0 \\ \hbar\omega_{2,3}(\vec{P}=\vec{K})=\pm\sqrt{(E(\vec{K})-\tilde{\mu}^{HF})^2+4(\nu^{Hf})^2} \tag{89}$$

Now the more general case will be considered introducing the small deviation of the vector $\vec{P}$ from the condensate wave vector $\vec{K}$ in the form $\vec{P}=\vec{K}+\vec{q}$ and using the series expansions on the small wave vector $\vec{q}$ as follows

$$E(\vec{P})=E(\vec{K}+\vec{q})=E(\vec{K})+\hbar\vec{\mathrm{v}}_{\mathrm{g}}(\vec{K})\vec{q}+\frac{\hbar^2q^2}{2M(\vec{K})} \\ \vec{\mathrm{v}}_{\mathrm{g}}(\vec{K})=\frac{\partial E(\vec{K})}{\partial\vec{K}}; \qquad M(\vec{K})=\frac{\hbar^2}{\frac{\partial^2E(\vec{K})}{(\partial K)^2}}; \\ E(\vec{K}-\vec{P})=E(\vec{q}); \qquad E(2\vec{K}-\vec{P})=E(\vec{K}-\vec{q}) \tag{90}$$

Here the group velocity $\vec{\mathrm{v}}_{\mathrm{g}}(\vec{K})$ and the magnetic mass $M(\vec{K})$ at the condensate wave vector $\vec{K}$ are introduced.

Then the coefficients of equation (88) will become

$$E(\vec{P})-E(2\vec{K}-\vec{P})=2\hbar\vec{v}_g(\vec{K})\vec{q}$$

$$\left(E(\vec{P})-\tilde{\mu}^{HF}\right)\left(E(2\vec{K}-\vec{P})-\tilde{\mu}^{HF}\right)=\left(E(\vec{K})-\tilde{\mu}^{HF}+\frac{\hbar^2q^2}{2M(\vec{K})}\right)^2-\left(\hbar\vec{v}_g(\vec{K})\vec{q}\right)^2\ ; \qquad (91)$$

$$E(\vec{K}-\vec{P})\left(E(\vec{P})-E(2\vec{K}-\vec{P})\right)=2E(\vec{q})\hbar\vec{v}_g(\vec{K})\vec{q}$$

The third order dispersion equation (88) looks as complete cubic equation

$$(\hbar\omega)^3+(\hbar\omega)^2\left[2\hbar\vec{v}_g\vec{q}-E(q)\right]-\hbar\omega\left[\left(E(\vec{K})-\tilde{\mu}^{HF}+\frac{\hbar^2q^2}{2M(\vec{K})}\right)^2-\left(\hbar\vec{v}_g\vec{q}\right)^2+2E(q)\hbar\vec{v}_g\vec{q}+4\left(\nu^{HF}\right)^2\right]+$$

$$E(q)\left[\left(E(K)-\tilde{\mu}^{HF}+\frac{\hbar^2q^2}{2M(\vec{K})}\right)^2-\left(\hbar\vec{v}_g\vec{q}\right)^2\right]-4\left(\nu^{HF}\right)^2\hbar\vec{v}_g\vec{q}=0 \qquad (92)$$

It can be transformed by the substitution

$$\hbar\omega(q)=y(q)+\frac{1}{3}\left(E(q)-2\hbar\vec{v}_g\vec{q}\right) \qquad (93)$$

into the incomplete cubic equation

$$y^3+py+g=0 \qquad (94)$$

with the coefficients $p(q)$ and $g(q)$

$$p(q)=-\left[\left(E(\vec{K})-\tilde{\mu}^{HF}+\frac{\hbar^2q^2}{2M(\vec{K})}\right)^2+4\left(\nu^{HF}\right)^2+\frac{1}{3}\left(\hbar\vec{v}_g\vec{q}+E(q)\right)^2\right]<0 \qquad (95)$$

$$g(q)=\frac{2}{3}\left(E(q)+\hbar\vec{v}_g\vec{q}\right)\left[\left(E(\vec{K})-\tilde{\mu}^{HF}+\frac{\hbar^2q^2}{2M(\vec{K})}\right)^2-2\left(\nu^{HF}\right)^2-\frac{1}{9}\left(E(q)+\hbar\vec{v}_g\vec{q}\right)^2\right] \qquad (96)$$

Because $p(q)<0$, the value $Q=\left(\frac{p}{3}\right)^3+\left(\frac{q}{2}\right)^2$ can be negative, if $\left(-\frac{p}{3}\right)^3>\left(\frac{q}{2}\right)^2$. In this irreducible case there are trigonometric solutions for three real roots of equation (94). They are [29]

$$y_1(q)=2\sqrt{-p(q)/3}\,Cos\frac{\alpha(q)}{3}$$

$$y_{2,3}=-2\sqrt{-p(q)/3}\,Cos\left(\frac{\alpha(q)}{3}\pm\frac{2\pi}{3}\right) \qquad (97)$$

$$Cos\alpha(q)=-\frac{g(q)}{2\sqrt{-\left(p(q)/3\right)^3}};$$

$\left|Cos\alpha(q)\right|<1.$

The final solutions for the dispersion relations are

$$\hbar\omega_1(q)=\frac{1}{3}E(q)-\frac{2}{3}\hbar\vec{\mathrm{v}}_g\vec{q}+2\sqrt{-p(q)/3}\,Cos\frac{\alpha(q)}{3}$$

$$\hbar\omega_{2,3}(q)=\frac{1}{3}E(q)-\frac{2}{3}\hbar\vec{\mathrm{v}}_g\vec{q}+2\sqrt{-p(q)/3}\,Cos\left(\frac{\alpha(q)}{3}\pm\frac{2\pi}{3}\right);\qquad -\left(\frac{p}{3}\right)^3>\left(\frac{g}{2}\right)^2 \tag{98}$$

$$Cos\alpha(q)=-\frac{g(q)}{2\sqrt{-\left(p(q)/3\right)^3}};$$

$$\hbar\omega_4(q)=E(q)$$

In the limit $q\to 0$

$$p(0)=-\left[\left(E(\vec{K})-\tilde{\mu}^{HF}\right)^2+4\left(\nu^{HF}\right)^2\right];\quad g(0)=0,\alpha(0)=\frac{3\pi}{2}$$

$$\frac{\alpha(0)}{3}=\frac{\pi}{2};\quad Cos\left(\frac{\alpha(0)}{3}\pm\frac{2\pi}{3}\right)=Cos\left(\frac{\pi}{2}\pm\frac{2\pi}{3}\right)=\mp\frac{\sqrt{3}}{2} \tag{99}$$

$$\hbar\omega_1(0)=\hbar\omega_4(0)=0;\quad \hbar\omega_{2,3}(0)=\pm\sqrt{\left(E(\vec{K})-\tilde{\mu}^{HF}\right)^2+4\left(\nu^{HF}\right)^2}$$

what coincides with formula (89). The fourth solution (86) $E(\vec{K}-\vec{P})$ equals $E(q)$ and also tends to zero when $q\to 0$.

Now the value ν and its relation with chemical potential μ will be confirmed from another side. To do it, we will start with motion equation (41) for the macroscopical large amplitude of the coherent magnetoexcitons with wave vector $\vec{K}$ neglecting the influence on it of the noncoherent quasiparticles. It has the form

$$i\hbar\frac{d}{dt}d(\vec{K})=\left(E(K)-\tilde{\mu}\right)d(K)-\nu\sqrt{N}e^{i\varphi}\left(1-2\mathrm{v}^2\right); \tag{100}$$

$$\left(E(K)-\tilde{\mu}\right)=\left(E(K)-\bar{\mu}\right)\left(1-2\mathrm{v}^2\right)$$

where we have put approximatively

$$\hat{\rho}(0)\cong\bar{N}_e-\bar{N}_h=0;\qquad \hat{D}(0)\approx\bar{N}_e+\bar{N}_h\approx 2\bar{N}_{ex}=2N\mathrm{v}^2 \tag{101}$$

where v^2 is the filling factor of the LLL. Equation (100) has the form, as it was discussed by Khadzhi in this theory of coherent nonlinear light propagation in the exciton range of spectrum [30]. The time-dependent solution of equation (100) was find [30] in the form

$$\underset{\delta\to+0}{d(K,t)}=\frac{\nu\sqrt{N}e^{i\varphi}}{\left(E(K)-\bar{\mu}\right)}+Ce^{-\frac{i\left(E(K)-\tilde{\mu}\right)t}{\hbar}-\delta t} \tag{102}$$

In the limit $t\to\infty$ the damped oscillatory term vanishes and the stationary solution is established. It was determined in [4] as equal to

$$d(K)=\sqrt{N_{ex}}e^{i\varphi}=e^{i\varphi}\sqrt{N}\,\mathrm{v}$$

Substituting it in equation (102) we will find in full accordance with (42)

$$\nu = \left(E(K) - \bar{\mu}\right) \mathrm{v} \tag{103}$$

It differs from expression (33) by the term $E(K)$, which is due to BEC on the state with $K \neq 0$. It is a general relation, which is true also for ν^{HF} and μ^{HF}.

In such a way we have all necessary parameters to investigate and calculate numerically the desirable dispersion relations on the base of analytical solutions (98)
obtained in the HFB approximation. The group velocity $V_g(k)$ is represented in fig.1, whereas the dispersion relations are drawn in plots 2-5, which correspond to condensate wave vectors $kl = 0$, 1;3,6 and 4,6. They are represented in three observation geometries when the wave vector $\vec{q}$ of the elementary excitation is parallel, anti parallel or perpendicular to the condensate wave vectors $\vec{k}$. There are four branches of the energy spectrum, two of which correspond to acoustical and optical plasmon branches. Other two branches belong to BEC-ed magnetoexcitons. One of them is named as quasienergy branch. Mathematically they appear due to the fact that in Bogoliubov theory of BEC side by side with the exciton annihilation operator $d(P)$ one must take also into account the complex of three operators $d^2(0)d^{\dagger}(-P)$. The states described by these operators have the bare energies $E_{ex}(P) = -I_l + E(P)$ and $2E_{ex}(0) - E_{ex}(-P) = -I_l - E(-P)$ correspondingly. Side by side with the branch $E(P)$ another branch $-E(-P)$ also appears, what is named as quasienergy branch.

From the physical point of view the BEC-te is nothing but an unlimited source of energy without a definite number of quanta, which permits to add or to substract to the energy quantum of any quasiparticle some energy quanta of the condensate. Just these four branches can be observed in fig.1. There are threefold degenerate branch $E(P)$ describing the two plasma branches and one energy branch of the BEC-ed magnetoexcitons. The fourth branch is a quasienergy branch and has a dispersion with the sign minus in comparison with the exciton energy branch. In the case $k = 0$ the two-dimensional magnetoexcitons form an ideal degenerate Bose gas because the interaction between the excitons without the motional dipole moments exactly equals zero. By this reason the energy branches of elementary excitations coincide with the energy spectrum of the bare noninteracting particles. The exciton-type branches of the collective elementary excitations do not contain the ionization potential I_l. It happens because in order to excite one exciton already existing in the componence of the condensate with wave vector $k = 0$ it is necessary to change the initial exciton energy $-I_l$ so as to transfer it in the state with wave vector q and final state energy $-I_l + E(q)$. The excitation energy is equal only to $E(q)$. This fact was mentioned first in [3].

When the condensate wave vector k increases so as kl equals 1;3,6 and 4,6 the attractive interaction between the magnetoexcitons appears, what makes the state of BEC-ed magnetoexcitons unstable. One can observe that in the next three figures one branch remains the same. It is not affected by the changes arised in other three branches. Only the acoustical plasmon branch is interconnected with two BEC-ed exciton branches. It results from the factorization of the fourth order determinant equation (66) and from subsequent equations (69), (71) and (77). Three remaining branches are interconnected and influence each other. When the condensate wave vector $\vec{k}$ increases it leads to the appearance of the growing attractive interaction in the system and to instabilities of the energy spectrum of the elementary excitations deduced in the frame of the HFBA. As was observed in the Introduction, the lowering of the positive energy spectrum of any branch in dependence on

the wave vector means the appearing of the soft mode. It testifies that the system tends to pass in another phase.

Dispersion relations (98) for $\omega_1, \omega_2, \omega_3$ depend on the group velocity $\vec{V}_g(\vec{k})$, in the form $-\frac{2}{3}\hbar\vec{V}_g(\vec{k})\vec{q}$, what is proportional to $-(\vec{k}\bullet\vec{q})$, because $\vec{V}_g(\vec{k})$ following (90) is proportional to $\vec{k}$. Due to such structure of expressions (98) there is a supplementary negative term in one geometry, when $\vec{q}$ is parallel to $\vec{k}$. This term becomes positive in the antiparallel orientation of $\vec{q}$ and $\vec{k}$ and turns to be zero when $\vec{q}$ is perpendicular to $\vec{k}$. The negative term leads to negative values of one branch of the energy spectrum of the elementary excitations and such behavior takes place at all three values of the condensate dimensionless wave number $kl = 1; 3, 6; 4, 6.$

In fig.1 the group velocity $\vec{V}_g(\vec{k})$ in dependence on kl is represented. It has a maximum in the region of $kl \cong 1$.

In the next four figures the energy spectra for different values of kl as well as for different geometries of observation are drawn. One can conclude that in the HFBA all energy spectra at kl different from zero and $v^2 = 0.32$ reveal the instabilities of the system due to the attractive exciton-exciton interaction.

Fig.1. The group velocity $V_g(k)$ of the magnetoexciton in units equal to $\frac{I_l l}{\hbar}$.

Fig.2.The energy spectrum of elementary excitations in the case when kl equals 0. The upper branch is threefold degenerate.

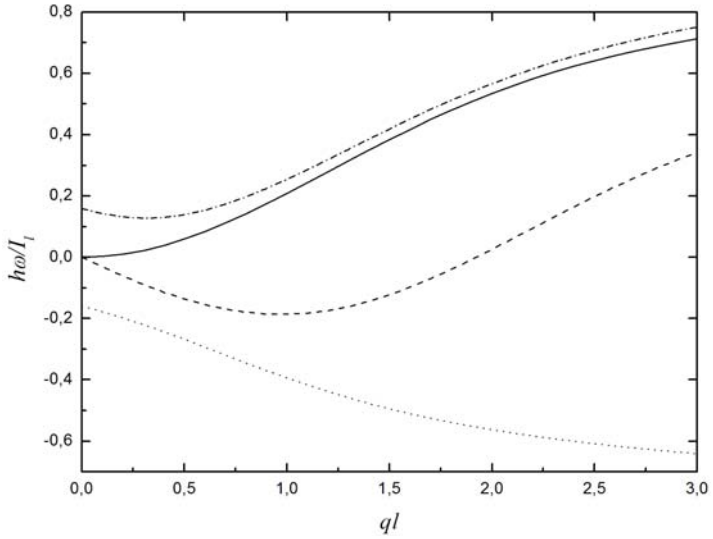

a) $\vec{q}$ parallel to $\vec{k}$

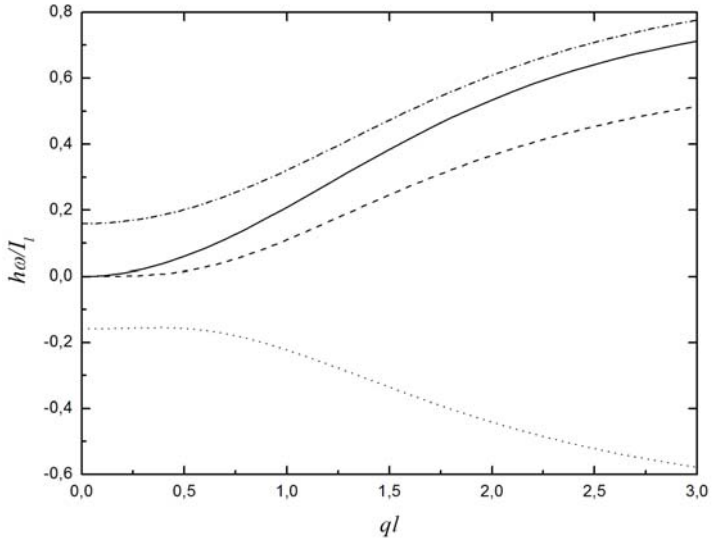

b) $\vec{q}$ perpendicular to $\vec{k}$

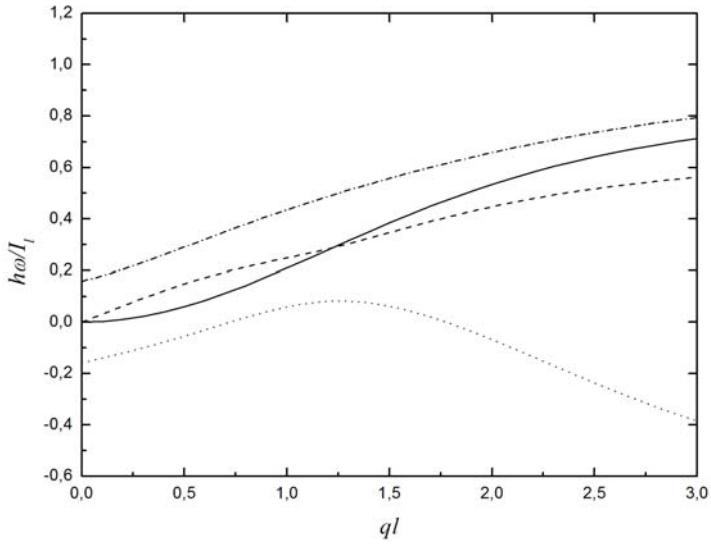

c) $\vec{q}$ antiparallel to $\vec{k}$

Fig.3. The energy spectrum of elementary excitations in the case when kl equals 1 for three different geometries of the observation:

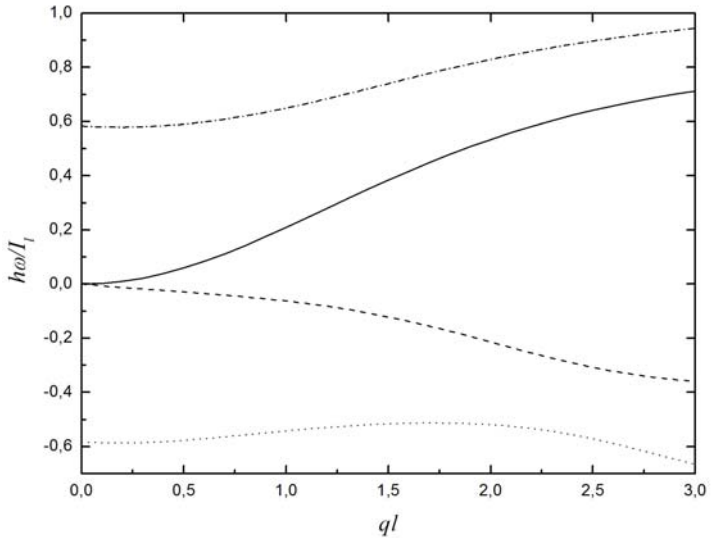

a) $\vec{q}$ parallel to $\vec{k}$

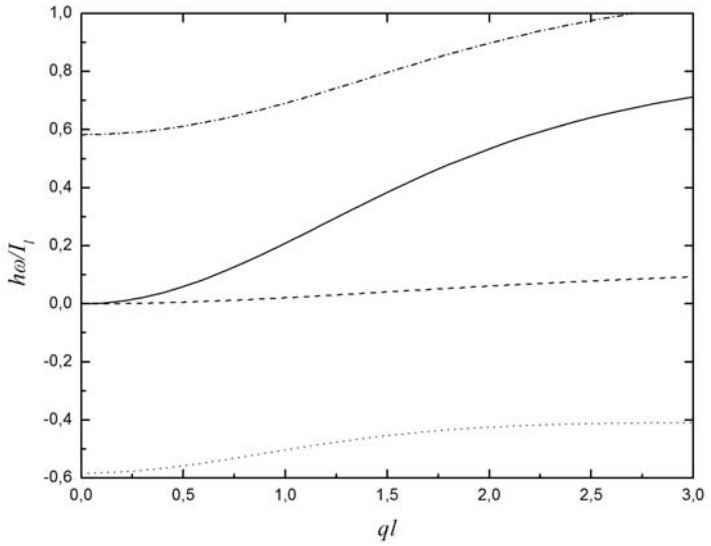

b) $\vec{q}$ perpendicular to $\vec{k}$

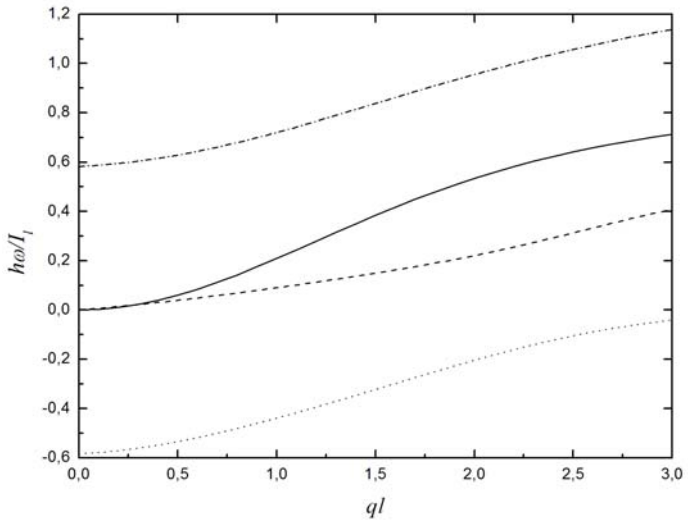

c) $\vec{q}$ antiparallel to $\vec{k}$

Fig.4. The energy spectrum of elementary excitations in the case when kl equals 3,6 for three different geometries of observation.

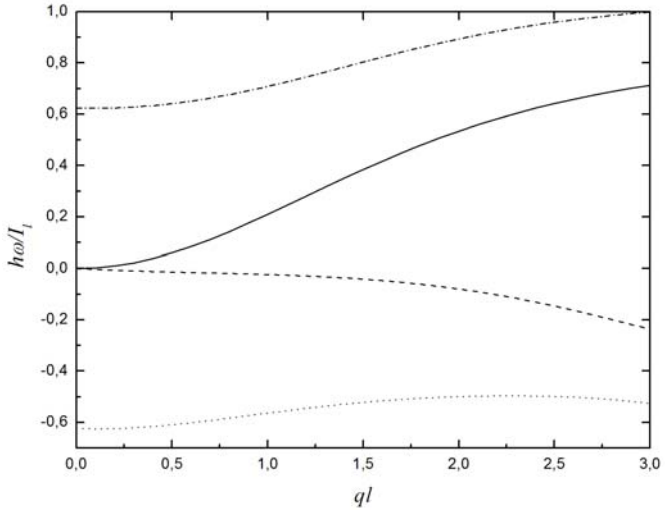

a) $\vec{q}$ parallel to $\vec{k}$

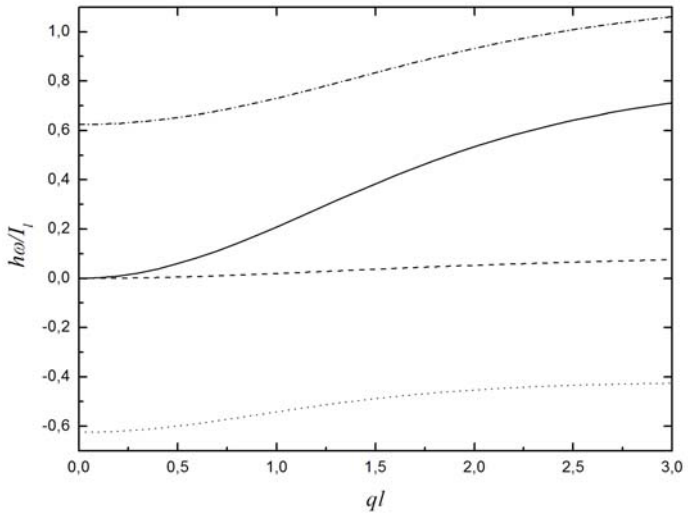

b) $\vec{q}$ perpendicular to $\vec{k}$

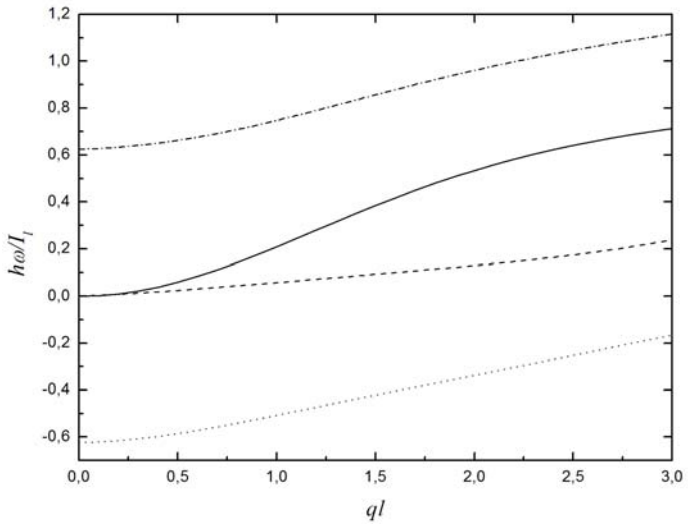

c) $\vec{q}$ antiparallel to $\vec{k}$

Fig.5. The energy spectrum of elementary excitations in the case when kl equals 4,6 for three different geometries of observation.

7. Self-energy parts in more complex expressions

The self-energy parts (69), (70) and (77) contain the average values of the types $\langle\hat{\rho}\hat{\rho}\rangle, \langle\hat{\rho}\hat{D}\rangle, \langle d^{\dagger}\hat{\rho}\rangle$ *and* $\langle\hat{\rho}d\rangle$. They may be calculated in different approximations. Because the more important averages happened to be of the type $\langle\hat{\rho}\hat{\rho}\rangle$, we will discuss below the different approximations on the base of this example. The simpler way is to use the ground state wave function $|\psi_g(k)\rangle$ (28) of the BEC-ed magnetoexcitons and to calculate the averages in this approximation using the α_p, β_p representation instead of a_p, b_p representation because the function $|\psi_g(k)\rangle$ plays the role of vacuum state for the α_p, β_p operators.

Transforming the operators $\hat{\rho}(\vec{Q}), D(\vec{Q}), d^{\dagger}(P)$ and $d(P)$ in α_p, β_p representation and using the Wick theorem [26] we have found

$$\langle\psi_g(k)|\hat{\rho}(\vec{Q})\hat{\rho}(-\vec{Q})|\psi_g(k)\rangle = 4u^2v^2NSin^2\left(\frac{[\vec{K}\times\vec{Q}]_z l^2}{2}\right)$$

$$\langle\psi_g(k)|\hat{\rho}(\vec{Q}+\vec{P}-\vec{K})\hat{\rho}(\vec{K}-\vec{P}-\vec{Q})|\psi_g(k)\rangle = 4u^2v^2NSin^2\left(\frac{[\vec{K}\times(\vec{Q}+\vec{P})]_z l^2}{2}\right)$$

$$\langle\psi_g(k)|\hat{\rho}(\vec{Q})\hat{D}(-\vec{Q})|\psi_g(k)\rangle = 2iu^2v^2NSin\left([\vec{K}\times\vec{Q}]_z l^2\right)$$

$$\langle\psi_g(k)|\hat{\rho}(\vec{Q}+\vec{P}-\vec{K})\hat{D}(\vec{K}-\vec{P}-\vec{Q})|\psi_g(k)\rangle = 2iu^2v^2NSin\left([\vec{K}\times(\vec{P}+\vec{Q})]_z l^2\right)$$

$$\langle\psi_g(k)|d^{\dagger}(\vec{K}-\vec{Q})\hat{\rho}(-\vec{Q})|\psi_g(k)\rangle\sqrt{N} = 2iuv^3NSin\left(\frac{[\vec{K}\times\vec{Q}]_z l^2}{2}\right)$$

$$\left\langle \psi_g(k) \mid d^{\dagger}(\vec{P}-\vec{Q})\hat{\rho}(\vec{P}-\vec{Q}-\vec{K}) \mid \psi_g(k) \right\rangle \sqrt{N} = 2iuv^3 NSin\left(\frac{[\vec{K}\times(\vec{P}-\vec{Q})]_z l^2}{2} \right)$$

$$\left\langle \psi_g(k) \mid \hat{\rho}(\vec{Q})d(\vec{K}-\vec{Q}) \mid \psi_g(k) \right\rangle \sqrt{N} = -2iuv^3 NSin\left(\frac{[\vec{K}\times\vec{Q}]_z l^2}{2} \right) \qquad (104)$$

$$\left\langle \psi_g(k) \mid \hat{\rho}(\vec{P}+\vec{Q}-\vec{K})d(2\vec{K}-\vec{P}-\vec{Q}) \mid \psi_g(k) \right\rangle \sqrt{N} = -2iuv^3 NSin\left(\frac{[\vec{K}\times(\vec{P}+\vec{Q})]_z l^2}{2} \right)$$

The first two averages contain the coherence factor $Sin^2\left(\frac{[\vec{K}\times\vec{Q}]_z l^2}{2} \right)$, which is sign well determined and positive function at any values of wave vector $\vec{Q}$, whereas the another averages are represented by sign variable dependences and this fact will diminish significantly in some cases their contributions to the self-energy parts. The calculation of the average $\langle \hat{\rho}\hat{\rho} \rangle$ is in strong relation with the determination of the ground state energy and of correlation energy in papers [4,5].

The starting expression in these papers is

$$\frac{1}{2} W_{\vec{Q}} \left\langle 0 \mid \hat{\rho}(\vec{Q})\hat{\rho}(-\vec{Q}) \mid 0 \right\rangle = \frac{1}{2} W_{\vec{Q}} \sum_n \left| \left(\hat{\rho}^{\dagger}(\vec{Q}) \right)_{n0} \right|^2 \quad , \qquad (105)$$

where $|0\rangle$ denotes the ground state wave function and $|n\rangle$ represents the wave function of the excited states. When the ground state wave function $|0\rangle$ was chosen in the form $|\psi_g(k)\rangle$ and the coherent excited states (46)-(56) [4] were used, they led to the expression

$$\frac{1}{2} W_{\vec{Q}} \sum_n \left| \left(\rho^{\dagger}(\vec{Q}) \right)_{n0} \right|^2 = -\int_0^{\infty} \frac{\hbar d\omega}{2\pi} \mathrm{Im}\left(\frac{1}{\varepsilon^{HF}(\vec{Q}\omega)} \right) \quad , \qquad (106)$$

which contains dielectric function of the system $\varepsilon^{HF}(\vec{Q},\omega)$ in the HF approximation. The idea suggested by Nozieres and Comte [31] and the method proposed by them is based on the affirmation that the more exact value of expression (105) can be obtained if the dielectric constant $\varepsilon^{RPA}(\vec{Q},\omega)$ in the random phase approximation (RPA) will be substituted in formula (106) instead of the value $\varepsilon^{HF}(\vec{Q},\omega)$.

This idea was applied when instead of approximation (82) in [4] the more exact expression (83) was used.

The possible ground in favour of this method is the supposition that the ground state wave function $|0\rangle$ of the BEC-ed magnetoexcitons in not exactly equal to $|\psi_g(k)\rangle$ but contains some superposition with other states, which make the variational wave function more flexible with lower energy of the ground state. As one can see from expression (2.154) [25] between new states engaged in this contribution there are the excited states with two free e-h pairs outside the condensate. On the same grounds we can expect that the more exact value of the chosen expression will be

$$\frac{1}{2} W_{\vec{Q}} \left\langle \hat{\rho}(\vec{Q})\hat{\rho}(-\vec{Q}) \right\rangle = -\int_0^{\infty} \frac{\hbar d\omega}{2\pi} \mathrm{Im}\left(\frac{1}{\varepsilon^{RPA}(\vec{Q},\omega)} \right) \qquad (107)$$

The both expressions of the dielectric constants $\varepsilon^{HF}(\vec{Q},\omega)$ and $\varepsilon^{RPA}(\vec{Q},\omega)$ differ by their dependences on the polarizability of the system $4\pi\alpha_0^{HF}(\vec{Q},\omega)$, as follows

$$\varepsilon^{RPA}(\vec{Q},\omega)=1+4\pi\alpha_0^{HF}(\vec{Q},\omega)$$
$$\frac{1}{\varepsilon^{HF}(\vec{Q},\omega)}=1-4\pi\alpha_0^{HF}(\vec{Q},\omega) \qquad (108)$$

In the case of BEC-ed magnetoexcitons their polarizability due to the coherent excited states in the frame of LLL approximation, without taking into account of the excited Landau levels (ELL) was deduced in [4] and has the form

$$4\pi\alpha_0^{HF}(\vec{Q},\omega)=-4u^2v^2NW_{\vec{Q}}Sin^2\left(\frac{[\vec{K}\times\vec{Q}]_z l^2}{2}\right)\left[\frac{1}{\hbar\omega-I_{ex}(k)+i\delta}-\frac{1}{\hbar\omega+I_{ex}(k)+i\delta}\right];\delta\to 0 \qquad (109)$$

It contains in the first fraction a resonant denominator, when $\hbar\omega$ equals the ionization potential $I_{ex}(k)$ of the magnetoexciton with wave vector $\vec{k}$. The singularity of expression (109) resulted in the case of correlation energy in its singular dependence of the type $\frac{1}{I_{ex}(k)}$ when $I_{ex}(k)$ tends to zero in the limit $k\to\infty$. To avoid both singularities in paper [5] instead of the infinitesimal value $\delta\to 0$ a finite value of the exciton level damping rate γ was introduced, which transforms expression (109) and its real and imaginary parts as follows

$$4\pi\alpha_0^{HF}(\vec{Q},\omega)=4\pi\alpha_{0,1}^{HF}(\vec{Q},\omega)+4i\pi\alpha_{0,2}^{HF}(\vec{Q},\omega)=$$
$$=-4u^2v^2NW_{\vec{Q}}Sin^2\left(\frac{[\vec{K}\times\vec{Q}]_z l^2}{2}\right)\left(\sum(\omega,\vec{k})+i\Gamma(\omega,\vec{k})\right), \qquad (110)$$

where

$$\sum(\omega,\vec{k})=\frac{\hbar\omega-I_{ex}(k)}{\left(\hbar\omega-I_{ex}(k)\right)^2+\gamma^2}-\frac{\hbar\omega+I_{ex}(k)}{\left(\hbar\omega+I_{ex}(k)\right)^2+\gamma^2},$$
$$\Gamma(\omega,\vec{k})=\gamma\left[\frac{1}{\left(\hbar\omega+I_{ex}(k)\right)^2+\gamma^2}-\frac{1}{\left(\hbar\omega-I_{ex}(k)\right)^2+\gamma^2}\right] \qquad (111)$$

The needed imaginary part approximately equals

$$\mathrm{Im}\left(\frac{1}{\varepsilon^{RPA}(\vec{Q},\omega)}\right)=-4\pi\alpha_{0,2}^{HF}(\vec{Q},\omega)+2*4\pi\alpha_{0,1}^{HF}(\vec{Q},\omega)*4\pi\alpha_{0,2}^{HF}(\vec{Q},\omega) \qquad (112)$$

It leads to the desirable average value

$$W_{\vec{Q}}\left\langle\hat{\rho}(\vec{Q})\hat{\rho}(-\vec{Q})\right\rangle=-\int_0^\infty\frac{\hbar d\omega}{\pi}\mathrm{Im}\left(\frac{1}{\varepsilon^{RPA}(\vec{Q},\omega)}\right)=$$
$$=4u^2v^2(NW_{\vec{Q}})Sin^2\left(\frac{\left[\vec{K}\times\vec{Q}\right]_z l^2}{2}\right)-\frac{16u^4v^4(W_{\vec{Q}}N)^2}{I_{ex}(k)}Sin^4\left(\frac{\left[\vec{K}\times\vec{Q}\right]_z l^2}{2}\right) \qquad (113)$$

if the infinitesimal damping rate $\delta\to+0$ is used. The first term of (113) coincides exactly with the result (104) obtained in the HFA. The second term of (113) corresponds to correlation energy corrections, when the ground state energy is calculated. It contains the singular dependence on $I_{ex}(k)$ discussed above. Taking into account the finite exciton damping rate γ and calculating the integral

$$S(k)=\int_0^{\infty}\frac{\hbar d\omega}{2\pi}\sum(\omega,k)\Gamma(\omega,k)=\frac{1}{2\pi}\left[\frac{\pi}{4I_{ex}(k)}-\right.$$
$$\left.-\frac{1}{2I_{ex}(k)}arctg\left(\frac{\gamma^2-I^2{}_{ex}(k)}{2\gamma I_{ex}(k)}\right)-\frac{\gamma}{I^2{}_{ex}(k)+\gamma^2}\right] \qquad (114)$$

we will obtain the chosen expression without singularity

$$W_{\vec{Q}}\left\langle\hat{\rho}(\vec{Q})\hat{\rho}(-\vec{Q})\right\rangle=4u^2\mathrm{v}^2\left(NW_{\vec{Q}}\right)Sin^2\left(\frac{\left[\vec{K}\times\vec{Q}\right]_z l^2}{2}\right)-$$
$$-\frac{16u^4\mathrm{v}^4T(k)}{I_{ex}(k)}\left(W_{\vec{Q}}N\right)^2Sin^4\left(\frac{\left[\vec{K}\times\vec{Q}\right]_z l^2}{2}\right), \qquad (115)$$

where $T(k)=4S(k)I_{ex}(k)$ has the limiting expressions

$$T(k)=1 \qquad T(k)=\frac{2}{3\pi}\left(\frac{I_{ex}(k)}{\gamma}\right)^3$$
$$\frac{\gamma}{I_{ex}(k)}\to 0 \qquad ; \qquad \frac{I_{ex}(k)}{\gamma}\to 0 \qquad (116)$$

Now the more complete expressions for the self - energy parts will be calculated. They are listed below.

The diagonal self - energy parts $\sum_{ii}(\vec{P},\omega)$ were calculated taking also into account the terms proportional to $u^4\mathrm{v}^4W_{\vec{Q}}{}^3$ side by side with $u^2\mathrm{v}^2W_{\vec{Q}}{}^2$.

$$\sum{}_{11}(\vec{P},\omega)=\hbar\omega-\widetilde{\mu}+E(P)-16u^2\mathrm{v}^2\sum_{\vec{Q}}W_{\vec{Q}}{}^2N\frac{Sin^2\left(\frac{\left[\vec{P}\times\vec{Q}\right]_z l^2}{2}\right)Sin^2\left(\frac{\left[\vec{K}\times\vec{Q}\right]_z l^2}{2}\right)}{\left[\hbar\omega-\widetilde{\mu}+E(\vec{P}-\vec{Q})-E(-\vec{Q})+i\delta\right]}+$$
$$+\frac{64u^4\mathrm{v}^4T(k)}{I_{ex}(k)}\sum_{\vec{Q}}W_{\vec{Q}}{}^3N^2\frac{Sin^2\left(\frac{\left[\vec{P}\times\vec{Q}\right]_z l^2}{2}\right)Sin^4\left(\frac{\left[\vec{K}\times\vec{Q}\right]_z l^2}{2}\right)}{\left[\hbar\omega-\widetilde{\mu}+E(\vec{P}-\vec{Q})-E(-\vec{Q})+i\delta\right]};$$

$$\sum_{22}(\vec{P},\omega)=\hbar\omega+\tilde{\mu}-E(2\vec{K}-\vec{P})-16u^2\mathrm{v}^2\sum_{\vec{Q}}W_{\vec{Q}}{}^2N\frac{Sin^2\left(\frac{\left[(2\vec{K}-\vec{P})\times\vec{Q}\right]_z l^2}{2}\right)Sin^2\left(\frac{\left[\vec{K}\times\vec{Q}\right]_z l^2}{2}\right)}{\left[\hbar\omega+\tilde{\mu}-E(2\vec{K}-\vec{P}-\vec{Q})-E(\vec{Q})+i\delta\right]}+$$

$$+\frac{64u^4\mathrm{v}^4T(k)}{I_{ex}(k)}\sum_{\vec{Q}}W_{\vec{Q}}{}^3N^2\frac{Sin^2\left(\frac{\left[(2\vec{K}-\vec{P})\times\vec{Q}\right]_z l^2}{2}\right)Sin^4\left(\frac{\left[\vec{K}\times\vec{Q}\right]_z l^2}{2}\right)}{\left[\hbar\omega+\tilde{\mu}-E(2\vec{K}-\vec{P}-\vec{Q})-E(\vec{Q})+i\delta\right]};$$

$$\sum_{33}(\vec{P},\omega)=\hbar\omega-E(\vec{K}-\vec{P})+16u^2\mathrm{v}^2\sum_{\vec{Q}}W_{\vec{Q}}Sin^2\left(\frac{\left[(\vec{K}-\vec{P})\times\vec{Q}\right]_z l^2}{2}\right)\times$$

$$\times\frac{\left[\left(W_{\vec{K}-\vec{P}}-W_{\vec{Q}}\right)NSin^2\left(\frac{\left[\vec{K}\times\vec{Q}\right]_z l^2}{2}\right)+\left(W_{\vec{Q}+\vec{P}-\vec{K}}-W_{\vec{K}-\vec{P}}\right)NSin^2\left(\frac{\left[\vec{K}\times(\vec{P}+\vec{Q})\right]_z l^2}{2}\right)\right]}{\left[\hbar\omega-E(\vec{Q})-E(\vec{K}-\vec{P}-\vec{Q})+i\delta\right]}-$$

$$-\frac{64u^4\mathrm{v}^4T(k)}{I_{ex}(k)}\sum_{\vec{Q}}W_{\vec{Q}}\frac{Sin^2\left(\frac{\left[(\vec{K}-\vec{P})\times\vec{Q}\right]_z l^2}{2}\right)}{\left[\hbar\omega-E(\vec{Q})-E(\vec{K}-\vec{P}-\vec{Q})+i\delta\right]}\times$$

$$\times\left[\left(W_{\vec{K}-\vec{P}}-W_{\vec{Q}}\right)N\left(W_{\vec{Q}}N\right)Sin^4\left(\frac{\left[\vec{K}\times\vec{Q}\right]_z l^2}{2}\right)+\left(W_{\vec{Q}+\vec{P}-\vec{K}}-W_{\vec{K}-\vec{P}}\right)N\left(W_{\vec{Q}+\vec{P}-\vec{K}}N\right)Sin^4\left(\frac{\left[\vec{K}\times(\vec{P}+\vec{Q})\right]_z l^2}{2}\right)\right];$$

$$\sum_{44}(\vec{P},\omega)=\hbar\omega-E(\vec{K}-\vec{P})-16u^2\mathrm{v}^2\sum_{\vec{Q}}W_{\vec{Q}}{}^2N\frac{Sin^2\left(\frac{\left[(\vec{K}-\vec{P})\times\vec{Q}\right]_z l^2}{2}\right)Sin^2\left(\frac{\left[\vec{K}\times\vec{Q}\right]_z l^2}{2}\right)}{\left[\hbar\omega-E(\vec{Q})-E(\vec{K}-\vec{P}-\vec{Q})+i\delta\right]}+$$

$$+\frac{64u^4\mathrm{v}^4T(k)}{I_{ex}(k)}\sum_{\vec{Q}}W_{\vec{Q}}{}^3N^2\frac{Sin^2\left(\frac{\left[(\vec{K}-\vec{P})\times\vec{Q}\right]_z l^2}{2}\right)Sin^4\left(\frac{\left[\vec{K}\times\vec{Q}\right]_z l^2}{2}\right)}{\left[\hbar\omega-E(\vec{Q})-E(\vec{K}-\vec{P}-\vec{Q})+i\delta\right]}. \quad (117)$$

The nondiagonal self - energy parts $\sum_{ij}(\vec{P},\omega)$ with $i\neq j$ do not contain the average $\left\langle\hat{\rho}(\vec{Q})\hat{\rho}(-\vec{Q})\right\rangle$ and in their expressions there are no terms proportional to $W_{\vec{Q}}{}^3$:

$$\sum_{31}(\vec{P},\omega)=-i\nu Sin\left(\frac{\left[\vec{P}\times\vec{K}\right]_z l^2}{2}\right)\left[1+\frac{2W_{\vec{P}-\vec{K}}N}{\left[\hbar\omega-\widetilde{\mu}+E(\vec{K})-E(\vec{K}-\vec{P})+i\delta\right]}\right]-$$

$$-\frac{4iuv^3E(\vec{K})\left(W_{\vec{P}-\vec{K}}N\right)Sin\left(\frac{\left[\vec{P}\times\vec{K}\right]_z l^2}{2}\right)}{\left[\hbar\omega-\widetilde{\mu}+E(\vec{K})-E(\vec{K}-\vec{P})+i\delta\right]}+8iuv^3\sum_{\vec{Q}}W_{\vec{Q}}\left(W_{\vec{P}-\vec{K}}N\right)\times$$

$$\times\frac{Sin\left(\frac{\left[\vec{P}\times\vec{Q}\right]_z l^2}{2}\right)Sin\left(\frac{\left[(\vec{P}-\vec{Q})\times(\vec{P}-\vec{K})\right]_z l^2}{2}\right)Sin\left(\frac{\left[\vec{K}\times\vec{Q}\right]_z l^2}{2}\right)}{\left[\hbar\omega-\widetilde{\mu}+E(\vec{P}-\vec{Q})-E(-\vec{Q})+i\delta\right]}+$$

$$+8iuv^3\sum_{\vec{Q}}W_{\vec{Q}}\left(W_{\vec{K}-\vec{P}}-W_{\vec{P}-\vec{K}-\vec{Q}}\right)N\frac{Sin\left(\frac{\left[\vec{P}\times\vec{K}\right]_z l^2}{2}\right)Sin\left(\frac{\left[(\vec{K}-\vec{P})\times\vec{Q}\right]_z l^2}{2}\right)Sin\left(\frac{\left[\vec{K}\times(\vec{P}-\vec{Q})\right]_z l^2}{2}\right)}{\left[\hbar\omega-\widetilde{\mu}+E(\vec{P}-\vec{Q})-E(-\vec{Q})+i\delta\right]};$$

$$\sum_{32}(\vec{P},\omega)=i\nu Sin\left(\frac{\left[\vec{P}\times\vec{K}\right]_z l^2}{2}\right)\left[1-\frac{2W_{\vec{K}-\vec{P}}N}{\hbar\omega+\widetilde{\mu}-E(\vec{K})-E(\vec{K}-\vec{P})+i\delta}\right]-$$

$$-\frac{4iuv^3E(\vec{K})W_{\vec{K}-\vec{P}}NSin\left(\frac{\left[\vec{P}\times\vec{K}\right]_z l^2}{2}\right)}{\hbar\omega+\widetilde{\mu}-E(\vec{K})-E(\vec{K}-\vec{P})+i\delta}-8iuv^3\sum_{\vec{Q}}W_{\vec{Q}}\left(W_{\vec{K}-\vec{P}}-W_{\vec{P}+\vec{Q}-\vec{K}}\right)N\times$$

$$\times\frac{NSin\left(\frac{\left[(2\vec{K}-\vec{P})\times\vec{Q}\right]_z l^2}{2}\right)Sin\left(\frac{\left[\vec{Q}\times(\vec{K}-\vec{P})\right]_z l^2}{2}\right)Sin\left(\frac{\left[\vec{K}\times(\vec{P}+\vec{Q})\right]_z l^2}{2}\right)}{\hbar\omega+\widetilde{\mu}-E(2\vec{K}-\vec{P}-\vec{Q})-E(\vec{Q})+i\delta}-$$

$$-8iuv^3\sum_{\vec{Q}}W_{\vec{Q}}W_{\vec{K}-\vec{P}}N\frac{Sin\left(\frac{\left[(2\vec{K}-\vec{P})\times\vec{Q}\right]_z l^2}{2}\right)Sin\left(\frac{\left[(\vec{K}-\vec{Q})\times(\vec{K}-\vec{P})\right]_z l^2}{2}\right)Sin\left(\frac{\left[\vec{K}\times\vec{Q}\right]_z l^2}{2}\right)}{\hbar\omega+\widetilde{\mu}-E(2\vec{K}-\vec{P}-\vec{Q})-E(\vec{Q})+i\delta};$$

$$\sum\nolimits_{34}(\vec{P},\omega)=8iu^2\mathrm{v}^2\sum_{\vec{Q}}W_{\vec{Q}}Sin^2\left(\frac{\left[(\vec{K}-\vec{P})\times\vec{Q}\right]_z l^2}{2}\right)\times$$
$$\times\frac{\left[\left(W_{\vec{Q}+\vec{P}-\vec{K}}\right)NSin\left(\left[\vec{K}\times(\vec{P}+\vec{Q})\right]_z l^2\right)+W_{\vec{Q}}NSin\left(\left[\vec{K}\times\vec{Q}\right]_z l^2\right)\right]}{\hbar\omega-E(\vec{Q})-E(\vec{K}-\vec{P}-\vec{Q})+i\delta}. \qquad (118)$$

First of all we are interested to determine the energy spectrum of the collective elementary excitations with the wave vectors $\vec{P}$ not so far from the condensate wave vector $\vec{K}$, so that $\vec{P}=\vec{K}+\vec{q}$. There are seven more cumbersome expressions $\sum_{ij}(\vec{P},\omega)$ (117) and (118) and the remaining other simpler expressions $\sum_{ij}(\vec{P},\omega)$ (69), (70) and (77), which in dependence on $\vec{q}$ and ω have the forms $\sum_{ij}(\vec{q},\omega)$

$$\sum\nolimits_{11}(\vec{q},\omega)=\hbar\omega-\tilde{\mu}+E(\vec{K}+\vec{q})-16u^2\mathrm{v}^2\sum_{\vec{Q}}W_{\vec{Q}}{}^2N\times$$
$$\times\frac{Sin^2\left(\frac{\left[(\vec{K}+\vec{q})\times\vec{Q}\right]_z l^2}{2}\right)Sin^2\left(\frac{\left[\vec{K}\times\vec{Q}\right]_z l^2}{2}\right)}{\hbar\omega-\tilde{\mu}+E(\vec{K}+\vec{q}-\vec{Q})-E(-\vec{Q})+i\delta}+ \qquad ;$$
$$+\frac{64u^4\mathrm{v}^4T(k)}{I_{ex}(k)}\sum_{\vec{Q}}W_{\vec{Q}}{}^3N^2\frac{Sin^2\left(\frac{\left[(\vec{K}+\vec{q})\times\vec{Q}\right]_z l^2}{2}\right)Sin^4\left(\frac{\left[\vec{K}\times\vec{Q}\right]_z l^2}{2}\right)}{\hbar\omega-\tilde{\mu}+E(\vec{K}+\vec{q}-\vec{Q})-E(-\vec{Q})+i\delta}$$

$$\sum\nolimits_{22}(\vec{q},\omega)=\hbar\omega+\tilde{\mu}-E(\vec{K}-\vec{q})-16u^2\mathrm{v}^2\sum_{\vec{Q}}W_{\vec{Q}}{}^2N\times$$
$$\times\frac{Sin^2\left(\frac{\left[(\vec{K}-\vec{q})\times\vec{Q}\right]_z l^2}{2}\right)Sin^2\left(\frac{\left[\vec{K}\times\vec{Q}\right]_z l^2}{2}\right)}{\hbar\omega+\tilde{\mu}-E(\vec{K}-\vec{q}-\vec{Q})-E(\vec{Q})+i\delta}+ \qquad ;$$
$$+\frac{64u^4\mathrm{v}^4T(k)}{I_{ex}(k)}\sum_{\vec{Q}}W_{\vec{Q}}{}^3N^2\frac{Sin^2\left(\frac{\left[(\vec{K}-\vec{q})\times\vec{Q}\right]_z l^2}{2}\right)Sin^4\left(\frac{\left[\vec{K}\times\vec{Q}\right]_z l^2}{2}\right)}{\hbar\omega+\tilde{\mu}-E(\vec{K}-\vec{q}-\vec{Q})-E(\vec{Q})+i\delta}$$

$$\sum_{33}(\vec{q},\omega)=\hbar\omega-E(\vec{q})+16u^2\mathrm{v}^2\sum_{\vec{Q}}W_{\vec{Q}}Sin^2\left(\frac{\left[\vec{q}\times\vec{Q}\right]_z l^2}{2}\right)\times$$

$$\times\frac{\left[\left(W_{\vec{q}}-W_{\vec{Q}}\right)NSin^2\left(\frac{\left[\vec{K}\times\vec{Q}\right]_z l^2}{2}\right)+\left(W_{\vec{Q}+\vec{q}}-W_{\vec{q}}\right)NSin^2\left(\frac{\left[\vec{K}\times\left(\vec{Q}+\vec{q}\right)\right]_z l^2}{2}\right)\right]}{\hbar\omega-E(\vec{Q})-E(-\vec{q}-\vec{Q})+i\delta}-$$

$$-\frac{64u^4\mathrm{v}^4T(k)}{I_{ex}(k)}\sum_{\vec{Q}}W_{\vec{Q}}Sin^2\left(\frac{\left[\vec{q}\times\vec{Q}\right]_z l^2}{2}\right)\times$$

$$\times\frac{\left[\left(W_{\vec{q}}-W_{\vec{Q}}\right)N\left(W_{\vec{Q}}N\right)Sin^4\left(\frac{\left[\vec{K}\times\vec{Q}\right]_z l^2}{2}\right)+\left(W_{\vec{Q}+\vec{q}}-W_{\vec{q}}\right)N\left(W_{\vec{Q}+\vec{q}}N\right)Sin^4\left(\frac{\left[\vec{K}\times\left(\vec{Q}+\vec{q}\right)\right]_z l^2}{2}\right)\right]}{\hbar\omega-E(\vec{Q})-E(-\vec{q}-\vec{Q})+i\delta}$$

$$\sum_{44}(\vec{q},\omega)=\hbar\omega-E(\vec{q})-16u^2\mathrm{v}^2\sum_{\vec{Q}}{W_{\vec{Q}}}^2N\frac{Sin^2\left(\frac{\left[\vec{q}\times\vec{Q}\right]_z l^2}{2}\right)Sin^2\left(\frac{\left[\vec{K}\times\vec{Q}\right]_z l^2}{2}\right)}{\hbar\omega-E(\vec{Q})-E(-\vec{q}-\vec{Q})+i\delta}+$$

$$+\frac{64u^4\mathrm{v}^4T(k)}{I_{ex}(k)}\sum_{\vec{Q}}{W_{\vec{Q}}}^3N^2\frac{Sin^2\left(\frac{\left[\vec{q}\times\vec{Q}\right]_z l^2}{2}\right)Sin^4\left(\frac{\left[\vec{K}\times\vec{Q}\right]_z l^2}{2}\right)}{\hbar\omega-E(\vec{Q})-E(-\vec{q}-\vec{Q})+i\delta} \qquad (119)$$

Three nondiagonal self-energy parts $\sum_{31}(\vec{q},\omega)$, $\sum_{32}(\vec{q},\omega)$ and $\sum_{34}(\vec{q},\omega)$ look as follows

$$\sum_{31}(\vec{q},\omega)=-i\nu Sin\left(\frac{\left[\vec{q}\times\vec{K}\right]_z l^2}{2}\right)\left[1+\frac{2W_{\vec{q}}N}{\hbar\omega-\tilde{\mu}+E(\vec{K})-E(-\vec{q})+i\delta}\right]-$$

$$-\frac{4iuv^3E(\vec{K})\left(W_{\vec{q}}N\right)Sin\left(\frac{\left[\vec{q}\times\vec{K}\right]_z l^2}{2}\right)}{\hbar\omega-\tilde{\mu}+E(\vec{K})-E(-\vec{q})+i\delta}-$$

$$-8iuv^3\sum_{\vec{Q}}W_{\vec{Q}}\left(W_{\vec{q}}N\right)\frac{Sin\left(\frac{\left[(\vec{K}+\vec{q})\times\vec{Q}\right]_z l^2}{2}\right)Sin\left(\frac{\left[\vec{q}\times\left(\vec{K}-\vec{Q}\right)\right]_z l^2}{2}\right)Sin\left(\frac{\left[\vec{K}\times\vec{Q}\right]_z l^2}{2}\right)}{\hbar\omega-\tilde{\mu}+E(\vec{K}+\vec{q}-\vec{Q})-E(-\vec{Q})+i\delta}-$$

$$-8iuv^3\sum_{\vec{Q}}W_{\vec{Q}}\left(W_{\vec{q}}-W_{\vec{q}-\vec{Q}}\right)N\frac{Sin\left(\frac{\left[\left(\vec{K}+\vec{q}\right)\times\vec{Q}\right]_z l^2}{2}\right)Sin\left(\frac{\left[\vec{q}\times\vec{Q}\right]_z l^2}{2}\right)Sin\left(\frac{\left[\vec{K}\times\left(\vec{q}-\vec{Q}\right)\right]_z l^2}{2}\right)}{\hbar\omega-\tilde{\mu}+E(\vec{K}+\vec{q}-\vec{Q})-E(-\vec{Q})+i\delta}$$

$$\sum_{32}(\vec{q},\omega)=i\nu Sin\left(\frac{\left[\vec{q}\times\vec{K}\right]_z l^2}{2}\right)\left[1-\frac{2W_{\vec{q}}N}{\hbar\omega+\widetilde{\mu}-E(\vec{K})-E(-\vec{q})+i\delta}\right]-$$

$$-\frac{4iu\nu^3E(\vec{K})\left(W_{\vec{q}}N\right)Sin\left(\frac{\left[\vec{q}\times\vec{K}\right]_z l^2}{2}\right)}{\hbar\omega+\widetilde{\mu}-E(\vec{K})-E(-\vec{q})+i\delta}-$$

$$-8iu\nu^3\sum_{\vec{Q}}W_{\vec{Q}}\left(W_{\vec{q}}-W_{\vec{q}+\vec{Q}}\right)N\frac{Sin\left(\frac{\left[\left(\vec{K}-\vec{q}\right)\times\vec{Q}\right]_z l^2}{2}\right)Sin\left(\frac{\left[\vec{q}\times\vec{Q}\right]_z l^2}{2}\right)Sin\left(\frac{\left[\vec{K}\times\left(\vec{q}+\vec{Q}\right)\right]_z l^2}{2}\right)}{\hbar\omega+\widetilde{\mu}-E(\vec{K}-\vec{q}-\vec{Q})-E(\vec{Q})+i\delta}-$$

$$-8iu\nu^3\sum_{\vec{Q}}W_{\vec{Q}}\left(W_{\vec{q}}N\right)\frac{Sin\left(\frac{\left[\left(\vec{K}-\vec{q}\right)\times\vec{Q}\right]_z l^2}{2}\right)Sin\left(\frac{\left[\vec{q}\times\left(\vec{K}-\vec{Q}\right)\right]_z l^2}{2}\right)Sin\left(\frac{\left[\vec{K}\times\vec{Q}\right]_z l^2}{2}\right)}{\hbar\omega+\widetilde{\mu}-E(\vec{K}-\vec{q}-\vec{Q})-E(\vec{Q})+i\delta};$$

$$\sum_{34}(\vec{q},\omega)=8iu^2\nu^2\sum_{\vec{Q}}W_{\vec{Q}}Sin^2\left(\frac{\left[\vec{q}\times\vec{Q}\right]_z l^2}{2}\right)\times$$

$$\times\frac{\left[\left(W_{\vec{q}+\vec{Q}}-W_{\vec{q}}\right)NSin\left(\left[\vec{K}\times\left(\vec{q}+\vec{Q}\right)\right]_z l^2\right)+W_{\vec{Q}}NSin\left(\left[\vec{K}\times\vec{Q}\right]_z l^2\right)\right]}{\left[\hbar\omega-E(\vec{Q})-E(-\vec{q}-\vec{Q})+i\delta\right]} \qquad (120)$$

The remaining nine self-energy parts containing only the terms proportional to the parameter ν are

$$\Sigma_{21}(\vec{q},\omega)=0; \qquad \Sigma_{12}(\vec{q},\omega)=0;\Sigma_{43}(\vec{q},\omega)=0;$$

$$\Sigma_{41}(\vec{q},\omega)=\nu Cos\left(\frac{[\vec{q}\times\vec{k}]_z l^2}{2}\right); \qquad \Sigma_{42}(\vec{q},\omega)=-\nu Cos\left(\frac{[\vec{q}\times\vec{k}]_z l^2}{2}\right);$$

$$\Sigma_{14}(\vec{q},\omega)=2\nu Cos\left(\frac{[\vec{q}\times\vec{k}]_z l^2}{2}\right); \qquad \Sigma_{24}(\vec{q},\omega)=-2\nu Cos\left(\frac{[\vec{q}\times\vec{k}]_z l^2}{2}\right); \qquad (121)$$

$$\Sigma_{13}(\vec{q},\omega)=2i\nu Sin\left(\frac{[\vec{q}\times\vec{k}]_z l^2}{2}\right); \qquad \Sigma_{23}(\vec{q},\omega)=-2i\nu Sin\left(\frac{[\vec{q}\times\vec{k}]_z l^2}{2}\right);$$

The full set of self-energy parts $\sum_{ij}(\vec{q},\omega)$ will be used below for the calculation of the energy spectrum of the collective excitations beyond the HFBA.

8. Energy spectrum beyond the HFBA in collinear geometry

The cumbersome dispersion equation in the form of fourth order determinant can be essentially simplified in collinear geometry when the vector product projection $[\vec{q}\times\vec{k}]_z = 0$. It takes place, when $\vec{q}$ is parallel as well is as antiparallel to condensate wave vector $\vec{k}$. At this condition two self-energy parts vanish

$$\Sigma_{13}(\vec{q},\omega) = \Sigma_{23}(\vec{q},\omega) = 0 \tag{122}$$

whereas other four self-energy parts equal to

$$\begin{aligned} &\Sigma_{14}(\vec{q},\omega) = 2\nu; \qquad &&\Sigma_{24}(\vec{q},\omega) = -2\nu; \\ &\Sigma_{41}(\vec{q},\omega) = \nu; \qquad &&\Sigma_{42}(\vec{q},\omega) = -\nu; \end{aligned} \tag{123}$$

The fourth order determinant becomes factorized in the form

$$\Sigma_{33}(\vec{q},\omega)\begin{vmatrix} \Sigma_{11}(\vec{q},\omega) & 0 & \nu \\ 0 & \Sigma_{22}(\vec{q},\omega) & -\nu \\ 2\nu & -2\nu & \Sigma_{44}(\vec{q},\omega) \end{vmatrix} = 0 \quad , \tag{124}$$

what leads to two dispersion equations. One of them is the separate equation determining the energy spectrum of an optical plasmon in the BEC-ed electron-hole system

$$\Sigma_{33}(\vec{q},\omega) = 0 \tag{125}$$

and another equation

$$\Sigma_{11}(\vec{q},\omega)\Sigma_{22}(\vec{q},\omega)\Sigma_{44}(\vec{q},\omega) - 2\nu^2(\Sigma_{11}(\vec{q},\omega) + \Sigma_{22}(\vec{q},\omega)) = 0 \tag{126}$$

determines the three interconnected branches. Two of them describe the collective elementary excitations of BEC-ed magnetoexcitons and the third branch describes the acoustical plasmon spectrum. Equation (126) is similar with equation (87) obtained in the HFBA, but their similitude is only apparent. Due to the chosen geometry the considerable simplification of the dispersion equation occurred. Below only the diagonal self-energy parts $\Sigma_{ii}(\vec{q},\omega)$ with $i = 1,2,4$ will be used, avoiding the more cumbersome components such as $\Sigma_{31}(\vec{q},\omega)$ and $\Sigma_{32}(\vec{q},\omega)$.

In spite of the condition $[\vec{q}\times\vec{k}]_z = 0$ equation (126) is not invariant under the inversion operation when $\vec{q}$ is substituted by $-\vec{q}$, because in the system there is a well selected direction determined by the BEC-ed wave vector $\vec{k}$. By this reason the elementary excitations with wave vectors $\vec{q}$ and $-\vec{q}$ have different energies.

The investigations in this direction are in progress.

Acknowledgements

One of the authors (S.A.M.) is grateful to Professor P.I.Khadzhi for the valuable proposal and useful discussions.

References

[1] I.V.Lerner and Yn.E.Lozovik, J.Low Temper.Phys. 38, 333 (1980)

[2] I.V.Lerner and Yn.E.Lozovik, Zh.Eksp.Teor.Fiz. 80, 1488 (1981) [Sov.Phys.-JETP 53, 763(1981)].

[3] D.Paquet, T.M.Rice and K.Ueda Phys.Rev.B, 32, 5208 (1985)
[4] S.A.Moskalenko, M.A.Liberman, D.W.Snoke and V.V.Botan Phys.Rev.B, 66, 245316 (2002)
[5] S.A.Moskalenko, M.A.Liberman, D.W.Snoke, V.V.Botan and B.Johansson Physica E, 19, 278-288 (2003)
[6] H.L.Stormer Rev.Mod.Phys. 71 №4, 875(1999)
[7] A.I.Baz`, Ya.B.Zeldovich and A.M.Perelomov Scattering, Reactions and delays in Nonrelativistic Quantum mechanics (Nauka, Moscow, 1971) (in Russian)
[8] D.Pines Elementary Excitations in Solids (Benjamin, New York, 1963)
[9] S.Das Sarma and A.Madhukar Phys.Rev.B 23, 805 (1981)
[10] S.V.Tovstonog, L.V.Kulik, I.V.Kukushkin at al. Phys.Rev.B 66 241308 (R) (2002)
[11] S.M.Girvin, A.H.MacDonald, and P.M.Platzman Phys.Rev.B 33 №4, 2481 (1986)
[12] R.B.Laughlin Phys.Rev. Lett. 50, 1395 (1981)
[13] R.P.Feynman Statistical Mechanics (Benjamin, Reading, Mass, 1972. Chap. 11)
[14] C.Kallin and B.I.Halperin Phys.Rev.B 30, 5655, 1984
[15] V.M.Apal`kov and E.I.Kashba Pis`ma Zh. Eksp.teor.Fiz. 54, 160, (1991); 55, 38, (1992)
[16] H.A.Fertig Phys.Rev.B 40, 1087, (1989)
[17] T.M.Rice, D.Paquet and K.Ueda Helv. Phys. Acta, 58, 410, (1985)
[18] Y.Kuramoto and C.Horie Solid State Commun.
[19] J.Eisenstein Abstracts of the International Conference on Spontaneous Coherence in Excitonic system. Champion, Pennsylvania, USA 25-28 May 2004, Edited by University of Pittsburgh, p.28.
[20] A.MacDonald Ibidem p.29
[21] X.M.Chen and J.J.Quinn Phys.Rev.Lett. 67, 895 (1991)
[22] X.M.Chen and J.J.Quinn Phys.Rev.B 45, 11054 (1992)
[23] N.N.Bogoliubov Collection of papers in three volumes (Naukova Dumka, Kiev, 1971) vol.2 and vol. 3 (in Russian)
[24] L.V.Keldysh and N.A.Kozlov Zv.Eksp.Teor.Fiz. 54 978 (1968) [Sov.Phys. JETP 27, 521 (1968)]
[25] S.A.Moskalenko and D.W.Snoke Bose-Einstein Condensation of Excitons and Biexcitons and Coherent Nonlinear Optics with Excitons (Cambridge University Press, Cambridge, New York, 2000)
[26] A.A.Abrikosov, L.P.Gor`kov and I.E. Dzyaloshinskii Methods of quantum field theory in statistical physics (Dover, New York, 1975).
[27] D.N.Zubarev Sov.Phys.Uspekhi Fiz.Nauk 71, 71(1960)
[28] P.W.Anderson Phys.Rev. 110, 827(1958)
[29] G.A.Korn and Th.M.Korn Mathematical Handbook for scientists and engineers Megraw-Hill Book Company N.Y. 1968
[30] P.I.Khadzhi Pis`ma Zh.Eksp.Teor.Fiz. 60, (85) (1994) [JETP Lett, 60, 89(1994)]
[31] P.Nozieres and C.Comte J.Phys. (Paris) 43 1083 (1982)

TEMPERATURE ANOMALIES OF OPTICAL PROPERTIES IN CADMIUM DIPHOSPHIDE CRYSTAL

I.T. Bodnar, V.M. Trukhan, A.U. Sheleg

Institute of Solid State and Semiconductors Physics of National Academy of Sciences of Belarus, 17 P. Brovki St., 220072 Minsk, Belarus, tel. +375(17)284-15-53;
E-mail: ivetta@ifttp.bas-net.by, truhan@ifttp.bas-net.by

The temperature dependence of refractive indices of ordinary and extraordinary rays (n_o, n_e) in the temperature region 20-110°C for different directions in cadmium diphosphide crystal are presented in the given work. It is obtained that n_o and n increase with temperature growth. It is shown the thermooptical coefficient for n_e depends on direction of laser beam relatively optical axis of the crystal and for n_o it doesn't depend. Several anomalies in the form of steps and bends are revealed on the curves of the temperature dependence of refractive indices. The detected features are connected with the transitions between commensurate and incommensurate phases.

Crystals of the tetragonal modification cadmium diphosphide belong to the A^2B^5 group and are a promising material to be used in the quantum electronics and laser techniques. Owing to large value of birefringence CdP_2 can be used as active elements in optoelectronics. Strong dependence of refractive indices on temperature and low heat conduction allow to produce deflectors of laser beam on the basis of CdP_2 single crystal. Placing a plate from the CdP_2 crystal into resonator of the ruby or neodim laser, it can be possible to change smoothly length of impulse from 20-25ns to 150-300ns with keeping of the impulse shape [1].

CdP_2 crystals have complex structure [2] and thus possess interesting optical properties. The crystal is of a dark red color, transparent in a limited range of wave's lengths in the visible spectrum part, optically negative and optically active.

The work aimed at determining temperature dependence differences of the refractive indices depending on the crystal orientation.

The temperature dependence of the ordinary and extraordinary ray refractive indices [3] in the region of 20-110°C for the red laser line is presented in the given work. The measurements were carried out by means of the least deviation method using five prisms of the same size but different orientation as the samples. The prisms with sizes of 10x10x5x3 mm were cut from the transparent crystal of high quality. Refractive angle of each of them was equal to 18°.

Laser beam propagates through investigated prisms under next angles to the optical axis of the crystal: ~90° (prisms 1 and 2, for vertical and horizontal plains), ~16°, ~28° and 50° (prisms 3, 4 and 5).

The prisms were placed into the optical furnace with two windows for the falling and refracted rays. Temperature measurements were carried out in regime of continuous heating or cooling which rate can be varied.

It is established that the refractive indices increase along with the temperature growth both for the ordinary and extraordinary rays. Beginning with 70°C the crystal gets darker and then it becomes black and nontransparent by the temperature of 100-110°C owing to the shift of the absorption line. Temperature dependence of refractive indices of ordinary and

extraordinary rays in direction perpendicular to the optical axis for the red laser line with wavelength 632,8 nm is shown in Fig.1.

Values n_o, n_e и Δn are equal to 3,4225; 3,2814 and -0,14 at room temperature in this direction. Temperature dependence n_o and n_e for the direction of laser beam in the crystal under the angle ~ 16° to the optical axis is presented in Fig.2. As one can see both curves are almost parallel. It means that thermooptical coefficients of both refractive indices are practically the same at comparatively small deflection of laser beam of the optical axis.

The temperature dependence of the ordinary ray is the same for all directions of the laser beam propagation within the crystal, and its thermooptical coefficient, dn_o/dt, is constant value.

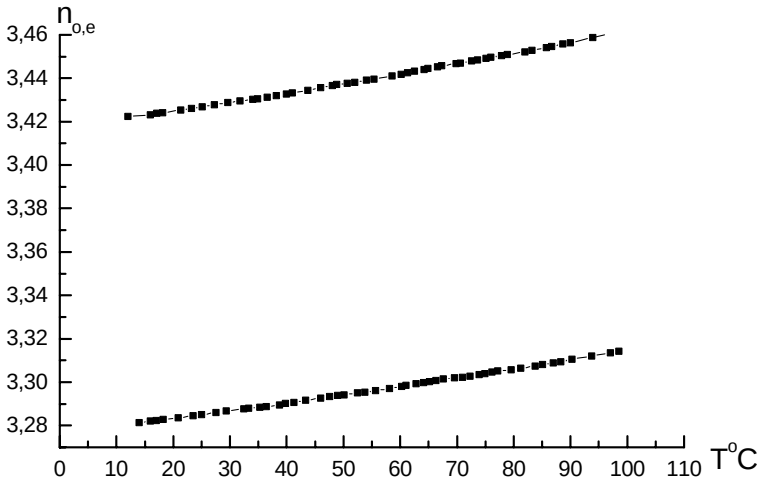

Fig.1. Temperature dependence of ordinary and extraordinary rays refracive indices measured in direction perpendicular to the optical axis.

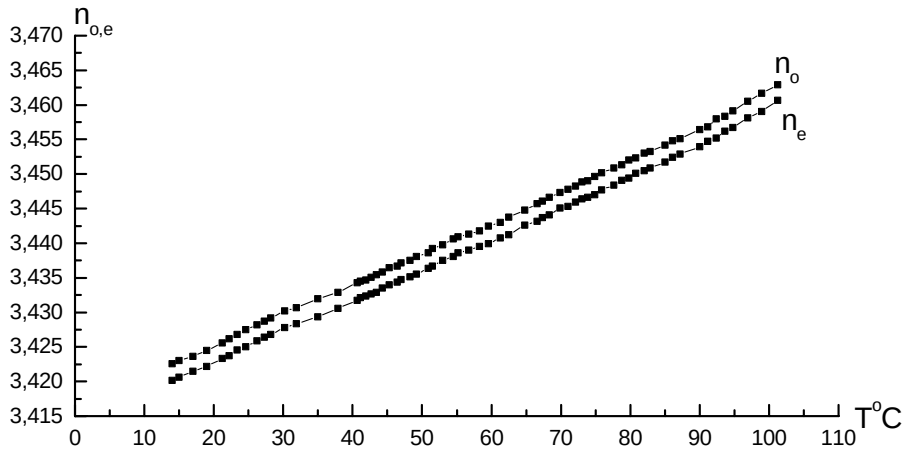

Fig.2. Temperature dependence of ordinary and extraordinary refractive indices measured under the angle 16° to the optical axis of CdP_2crystal

The temperature dependence of extraordinary refractive index is not usual. It is revealed that not only the value of the extraordinary refractive index depends on the direction of light propagation within the crystal but also its thermooptical coefficient also depends on the direction. Therefore thermooptical coefficient dn_o/dt is constant and does not depend on direction of laser beam in the crystal and dn_e/dt is variable and depends on direction of laser beam in the crystal.

The increasing of deviation of laser beam of the optical axis results in decreasing of dn_e/dt. Two waves ordinary and extraordinary with reciprocally orthogonal polarization propagate along the optical axis with rate of ordinary wave, i.e. $n_o = n_e$ in the temperature region 20-110°C, and their thermooptical coefficients are equal in this direction too. These two waves have not only different refractive indices in direction perpendicular to the optical axis, but also different thermooptical coefficients.

Fig. 3 shows dependence of thermooptical coefficient of extraordinary beam dn_e/dt on the angle between the optical axis of the crystal and direction of laser beam. It is seen that increasing of laser beam deflection of the optical axis results in decreasing dn_e/dt.

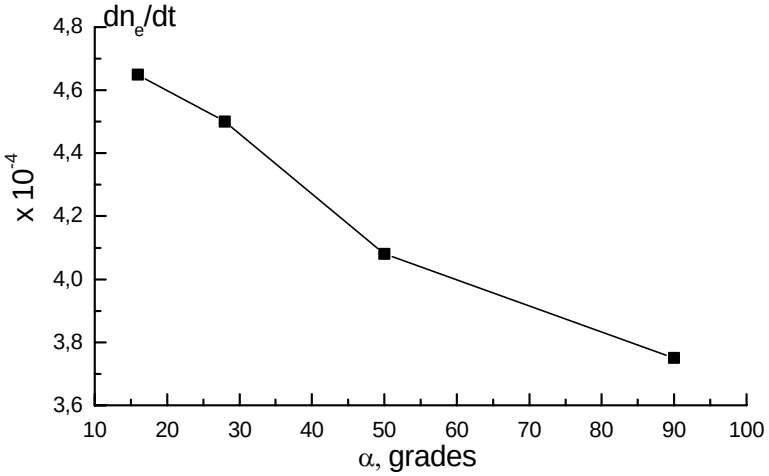

Fig.3. Dependence of thermooptical coefficient of extraordinary ray refractive index on the angle between direction of laser beam and optica axis.

From the Fig.3 it follows also that the smaller angle of deflection of laser beam of optical axis the nearer value dn_e/dt to dn_o/dt.

It means that thermooptical coefficients of both ordinary and extraordinary rays along the optical axis of CdP_2 crystal are equal in the whole temperature region 20-110°C, $dn_e/dt = dn_o/dt \approx 4{,}7 \cdot 10^{-4}$.

At small ″steps″ of temperature measurements equal to 2-3°, there is a succession of anomalies on all curves $n_{o,e} = f(t)$. Sections of the curves between the anomalies are rectilinear. The revealed anomalies take place nearly at the same temperatures for all investigated samples: 20°C, 35°C, 50°- 55°C°, 70°- 75°C, 85°- 90°C.

The temperature dependence of the extraordinary ray refractive index for two samples (1,2) in direction perpendicular to the optical axis, but in reciprocally perpendicular planes, is presented in Fig.4.

At the same time temperature behavior of refractive indices for each direction in CdP_2 crystal is specific.

The bend point at 20° is clearly seen in the graphs obtained at measuring of refractive indices of prisms 1,2 and 3. The bend point at 35-37°C is observed on every curve $n_{o,e} = f(t)$, but it reveals especially distinctly in shape of "step" at propagation of light through the prism

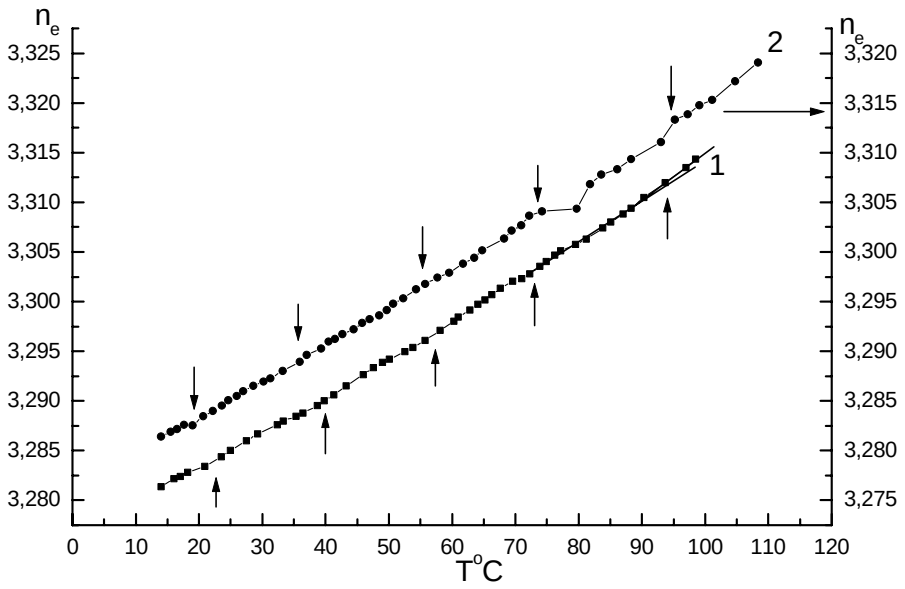

Fig.4.Temperature dependence of refractive index of extraordinary ray for the prisms 1 and 2 measured in direction perpendicular to the optical axis but in two perpendicular planes. Arrows show bend points on the curves.

4 under the angle 28° to the optical axis. The bend at 50°C is good seen at the measurements of the prisms 2 and 3, and for the other ones it is smoothed. Transition in the temperature region 85-87°C is revealed on every curve, and for the prisms 2 and 5 it presents in the shape of "step". At frequent measurements the steps can be smoothed, but the bends and change of the slope angle of the rectilinear sections are kept.

We suggest that pointed anomalies are connected with phase transitions between incommensurate phases of type of ″devils staircase″ [4].

References

[1] V.M. Truhan, Abstracts of International Conference to 40th anniversary of Institute of Solid State and Semiconductors Physics of National Academy of Sciences of Belarus and to 90 years of the founder of Institute academician N.N.Sirota, 4-6 of November 2003. Edition center of Belarusian State University, Minsk, P.264, 2003.

[2] V.B. Lasarev, V.Ya. Shevchenko, Ya.H. Grinberg, V.V. Sobolev, Semiconductors compounds of $A^{II}B^{V}$ group, Edition "Nauka", Moscow, 1978.

[3] I.T. Bodnar, A.U. Sheleg, Sbornik dokladov seminara "Novoe v poluchenii i primenenii fosfidov ", Alma-Ata, V.2, 1988.

[4] A.U. Sheleg, V.P. Novikov, Fisika tverdogo tela (rus), 24, 11, 1982.

DIELECTRIC AND ELASTIC PROPERTIES OF CdP_2, ZnP_2 AND $ZnAs_2$ SINGLE CRYSTALS

L.E. Soshnikov[1], V.M. Trukhan[1], T.V. Haliakevich[1], H.L. Soshnikava[2]

[1]Institute of Solid State and Semiconductor Physics, National Academy of Sciences of Belarus
P. Brovki str. 17, Minsk, 220072, Belarus
[2]Belorussian State University, Skoriny Ave. 4, Minsk, 220050, Belarus

The study of dielectric and elastic properties of CdP_2, ZnP_2, $ZnAs_2$ single crystals was carried out at frequencies 10^2, 10^3, 10^4, 10^6 Hz and 10^7 Hz relatively over the temperature range 78-400 K. Dielectric constant has values ($\varepsilon = 10^2 – 10^3$) over a wide temperature range between 150 K and 400 K. Lower than 150 K the value drops abruptly by almost two orders of magnitude and the dielectric constant is about 9-14 over a temperature range 78-100K. Conductivity σ of materials is composed of two parts: frequency-dependent (hopping) σ_h part and typical for semiconductors σ_s part. Hopping conductivity $\sigma_h \sim \omega^\alpha$ is described by sublinear ($\alpha < 1$) and superlinear ($\alpha > 1$) power laws at low and high temperatures respectively. The sound velocities of single crystals were measured over temperature range of 78 - 400 K and elastic constants were calculated. Elastic properties show anomalous softening at small ranges about ΔT = 10-20 K with the following change of curve slope to the temperature axis.

1. Introduction

$A^{II}B^V$ compounds attract special attention due to such phenomena as the incommensurate phases, polytypicism and "devil's staircase", which are observed in CdP_2 and ZnP_2 representatives of this family. The compounds crystallize to isomorphous tetragonal α-ZnP_2 and β-CdP_2 crystals and to isomorphous monoclinic β-ZnP_2 and $ZnAs_2$ crystals with tetrahedral atomic coordination, implicit layer structure and anion chains penetrating over the crystal. $ZnAs_2$ is relatively weakly studied in consequence of the difficulties of growing perfect single crystals, and large structurally perfect crystals were obtained only during the latest years.

The semiconductors of $A^{II}B^V$ group in technical applied aspect are represented as functional materials owing to prospects to use them as working elements of optical, electronic and thermal detectors, photovoltaic cells, solar batteries and thermal radiation receivers. At the same time $A^{II}B^V$ compounds have the complex phase diagrams that are reflected in existence of several compounds in systems in polymorphism of a line of compounds, available of metastable and amorphous phases and wide areas of homogeneity [1]. The distortions of structures and characteristic structural transformations, connected to them concern also to features of $A^{II}B^V$ compounds. The special place among semiconductors of $A^{II}B^V$ group is occupied by cadmium and zinc diphosphides intensively investigated last years.

The interest to study of properties and structural transformations in crystals of $A^{II}B^V$ compounds is connected to features of their crystal structure. The crystals are tetrahedral coordinated mainly with covalent bond of the uncentral character and share of ionic bond. The tetrahedrons, forming a continuous grid, are strongly deformed, that entails the instability of a lattice in relation to structural transformations and formation of various superstructures. In

diphosphide crystals, in which at the simple chemical formula the elementary cell consists of 24 atoms and the zigzag chains of atoms of phosphorus pass through all crystal, forming huge molecules, it is possible to expect presence of strong nonlinear effects and anharmonic instability [2]. And, though the structure distortions and characteristic transformations, connected to them, concern to features of $A^{II}B^{V}$ compounds, the mechanisms of lattice distortions formation and of structural transformations in crystals are not clear enough. The electronic subsystem in semiconductors also rather strongly influences structural properties and the interaction of phonon (lattice) and electronic subsystems can cause the shift of phase transition temperature, the thermal memory effects and occurrence of metastable states with phase transitions.

Under the formula $A^{II}B^{V}_2$ in zinc - phosphorus, cadmium - phosphorus, zinc - arsenic systems two modifications of CdP_2 (orthorhombic α-CdP_2 and tetragonal β-CdP_2), two modifications of ZnP_2 (tetragonal α-ZnP_2 and monoclinic β-ZnP_2) and monoclinic $ZnAs_2$ are formed. The structure of crystals is characterized by tetrahedral coordination of atoms. Each atom of metal M (M ≡ Cd, Zn) is surrounded with four atoms of anion A (A ≡ As, P) and each atom A is surrounded with two atoms M and two atoms A. Atomic radius A is about 0.1 nm and, as A-A distance is 0.21 nm approximately, the chemical bond between anions is rather strong. In structures of diphosphides the atoms of anions form the zigzag chains which are penetrating through over the crystal [1]. The atoms of metal M are at the centre of deformed tetrahedron and connect the chains of anions in 3D structure. In compounds the complex character of chemical bond is observed; phosphorus - phosphorus and arsenic - arsenic bond carries covalent character, in metal-anion bond the certain share of ionic bond (from 16 up to 54 % by different estimations) is present [3].

Elementary cell consists of four layers revolved from each other on 90 degrees. The sequence of packing of layers is frequently broken and instead of four it is possible to observe the multiplets of six, less often five layers. The infringements of a sequence of packing are entailed with formation of polytypes in a crystal [4]. The transformations of polytypes carry thermoactivated character and have served as an explanation of observed in [5] an unusual sequence of structural phase transitions existing in a wide temperature range from 80 K to 400 K. The temperature dependences of lattice parameters have anomalous areas about $\Delta T \approx 20$ K with thermal expansion near zero. The superstructure with period from 60 nm at 80 K to 20 nm at 400 K, quickly changes in area of "plateau" and remains almost constant in areas with usual thermal expansion. It has given the basis to determine the existence of incommensurate phase and "incomplete devil's staircase" [6-9] in α-ZnP_2 crystal [5]. In β-ZnP_2 [10] crystals the incommensurate phase has not been observed, however there is an original superstructure formed by the microtwins with the sizes of the twins about several elementary cells [4]. Structure and the properties of crystals have not brightly expressed anisotropy, which is peculiar to layered crystals [11]. However, rather large deviations of lengths and corners of chemical bonds in deformed tetrahedrons result in various local distortions in a crystal.

2. Experimental procedures

Single crystals of β-CdP_2, α-ZnP_2, β-ZnP_2 and $ZnAs_2$ were grown from gas phase, where cut parallel to the (001), (100), (010), (110) planes and polished to the desired thickness.

Dielectric measurements were performed using a parallel-plate capacitor arrangement. The samples were formed into thin plates with smooth polished faces onto which aquadag electrodes were painted. Samples were placed among polish brass electrodes. Stray

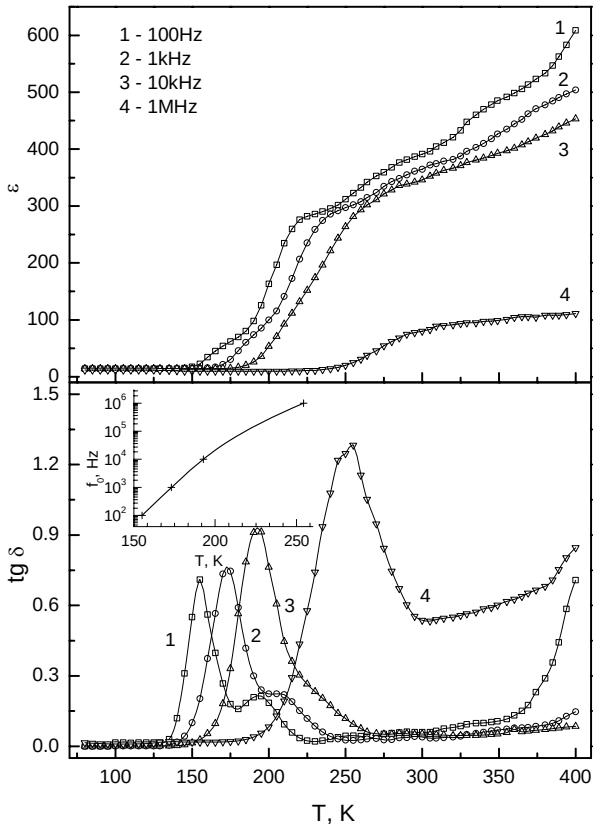

Fig. 1. Temperature-dependence of the dielectric constant ε(T) and tan δ(T) along [001] axis at the different frequencies of single crystal β-CdP_2.

capacitance of holder with conductors was at most 0.7 pF. Data were taken with E8-14 type digital LCR meter operating at 100 Hz, 1 kHz, 10 kHz and E8-12 type LCR meter operating at 1MHz. It is assumed that the loss component of the impedance is in parallel with the capacitive component in all of the dielectric measurements.

Elastic properties of compounds have been studied with ultrasonic echo-pulse technique at 10 MHz frequency. Samples for ultrasonic measurements were formed into parallelepipeds with polished faces. Longitudinal and shear sound velocities were measured i) along ***a, c*** crystallographic axes of β-CdP_2, α-ZnP_2 and along ***a***, ***b***, ***c*** axes of β-ZnP_2 ii) longitudinal sound velocities along ***a***, ***b, c*** axes of $ZnAs_2$.

The dielectric and ultrasound measurements were carried out in 78-400 K temperature range in a mode of slow heating/cooling with velocity 0.1 - 0.05 K/min. Accuracy of dielectric measurements and of relative measurements of sound velocity was not worse 0,1 %, of temperature - 0.1 K.

3. Experimental results

3.1. Dielectric properties and conductivity

In Fig. 1 typical temperature dependence of the dielectric constant ε(T) and the loss component tan δ(T) along ***c*** axis of β-CdP_2 and α-ZnP_2 samples for different (f = 10^2, 10^3, 10^4, 10^6 Hz) frequencies is shown. The low temperature values $\varepsilon_c \approx 7 - 8$ along ***c*** and $\varepsilon_{a,b} \approx 12 - 13$ along ***a, b*** axes agree with those obtained from optical measurements [3].

Over the temperature range of 150–350 K, ε(T) is large (ε ~ 10^2 - 10^3) and only weakly temperature dependent. However, on cooling below 150 K, ε(T) drops by a factor of 100. This drop in ε(T) is accompanied by a peak in tan*δ(T)*. It is seen that the temperature of the sharp anomaly in ε(T) is strongly affected by ***f*** measuring frequency, increasing from 150 to 250 K between 10^2 and 10^6 Hz. The temperature-frequency dependence of the dielectric constant (ε) and the loss component (tan δ) along ***a*** axis (for β-CdP_2 and α-ZnP_2 samples) is qualitatively similar. Peak values of tan δ(T) increase when the measuring frequency increases that possible to describe $\tan\delta_{max}=0.332+0.144\cdot\lg f$ dependence. At the temperature above 350 K the growth of tan δ due to through conductivity is observed. The characteristic frequency f_0, extracted from the peak in the loss data, as a function of temperature is shown in the inset of

Fig.1. The large change in f_0 with temperature is unusual for a thermally driven phase transition and rather points to a relaxation process.

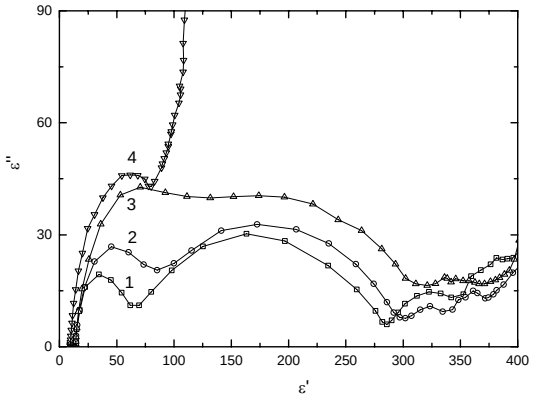

Fig. 2. The temperature dependence of Davidson-Cole diagram of β-CdP_2 crystal along [001] axis at the frequencies: 1 – 100 Hz; 2 – 1 kHz; 3 – 10 kHz; 4 – 1 MHz**.**

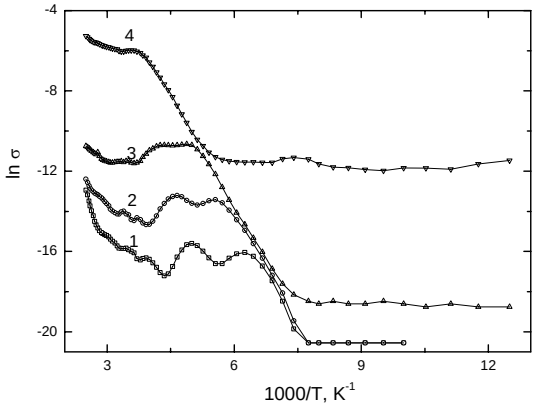

Fig. 3. The temperature dependence of conductivity of β-CdP_2 crystal along [001] axis at the frequencies: 1 – 100 Hz; 2 – 1 kHz; 3 – 10 kHz; 4 – 1 MHz.

The imaginary part of the dielectric constant ε″ of β-CdP_2 is shown in Fig. 2 as a function of the real part ε′, namely Davidson-Cole [12-13] plot.

In Fig. 3 the experimental dependence of conductivity on temperatures measured at the frequencies f = 10^2, 10^3, 10^4, 10^6 Hz is submitted. The conductivity has the brightly expressed frequency dependence, which is caused by imposing of conductivity of usual semiconductor character and hopping conductivity.

3.2. Elastic properties β-CdP_2, α-ZnP_2, β-ZnP_2 and $ZnAs_2$ single crystals

The elastic properties of zinc and cadmium diphosphides were investigated by measurements of ultrasound velocities along [001], [100] and [110] crystallographic directions of single crystal samples. Elastic properties of zinc arsenide were investigated by measurements of ultrasound velocities along [100], [010] and [001] crystallographic directions of single crystal samples. The results of measurements of ultrasound velocities in researched compounds and literature data are given in Table 1.

Table 1. Ultrasound velocities of β-CdP_2, α-ZnP_2, β-ZnP_2 and $ZnAs_2$ V_{ijk}^{lmn} at room temperature (T_r = 300 K). The subscript means a direction of a wave vector of an elastic wave, superscript - direction of polarization vector.

V_{ijk}^{lmn}, m/s Compound	V_{100}^{100}	V_{010}^{010}	V_{001}^{001}	V_{001}^{010}	V_{110}^{010}	$V_{110}^{1\bar{1}0}$	V_{110}^{110}	V_{110}^{001}	References
β-CdP_2	4340		4878	2506	2699	-	4671		
	4415		4735	2539	2906		4705		[14]
α–ZnP_2	5394		5742	3494	3852	2780	5811		
	6433		6017	3544			5820		[15]
β-ZnP_2			6337				6264	4355	
$ZnAs_2$	4147	4050	4417						

The measured values of ultrasound velocities are a basis for calculation of elastic modules (C_{ij} components of elastic constant tensor) at room temperature under the formula $C=\rho V^2$, where ρ is density of a crystal, which for β-CdP_2 is $4.18\cdot10^3$ kg/m^3, α-ZnP_2 - $3.51\cdot10^3$ kg/m^3, $ZnAs_2$ - $5.245\cdot10^3$ kg/m^3 (Table 2).

Table 2. Elastic constants Cij of β-CdP_2, α-ZnP_2 and $ZnAs_2$ single crystals at room temperature (T_r = 300 K).

C_{ij}, GPa / Compound	C_{11}	C_{22}	C_{33}	C_{44}	C_{66}	C_{12}	C'	C"	Θ_D, K	References
β-CdP_2	78.7		99.5	26.25	30.45	42.79	91.21	32.73	198.2	
	91.6		109.7	30.0	39	52			206	[16]
α–ZnP_2	102.1		115.7	42.85	52.08	30.76	118.5	27.13	280.2	
	144.2		126.1	43.8	31.2	29.4	118		432	[15]
$ZnAs_2$	95.63	102.5	112.7	20.76	40.45	31.47				[17]
		86.04								

Temperature dependence of the elasticity tensor components C_{11}, C_{33}, C_{44}, C_{66}, $C'=1/2(C_{11}+C_{12}+2C_{66})$ and $C''=1/2(C_{11}-C_{12})$ of the tetragonal modifications of cadmium and zinc diphosphide β-CdP_2 and α-ZnP_2 was calculated from the measured values of velocities of longitudinal and shear elastic waves along the crystallographic directions [001], [010] and [110]. Typical temperature dependence of the elastic module $C_{ij}(T)$ of tetragonal modifications of single crystals coincides with x-ray diffraction measurements of corresponding parameter of lattice (Fig. 4).

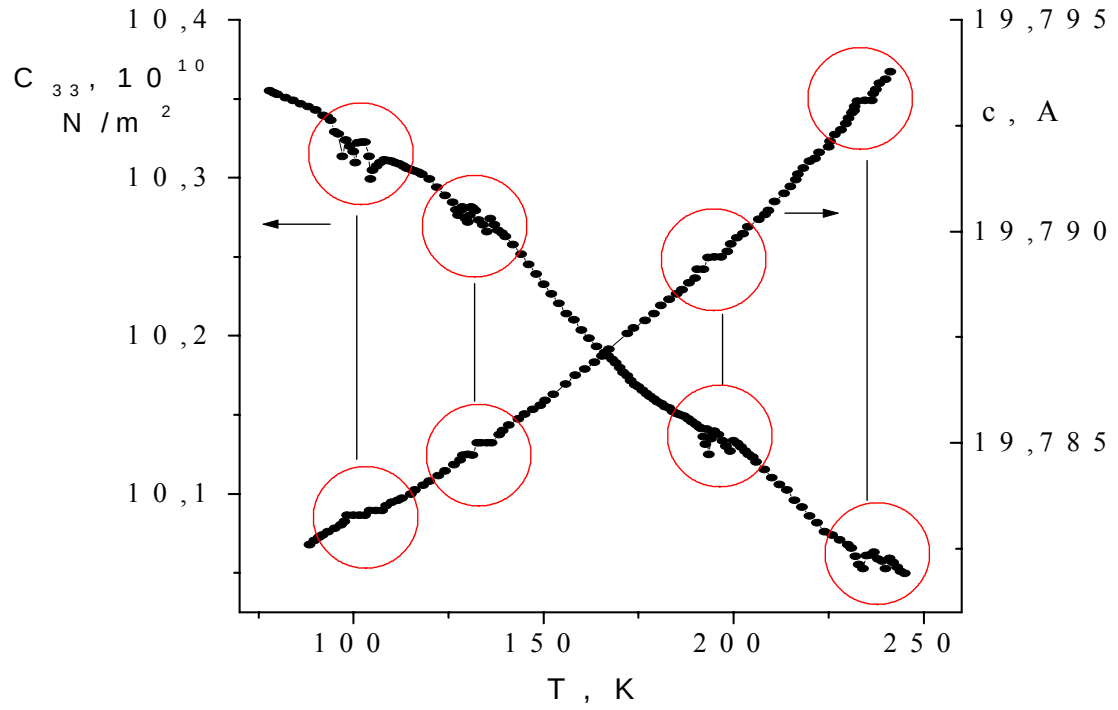

Fig. 4. The temperature dependence of elastic constant $C_{33}(T)$ and of ***c***(T) lattice parameter of β-CdP_2 single crystal.

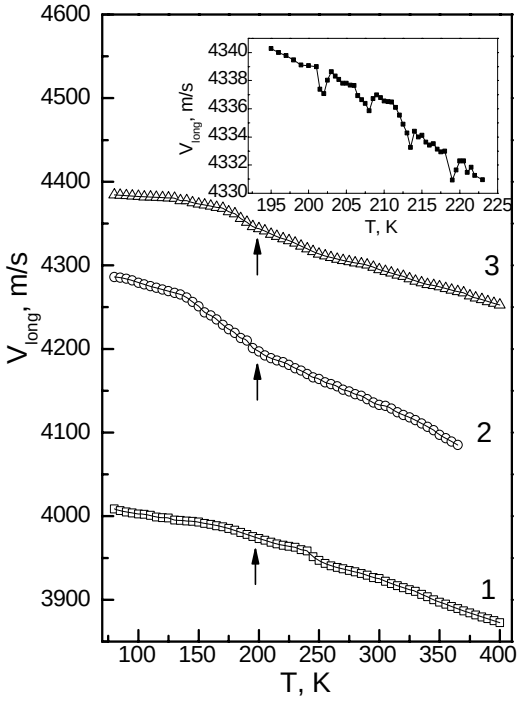

Fig.5. Temperature dependence of the longitudinal sound velocity $V_{long}(T)$ along ***a***, ***b*** and ***c*** axes of $ZnAs_2$ single crystal.

The temperature dependence of the longitudinal ultrasonic velocities in $ZnAs_2$ measured along axes ***a, b, c*** in the temperature range of 78-400 K are shown in Fig.5. The arrows indicate the temperature regions of anomalies of ultrasonic velocities, where the slope of curves is breaking. In inset in Fig. 5 the temperature range of anomalous changes of sound velocity is shown.

4. Discussion

4.1. Dielectric properties and conductivity.

Cadmium and zinc diphosphide and zinc arsenide crystals are wide-band gap semiconductors with *p*-type of conductivity and the band gap width is $E_g \cong 2.03$ eV, $E_g \cong$ 2.05-2.22 eV in tetragonal β-CdP_2 and α-ZnP_2 accordingly, and the band gap width is $E_g \cong$ 1.44 - 1.602eV, $E_g \cong 0.89$eV in the monoclinic β-ZnP_2. and $ZnAs_2$ accordingly [15, 18 - 20].

Temperature-frequency dependence of the complex dielectric constant ε*(ω, T) points dielectric relaxation of orientation type. As from the experimental data on $A^{II}B^{V}$ it is possible to make a conclusion about the absence of structural transition of ferroelectric type, obtained values of dielectric constant are caused by mechanisms of dielectric relaxation. Let us consider several possible models.

Maxwell-Wagner mechanism describes strong dielectric relaxation in the ceramic semiconductors [21]. In our case researched samples are practically perfect single crystals with a small concentration of defects, in which there are no the areas acting in a role of grains. If we consider all crystal as the grain, the Maxwell-Wagner relaxation can be caused by the air capacity between electrode and a crystal surface. Semi-insulating graphite layer between sample surface and electrodes has been used to avoid this. Hence, relaxation of Maxwell-Wagner in this case is improbable.

The model of charge exchange was proposed for explaining the thermally activated growth of dielectric constant in the ternary semiconductor compounds $Cd_{1-x}Mn_xTe$ ($0 \le x \le 0.7$) [22]. According to this model the charge exchange of multicharged defects, contributing the deep levels into the band gap, in the presence of external electric field must lead to the dielectric constant increase. However such mechanism is poorly probable in our case, because for the ε increase to values $\varepsilon \approx 200$ defect concentration about 10^{19}–10^{20} sm^{-3} is necessary, i.e. the sample must be strongly defective, but used single crystals are much more perfect and defect concentration in them does not exceed 10^{13}–10^{17} sm^{-3}.

Model, proposed by Ramirez A.P. [23] for explaining the high values of the dielectric constant in $CaCu_3Ti_4O_{12}$, gives the most probable description of processes, occurring in researched materials. In this case P-vacancies (VP), which disrupt the initial crystal structure, can play a role of isolated defects. Under action of an external variable electric field the defective areas are exposed to distortions and relax between the alternative equivalent configurations preserving, on the average, crystal structure. This model describes well the obtained results. Typical experimental temperature dependence of conductivity of sample β-CdP_2 in the form lnσ (1/T) at frequencies of 10^2, 10^3, 10^4, 10^6 Hz is represented in Fig. 3. The kind of a curve is similar for all experimental dependences of conductivity. The curves of temperature dependence of conductivity lnσ versus (1/T) have characteristic of semiconductors type. Different sections of curve correspond to different conductivity types. It is possible to calculate activation energy ΔE_a of carriers for the certain frequency from the formula of conductivity for semiconductors $\sigma=\sigma_0 * \exp(-\Delta E_a/2kT)$ by lnσ (1/T) line slope. The calculated values are given in Table 3.

Table 3. Activation energy ΔE_a (eV) in various sections at the certain frequency

Frequency, Hz / ΔT, K	10^2	10^3	10^4	10^6
80÷130	–	–	0,01	0.003
130 ÷ 260	0.6546	0.7305	0.5916	0.5889
260 ÷ 350	0.04	0.0016	0.001	0.12
350 ÷ 400	1.2	0.38	-	-

The values of the activation energy differ for the different frequency that is connected with the frequency dependence, characteristic of the hopping conductivity. Conductivity possesses strongly pronounced frequency dependence, which is caused by imposing of usual conductivity and hopping conductivity. At low temperatures $\sigma(f) \sim f^{\alpha}$ ($\alpha \approx 0{,}75$ - $0{,}85$), at high temperatures $\sigma(f) \sim f^{\beta}$ ($\beta > 1$).

4.2. Elastic properties and structural distortions

There is the only one possible orientation of layers in the tetragonal crystals – perpendicular to the symmetry axis of higher order. C_{11}, C_{12} and C_{66} elastic modules characterize binding forces inside layer (intra-layer modules) and C_{33}, C_{13} and C_{44} elastic constants substantially characterize binding forces between the layers (interlayer constants).The anisotropy of elastic properties in tetragonal β-CdP_2 and α-ZnP_2 is unusual - although "interlayer" and "intra-layer" shear elastic modules correspond to layered crystal structure and $C_{44}<C_{66}$, however, the value of "interlayer" longitudinal elastic module C_{33} is higher than the "intra-layer" elastic module C_{11}. This fact was observed by many researchers and deviation falls outside the experiment errors. The elastic module decrease along layers can be partly caused by the dislocation mechanism (on 1-2 %), since the dislocation

concentration in the direction of ***c*** axis is by an order below in the value of the dislocation concentration in the direction, perpendicular to ***c*** axis. However, the value of C_{11} module is lower than the value of C_{33} module by 10-20 %, what is anomalous and testifies, in our opinion, to the softening of the corresponding phonon modes and tendency toward the structural distortions in the plane of layers (in the plane, perpendicular axis *c*). Anisotropy of elastic properties in crystals is characterized by coefficient of anisotropy $A=2C_{44}/(C_{11}-C_{12})$ and deviations from ratio of Cauchy $G_{kk}=C_{ij}-C_{9\text{-}i\text{-}j,\ 9\text{-}i\text{-}j}$, where $(i \neq j \neq k; i, j, k = 1, 2, 3)$, caused by noncentral character of atom interaction. Elastic anisotropy in β-CdP_2 is higher, than elastic anisotropy into α-ZnP_2 that, apparently, is connected with the fact that Cd ionic radius is more than the Zn ionic radius and distortion of tetrahedrons in β-CdP_2 is more than in α-ZnP_2 (Table 4). Deviations from ratio of Cauchy speak that the model of the central forces in the cadmium and zinc diphosphide crystals is not carried out.

Table 4. Parameter of the elastic anisotropy A, G_{kk} and δ deviations from the ratio of Cauchy for the β-CdP_2 and α-ZnP_2 crystals at room temperature

Anisotropy	α–ZnP_2	β-CdP_2
$A = 2C_{44}/(C_{11} - C_{12})$	1.2	1.46
$\delta = (C_{44} - C_{12})/C_{11}$	0.12	- 0.21
$G_{11} = C_{23} - C_{44}$, GPa	6.5	32
$G_{33} = C_{12} - C_{66}$, GPa	-21.4	12.4
C_{11}/ C_{33}	0,88	0,79
C_{11}/ C_{44}	2,4	3
C_{66}/ C_{44}	1,22	1,16

Gruneisen's parameters are the important characteristics of solids and determine nonlinear (anharmonic) properties of crystals. Gruneisen's constant $\gamma_{ij} = \frac{M}{\rho c_p}\alpha_{kl}c^s_{ijkl}$ where M is molecular weight, ρ is density, α is thermal-expansion coefficient, c_p is specific heat, c^s_{ijkl} is adiabatic elastic constants. Gruneisen's parameters characterize anharmonicity of thermal fluctuations and for tetragonal crystals have two components - along and perpendicular to axis of symmetry of 4-th order:

$$\gamma_{II} = \frac{(C^S_{33}\alpha_{II} + 2C^S_{13}\alpha_{\perp})M}{\rho c_p}, \gamma_{\perp} = \frac{\left[\left(C^S_{11} + C^S_{12}\right)\alpha_{\perp} + C^S_{13}\alpha_{II}\right]M}{\rho c_p},$$

where $\alpha_{||}$ и $\alpha_{\perp}$ are thermal expansion coefficients along and perpendicular to axes of symmetry of 4-th order (Table 5).

Table 5. Debye temperatures Θ, the value of the average ultrasonic velocity V_m, volume K and shear G modules and Gruneisen's constants γ.

Compound	Θ, K	V_m, m/s	K, GPa	G, GPa	γ_{II}	$\gamma_{\perp}$	$\gamma_{\perp}/\gamma_{II}$
α-ZnP_2	280.2	3708.1	63.6	39.3	0.632	0.723	1.144
β-CdP_2	198.2	2603.3	64.2	22.1	0.449	0.46	1.024

Gruneisen's parameters and anharmonicity in α-ZnP_2 are above in comparison with β-CdP_2. The anharmonicity of the thermal atom oscillations in cadmium and zinc diphosphide

of tetragonal modification is higher in the layer plane than along the axis of the 4th degree of symmetry.The tetragonal modifications of cadmium and zinc diphosphides have implicitly expressed layered structure and their elastic and dielectric properties are characterized by the anisotropy of elastic modules and of static dielectric constant $\varepsilon_0(\mathbf{E} \perp \mathbf{c}) > \varepsilon_0(\mathbf{E} // \mathbf{c})$ along and perpendicular to layers. Anions in the layers are asymmetric coordinated and dipoles formed on the anions are oriented perpendicular to layers what leads to the softening of lattice modes. As a result of the rigidity of phosphorus atom sublattice, displacements of cations will play main role in the spontaneous distortion of lattice and structural distortions acquire the complex character of incommensurate superstructure modulation.

In Fig. 4 temperature dependence of elastic modules $C_{ij}(T)$ is shown. Temperature dependences of elastic constant crystals, in general, are sufficiently monotonic and linear, describing by a sufficiently simple equation such as $C_{ij}(T)=C^{o}_{ij} + A_{ij}T$. However, at the certain temperatures linear dependences are interrupted by areas of width $\Delta T \cong 10$ -20 K with anomalous behavior of modules. These regions change a curve slope and value of a derivative dC_{ij}/dT. In the investigated temperature range of 78–410 K the elastic modules have abnormal changes in the form of the small minima with the amount of deviation 0,1-0,4%. On curves of temperature dependence of longitudinal ultrasonic velocity in monoclinic $ZnAs_2$ (Fig. 5) sections of width of $\Delta T \cong 20$ K with the anomalous behavior of ultrasonic velocity are observed.

5. Conclusions

Dielectric properties of β-CdP_2, α-ZnP_2, β-ZnP_2 and $ZnAs_2$ single crystals - dielectric constant ε, tan δ and conductivity σ are investigated depending on temperature and frequency of an external field. Dielectric constant grows up from values $\varepsilon \approx 7$-13 at low temperatures to values $\varepsilon = 10^3$ at high temperatures (T = 400 K) without structural transition. Conductivity is composed of usual conductivity, characteristic of semiconductors, and hopping conductivity. Activation energies are calculated and Davidson - Cole's diagrams are constructed.

Ultrasonic velocities in the basic crystallographic directions of β-CdP_2, α-ZnP_2, β-ZnP_2 and $ZnAs_2$ single crystals are measured and their temperature dependences are investigated. Elastic properties of single crystals over 78 – 400 K temperature range are studied and their elastic characteristics in the basic crystallographic directions are calculated.

References

[1] V.B. Lazarev, V.Ya. Shevchenko, Ya.H. Grinberg, V.V. Sobolev, Semiconductor compounds of A^2B^5 group. M.: Science, 1978. – pp. 256 (in Russian).
[2] J. A. Krumhansl, R. J. Gooding Physical Review B. 39, 5, 3047 (1989).
[3] N.N. Sirbu, V.E. Lvin Physics and technics of semiconductors (Russian), 25, 7, 1136 (1991).
[4] C. Manolikas, J. van Tendeloo, S. Amelinckx Physica Status Solidi. A97, 1, 87 (1986).
[5] A. U. Sheleg, V. V. Zaretskii Physica status solidi. A86, 2, 517 (1984). S. J. Aubry, Phys. (Fr.), 44, 2, 147 (1983).
[6] J.S. Aubry, Phys. (Fr.), 44, 2, 147 (1983).
[7] J.S. Aubry, Phys. C: Solid State Phys. 16, 3, 2497 (1983).
[8] P. Bak Rep. Prog. Phys. 45, 6, 587 (1982).
[9] P. Bak, R. Bruinsma Phys. Rev. Lett. 49, 4, 249 (1982)

[10] J. J. Hegyi, E. E. Loebner, E. W. Poor, J. G. White J. Phys. and Chem. Solids, 24, 2, 333 (1963).
[11] G. L. Belenkii, E. Yu. Salaev, R. A. Suleimanov, N. A. Abdullaev, V. Ya. Steinshraiber Solid state communications. 53, 11, 967 (1985).
[12] K.S. Cole and R.H. Cole, J. Chem. Physics 9, 341 (1941).
[13] D.W. Davidson and R.H. Cole, J. Chem. Physics 19, 1484 (1951).
[14] K.S. Dubrova, V.S. Koval, V.Ya. Kuryachii, N.V. Stuchinskaya Ukr. Phys. J. 33, 8, 1259 (1988).
[15] E. Karajamaki, R. Laiho, T. Levola, A. U. Sheleg Semicond. and Insul. 5, 153 (1980).
[16] V.Ya. Kuryachii, V.P. Michalchenko, N.V. Stuchinskaya, I.I. Tichina Ukr. Phys. J. 30, 2, 248 (1985).
[17] V.N. Balazuk, G.U. Bogachev, V.Ya. Kuryachii, S.F. Marenkin, V.P. Mihalchenko, D.I. Pishikov, A.I. Rarenko Solid State Physics (in Russian), **33**, 9, 2777 (1982).
[18] V.V. Sobolev, A.I. Kozlov, Yu.I. Polygalov, V. E. Tupitsyn, A.S. Poplavnoi Phys. stat. sol. (b).**154**, 1, 377 (1989).
[19] R. S. Berg, P. Y. Yu Solid state commun. **46**, 2, 101 (1983).
[20] V.A. Morozova, S.F. Marenkin, O.G. Koshelev Inorg. Mat. **38**, 4, 409 (2002).
[21] V.V. Lemanov, A.V. Sotnikov, E.P. Smirnova, M. Weihnacht Solid State Phis. **44**, 11, 1948 (2002).
[22] P.V. Zhukovskii, A. Rodzik, U.A. Shostak Phys. Techn. Semicond. **31**, 6, 714 (1997).
[23] A.P. Ramirez, M.A. Subramanian, M. Gardel, G. Blumberg, D. Li, T. Vogt, S.M. Shapiro Solid State Communications, 115, 217 (2000).

OPTICAL PROPERTIES OF CRYSTALS GaSe AND InSe DOPED WITH Cu

Ig. Evtodiev, El. Cuculescu, M. Caraman, S. Anghel, M. Petrov

State University of Moldova, Department of Physics, A. Mateevici 60, Republic of Moldova , MD 2009

The anisotropy of absorption spectra in the range of the margin of fundamental band of the crystals GaSe and InSe doped with Cu in the percentage quantities up to 0.5 % at. from which the implementation mechanism of the impurity atoms of Cu in the hexagonal crystal grating of the GaSe and InSe crystals and the localization energy of the impurity levels in the forbidden energetic band is studied.

Introduction

The compounds GaSe and β-InSe are crystallized in the stratified structure (symmetric spatial group D_{6h}). The crystalline grating of the compounds belonging to this structural type is formed by four stratified packages of X-M-M-X type. Each atom of Ga (In) belongs to the tetrahedral neighbor of the Se atoms and one atom of Ga (In) [1]. In the internal part of stratified package the ionic-covalent preponderant bonds are active, but the bonds between package are realized by polarization forces [2]. The presence of weak bonds between layers leads to the anisotropy of electronic states.

The impurity atoms in the stratified structures of $A^{III}B^{VI}$ type are localized in the space between stratified packages, modifying so the character of chemical bonds between layers. But the presence of impurity atoms in the space between the planes of halogen atoms (Se) leads also to the modification of energetic spectrum especially on the axis direction with the high symmetry C_6.

The presence of vibration modes at low frequencies is among characteristic peculiarities of weak interaction, which correspond to the removing of atomic layers one with respect to another. The atoms from the interior of the stratified package at vibration do not remove one with respect to another. The presence of impurity atoms of Cu in the crystals GaSe and InSe with the modification of vibration spectrum of the crystalline grating leads to the formation of new energetic states in the forbidden energetic band.

Application in practice of GaSe and InSe crystals is determined by solution of the preparation problem of crystals with the electrical conductivity and energetic level diagram that will assure this.

The small mechanical deformations of the monocrystals lead to the increasing of the concentration of surface states. The energy of capture levels which are localized at ~ 0.18÷0.05 eV from the top of valence band modifies the character of absorption and photoconductivity in the range of absorption band margin.

Method of experiment

The crystals of GaSe and InSe were grown by Bridgman method from the elementary components Ga, In and Se which are pure spectral. The doping of the crystals GaSe and InSe with the Cu atoms in the concentrations from 0.01 up to 0.5% at was effected in the process of synthesis of the respective compounds. The samples of researches were obtained by

cleaving from the massive crystals and had the thickness in the limits from 0.1 up to 15 mm and the area 250÷350 mm^2. The cleaving is made in the direction perpendicular to the axis C_6. As the result of cleaving the plan parallel surfaces at the atomic level are obtained.

In order to obtain the information about the absorption of linear light polarization on the direction $\overline{E}II\overline{C}$, the light beam falls on the surface of crystal under the angle 45^o.

The absorption spectra and reflection ones at the temperature of 78K and 293 K were recorded on the spectrophotometer installation with the monochromator MDR-2 with the energetic resolution of about 0.5 meV.

Experimental results and their explanation

The spectral dependence of absorption coefficient in the range of fundamental band margin of the crystals ε-GaSe special non-doped is presented in fig.1. The margin of absorption band is formed by excitonic absorption both in the polarization $\overline{E}II\overline{C}$ (curve 1) and $\overline{E} \perp \overline{C}$ (curve 2). The states n=1 and n=2 are underlined clearly in both polarizations at the temperature of 78 K. The maxima of absorption excitonic lines n=1 and n=2 are localized at 2.105 and 2.106 eV.

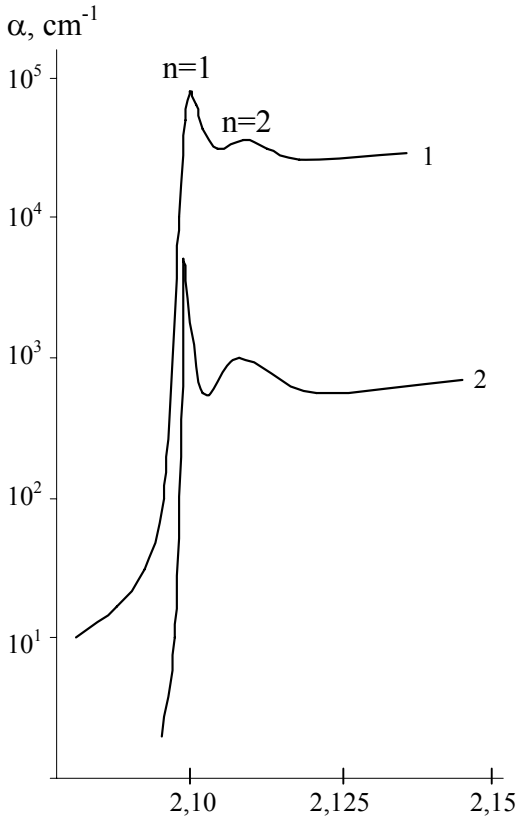

Fig.1. The absorption spectra of GaSe crystals in the polarization $\vec{E}II\vec{C}$ (1) and $\vec{E}\perp\vec{C}$ (2), T=78 K.

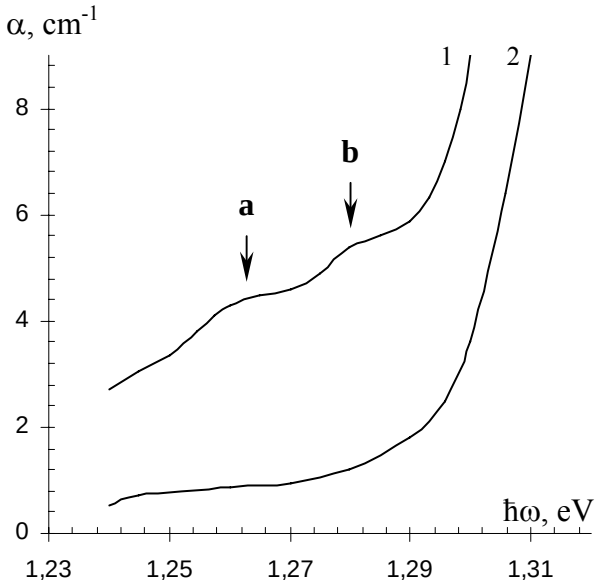

Fig.2. The margin of the absorption band of InSe in the polarization $\vec{E}II\vec{C}$ (1) and $\vec{E}\perp\vec{C}$ (2), T=78K.

The ration between the absorption coefficient in the maximum of excitonic line n=1 for the polarization $\overline{E}II\overline{C}$ and respectively $\overline{E} \perp \overline{C}$ is equal to 17 which is the value that correlates better with the coefficient of anisotropy calculated from the effective mass equal to 16 [3]. This ratio for the line n=2 is greater by 1.7 times than for the line n=1. Such an increasing of anisotropy of absorption coefficient in the range of the line n=2 is possible because in this field the absorption for the lines n≥2 is add and also it is necessary to take into consideration that the optical transitions in the polarization $\overline{E}II\overline{C}$ are permitted, but for $\overline{E} \perp \overline{C}$ are forbidden [2]. Also, the margin of absorption band of the crystals InSe special non doped is described by an exponential decreasing of the absorption coefficient with the energy of incident photons on the sample. The background absorption in the polarization $\overline{E} \perp \overline{C}$ is ~ 0.75 cm^{-1}. In the polarization $\overline{E}II\overline{C}$ at the energies $\hbar\omega$<1.29 eV, the absorption coefficient α decreases at ~ 5.5 cm^{-1} up to 2.5 cm^{-1} at the energy $\hbar\omega$<1.24 eV. Two maxima **a** and **b** (fig.2) are distinguished in this spectral domain respectively at 1.278 eV and 1.264 eV and the presence of these peculiarities is probably determined by the surface states, their concentration is considerable in the samples of GaSe and InSe which are studied in this polarization. The energetic levels of the surface states are localized at ~ 42 meV and 56 meV from the minimum of conduction band of the crystals InSe.

The absorption of light in the range $\hbar\omega$<1.26 eV in the polarization $\overline{E}II\overline{C}$ (in the crystals InSe (see fig.2, curve 1) can be interpreted as the process determined by indirect optical transitions, permitted by this polarization).

The doping of the crystals GaSe with the impurity atoms of Cu in the quantities up to 0.04% at. leads to the liquidation of the proper defects in the sub grating of metal which is the process that is manifested by the increasing of the intensity of excitonic line n=1 by 1.2 times, but for the line n=2 by ~ 3 times in the absorption spectra (fig.3) and 1.6 times for the line n=1 and 2.1 times for the line n=2 in the luminescence spectra. The intensity of impurity band in the absorption spectra is increased rapidly at the continuing increasing of the concentration of impurity atoms of Cu from 0.05 up to 0.1% at.

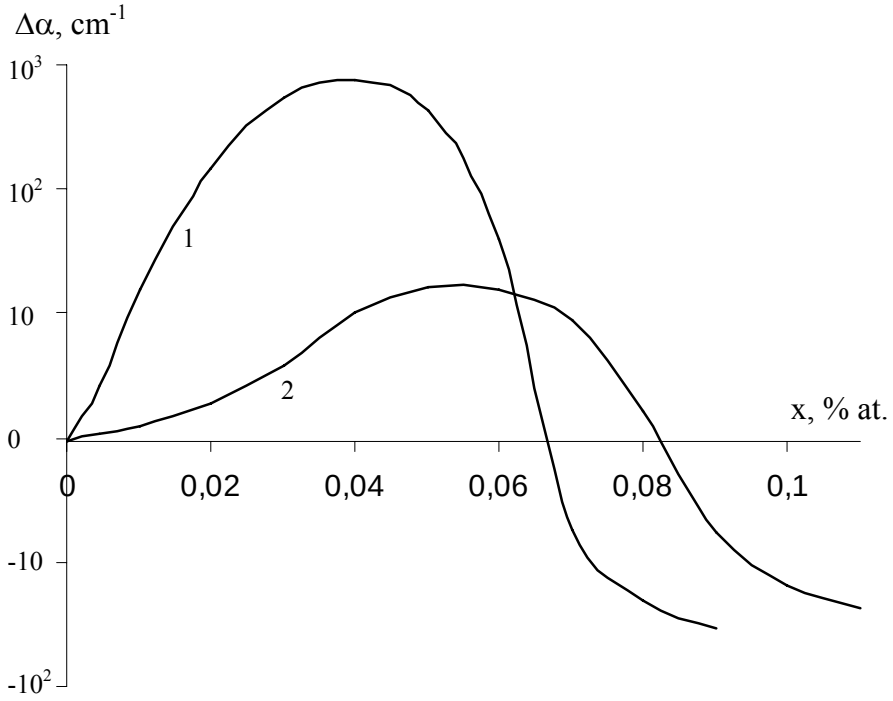

Fig.3. The variation of absorption coefficient of percentage concentration of copper in GaSe (1) and InSe (2) in the maximum of excitonic line n=1.

The impurity absorption reaches the value of about 12 cm^{-1} at the concentration of Cu of the order 0.08% at. Although the mechanism of electrical conductivity and the type of majority charge carriers in the process of doping of the crystals of ε-GaSe is not changed we can consider that the impurity atoms of Cu create in the forbidden band of the gallium monosellenium the acceptor levels. So, the impurity level that forms the threshold A^* (fig.4b) is localized at ~ 50 meV from the top of the valence band.

The impurity copper of InSe as in the GaSe leads to the liquidation of the defects in the sub grating of the metal for small concentrations (x<0.06 % at.). As we can see from fig.3 (curve 2) the absorption coefficient in the center of exitonic line slowly increases with the increasing of doping concentration, although the variation of absorption coefficient with the concentration is distinguished more weakly than in the GaSe (curve 1).

The light absorption spectra of the InSe crystals special non doped (curve 1) and doped with Cu up to 0.06% at. (curve 2) are presented in fig.4a. The presence of impurity atoms of Cu leads to the decreasing of absorption coefficient in the field of excitonic line n=1, modifies the character of dependence $\alpha(\hbar\omega)$ on the band of small energies of the excitonic line and forms a supplemental band of absorption in the range 1.26÷1.30 eV. The absorption coefficient in the impurity band of the crystals InSe (Cu) is of the same order of value (18÷20) cm^{-1} as for the crystals GaSe for which the atoms of Cu consist ~ 0.08% at. (fig.4b).

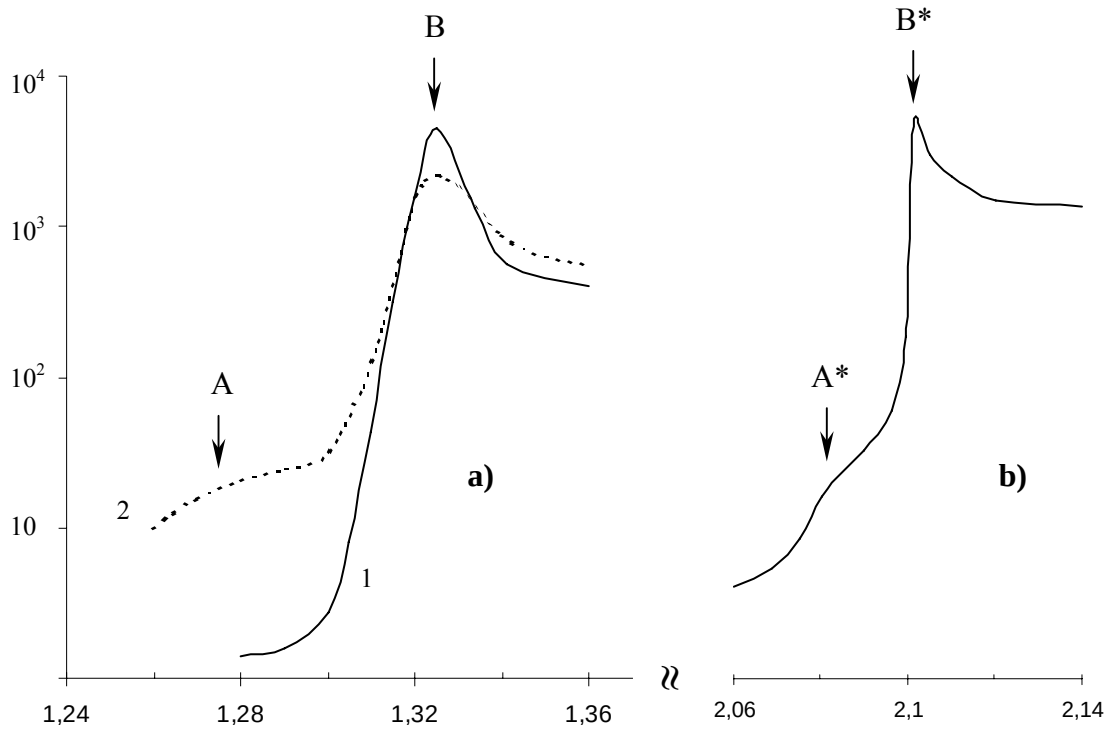

Fig.4. The spectral dependencies of the absorption coefficient of the photon energy in the range of absorption band margin for the crystals InSe (a) and GaSe (b) at the temperature T=78K.

The copper in the quantities greater than 0.05% at. both in the crystals GaSe and InSe screens the hole-electron bonds leading so to the liquidation of the line n=2. But a weak increasing of the absorption coefficient of the light at the energies from the fundamental

absorption band is determined by band – band optical transitions and the impurity levels of Cu localized at ~58 meV from the top of valence band in the crystals ε-GaSe.

The impurity absorption band in the crystals InSe (Cu) does not differ from those of GaSe by the form. The absorption coefficient in the field of energies 1.25 eV is increased by ~1.3 times with the increasing of the concentrations of Cu atoms from 0.05% at. up to 0.1% at. Though, for the quantities of Cu atoms included in the limits from 0.01% up to 0.1% at. the type of major charge carriers is not changed, the character of absorption of the light in the range of the margin of fundamental band allows to suppose that in the same time with the creation of the supplemental donor levels the atoms of Cu create also the acceptor levels in the forbidden band of the compound InSe localized at ~ 0.07 eV from the top of the valence band.

Conclusions

The value of the absorption coefficient in the center of excitonic line at the temperature of 78K and the influence of incident light polarization on the dependence $\alpha(\hbar\omega)$ in the range of fundamental band absorption band margin was established from the analysis of absorption spectra of the crystals ε-GaSe special non doped with Cu. The increasing of absorption coefficient in the range $\hbar\omega$>2.1 eV in the polarization $\overline{E}II\overline{C}$ with respect to $\overline{E} \perp \overline{C}$ polarization is influenced by the increasing of the probability of respective optical transitions.

The impurity atoms of Cu at small concentrations (Cu<0.04% at.) in the GaSe and <0.06% at. in the InSe liquidate the defects in the sub grating of the metal, and so that the intensity of excitonic absorption is increased. At bigger concentrations, both in the GaSe and InSe the impurity atoms of Cu screen the hole-electron interaction contributing so to the decreasing of absorption coefficient in the excitonic line. The process of screening of the excitonic bonds by impurity atoms of Cu both in the GaSe and InSe has the tendency to saturation.

The dissolved copper in the GaSe crystals creates the acceptor levels, the average energy of which is ~ 58 meV, but in the crystals InSe the acceptor levels are formed with the donor levels, average energy of which is about 70 meV.

References

[1] A. Kuhu, A. Chery, R. Chevallier Crystall structures and interatomic distance in GaSe. Phys. Stat. Sol. (a), v. 31, N1, p.469-475 (1975).

[2] E. Mooser, J. Ch. Schluter, M. Schluter – J. Phys. Chem. Sol., v.35, p.1269 (1974).

[3] Г. Л. Беленький, В. Б. Стопочинский Электронные и колебательные спектры слоистых полупроводников типа $A^{III}B^{VI}$. УФН, т.140, вып.2, с.233-270 (1983).

[4] Б. С. Разбирин, А. Н. Старухин, Е. М. Гамарц и др. – Письма в ЖЭТФ, т.27, N6, с.341-344 (1978). Магнето-Штарк Эффект в слоистом кристалле.

STUDY OF RECOMBINATION MECHANISMS IN CRYSTALS GaSe DOPED WITH Cu, Cd AND Sn

Ig. Evtodiev[1], El. Cuculescu[1], M. Rusu[2], M. Caraman[1]

[1]*Faculty of Physics, Moldavian State University, Kishinev, Moldova*
[2]*Faculty of Physics, "Al. I. Cuza", University, Iassy, Romania*

The energetic diagram of the localized states in the forbidden band energy of the crystals ε-GaSe doped with Cu, Cd and Sn is determined from the analysis of absorption spectra in the field of impurity band, luminescent emissive spectra and thermo luminescent ones.

Introduction

The stratified crystals of GaSe type serve as the basic element in different optoelectronic devices such as the micro lasers (the excitation with the electron beam), optoelectronic modulators for a large domain of wavelengths [1]. In order to enlarge the domain of application of gallium monoselenium and of analogical compounds by the structure and physical mechanical properties (GaS and InSe) it is necessary to increase the variety of characteristic physical properties of these compounds.

The studies of optical properties and photoelectrical ones of the crystals GaS, GaSe and InSe pure nondoped prove that on their base the optoelectronic devices can be elaborated for the visible range and the near IR. In order to reach the conquerable parameters with the existent elaborations (on the base of semiconductors $A^{II}B^{VI}$, $A^{III}B^{VI}$) it is necessary to vary controllably with the diagram of localized states in the forbidden band of these crystals.

It is known [2] that the impurity atoms in the crystals of GaSe type, after the liquidation of structural defects in the sub grid of the metal from the interior of stratified packages Hal-M-M-Hal are localized in the space among the planes of the neighbor packages contributing so to the increasing of cohesion force among packages. These atoms will be situated on the surface of cleaving on the direction perpendicular to C contributing so to the formation of the ionized surface states. The physical properties of the extra fine monocrystalline films are modified by the surface states in which the characteristic properties of the structures with the reduced sizes are manifested.

The method of experiment and the technology of preparation of the samples

The absorption coefficient of the light in the field of impurity bands of the crystals GaSe and GaS is of order 10 cm^{-1} [2]., so in order that the error in the optical determinations does not exceed the order of 5% it is necessary to have the homogenous samples with the thickness of 1 cm. The necessary samples were prepared by cleaving from the homogenous optical monocrystals which were grown by Bridgman-Stockbarger method. The doping of the crystals GaSe with Cu, Cd and Sn was performed in the process of synthesis of the respective chemical compound. The distribution of impurity atoms in the volume of the crystal was established by the method of emission spectral analysis after the characteristic last lines of the respective atoms. The analytical spectra were registered by the spectrograph DFS-8 with the diffraction grating 600 mm^{-1}.

The absorption coefficient α was determined from measurements of spectral dependences of the transmission and reflection of the light from the natural mirror surfaces.

The emissive luminescent spectra and of thermoluminescence were recorded at the combined installation on the base of monochromator MDR-2 with the diffraction grating of 600 mm^{-1} and 1200 mm^{-1}. The luminescence of crystals GaSe was excited with the radiation of laser He-Ne (λ=0.6328 μm, P≈40 mWt), but in the case of thermo luminescence the light source was of Hg steam with the spectrum from the UV domain. The necessary spectral domain for the excitation of luminescence was selected with a set of optical filters.

Experimental results and their explanation

The spectral dependence of absorption coefficient is strongly emphasized by the shape. In the case of transitions valence band – ionized donor at the energies $\hbar\omega \approx E_g^d - E_d^i$ (E_d^i is the energy of ionization of the donor) a line is formed, but in the case of transitions acceptor level with small energy to conduction band the absorption coefficient $\alpha(\hbar\omega)$ is described with the analogical function for the direct optical transitions

$$\alpha(\hbar\omega) = A(\hbar\omega - E_g^d + E_A)^{1/2} \quad (1)$$

where the coefficient A receives the value smaller than the respective coefficient in the case of band – band transition, E_A is the energy of respective acceptor level.

The absorption spectra in the coordinates $\alpha^{1/2}=f(\hbar\omega)$ are presented in fig.1 for the crystals ε-GaSe doped with Cu, Cd and Sn at two temperatures: 78 and 293 K.

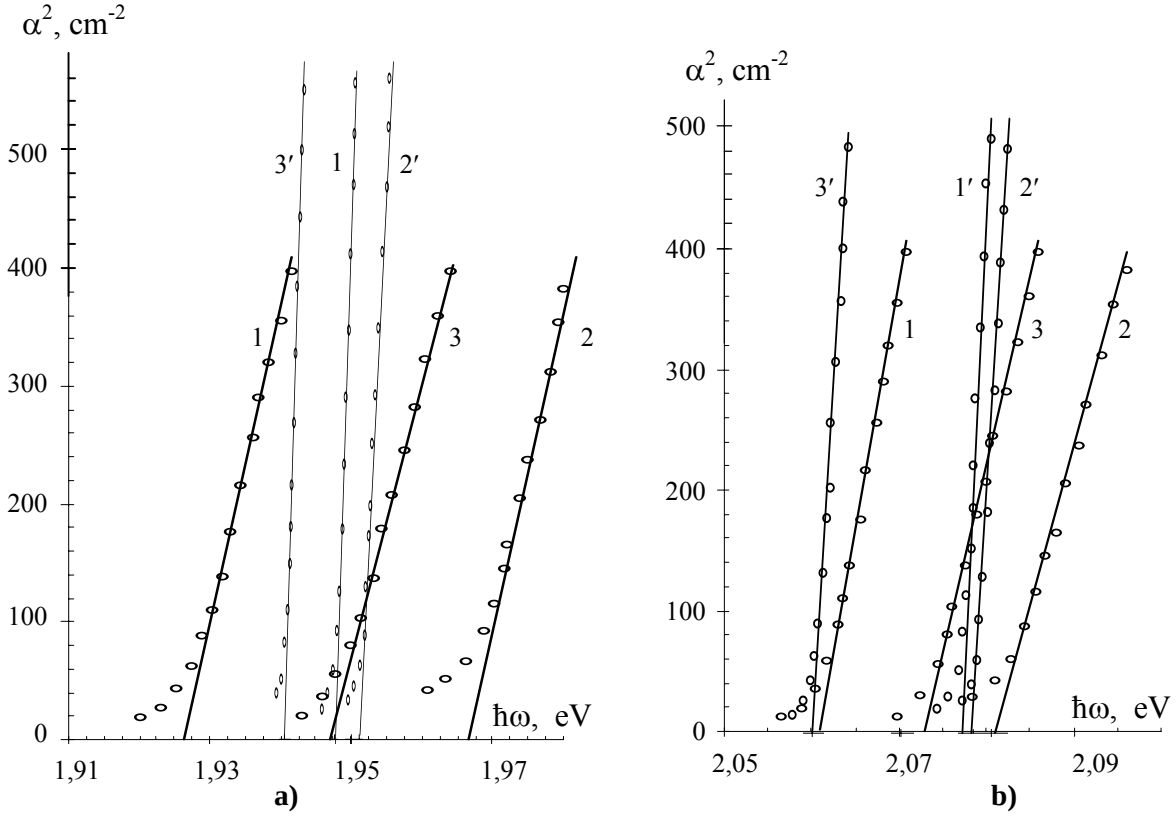

Fig.1. The spectral dependence of absorption coefficient of GaSe crystals doped with Cu (1, 1′); Cd (2, 2′); Sn (3, 3′); 1,2,3 - 0,05% at., 1′,2′,3′ - 0,50% at.; T, K: a – 293; b – 78.

As we can easily observe the experimental points are arranged on the segments of straight line in accordance with the function (1). Extrapolating the segments of straight line to the value $\alpha=0$ the energetic interval was determined between the minimum of conduction band and the acceptor level. Knowing the width of forbidden energy band of the crystals ε-GaSe special nondoped and equal to 2.132 eV and 2.037 eV respectively at the temperature 78 K and 293 K the average energy of ionization of the acceptor levels was determined created with Cu, Cd, and Sn, which are values introduced in table 1. As we can see from the table with the increasing of the Cu quantity in GaSe the ionization energy of the respective acceptor is decreased.

Table 1.

Chemical compound, % at.	GaSe: Cu		GaSe: Cd		GaSe: Sn	
	E / E_A, eV (T=78K)	E / E_A, eV (T=300K)	E / E_A, eV (T=78K)	E / E_A, eV (T=300K)	E / E_A, eV (T=78K)	E / E_A, eV (T=300K)
0.05	2.061 / 71	1.927 / 110	2.081/ 51	1.957 / 80	2.073 / 59	1.947 / 90
0.10	2.063 / 69	1.930 / 107	2.066 / 56	1.927 / 110	2.068 / 64	1.945 / 92
0.20	2.070 / 62	1.943 / 94	2.073 / 53	1.942 / 95	2.080 / 52	1.955 / 82
0.50	2.077 / 55	1.948 / 90	2.078 / 58	1.951 / 86	2.060 / 72	1.942 / 95

The photoluminescence spectra of the crystals GaSe doped with Cu, Cd and Sn are presented in fig.2.

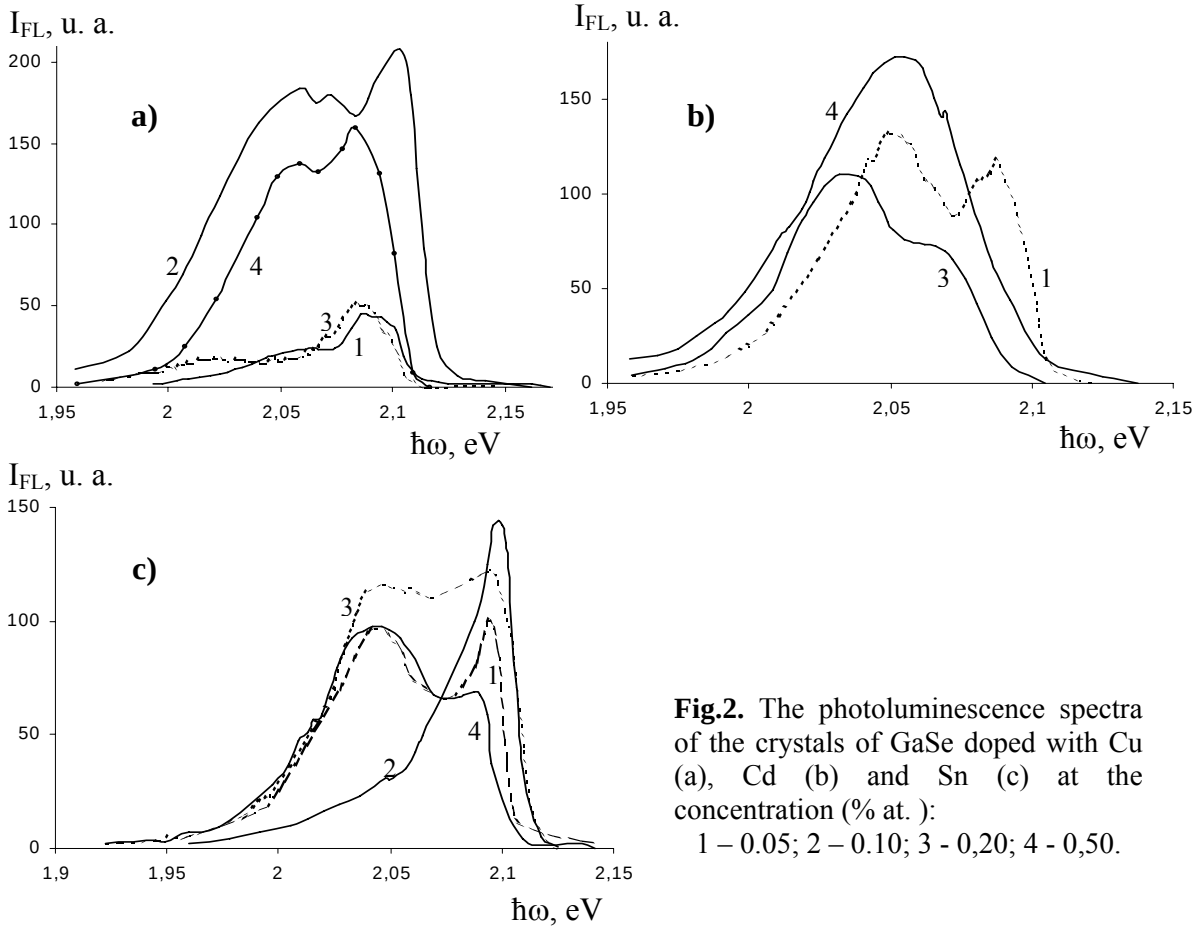

Fig.2. The photoluminescence spectra of the crystals of GaSe doped with Cu (a), Cd (b) and Sn (c) at the concentration (% at.):
1 – 0.05; 2 – 0.10; 3 - 0,20; 4 - 0,50.

The luminescence is initiated in the field of excitonic line n=1 and for all types of samples is composed of two intensive bands localized at red frontier of fundamental band of absorption. The energies of maximal intensity are introduced in tab.2. The excitonic luminescence (n=1) is emphasized clearly in the compounds GaSe with the impurity atoms of Cu in the quantities up to 0.2% at. with a maximum at 2.101 eV. The intensity of this line is in increasing from 0.05% at. of Cu up to 0.1% and further is rapidly decreased which is the fact that allows us to suppose that at small concentrations Cu compensates the structural defects in the subgrid of the metal from the interior of stratified packages. At the concentrations bigger than 0.2% at. copper creates the acceptor levels by which the luminescence band is formed with the maximum at 2.06÷2.08 eV that correlates better with the impurity absorption spectra (tab.1).

Table 2.

Concentration of the doped substance, % at.		E_1, eV	E_2, eV	E_3, eV	E_4, eV
GaSe: Cu	0.05	2.060	2.088	2.098	2.101
	0.10	2.073	2.092	2.098	2.100
	0.20	2.065	2.089	2.098	2.105
	0.50	2.055	2.080	2.086	-
GaSe: Cd	0.05	2.042	2.08	2.09	-
	0.20	1.990	2.04	2.09	-
	0.50	2.060	-	-	-
GaSe: Sn	0.05	-	-	2.100	-
	0.10	2.04	-	2.098	-
	0.20	2.05	-	2.100	-
	0.50	2.05	-	2.095	-

The doping of GaSe crystals with Cd in quantities from 0.05% at. up to 0.5% at. leads to the formation both of bond centers of excitons which their irradiative annihilation forms the luminescent band with the maximum at 2.08÷2.09 eV and acceptor levels by which the maximum bands at 2.04÷2.06 eV are created.

The photoluminescence spectra of the crystals GaSe doped with Sn in quantities up to 0.5% are composed of two localized bands at the margin of absorption band. The presence of excitonic line indicates us that the Sn in the small concentrations as Cu liquidates the defects of Ga and forms the acceptor levels localized at ~ 60 meV from the top of valence band.

The energetical diagram of the surface states (capture) in the crystals GaSe doped with Cu, Cd and Sn was established from the thermoluminescent analysis in the interval of temperatures from 78K up to 250 K.

The TLS spectra recorded from researched crystals contain a series of bands, their shapes are in the function of kinetic of TLS [3], of the speed of heating, the number of charge carriers captured on the capturing centers etc. We will take into consideration two limit cases of capturing of nonequilibrium charge carriers and especially:

a) *the linear kinetic of TLS*, for which $\gamma_t N_t << \gamma P_r$, where γ_t is the capture coefficient of the electrons on the capturing centers; γ is the recombination coefficient; N_t is concentration of capturing centers; P_r is the concentration of holes on the recombination centers.

b) *the square kinetic of TLS*, so when the probability of secondary capture of the electrons on the capturing centers is greater than the probability of their recombination on luminescent centers:

$$\gamma_t N_t >> \gamma P_r$$

The theoretical shapes were calculated in paper [4] of TLS spectra for the types of linear and square kinetics. For the linear kinetic the straight of the shape from the domain of low temperatures has a large "stretching "with respect to the domain of high temperatures, but for square kinetic has the inversed symmetry.

The respective temperature is determined by the shape of TLS, its intensity of the band is maximal (T_m); the half-length of the shape of TLS (δ) equal with the temperature differences T_2-T_1 for which the intensity of TLS is ½ from its maximal intensity; the surface (S) margined by the shape of TLS – I(T) and the axis of temperatures.

It is necessary to take into consideration that the form of the shape and the position of the maxima of TLS on the axis of temperatures is influenced both by the kinetic of TLS and the speed of releasing (β_0) of charge carriers from the capture centers at the determination of energy of surface states.

The energies of capture levels determined from the analysis of thermal stimulated luminescence are presented in table 3.

Table 3.

Concentration of the doped substance, % at.		E_t, eV
GaSe: Cu	0.05	0.161; 0.236
	0.10	0.145; 0.148; 0.163; 0.185
	0.20	0.189; 0.337
	0.50	0.147; 0.150; 0.178; 0.228
GaSe: Cd	0.05	0.189; 0.196; 0.516; 0.541; 0.604; 0.710
	0.10	0.185; 0.218; 0.509; 0.544; 0.654
	0.20	0.189; 0.561; 0.601; 0.633; 0.676
	0.50	0.204; 0.246
GaSe: Sn	0.05	0.161; 0.362; 0.370; 0.605; 0.679
	0.10	0.186; 0.376; 0.480
	0.20	0.196; 0.376; 0.199; 0.386
	0.50	0.281; 0.321; 0.343; 0.353; 0.500

Conclusions

The margin of fundamental band of absorption of the crystals GaSe is formed by the optical transitions with the formation of excitonic complexes. The maximum of excitonic absorption line in the state n=1 is localized at 2.102 eV (T=78K). The impurity atoms of Cu, Cd and Sn create the acceptor levels. The energy of created levels of Cu is in the slow decreasing from 110 meV up to 90 meV with the increasing of their concentration from 0.05% at.up to 0.5% at. With the decreasing of the sample temperature from 293 K up to 78 K the energy of acceptor levels of Cu, Cd and Sn is in weak decreasing.

The impurity atoms of Cu in the quantities up to 0.2% at. and of Sn up to 0.1% at. are arranged in the vacancies of Ga from the interior of stratified packages and lead to the

amplification of the intensity of excitonic line n=1 in the photoluminescence spectra. The impurity atoms create the acceptor levels which lead to the formation of the bands in the photoluminescence spectra.

The energetic diagram of the surface states in the crystals GaSe doped with Cu, Cd and Sn in the quantities up to 0.5% at. was established from the analysis of thermal stimulated luminescence.

References

[1] А. С. Медведева Халькогениды элементов $III^{Б}$ группы таблицы химических элементов. М., Наука, 1969.

[2] М. И. Караман, В. П. Мушинский. Роль прямых и непрямых переходов в формировании края фундаментального поглощения в кристаллах ε-GaSe. Мат. XI Всесоюзной конференции по физике полупроводников, Кишинев, 1988, с.64-65.

[3] В. П. Грибков Теория поглощения и испускания света в полупроводниках. 1975.

[4] В. В. Сердюк, Ю. Ф. Ваксман Люминесценция полупроводников. - К.; Одесса: Изд. “Выща школа”, 1988, 200 с.

GALLIUM ARSENATE REMOVAL FROM WASTE WATERS

S. Baranov, B. Cinic, J. Redwing[1] and V. Stavila

Scientific and Engineering Center "INFORMINSTRUMENT" SA, 6 str. Puskin, Chisinau, MD-2009, Republic of Moldova;
[1] Material Science and Engineering Department, Pen State University, 108 Steidle Bldg, University Park, PA 16802, USA.

Abstract

The aim of this paper is to study the loss of gallium (Ga) and arsenic (As) loss during the sedimentation of gallium arsenate ($GaAsO_4$) from waste solutions of GaAs epitaxial production by chloride method. The solid wastes of this semiconductor manufacturing process are removed from technological equipment by dissolution in an acidic etching solution. In order to recover valuable Ga and very toxic As from these waste solutions we proposed to precipitate them as gallium arsenate. Experiments have been conducted to determine the migration of the two elements in filtrate and washing solutions as a function of pH for both model and real industrial wastes. It has been determined the optimal interval of pH for sedimentation, the losses of Ga and As present 0,01-0,053%. For model solutions the sedimentation is optimal in the range of pH from 3,2 to 4,3, while in the case of real waste solution this interval is 3,6-5,0. Comparative evaluation of the precipitation efficiency revealed that for model solutions the arsenic loss during the precipitation is higher (0,5%), and this can be explained by a different ratio of initial Ga^{3+} and AsO_4^{3-} in model and real solutions. The results described in this paper provide important guidelines for the sedimentation of gallium arsenate from acidic waste solutions and indicate an overall efficiency of the process that could lead to savings in cost and process time for industrial effluent treatment technologies.

1. Introduction

The semiconductor gallium arsenide (GaAs) manufacturing processes generate large amount of solid wastes containing valuable gallium and toxic arsenic [1]. The dissolution of these wastes in specific etching solutions is an inevitable process. For instance in the case of growing GaAs layers from gaseous phase by chloride epitaxial method the technological equipment should be periodically treated with an etching solution to remove the solid deposit from the surface. Usually the solutions for etching contain a solubilizing and an oxidazing agent. In general it is desirable to use chemical agents which oxidaze arsenic to +5 valence state, since the use of acids without oxidizer leads to generation of a highly toxic gas arsine AsH_3. A number of chemicals have been used for these purposes, the most commonly used oxidants being hydrogen peroxide, hypochlorites, and nitric acid. The combination of the nitric with hydrochloric acid is especially attractive, since the resulted solution is characterized by a high etching activity and short reaction time. The dissolution process produces an acidic waste solution that may contain up to 2 mol/l of gallium(III) and arsenic(V). At such concentrations, the aqueous wastes require subsequent treatment for recovery of Ga and removal of As, prior to discharge of the waste from the manufacturing plant. For example, during the process of growing epitaxial GaAs semiconductor layers from

gaseous phase by chloride method the resulting waste solution from etching technological equipment in HCl/HNO_3 may contain up to 70% of the initial materials of high purity [2, 3]. The same category of liquid wastes results from dissolution of residual epitaxial GaAs plates in such acidic solutions. Since the aqueous waste itself contains gallium and arsenic of high semiconductor purity there is a critical need in developing appropriate technologies for their recovery. Recycling of such wastewater offers tremendous benefits from both reduced cost of production and environmental liability [1]. For example, gallium is particularly expensive and its recovery is economically advantageous to semiconductor manufacturers. However, there is a lack of technologies dealing with recovery of Ga and As from waste solutions containing g/l concentrations of these elements. It is clear that management of such hazardous wastes containing huge concentration of As is a very serious problem [4].

The environmental issues facing semiconductor industry have recently considerably expanded and become increasingly important concerns. For instance, the management and disposal of hazardous wastes, such as arsenic, receive significant attention because of strict regulation [4, 5]. Therefore, it is desirable to treat the wastewaters at the production plants, avoiding the costs and risks of eventual transportation to specialized mills. This strategy would permit to reduce production costs, conserve natural resources, and prevent pollution.

We propose a simple and robust method for recovery of both Ga and As from waste solutions derived from dissolution of GaAs in acidic solutions. This method involves the sedimentation of gallium arsenate ($GaAsO_4$) by adjusting the pH of the solution. The present study is devoted to the study of gallium arsenate sedimentation by titration of corresponding acidic solutions with an alkaline base (NaOH or KOH) and analysis of Ga and As removal at different pH, as well as the loss of these elements during the precipitation and washing of the sediment.

2. Experimental Section

2.1. Materials

Three model and one real waste solutions were considered for the present study. The three model waste solutions have been obtained by dissolution of GaAs plates in an acidic solution of nitric and hydrochloric acid and contain respectively 297.524, 244.586 and 92.425 g of GaAs in 1 litre of solution. The real waste solution results from etching technological equipment of GaAs epitaxial layers growing from gaseous phase from the $Ga\text{-}AsCl_3\text{-}H_2$ system. The other chemicals were analytical reagent grade and were used without any further purification. All solutions were prepared in deionised pure grade water. All glassware were cleaned with water and 1 N HCl and then rinsed with distilled water. KOH and NaOH stock solutions were standardized with a solution of hydrochloric acids (C_N=1.000 mol/l). The intermediate and secondary standards of working solutions were prepared freshly for each experiment. The separation of the sediment was performed using FILTRAK paper filters of medium porosity.

2.2. Procedure

2.2.1. Precipitation

The sedimentation experiments were carried out at 20±1 °C. The pH of the waste solutions was adjusted by adding either aqueous NaOH or KOH. An initial volume of 2ml of

the acidic solutions was added in 11 beakers, each of 50 ml. To each beaker 20 ml of deionised water was added to dilute the solutions in order to minimise the possible co-precipitation effects. Then to the first beaker a solution of the alkaline base was added gradually to the point of incipient precipitation. To the rest of the beakers a step-wise increased volume of the alkaline base was added under continuous stirring. For instance in the case of potassium hydroxide solution with a concentration of T=0.05743 g/l, this volume was in the range 0.3-0.7 ml, and it was individual for each acidic solution, function of the concentration of gallium and arsenic. These concentrations were preliminary measured by means of a spectrophotometric method [3]. The final volume of the solutions was adjusted to 50 ml with deionised water and the samples were left to equilibrate for 4 hours.

2.2.2. Filtration and Washing

The separation of the obtained gallium arsenate sediment was performed by filtration on the paper filters. The filters were preliminarily stored at 120 C° for 40 min and weighted on a balance with a precision of 0.5 mg. The time of contact of the filters with the atmosphere is minimised and is maintained constant for each sample. The sediments were separated by filtration. The filtrate solutions have different values of pH and present the first source of gallium and arsenic losses during the sedimentation of $GaAsO_4$. The obtained gallium arsenate sediment was washed with 50 ml of deionised water directly on the filter. The washing solutions present the second source of gallium and arsenic losses.

2.2.3. Drying of the sediment

The filters containing the gallium arsenate were dried at 120 °C for 90 min and then weighted. The obtained gallium arsenate presents a white amorphous solid, slightly hygroscopic. The weighting is performed in the same conditions for all samples, during the same period of time, determined by the cooling the samples to room temperature in a desiccator. The weight of the gallium arsenate was determined as the difference of the weight of the filter with and without sediment.

3. Measurements

The weight of the samples was measured by means of a laboratory balance VLR-200 (class of precision - 2). The pH measurements of the solutions were performed with an 3310 pH meter by means of glass and Ag/AgCl electrodes, the later filled with saturated potassium chloride solution.

The concentrations of gallium (Ga) and arsenic (As) in solutions have been measured by atomic-absorption spectroscopy method. The measurements have been performed by an atomic-absorption spectrophotometer AAnalyst-800 (Perkin-Elmer, USA), supplied with a flame atomizer with pneumatic nebulizer and interchangeable burner heads, the thermo-electric atomizer transversely-heated graphite furnace THGA incorporating an electromagnet for longitudinal Zeeman-effect background correction and flow injection system FIAS-400. As a line radiation source we have used the hollow cathode HCL lamp for determination of Ga and the electrode less discharge EDL lamp for determination of arsenic. A P-E firm AA Win Lab 4.1 program with utilisation of the computer controlled machine work and the analysis process. This method has found exhaustive use for determination of small concentrations of arsenic [6] and gallium [7] for determination of trace amounts of gallium by

tungsten metal furnace. The filtrate solutions contain 1-680 mg/l of gallium and 55-880 mg/l of arsenic, depending on the value of the pH of sedimentation. For this reason it is necessary to dilute the investigated solutions for using the described methods [8, 9]. The dilution of solutions is only of 5-20 times for atomisation method in flame, and of 100-1,000 times for thermal method and up to 10,000 times for hydride technique is necessary.

4. Results and Discussion

Three different model and one real waste solutions have been selected for the gallium arsenate sedimentation studies. The purpose for selecting those solutions was to study the effect of concentration of the dissolved gallium and arsenic, as well as their ratio. The results of the sedimentation of the gallium arsenate from acidic wastes are shown in Fig. 1. As expected, at higher concentrations of Ga(III) and As(V) the quantity the gallium arsenate sediment is higher. The interval of pH for optimum sedimentation for the solution with the concentration of GaAs 2.06 mol/l is between 3.2 and 4.4 with 3.1% loss from the weight of the sediment. At the concentration of GaAs 0.64 mol/l this interval is between pH 3.2 and 5.0 with the same amount of loss of the sediment.

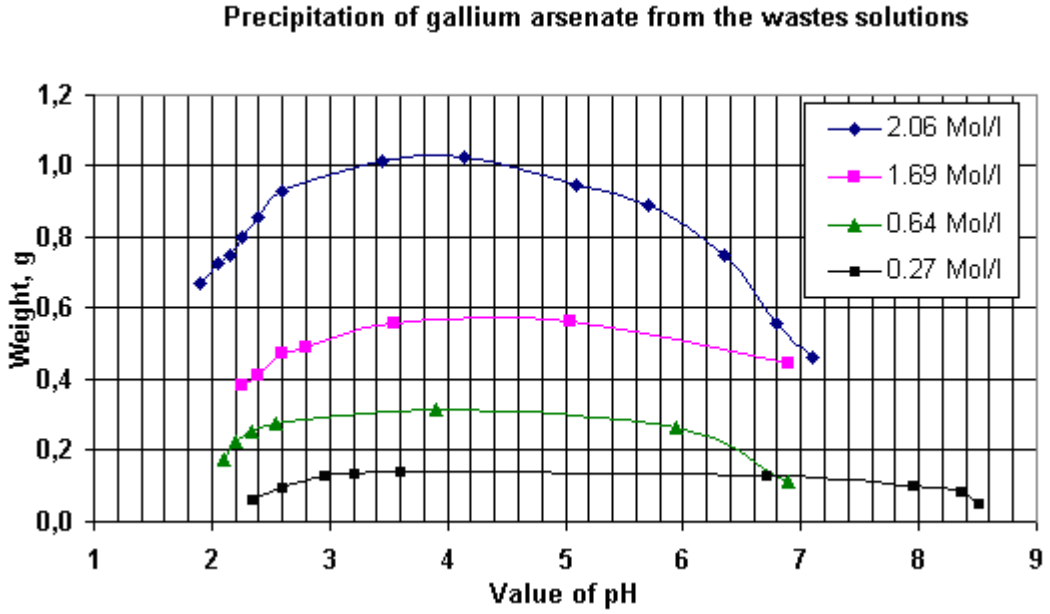

Fig.1. Precipitation of gallium arsenate from waste solutions

For the real waste solution with a concentration of Ga 0.27 mol/l the highest removal was obtained at a pH between 3.6 and 6.7, but the losses are smaller than 1% from the total weight. To be noted that the ratio of Ga to As in the real waste solution is close to 2:1, while in the model solutions this ratio is 1:1. The efficiency of the precipitation is higher for the more diluted solutions. The weight of the sediment obtained in the range of optimal pH values is about 20% higher as the calculated for anhydrous gallium arsenate. This increase in mass can be explained by the hygroscope properties of the obtained gallium arsenate, that can incorporate water molecules, as well as co-precipitate other ions presented in solutions.

The experiments were conducted with both KOH and NaOH solutions, the results are identical in both cases. The loss of gallium and arsenic calculated from gravimetric measurements presents a general characteristic of the precipitation process, but does not contain information about absolute losses of these elements. The atomic absorption method

permits to measure directly the concentrations of Ga and As, both in filtrate and washing solutions.

As observed in Fig. 2, in the filtrate solution resulted from the model waste samples the total concentrations of arsenic in the investigated pH range are between 0.5 and 0.9 mol/l, while the gallium concentrations are between 36 mg/l to 120 mg/l with the highest removal between pH 3.2 and 4.3.

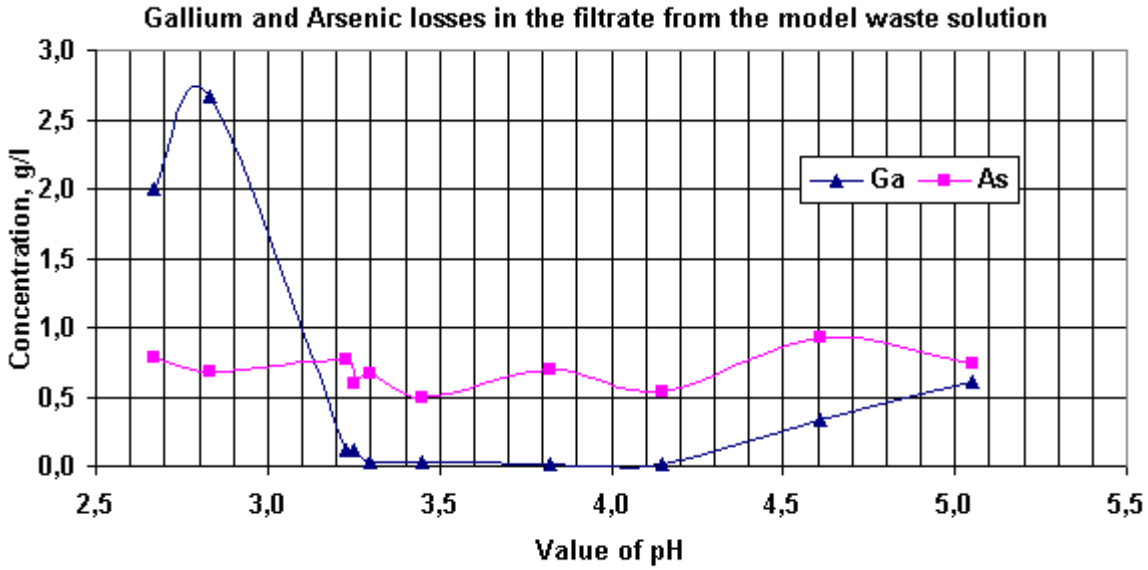

Fig. 2. Ga and As losses in the filtrate from the model waste solution

It is clear that for the real waste solution the composition of the sediment is different from stoechiometric, and can be formulated as $Ga(AsO_4)_x$. The occurrence of both stoechiometric and non-stoechiometric gallium arsenates has been previously reported [10-12]. A possible reason for the increase of gallium concentrations in the filtrate at pH higher than 4.3 may be formation of soluble Ga species. The speciation of gallium(III) solution chemistry and formation of hydroxo-complexes is well documented [13].

The solution chemistry of gallium(III) is very sensitive to pH due to hydrolysis reactions. For instance, Ga(III) solutions with more than 0.1 g/L or 1.4 mM Ga, one or more polynuclear species, such as $[Ga_{26}(OH)_{65}]^{13-}$, can exist at pH above 3. Below 0.01 g/L or 0.14 mM Ga, four mononuclear complexes are reported: $GaOH^{2+}$ (pK_{a1}=3.09), $Ga(OH)_2^+$ (pK_{a2}=3.55), $Ga(OH)_3$ (pK_{a3}=4,40) and $Ga(OH)_4^-$ (pK_{a4}=6.0) [13]. In our case the existence of soluble polynuclear Ga(III) complexes is very likely and this can explain the increase of Ga(III) concentration in the filtrate at pH higher than 4.3. The same conclusion may be made based on the results of the measuring gallium concentrations in washing solutions.

For washing solutions, as shown on Fig. 3, the concentrations of arsenic at pH higher than 4.3 increase to a value of 0.26 g/l, and at pH 5.05 reach 0.73 g/l and are higher than in the filtrate 0.61 g/l, while at the more acidic pH the As concentrations are in the range 58-90 mg/l.

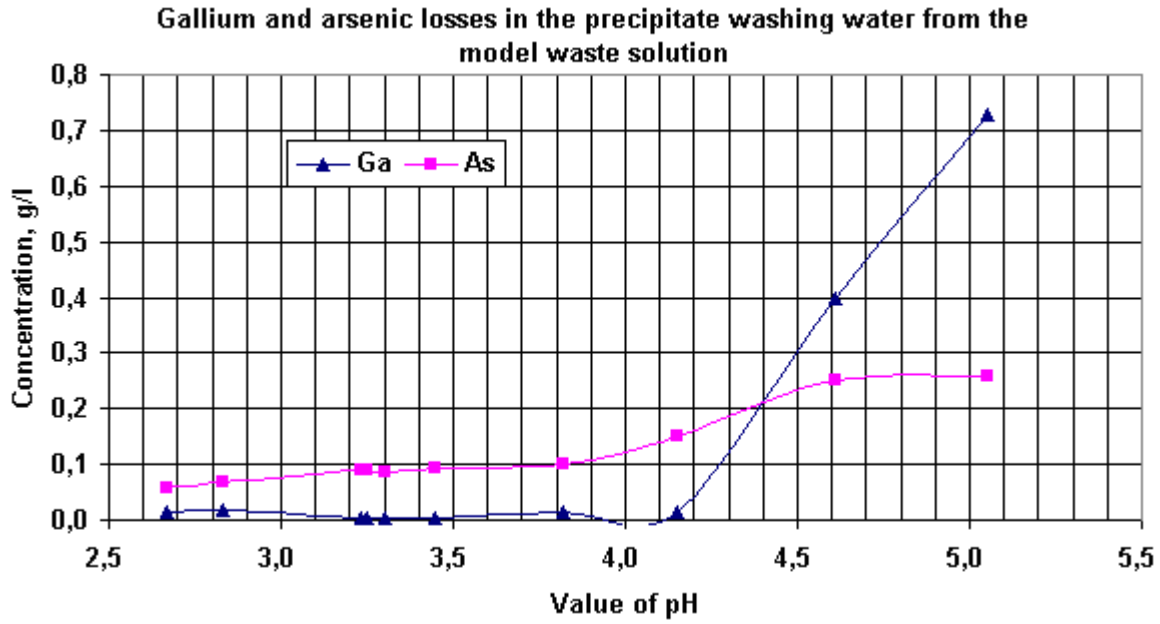

Fig. 3. Ga and As losses in the precipitate washing water from model waste solution

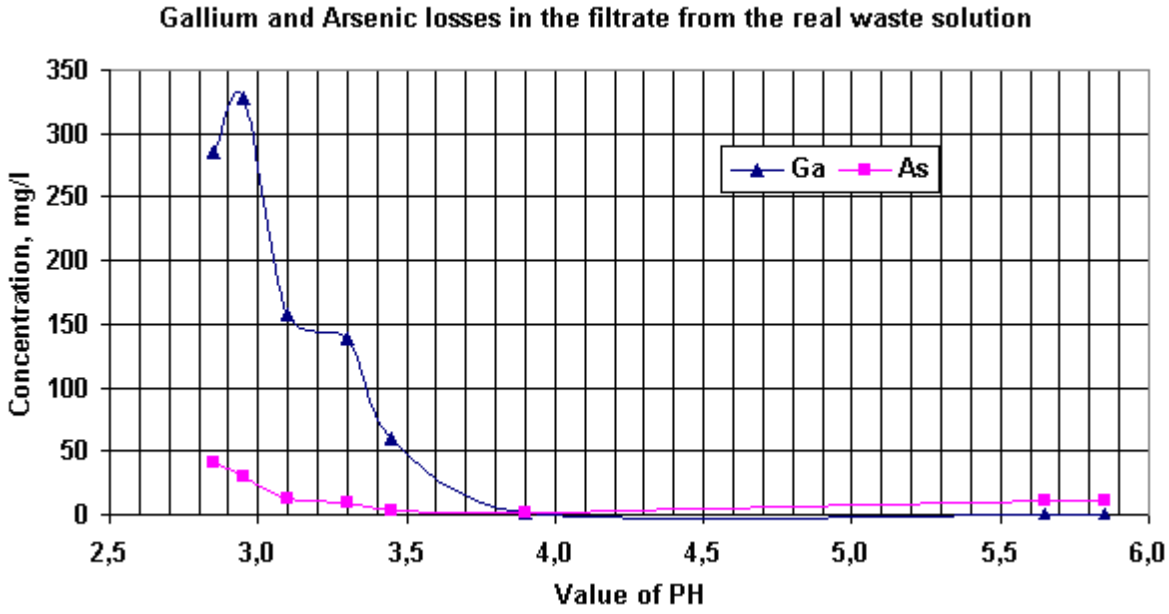

Fig. 4. Ga and As losses in the filtrate from the real waste solution

The effect of pH on the removal of gallium and arsenic from the real waste solution with the ratio Ga/As=2:1 is presented in Fig. 4. It can be seen from the figure that the concentrations of these elements in filtrate are smaller, probably due to their lower content in initial solution. The concentrations of As in filtrate decrease with pH from 42 mg/l to 2.2 mg/l at pH=3.9. The gallium concentrations also diminish from 328 mg/l to 1.7 mg/l at pH=3.9., but the beginning of the optimal sedimentation is at a slightly higher pH, 3.5 versus 3.2 for model solutions. A possible reason for this behaviour may be the different ratio of gallium to arsenic in solution.

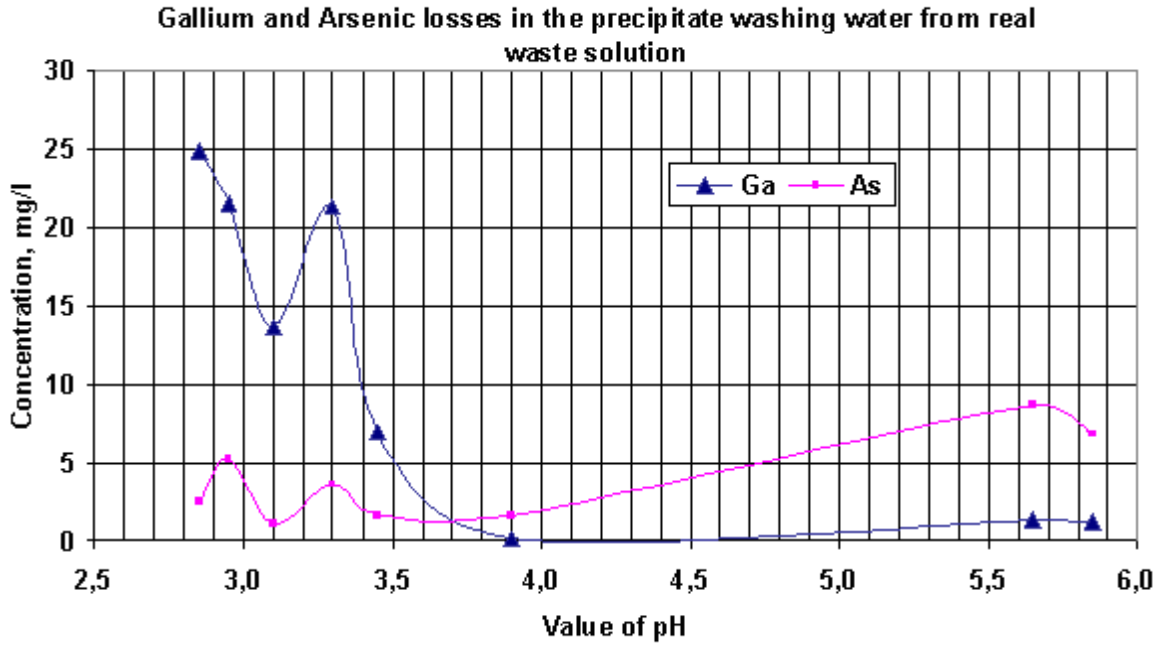

Fig. 5. Ga and As losses in the precipitate washing water from real waste solution

Fig. 5 shows the losses of Ga and As during the washing of the sediment obtained from real wastes. It can be seen from the figure that in the range of pH 2.75-3.50 the character of dependence of Ga concentrations in solutions is similar, the absolute values diminish, however, due to dilution 1:1 at washing. The concentrations of arsenic diminish as well, but the dependence is not the same any more. At higher pH values the concentration of Ga (1.30 mg/l) is over the respective in filtrate (0.30 mg/l) with even a higher ratio than the corresponding value in the case of model samples. In contrast to this, As concentrations in this interval of pH values have the same behaviour as in the case of model solutions. To sum up, the precipitation experiments with model and real solutions proved that the interval of optimal removal of gallium arsenate is different in the two cases.

Results of the efficiency of gallium and arsenic removal in the process of gallium arsenate sedimentation at optimal values of pH are presented in Table 1.

Table 1. The efficiency of gallium arsenate sedimentation.

Element	pH range	Concentration , g/l	Losses at filtratioin, mg/l	Losses at washing, mg/l	Total losses, mg/l	Total losses, %
Ga	3.2-4.3	143.4	65.5	10.1	75.6	0.053
Ga	3.6-5.0	18.96	1.7	0.15	1.85	0.010
As	3.2-4.3	154.1	655.0	119.5	774.5	0.500
As	3.6-5.0	10.19	1.6	1.6	3.8	0.037

As can be seen from Table 1, the total losses of Ga are function of initial concentration of this element and constitute 0.01-0.053%. The corresponding As losses during the precipitation from the real waste solution are of the same order that those of Ga and present 0.037%. Contrary, the removal of As from model solutions is less efficient and the losses present about 0.5%. There is a difference of one order between the losses of Ga and As, it

seems that there is no correlation with the initial concentrations of these elements, and probably it is connected with the ratio of Ga to As at the precipitation and co-precipitation of the species existing in solutions.

It is known that some high-pressure modifications of gallium arsenate present promising electronic materials [14-16] with useful opto-electronic and piezoelectric properties in a large range of temperature, between 15 and 1073K. A study is in course to reveal the respective properties of the obtained material from our sedimentation experiments. In parallel we are currently developing a technology of processing the obtained gallium arsenate in order to recover pure gallium and arsenic. The obtained filtrate and washing solutions still contain huge quantities of As and in order to remove the contaminant from the resulting wastewater one of the available commonly used technologies can be used, for instance precipitation and adsorption by iron(III).

5. Conclusions

The precipitation of gallium arsenate may be considered as a serious option for removal of both gallium and arsenic from acidic aqueous wastes of GaAs semiconductor industry. The sedimentation from the real waste with a ratio of Ga to As of 2:1 is particularly effective with the optimal pH range of the process between pH 3.6-5.0. In the case of three model solutions with a ratio Ga:As=1:1 this interval is between 3.2-4.3. The losses of Ga and As present 0.01 to 0.053% in the optimal conditions, with a mention that in the case of model solutions the loss of As is higher and constitutes about 0.5%. The obtained results are promising and showed that removal of gallium arsenate from acidic solutions can be performed with losses less than 0.5%. The obtained gallium arsenate can be further processed to isolate pure gallium and arsenic, while the remaining waste solution can be treated with a conventional technology for arsenic removal. Implementation of this process may have a positive role on the waste minimisation and pollution prevention within industrial process of GaAs layers production.

Acknowledgements

The research described in this publication was made possible in part by Award No. MP2-3048 of the Moldovan Research and Development Association (MRDA) and the U.S. Civilian Research and Development Foundation for the Independent States of the Former Soviet Union (CRDF). Any opinions, findings and conclusions or recommendations expressed in this material are those of the authors and do not necessarily reflect those of the MRDA or CRDF.

6. References

[1] T. Joseph and A. Jeffrey Reduction of Arsenic Wastes in the Semiconductor Industry. University of Dayton Research Institute Environmental Science and Engineering Group, Dayton OH 45469-0132, EPA/600/R-02/089, (1998). www.epa.gov/ORD/NRMRL/Pubs/600R02089/600R02089htm.

[2] S. Baranov, B. Cinic, V. Stavila, Waste Formation in Epitaxial Production of GaAs From Processing Technological Equipment in The Etching Solution. Proceeding of the 3rd International Conference on "Microelectronics and Computer Science", p.130-133, sept.26-28, 2002, Chisinau, Moldova.

[3] J. Redwing, S. Baranov, V. Stavila, B. Cinic, Study of the Waste Formation Process in Etching Solution Derived From Manufacture of Epitaxial GaAs Structures. Scientific Annals of State University of Moldova, ISBN 9975-70-305-4, series "Physics and Mathematics Sciences", pp.129-133, 2003

[4] B.K. Mandal and K.T. Suzuki. Arsenic round the world: a review. Talanta vol. 58 (2002), pp. 201–235.

[5] M. Leist, R. J. Casey and D. Caridi. The management of arsenic wastes: problems and prospects. Journal of Hazardous Materials. vol. 76, Issue 1, (2000), pp. 125-138.

[6] P. Palfy, E. Vircicova, L. Molnar Processing of arsenic waste by precipitation and solidification. Waste Management 19, 1999, pp. 55-59.

[7] A. Uzawa, H. Minamisawa, T. Okutani, Determination of trace amounts of gallium by tungsten metal furnace atomic absorption spectrometry after preconcentration on activated carbon impregnated with 8-quinolinol. Analytical Sciences (2000), 16(10), 1085-1088.

[8] J. Regwing, D.N. Izmailova, S.I. Baranov, O.P. Bogdevici Determination of Gallium and Arsenic in Technological Solutions by Absorption Spectrometry Metod. Scientific and Practical Conference Odessa National University, "Quality and Safety. Methodology and Metrology of Chemocal Analyses Questions", Odessa, Ukraina, 15-19 November 2004, pp. 15-19.

[9] S. Baranov, J. Redwing, O. Bogdevici, B. Cinic and D. Izmailov A method of Study the Gallium and Arsenic Losses in Technology of Gallium Arsenate Obtained From Wastes. In Press. Moldavian Journal of the Physical Sciences. 16.12.2004.

[10] M. Ronis, F. D'Yvoire, Trivalent metal arsenates. Preparation and study of the stoichiometric dihydrates MAsO4. 2H2O (M = aluminum, gallium, chromium, iron) and the nonstoichiometric dihydrates M1-xH3xAsO4.2H2O. Bulletin de la Societe Chimique de France (1974), (1-2, Pt. 1), pp. 78-82.

[11] M. Ronis, F. D'Yvoire, H. Guerin, Trivalent metal arsenates. I. M2O3-As2O5-H2O systems at 60.deg. (M = aluminum, gallium, chromium, iron). Bulletin de la Societe Chimique de France (1972), (7), pp. 2575-2580.

[12] M. Ronis. Gallium arsenates. Comptes Rendus des Seances de l'Academie des Sciences, Serie C: Sciences Chimiques (1970), 270(12), pp. 1113-1115.

[13] Baes and Mesmer, 1976 C.F. Baes and Jr.R.E. Mesmer, The hydrolysis of cations, Wiley Interscience publication, New York (1976).

[14] D. M. Christie and J. R. Chelikowsky, Electronic and structural properties of $GaAsO_4$, Journal of Physics and Chemistry of Solids. pp.617-624, Issue 5, v. 59, 1998.

[15] St. Dick The Structure of GaAsO4*2H2O: A New Member of the Variscite Family. Z. Naturforsch. B 1997, 52 11 p.p. 1337-1340.

[16] E. Philipot, P. Armand, P. Yot, O. Cambon, A. Goiffon, G. J. Mcintyre and P. Bordet Neutron and X-Ray Structure Refine ments between 15 and 1073 K of Piezoelectric Gallium Arsenate, $GaAsO_4$: Temperature and Presure Behavior Compared with Other α-Quartz Materials. Journal of Solid State Chemistry, 146, iss.1, 1999, pp. 114-123.

TECHNOLOGY FOR PREPARATION OF THERMAL ELEMENTS OF SbBiTe ALLOYS FOR THERMOELECTRIC COOLERS

M.P.Dyntu, V.G. Kantser, D.F.Meglei, A.I.Rusu

International Laboratory of Superconductivity and Solid State Electronics, Academy of Sciences, Academiei str., 3/3, Chisinau - 2028 MD, Republic of Moldova

An improved technology for treatment of thermal elements of SbBiTe alloys is given. Optimal technological regimes for their cutting, mechanical and chemical polishing are found. The electric spark method of cutting, double-sided mechanical polishing without preliminary grinding are found to improve the surface state, to increase output of valid thermal elements and to save material. Optimal conditions for chemical plating of nickel on butt-ends of thermal elements are found.

1. Introduction

Solid solutions of SbBiTe are the most efficient materials for preparation of thermoelectric cooling devices in the region of low temperatures [1,2]. Efficient work of thermocooling devices depends on both physical parameters of a semiconductor material they are made of and a technology for preparation of thermal elements themselves. The thermal element surface state influences greatly the quality of thermoelectric devices, however the process of cutting of thermal elements and their treatment is not well studied in literature.

Low hardness and layered crystal structure of these alloys determine formation of broken surface layers of a significant thickness in the process of cutting and abrasive mechanical treatment. Due to this, it is practically impossible to obtain a perfect surface of thermal elements of given parameters without a post-treatment.

Hence, this paper shows results of improvement of the technology for treatment of thermal elements based on SbBiTe alloys of p- and n-types of conductivity, with the purpose to achieve high values of thermal efficiency $Z=3\bullet10^{-3}$ K^{-1} and approximately equal values of parameters of the thermopower α, conductivity σ and thermal conductivity κ of the branches of both conductivity types in the temperature range 300-200 K.

2. Experimental results

We studied the technology for treatment of thermal elements having the sizes 1,1x1,1x1,8 mm^3 and 0,95x0,95x1,4 mm^3 cut out of SbBiTe alloys of p- and n-types of conductivity with the figure of merit Z no less than $3,1\bullet10^{-3}$ 1/K and σ=(1100-1200) $Ohm^{-1}cm^{-1}$. Fragility and splitting along the cleavage plane restrict the methods of cutting and mechanical polishing of thermal elements.

The following methods were studied: cutting with metal saw, diamond disks and electric spark cutting. It was found that the first two methods are not suitable since the cutting process causes appearance of large splits along the cut planes due to fragility of this material, and is accompanied by a rivet formation. The electric spark cutting gives a positive result.

The cutting was carried out using the electric spark device of the type A207.23 allowing to decrease thermal and mechanical overloads and the sample deformation. As a washing liquid 25% spirit solution in distilled water was used.

The wire diameter determined the cutting regime. Thus, for example, for a nickel wire of the diameter 0,065 mm, the open-circuit voltage is U=55 V, the short-circuit current is equal to I=0,1÷0,2 A. For a brass wire of the diameter 0,09 mm, U=70 V, and I=0,15 ÷0,2 A.

A condensation battery in machine-tools of this type is built in the power supply of the RC generator. Due to this, the cutting regime may be controlled only by the supply voltage and short-circuit current. Higher values of the latter cause splitting of a larger number of thermal elements while cutting. Thus, for example, at U=70 V, I=0,15 A the output coefficient is 88%, and at U=70 V, I=0,2A it decreases down to 73%. Optimal regimes for cutting of SbBiTe alloys were found when the coefficient of the thermal element output was ~100%.

Mild regime of cutting, in spite of the low electric erosion stability of this material, allows to obtain rather high roughness of the thermal element surface - ∇6-∇8, and the deformed layer is about 20-50 μm.

An attempt to polish the deformed layer obtained after the sample cutting with diamond pastes resulted in the broken layer increase and in a breaking of thermal elements along the cleavage plane. Therefore, in order to remove the broken layer of the butt-ends, double-sided mechanical polishing on felt with the chromium oxide powder was used, without the grinding process. As a result, a layer having the thickness of about 20-30 μm was removed. Microscopic investigations of the thermal element surfaces after polishing have shown that they were light, without cuts and breaks, and corresponded to the ∇8-∇9 purity class. Let us also note that the double-sided polishing of the samples eliminated the necessity of rejection of spoilage of the thermal elements according to height.

After the chemical polishing the thermal elements were repeatedly washed in organic dissolvents (benzine, toluene, isotropil spirits, acetone) in order to remove contamination, then they were washed in distilled water and went to chemical treatment of the surface.

The analysis of the literature data has shown that for thermoelectric alloys of bismuth telluride two types of polishing etching - electrolytic and chemical are used with an etchant based on HNO_3-HCl and CH_3COOH-Br_2 [3-5]. Use of electrolytic etching of thermal elements has not given a practical result due to the fact that on the sample surface there took place formation of films of yellow or black colour, i.e. films of oxides and products of the sample interaction with the etchant, which are not always dissolved. Besides, the etching kinetics is significantly influenced by the temperature, density of the current and concentration of the solution, that impedes obtaining of demanded sizes of the thermal elements.

One of the peculiarities of the etchants given in literature is that usually they are intended for one plane, in the majority of cases for the cleavage plane of perfect crystals, while thermal elements are cut usually not of perfect crystals, but of ingots with a special texture of the cleavage plane due to necessity to increase mechanical strength of branches of the thermal elements.

The chemical etching of the thermal elements was carried out in etchants of different composition for one and the same material, they were composed both as it is recommended in literature and on our own.

It is found that the chemical polishing of the thermal elements includes two stages of etching: the first is etching in a solution of mineral acids (3_2NHO_3 + 1_2HCl during 5-10 sec.)

and the second is etching in a solution containing 20-25 g of $CH_3COOH + 1_2Br_2$ during 30-60 sec.

After the mechanical polishing, the thermal elements underwent the chemical one. It was noted that the degree of the material removal while polishing depended on the surface state, composition of the material, temperature and freshness of etching solutions.

Optimal conditions for chemical polishing of the thermal elements were found, resulting in pure surfaces, without residuum of oxide film, with a metal glitter and with the surface roughness of ∇10-∇11 purity class. The etching regime ensuring the demanded sizes of the thermal elements was found as well.

Then a possibility of chemical plating of nickel film layer [3] on butt-ends of the thermal elements after the above mentioned preparation of the surface was studied. Main advantages of chemical nickel-plating in comparison with other metal coverings are the following: the possibility to plate nickel as a uniform layer upon parts of any configuration, absence of pores, the possibility to plate nickel simultaneously on a large number of thermal elements under similar conditions. Besides, nickel-plating of working butt-ends of thermal elements of SbBiTe alloys allows using solders which do not wet the thermoelectric material, that is solders of series ПОС and ПОСК with a flux consisting of a saturated solution of ammonium chloride in glycerine.

Chemically polished butt-ends of thermal elements after washing with hot and then cold distilled water were subjected to chemical activation, whereupon nickel-plating was performed in the following solution, g/l:

nickel chloride - 21;
sodium hypophosphite - 24;
sodium cytrate - 45;
ammonium chloride - 30;
distilled water up to 1 l,

during 30 minutes at the temperature 50-60°C, and the solution PH was corrected with the 30% aqueous solution of ammonia. However, coverings obtained of this solution are often fragile, this impeding their use for thermal elements.

It turned out that sodium hypophosphite significantly influences the quality of covering of thermal elements of SbBiTe based alloys. The best result is obtained when its content is 10-15 g/l. If its amount is less than 7 g/l the covering is porous and has weak adhesion. When hypophosphite content is increased higher than 20 g/l the covering is fragile and rough, and the solution stability decreases.

It should be noted that in order to obtain a uniform covering and the solution stability nickel-plating should be performed while the solution mixing. For increasing of adhesion and decreasing of the resistance of the contact after plating of nickel the thermal treatment was carried out in vacuum $5 \bullet 10^{-6}$-$1 \bullet 10^{-5}$ mm Hg during 30-45 min at the temperature 250-300°C. In order to avoid large mechanical stresses the cooling velocity did not exceed 5 degree/min.

Investigation of the covering microstructure has shown that it is expedient to plate nickel layer of the thickness 8-12 μm, because the thin covering having the thickness 3-5 μm was dissolved by the solder in some places while soldering.

The plated nickel turned out light, dead, and the pitting phenomenon is not observed. At this treatment of the thermal element surface the covering adhesion was 46-68 kH/cm^2. This, in its turn, increases reliability of operation of thermoelectric coolers assembled of the branches with these nickel layers.

3. Conclusions

Optimal technological regimes for cutting and for treatment of thermal elements after cutting are selected. The spark method of cutting allows to increase the output of valid thermal elements, to improve their quality and to save the material. It is shown that the doubled-sided mechanical polishing, without the grinding process, improves the state of the thermal element surface and eliminates the necessity of rejection of spoilage of the elements according to height. For decrease of the contact resistance of thermal elements and for increase of their mechanical and thermal durability optimal conditions for chemical plating of nickel on butt-ends of thermal elements of alloys based on SbBiTe solid solution are found.

References

[1] L.I.Anatychuk. Kiev, Naukova dumka (1989).
[2] B.M.Goltsman, V.I.Lyashchenok. USSR Patent application N 4086479 (1986).
[3] K.Sangval. Moscow, "MIr" (1990).
[4] Iu.S.Volkov. Methods for selection of electrolyte for size electrochemical treatment of metals (in Russian) (1968).
[5] "Etching of semiconductors". Translation from English of S.N.Gorin., Moscow, "Mir" (1965).
[6] T.I.Sturov, N.F.Shatanov. USSR Patent N 213512 (1976).

PARACONDUCTIVITY ANALYSIS FOR Ni-DOPED BSCCO

I.T. Dihor

Superconductivity & Magnetism Laboratory, State University of Moldova, MD2009 Chisinau, ReMoldova

Abstract

The paraconductivity effect of Ni-doped 2223 BSCCO ceramic samples was studied using data obtained from resistive measurements. The temperature ranges of 2D and 3D regimes of fluctuation conductivity as well as the crossover between different temperature regimes were determined in terms of the Lawrence and Doniach theory of fluctuations.

Introduction

Although a superconductor exhibits superconductivity only below T_c, there are superconducting electron pairs present also above T_c. These pairs are referred to as superconducting fluctuations. They are caused by thermodynamic fluctuations, which continuously create and destroy electron pairs. There is always a certain number of pairs present: the closer to T_c, the more pairs. It is, however, only below T_c that a superconducting condensate penetrates the material and the resistivity is zero. Superconducting fluctuations have a number of measurable effects. They influence, for example, electrical, thermal, and magnetic properties. Fluctuations have particularly large effects in high T_c superconductors (HTS), partly because of their high anisotropy. The fluctuation effects in HTS are large and easily observable, thanks to the short coherence lengths, the high temperatures involved, and the layered structure.

One easily observable effect of fluctuations is a fluctuation resistivity (conductivity) or more commonly the paraconductivity. The resistivity curve is linear, but bends down just above T_c. This decrease in resistivity can be attributed to the superconducting fluctuations.

In this paper we study the influence of Ni doping ions on paraconductivity of two types of superconductors: $Bi_{1.8}Pb_{0.46}Sr_{1.88}(Ca_{1-x}Ni_x)_{2.06}Cu_3O_y$ (I) and $Bi_{1.6}Pb_{0.4}Sr_{1.8}Ba_{0.2}(Ca_{1-x}Ni_x)_2Cu_3O_y$ (II) using the Lawrence-Doniach (LD) model of fluctuations. Here x denote the concentration of doping metal x=0, 0.02, 0.05.

The Aslamazov-Larkin (AL) model [1] is the most intuitive one, simply reflecting the fact that the superconducting electron pairs contribute to the conduction. Hence, this term gives a positive contribution to the conductivity (i.e. a decrease of the resistance against temperature decrease). The AL model was the first model to be derived and was treated for layered structures already in 1970 by Lawrence and Doniach [2]. In this model, each Cu-O plane is considered to be a two-dimensional (2D) superconductor, separated from the neighboring planes by insulating regions. The layers are coupled by Josephson tunneling. Close to T_c, where the coherence length perpendicular to the plane is much larger than the inter-plane distance, the material shows the 3D anisotropic superconductor behavior. Far away from T_c, where the coherence lengths are shorter than the inter-plane distance, it follows a 2D behavior.

In the LD model, the AL conductivity above T_c can be written as

$$\sigma_{LD}^{AL} = \frac{e^2}{16\hbar s}\frac{1}{\left[\varepsilon\left(\varepsilon+\delta\right)\right]^{1/2}} \tag{1}$$

where $\varepsilon = (T - T_c)/T_c$ is reduced temperature, $\delta = \frac{4\xi_c^2(0)}{s^2}$ is an anisotropy parameter, $\xi_c(0)$ is the coherence length perpendicular to the planes at zero temperature, and s is the inter-plane distance.

At T_c ($\varepsilon << \delta$) expression (1) approaches

$$\sigma_{3D}^{AL} = \frac{e^2}{32\hbar\xi(0)}\varepsilon^{-1/2} \qquad (\lambda = -1/2) \tag{2}$$

and at higher temperature ($\varepsilon >> \delta$) it approaches

$$\sigma_{2D}^{AL} = \frac{e^2}{16\hbar s}\varepsilon^{-1} \qquad (\lambda = -1) \tag{3}$$

The crossover from 2D to 3D regime of fluctuations occurs when $\varepsilon \approx \delta$. This corresponds to $\xi_c^2(T) \approx s/2$ with crossover temperature T_{cross} determined by

$$T_{cross} = T_c\left(1+\delta\right) \tag{4}$$

Result and analysis

In Fig.1 and Fig.2 the temperature dependences of resistivity superconductors of types I and II with different level of doping respectively are presented.

We assumed that T_c is the temperature where $d\rho/dT$ is a maximum, although there are other several methods to find T_c listed in the literature [3]. The linear (metallic) behavior of $\rho(T)$ dependence is considered to be above $2T_c$ temperature and could be fitted to $\rho_N(T) = \rho(0) + BT$.

Using the normal and total resistivity data shown in Fig.1, 2 and expression (1) we can extract the paraconductivity of these samples. The results are shown in Fig.3, 4 in a *log-log* scale. In brackets the R-squared coefficient of determination of fitted lines is indicated.

From these diagrams the crossover from 2D (λ = -1) to 3D (λ = -0.5) regime of superconducting fluctuations of studied samples except $Bi_{1.6}Pb_{0.4}Sr_{1.8}Ba_{0.2}(Ca_{1-x}Ni_x)_2Cu_3O_y$ with x=0.02 was identified (table 1). For above mentioned sample the 2D regime was not identified: the dimensional crossover occurs from 1D (λ = -1.5) regime directly to 3D regime (λ = -0.5). This sample contains 90% of 2223 phase with some 2212 and 2201 phase. Probably these small phases distributed randomly in the 2223 phase form wire type conductivity. In case of $Bi_{1.6}Pb_{0.4}Sr_{1.8}Ba_{0.2}(Ca_{1-x}Ni_x)_2Cu_3O_y$ sample with x=0.05 the phase content of 2223 is 65% and 2212 phase is 25%. Here the 2D regime of conductivity occurs. The superconductor type I with x=0.02 contain 90% of 2223 phase without any other phases while for x=0.05 this superconductor contains 25% of 2223 phase and 65% of 2212 phase.

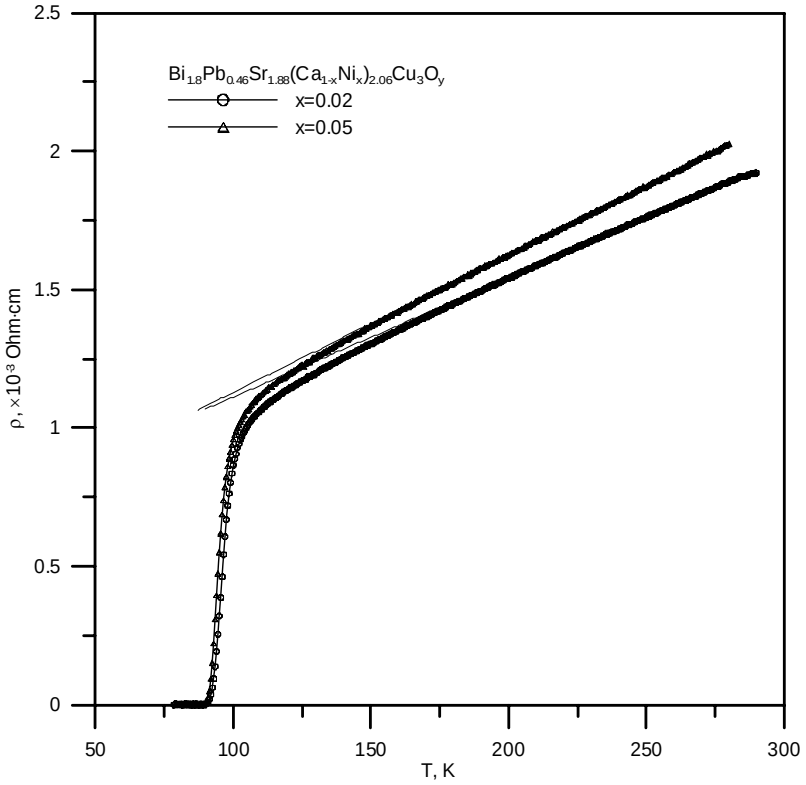

Fig.1. The temperature dependence of resistivity for type I superconductor.

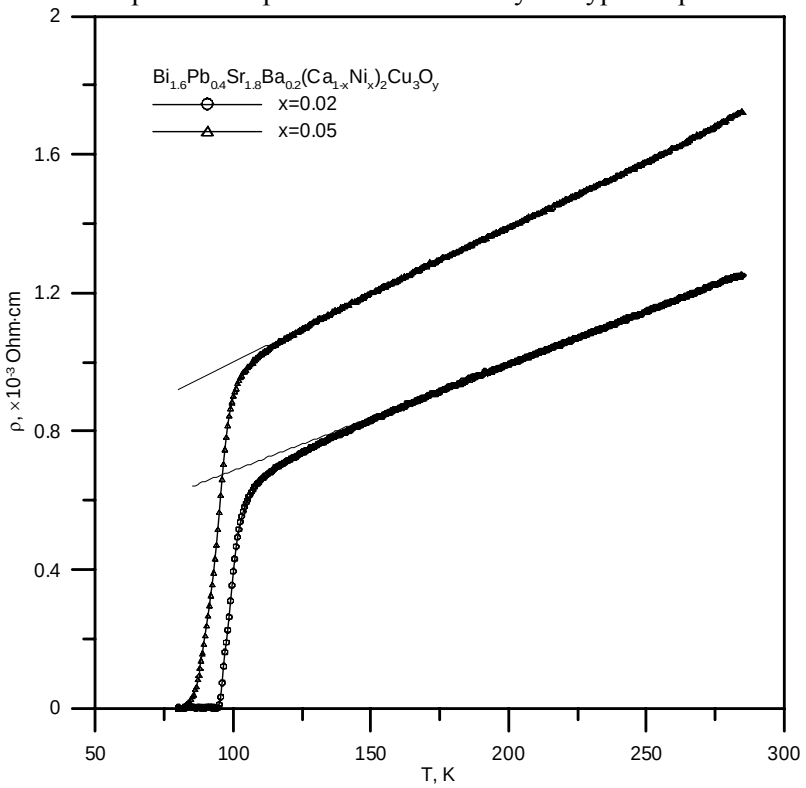

Fig.2. The temperature dependence of resistivity for type II superconductor.

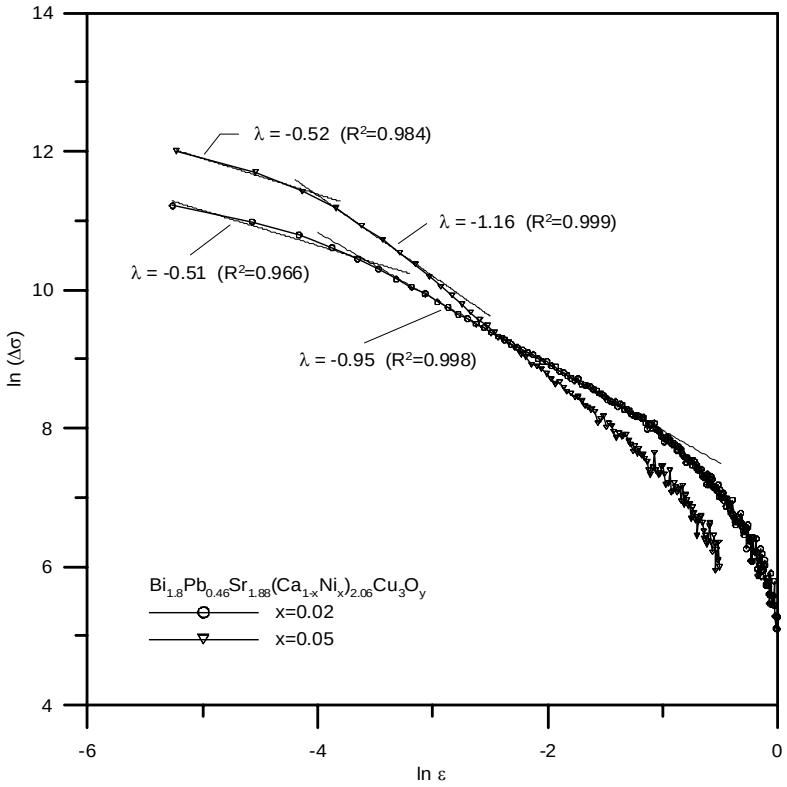

Fig.3. The ln(Δσ) vs lnε plot for type I superconductor.

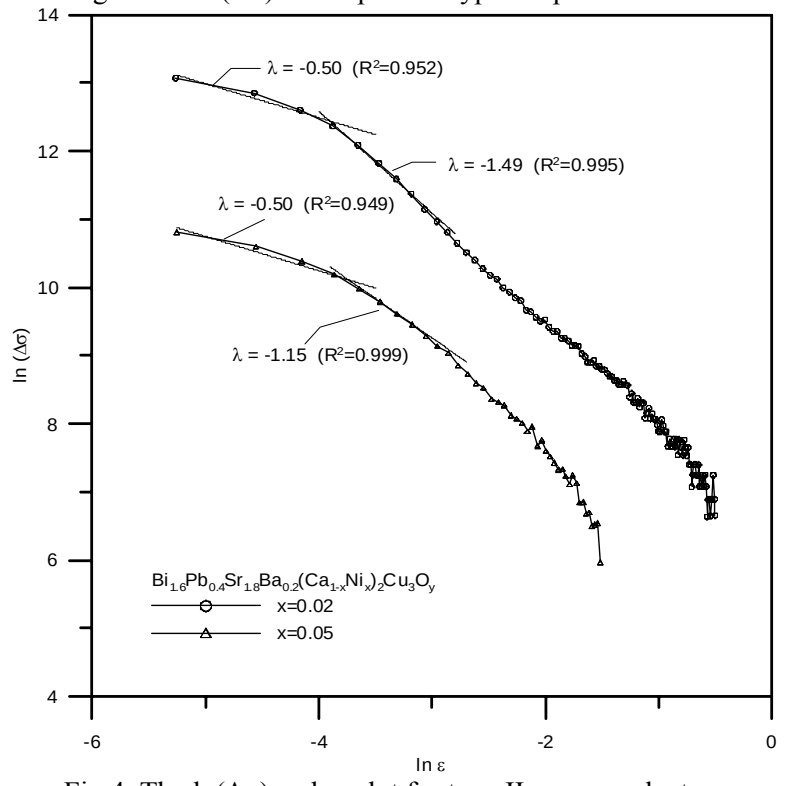

Fig.4. The ln(Δσ) vs lnε plot for type II superconductor.

Table 1. The parameters obtained from Fig.3, 4

	$Bi_{1.8}Pb_{0.46}Sr_{1.88}(Ca_{1-}$□$Ni$□$)_{2.06}Cu_3O_y$		$Bi_{1.6}Pb_{0.4}Sr_{1.8}Ba_{0.2}(Ca_{1-}$□$Ni$□$)_2Cu_3O_y$	
□□	0.02	0.05	0.02	0.05
□□, **K**	96.5	93.5	96.5	95.5
□□□□□, **K**	99.3	95.1	98.5	97.7
***ξ*(0), Å**	13.9	6.9	2.1	20.4
***δ*□**	0.029	0.017	0.021	0.023
3D regime	$-5.3 < \ln \varepsilon < -3.5$	$-5.3 < \ln \varepsilon < -3.9$	$-5.3 < \ln \varepsilon < -3.8$	$-5.3 < \ln \varepsilon < -3.8$
2D regime	$-3.4 < \ln \varepsilon < -1.5$	$-3.8 < \ln \varepsilon < -3.0$	-	$-3.7 < \ln \varepsilon < -3.0$

In [4] the dimensional crossover from 0D to 1D near T_c was identified. The authors refer this crossover to fact that small islands of the 2223 phase distributed in 2212 phase could form quiasi-1D dimensional percolation structure above T_c.

Conclusion

The investigation of 2D and 3D conduction in Ni-doped 2223 BSCCO ceramic samples has confirmed the usefulness of the paraconductivity in the identified temperature ranges over which copper planes and chains conduct. For all samples the crossover occurs at the temperature $T_{cross} \approx 1.03T_c$. However in the case of $Bi_{1.6}Pb_{0.4}Sr_{1.8}Ba_{0.2}(Ca_{1-x}Ni_x)_2Cu_3O_y$ sample (x=0.02) the crossover from 1D to 3D regime was identified. Also, the coherence length $\xi(0)$ at temperature T = 0K was determined (Table 1).

References

[1] L. G. Aslamazov and A. I. Larkin, *Phys. Lett.* **26A**, p.238 (1968); L. G. Aslamazov and A. I. Larkin, *Sov. Phys. Solid State* **10**, p.875 (1968).
[2] W. E. Lawrence and S. Doniach, in *Proc. 12th Int. Conf. on Low Temp. Phys*., edited by E. Kanda (Keigaku, Tokyo, 1971), p.361.
[3] S. N. Bhatia and C. P. Dhard, *Phys. Rev. B* . **49,** p.12206, (1994).
[4] H. Enomoto, N. Mori, I. Matsubara, and H. Ozaki, *Physica B*, 284-288, p.579, (2000).

OPTICAL PROPERTIES OF FULLERITE C_{60} NANOSTRUCTURES IN WATER

I.T. Dihor

Superconductivity & Magnetism Laboratory, State University of Moldova, MD2009 Chisinau, Moldova

Abstract

The colloidal solution of fullerene C_{60} in water has been investigated by UV-VIS spectroscopy. It is shown that the peculiarities of colloidal solution spectrum are similar to UV-VIS spectrum for solid state C_{60}. The direct and indirect optical transitions were found for this colloidal solution of fullerene. The existence of indirect transitions proves the presence of solid state C_{60} in water. The influence of IR laser irradiation on the colloidal solution of fullerene in water was also investigated. It is shown that under action of high power laser radiation the red shift of the optical line corresponding to $h_u \leftrightarrow t_{1u}$ (HOMO-LUMO) transitions arises. Other transitions are not affected by IR laser.

Since its discovery in 1985 [1], carbon-60 (C_{60}), a newly found all-carbon molecule, has captured the attention of scientists all over the world. The investigation of its physical and chemical properties, as well as the properties of its compounds, became one of the most popular topics of today's research in solid state physics, material science, chemistry and biomedicine.

The main contribution of the present work has been the research of optical properties of fullerite C_{60} nanostructures in water and changes in the structure of the optical spectra of the fullerene C_{60} water solution under influence of IR laser irradiation. It is known that the fullerenes are characterized by poor solubility in water. In [2] it has been proposed a method for obtaining the molecular-colloidal dispersions of fullerenes in water without any stabilizers and this resulted in the generation of solutions with fullerene aggregate sizes from several nanometers to 200.

For investigation of fullerene C_{60} aggregates in water a solution with initial concentration c=0.3 mg/ml was used. The parameters of electronic spectrum of this solution were obtained in the 1.6-6.2 eV range using SPECORD M40 UV-VIS spectrometer.

In Fig.1 the absorption spectrum of non-irradiated (○) fullerene C_{60} aggregates in water is presented. The UV-VIS spectrum of colloidal fullerene water solution does not significantly differ from UV-VIS spectrum of fullerite C_{60} having the same positions of spectral lines. The similarity of spectra of C_{60} solid films and C_{60} in solution suggests the same origin for the transitions in both cases and shows the molecular character of the solid. Four intensive lines of absorption with maxima at 2.92, 3.62, 4.66 and 5.63 eV are caused by dipole allowed transitions. The positions of these lines correspond to data of ellipsometric and optical transparency measurements for crystalline C_{60} [3-7]. The line of small intensity caused by optical dipolar-forbidden transition $h_u \leftrightarrow t_{1u}$ (HOMO↔LUMO) is also noticed in the range of fundamental absorption edge (~2 eV).

The existence of the direct forbidden transitions $h_u \leftrightarrow t_{1u}$, direct allowed transitions ($h_u \leftrightarrow t_{1g}$, $(h_g+g_g) \leftrightarrow t_{1u}$, $h_u \leftrightarrow h_g$, $(h_g+g_g) \leftrightarrow t_{2u}$), indirect allowed optical transitions ($h_u \leftrightarrow t_{1g}$, $(h_g+g_g) \leftrightarrow t_{1u}$) and indirect forbidden optical transitions ($h_u \leftrightarrow t_{1g}$, $(h_g+g_g) \leftrightarrow t_{1u}$) in the C_{60} fullerene aggregates in water is shown in Fig.2 and Fig.3 for non-irradiated samples. The

presence of indirect optical transitions is characteristic only of solid state and in the case of C_{60} colloidal water solution existence of such transitions certainly proves the C_{60} crystalline type in water. For transitions $h_u \leftrightarrow h_g$, $(h_g+g_g) \leftrightarrow t_{2u}$ the indirect allowed or forbidden transitions were not identified. The notations for indirect transitions used above are conditional, since the final states at these transitions belong to group of wave vector.

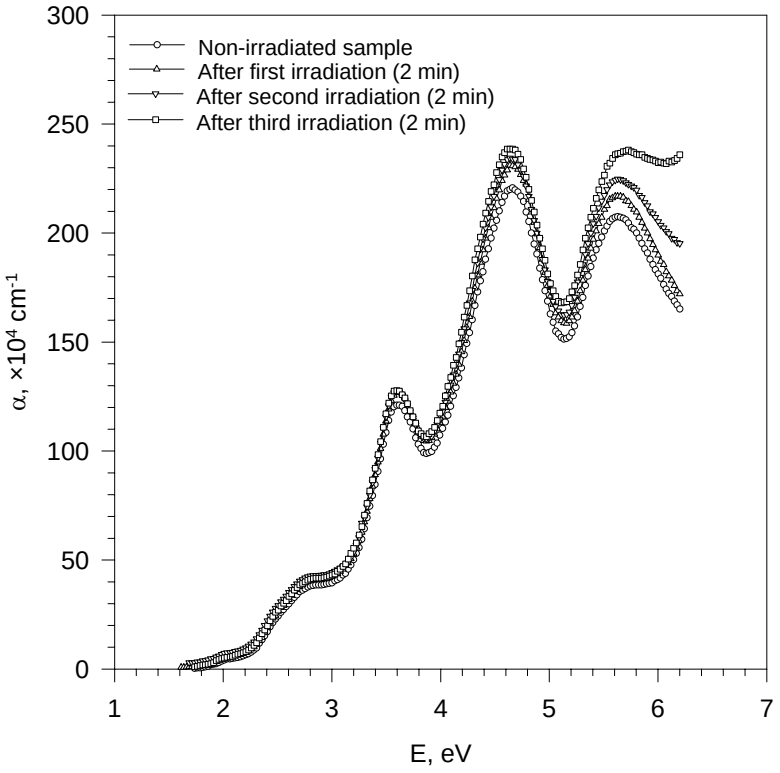

Fig.1 The absorption spectra for non-irradiated (○) and irradiated (Δ, ∇, □) by high power IR laser (P=40 W) samples of fullerene C_{60} aggregates in water.

The values of E_g for direct and indirect dipole forbidden and dipole allowed transitions, as well as energy of phonons, which participate in indirect optical transitions, are represented in Table 1. Index γ in Table 1 marks the exponent of multiplying $E \cdot \alpha$ of dependence $(E \cdot \alpha)^{\gamma} = f(E)$.

Table 1.

The energy gaps determined from direct and indirect optical transitions data for the fullerene aggregates C_{60} in water.

Type of transition	Direct forbidden	Direct allowed	Indirect allowed		Indirect forbidden	
	E_g, eV	E_g, eV	E_g, eV	E_{ph}, cm^{-1}	E_g, eV	E_{ph}, cm^{-1}
$h_u \leftrightarrow t_{1u}$	1.77	-	-	-	-	-
$h_u \leftrightarrow t_{1g}$	-	2.37	1.89	879.28	1.71	903.48
$(h_g+g_g) \leftrightarrow t_{1u}$	-	3.27	2.56	1097.098	2.14	1900
$h_u \leftrightarrow h_g$	-	4.02	-	-	-	-
$(h_g+g_g) \leftrightarrow t_{2u}$	-	4.90	-	-	-	-
γ	2/3	2	1/2		1/3	

We see from Table 1 that in the case of indirect forbidden transition $(h_g+g_g)\leftrightarrow t_{1u}$ the energy of phonon E_{ph}=1900 cm^{-1} exceeds the limiting energy for "intern" phonons of the fullerite C_{60}. In this transition, probably, two phonons with summary energy equal to 1900 cm^{-1} participate.

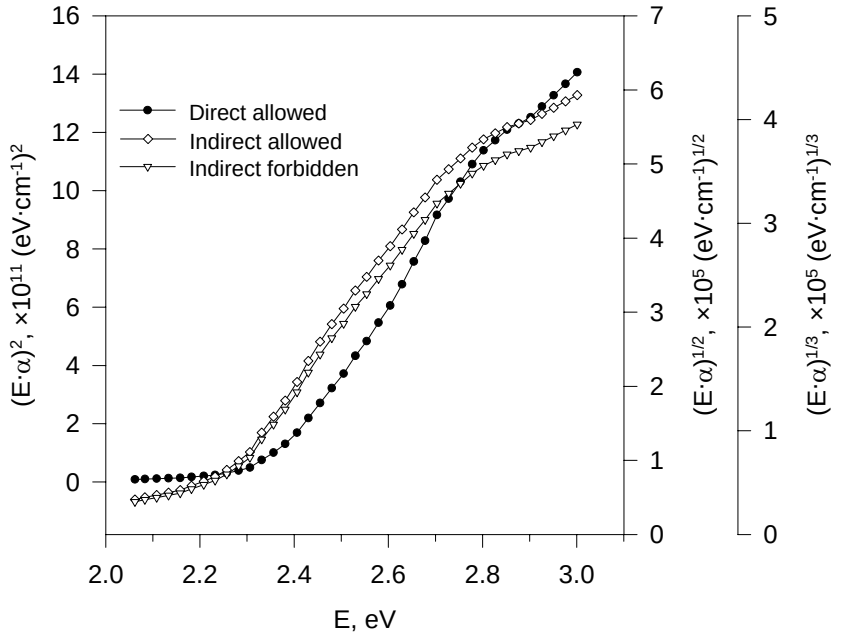

Fig.2 The direct allowed transitions (•), indirect allowed transitions (◊) and indirect forbidden transitions (∇) in the C_{60} fullerene aggregates in water in (2-3.1) eV range.

The solution of fullerene aggregates C_{60} in water was irradiated by IR laser type LTN-101 with wavelength λ=1064.1 nm (emitted power ≈ 40 W) for 3 times, every time being with 2 min duration. The absorption optical spectra for irradiated samples (Δ, ∇, □) are presented in Fig.1. The increasing of optical absorption with increasing of irradiation dose is caused by evaporation of the water with increasing of fullerene aggregate concentration during the irradiation processes. In the case of irradiated samples the change of E_g occurs. Namely, for the direct forbidden transitions $h_u\leftrightarrow t_{1u}$ the decrease of E_g after IR laser irradiation was found. This decreasing depends on irradiation dose: 1.77 eV before irradiation, 1.68 eV after the first irradiation, 1.62 eV after the second irradiation, 1.57 eV after the third irradiation (Fig.4). The influence of high power IR laser irradiation on $h_u\leftrightarrow t_{1u}$ (HOMO↔LUMO) transitions in C_{60} thin films was also examined. But in this case no change of E_g value was observed. Thereby the red shift of HOMO↔LUMO E_g only for fullerite C_{60} nanostructures in water occurs. The decreasing of E_g during the high power irradiation of fullerene C_{60} aggregates in water is linear type dependence in the first approximation.

In [8] the effect of energy blue shift of star-like $C_{60}PS_n$ macromolecule (PS polystyrene, n=1, 2, 3, 4) photoluminescence spectra was observed. This shift is assumed to HOMO-LUMO gap increasing. According to [8] the increasing of HOMO↔LUMO gap is caused by formation of new covalent bonds between fullerene C_{60} and polystyrene chains. The type of such bonds can affect the values of Hamiltonian matrix elements W_1 and W_2 of states mixing

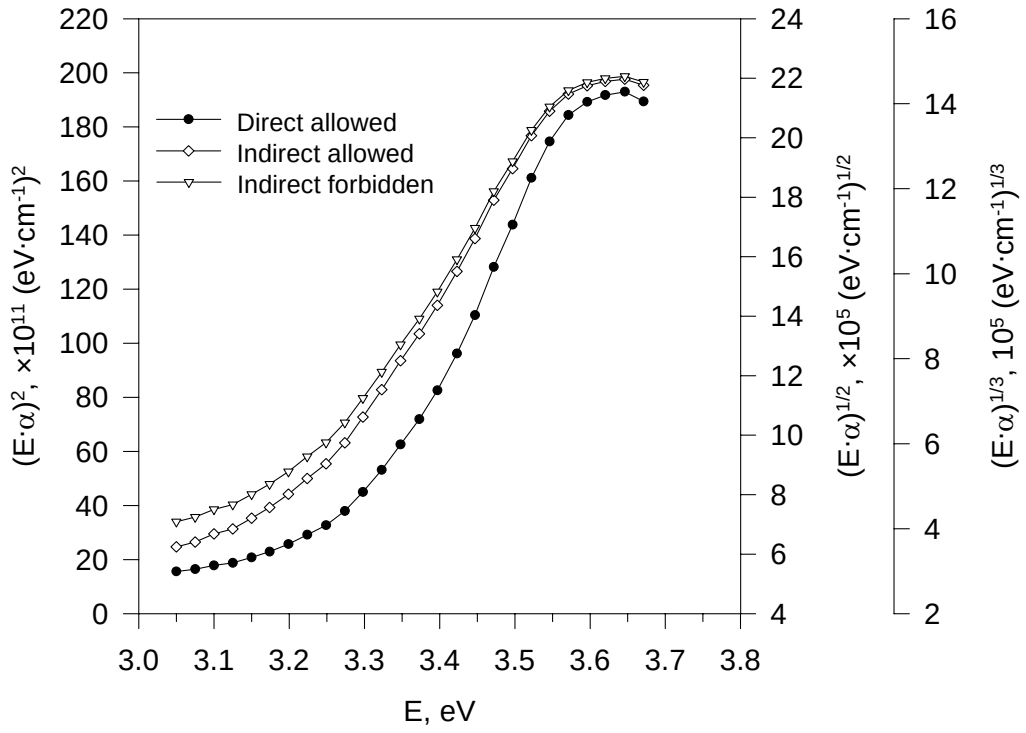

Fig.3 The direct allowed transitions (•), indirect allowed transitions (◊) and indirect forbidden transitions (∇) in the C_{60} fullerene aggregates in water in (3-3.8) eV range.

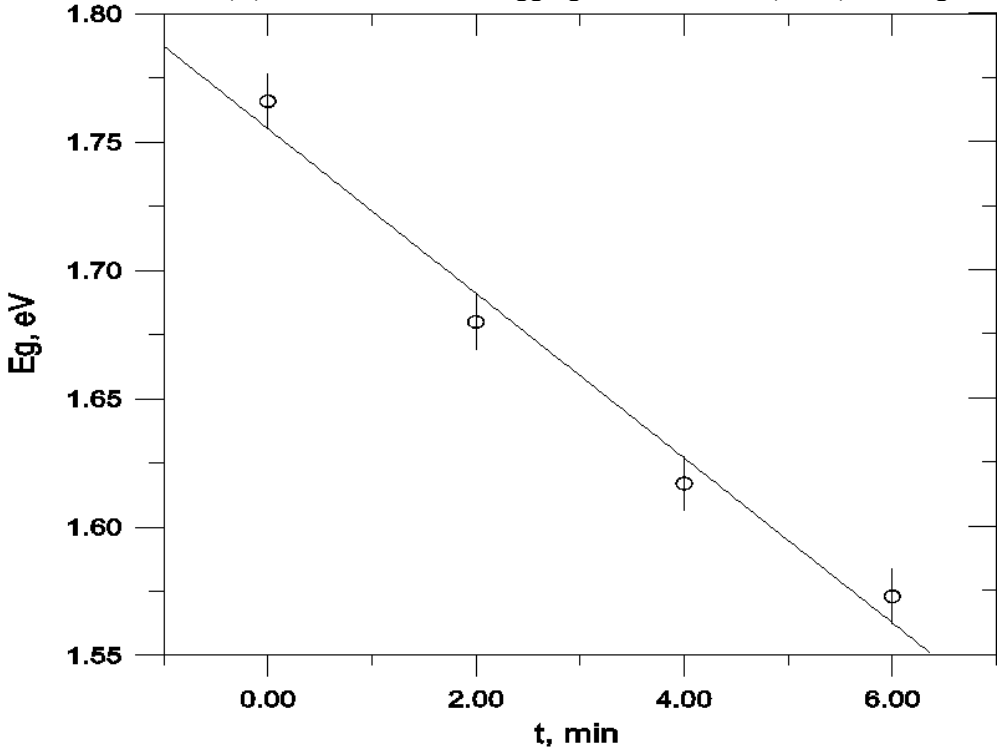

Fig.4. The decreasing of E_g corresponding to $h_u \leftrightarrow t_{1u}$ (HOMO↔LUMO) direct dipole forbidden transitions under action of high power IR laser irradiation vs. irradiation time

for cases of C-C and C-H bond formation, respectively. These matrix elements determine the following dependence of the HOMO↔LUMO transition quantum [9]

$$h\nu=[\Delta^2+n(W_1^2+W_2^2)]^{1/2},$$

where Δ is initial HOMO-LUMO gap of unperturbated fullerene and n is number of new formed chemical bond pairs. The dependence of HOMO↔LUMO gap vs. n at n<9 is linear function in accordance with experimental data (blue HOMO↔LUMO transition shift) [8]. Moreover, this behavior weakly depends on peculiarities of full polymer chain or other ligands attached to fullerene, but strongly depends on the nearest neighbors of C_{60} linked to fullerene by covalent bonds. In contrast to the fullerene $C_{60}PS_n$ blue HOMO↔LUMO shift at decreasing of n the red shift of HOMO↔LUMO transitions must be observed. This effect was observed in our experiments at action of high power IR laser irradiation on the fullerite C_{60} in water.

The fullerene water solution consists of isolated C_{60} molecules in hydrated state, $C_{60}@\{H_2O\}_n$ complexes and of their small spherical clusters. The complexes $C_{60}@\{H_2O\}_n$ are surrounded by spherical layers of interconnected water molecules and can be noticed as $[C_{60}@\{H_2O\}_n]_m$ [10]. In such a structure the carbon atoms are centers of electron-deficiency and capable of interacting with electrons donated by extra water molecules. Under action of the high power IR laser irradiation the breaking of these bonds takes places. This leads to decreasing of HOMO↔LUMO gap. The high power IR laser irradiation leads also to breaking of the bonds between $C_{60}@\{H_2O\}_n$ complexes in spherical fractal clusters of hydrated fullerenes. However at these breakings the HOMO-LUMO gap remains unchanged.

According to our experiments, unlike HOMO-LUMO transitions, the value of E_g corresponding to direct allowed optical transitions ($h_u \leftrightarrow t_{1g}$, $(h_g+g_g) \leftrightarrow t_{1u}$, $h_u \leftrightarrow h_g$, $(h_g+g_g) \leftrightarrow t_{2u}$), indirect allowed optical transitions ($h_u \leftrightarrow t_{1g}$, $(h_g+g_g) \leftrightarrow t_{1u}$) and indirect forbidden optical transitions ($h_u \leftrightarrow t_{1g}$, $(h_g+g_g) \leftrightarrow t_{1u}$) for fullerene C_{60} aggregates in water is not affected by high power IR laser irradiation.

References

[1] H. W. Kroto, J. R. Heath, S. C. O'Brien, R. F. Curl, and R. E. Smalley, Space, stars, C60 and soot, Nature (London), 318:162-163, 1985.

[2] G.V. Andrievsky, M.V. Kosevich, O.M. Vovk, V.S. Shelkovsky, L.A. Vashchenko, J.Chem.Soc. Chem.Commun., 1995, l2, l28l.

[3] S.L. Ren, Y. Wang, A.M. Lee, H.F. Ni, J. Selegne, P.C. Eklund, Appl. Phys. Lett., 1991, 59, 2678.

[4] V.I. Srdanov, C.H. Lee, N.S. Sariciftci, Thin Solid Films, 1995, 257, 233.

[5] E. Sohmen, J. Fink, Phys. Rev. B., 1993, 47, 14532.

[6] S. Modesti, S. Gerasari, P. Rudolf, Phys. Rev. Lett., 1993, 71, 2469.

[7] G. Gensterblum, J.J. Pireaux, P.A. Thiry, R. Caudano, J.P. Vigneron, P. Lambin, A.A. Lucas, W. Kratschmer, Phys. Rev. Lett., 1991, 67, 2171.

[8] A. N. Aleshin, Yu. F. Biryulin, N. B. Mironkov, L. V. Sharonova, E. N. Fadeeva, V.N. Zgonnik, Fullerene Science and Technology 1998, 6, *3*, 545.

[9] Yu. F. Biryulin, V. S. Vihnin, V.N. Zgonnik, FTT, 2000, 42, 188.

[10] G. V. Andrievsky, V. K. Klochkov, A. Bordyuh and G. I. Dovbeshko, Chem. Phys. Lett. 364 (2002).

DEVELOPMENT OF DISSIPATIVE STRUCTURES ON SURFACE OF DIELECTRIC LIQUID IN ELECTROSTATIC FIELD

B. Constantinov[1], V. Bocan[1,3], T. Pasechnic[2], P. Untila[3], M. Petrov[4], S. Sircu[1]

[1]*Technical University of Moldova,* [2]*State University of Moldova,* [3]*State University of Tyraspol,* [4]*State University of Medicine N. Testemitsanu.*

The transition of plane surface of liquid dielectric charged with the electrical charge in the electrostatic field in the periodical gofer surface of crater type deformation is researched. It was proved for the first time that the apparition of dissipative structures keeps not optical character but thermal and is not conditioned by the presence of the photo sensible semiconductor layer. It was established that the development of dissipative structures on the surface of dielectric liquid includes in itself the mechanism of initiation of germination deformations and a mechanism of multiplication of the centers of new deformations in the free volume of germination deformation.

Introduction

The thermoplastic layer of photo thermoplastic career of information (PTPCI) during the development of deformations on the local microzones with the values of sizes within the limits (6÷25)μm are behavioral as the liquid dielectric during $t\approx(0.3\div1)s$ of sensitizing (deposition of electrical charges) in the electrostatic field [1-5]. This allowed authors [6] by numerical methods to separate the development of wave shock of substance masses in the normal plane on the substrate of the sample of liquid dielectric-solid metal substrate of the development of the wave of mass transportation of substances in the radial plane [2]. Taking into consideration that the "depth" of deformations determines the value of penetrated light flux through the liquid layer, in [7] the numerical processing 3*D* of optical images 2*D* was applied. The basic idea consists in the storage of penetrated light through PTPCI in the memory of computer. The structure 3D approximated of the deformation of relief portable surface was represented by the association of each point (***x, y***) of the image with the pseudo spatial parameter of color (***h***). This allowed the definition of expression of some new physical value Q – the quality factor of pseudo spatial optical images.

1. Method of research and the processing of results

The method of research was elaborated in [8]. The numerical method of calculation evidentiated the non linear character of the phenomenon of apparition of the grey points $\mathbf{n_{ij}}$ (grey pixels) on the curves of histogram of optical image and the interconnection with the mechanism of development of the deformations of crater type on the free surface of PTPCI.
The model of development of the deformations elaborated in paper [1] does not explain and does not suppose the apparition of spatial structures in group or sets of groups. The elaboration of structural model that will give good results must take into consideration the factors that assure the apparition of one group with square symmetry of the deformation of crater type – "attack figure". The attack figure is multiplied into the structure of hexagonal symmetry of deformation. Taking into the consideration the possibility of the apparition "of

the crystallization of coulomb type" on the surface of some liquid dielectric media (see [9]), the computational modeling was applied. Applying special programs, the structured models were obtained that describe the process of germination and multiplication of thermoplastic deformations in group by the algorithm represented in fig. 1. On the base of computational calculations the results of theoretical researches were taken [8, 9]. The results of theoretical researches indicate that the first non stable harmonics are excited for which the deformation of hexagonal micro relief is nonvariant with respect to the rotation with 120° around the perpendicular axis on the plane of the surface of liquid.

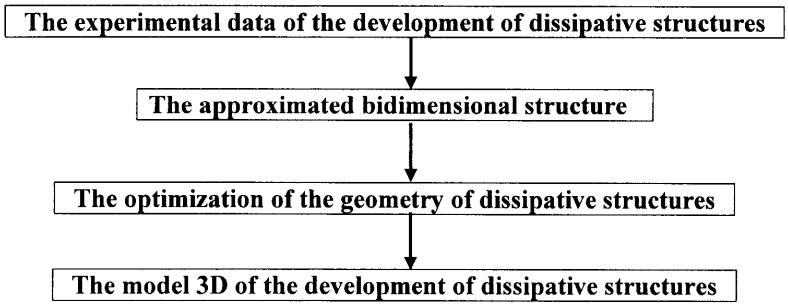

Fig. 1 The algorithm of pseudorepresentation 2D – 3D of the development of dissipative structures

From those mentioned above, further we will analyze the mechanism of initializations of periodic –spatial deformed structures for which the germination deformation $\boldsymbol{C_o}$ can initiate three centers of deformation $\boldsymbol{C_s}$ respectively only two on the selected micro zone. The experimental researches [see 10, 11] indicate that one more mechanism of initialization exists that can be observed in the samples with ultra fine liquid layers. The modification of dissipative structures can be performed in these samples from the hexapole to the octapole because the distance between $\boldsymbol{C_o}$ and $\boldsymbol{C_s}$ is greater as the radial values of the thermoplastic deformations. The modification is described by computational modeling for which C_0 can initiate on the selected microzone four centers of deformations $\boldsymbol{C_s}$, but C_s only two respectively. It was established by computational modeling that on the free surface of researched samples the structural groups (units) can exist formed of germination deformations of crater type - $\boldsymbol{C_o}$ with the approached geometrical structure (local) of satellite deformations – ($\boldsymbol{C_s}$) and the packing configuration: $\mathbf{1}\boldsymbol{C_o}\mathbf{-2}\boldsymbol{C_s}$; $\mathbf{1}\boldsymbol{C_o}\mathbf{-3}\boldsymbol{C_s}$; $\mathbf{1}\boldsymbol{C_o}\mathbf{-4}\boldsymbol{C_s}$; $\mathbf{1}\boldsymbol{C_o}\mathbf{-5}\boldsymbol{C_s}$; $\mathbf{1}\boldsymbol{C_o}\mathbf{-6}\boldsymbol{C_s}$; that are increased up to the structure with removed order of one set of groups: $\mathbf{2}\boldsymbol{C_o}\mathbf{-10}\boldsymbol{C_s}$.

It was observed from computational modeling that in the experimental situation the sets of group can form a periodical lattice that formally can be described by structural unit of the type:

$$x\boldsymbol{C_o}\rightarrow(2x^2+x)\boldsymbol{C_s} \text{ of } \boldsymbol{C_{o(x)}}\rightarrow \boldsymbol{C_{s(2x^2+x)}}\text{; where } x=1, 2, \ldots \quad (1)$$

here $x=f_{(\omega)}$ is the multiplication coefficient of the centers of new deformations as the function of the increment of formation of deformation ω, thermal stable also in the electrical field.
The existence of elementary structural unit (x=1) results from relation (1) that assures the mechanism of multiplication of the centers of new deformations that correspond to the geometrical configuration of packing:

$$(\mathbf{1}\boldsymbol{C_o}\rightarrow\mathbf{3}\boldsymbol{C_s}) \quad (2)$$

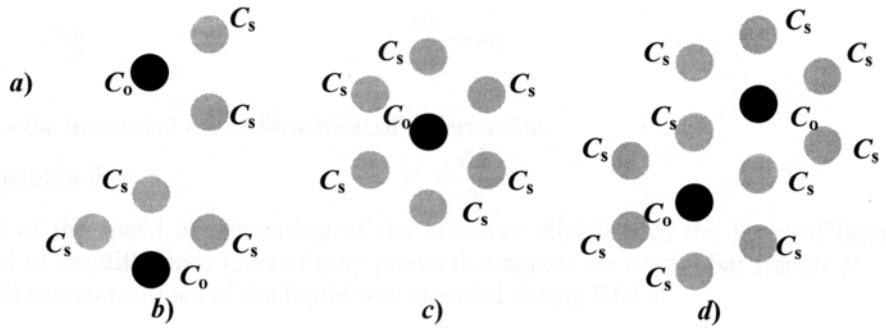

Fig. 2 Structural units induced by electrostatic field on the surface of liquid dielectric:
a) - ($1C_o - 2C_s$); b) - ($1\ C_o - 3C_s$); c) - ($1C_o - 6C_s$); d) ($1C_o - 10C_s$) $\leftrightarrow C_{o\,x} \rightarrow C_{s(2x^2+x)}$

Several examples of structural units are proposed in fig. 2 that are realized during the development of the deformation of crater type at the projection of optical images on the free surface of liquid dielectric. The model is characterized by the coefficients α, β, γ [2]. The defined structural relations are classified by the analogy with the structures for which the electrical bonds are established (chemical). So that, the mechanisms of initialization of the series of stable structures for which the intermediary states do not exist can be defined by the general relation of type: $\boldsymbol{C_o^X C_s^Y}_{\mathbf{XY}}$, where **X**,**Y** is the number of harmonics (waves) totally initiated by $\boldsymbol{C_o}$. So, all geometrical forms are calculated of stable structures that can be realized in the process of formation and restructure of the deformation of the surface of liquid dielectric, researched in paper [8]: $\boldsymbol{C_o^3 C_s^2}_{\mathbf{6}}$ and $\boldsymbol{C_o^4 C_s^2}_{\mathbf{8.}}$ The research of the mechanisms of formation of stable structure – $(\boldsymbol{C_o^4 C_s^2}_{\mathbf{8}})$ formed of germination deformation and 8 satellite craters on the perimeter are outside of the objectives of the recent paper. The statistical modifications of the geometry of the structure $\boldsymbol{C_o^4 C_s^2}_{\mathbf{8}}$ were emphasized in [8], but the dynamical modifications will be researched in the future papers. The limit of applicability of the model of the mechanisms of initialization of the harmonics represents the case X=Y=2 for which the stable form would be $\boldsymbol{C_o^2 C_s^2}_{\mathbf{4}}$ described by relation (2) that results from the mechanism of multiplication of the centers of new thermoplastic deformations. From the evident form of relation $\boldsymbol{C_o^2 C_s^2}_{\mathbf{4}}$ the dissipative structure represents a group of four thermoplastic deformation centers that are multiplied, independent of initial deformation C_0. Then the theoretical and experimental results will be synthesized by approximated numerical methods.

2. Theoretical investigations.

The numerical interpretation of the process of development of the deformation emphasized the thermal character of it and the dependence on rheology. An important factor in the research of the process of initialization of the deformations represents the phenomenon of the decreasing of effective thickness of the visualized structure under the action of the pressure of electrical forces. The value of relative deformation of the surface of liquid is represented by form:

$$\frac{\Delta \xi_N}{z} \approx e^{\delta t_N} \tag{3}$$

In this case the equation of the removing of the mass of liquid in the real coordinates of the space and time is represented as:

$$\frac{d\xi}{dt} = \omega\xi \tag{4}$$

here: $\boldsymbol{\omega}$ is the increment of the formation of deformation.

We will mention that: $V_z = \dfrac{\partial \xi}{\partial t}$

The value of the speed of decreasing of the effective thickness of the layer of liquid was determined as the difference ($\Delta \boldsymbol{n}$) of grey points that appear on 2 neighbor frames *N*. In fig. 3 the dynamical surface of the liquid was modeled during 0.04 s:

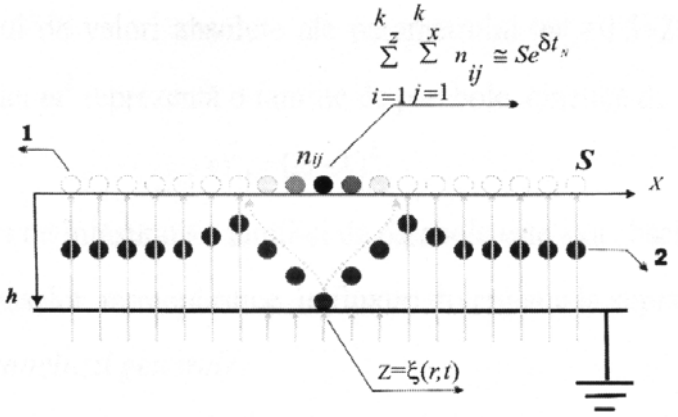

Fig. 3 The numerical representation of the development of dissipative structures:
1 – the "numerical" removing of the points of one Newtonian liquid – 2, from the dynamical surface - $\xi(\vec{r},t)$.

So in the linear approximation by the amplitude the solution of the equation of profile of dynamical surface of the liquid is defined as:

$$\xi_i = \int V dt \tag{5}$$

The value V_z is interpreted as sum of $\boldsymbol{n_{ij}}$ bits stored in the memory of computer in the interval of time d*t*=0.04s. From the expression of the calculation of total information that is contained by optical image results:

$$S = \sum_{i,j} n_j n_i \log_2 I \tag{6}$$

Where (*I*) is given by relation (4) and represents the gradation from white to black of each point, ($\boldsymbol{n_i}$) is the number of points from the row (*I*) and ($\boldsymbol{n_j}$) - from the column j. For I=256 (the black nuance), a point of one image will contain the information of S=8bits=1 byte (1 pixel), S has the physical meaning of maximal deformation of 8 bits of thermoplastic sample in the point of liquid surface with the real coordinate of the space $\xi(\vec{r},t) = z$. Then the stock of numerical data from the memory of computer from a base of $\boldsymbol{n_{ij}}$ bytes will describe the formation of radial deformation with the characteristic dimensions ($\boldsymbol{\lambda}$). Then the sum of $\boldsymbol{n_{ij}}$ bytes is represented as:

$$\sum_{i=1}^{k_y}\sum_{j=1}^{k_x} n_{ij} \equiv \xi_i ; \qquad \frac{1}{S}\sum_{i=1}^{k_y}\sum_{j=1}^{k_x} n_{ij} = h_i \tag{7}$$

The synthesis of numerical data and experimental ones is described by the relation of numerical calculation:

$$\frac{1}{S}\sum_{i=1}^{k_y}\sum_{j=1}^{k_x} n_{ij} \equiv \frac{\xi}{\lambda} \le 1 \tag{8}$$

Here: (ξ) is the removing of the points of the liquid surface: (λ) is the radial dimensions of the selected micro zone at the moment t. The numerical relation (8) taking into consideration the relations (6) expresses the process of apparition of grey points n_{ij} on the selected micro zone, that represents a data base which is increased exponentially. From the experimental data a numerical model was developed in accordance with relation (3):

$$\sum_{i=1}^{k_z}\sum_{j=1}^{k_x} n_{ij} \cong Se^{\delta t_N} \text{ were } \delta \equiv \omega \cong \frac{1}{t_N}\ln\frac{1}{S}\sum_{i=1}^{k_z}\sum_{j=1}^{k_x} n_{ij} \text{ and } \omega_{(t)} \approx \alpha t^{-1} \tag{9}$$

Here: $\alpha \le 1$ is the parameter that characterizes the dispersion; δ is interpreted as the speed (the increment ω) of formation of deformation.

3. The processing of experimental material

In these conditions of experiment described in paper [9] the value of increment calculated by relation (9) varies in limits ω=0.35÷28s^{-1}. In this segment the values: ω≈0.7÷7s^{-1} indicated in paper [2] are also included. The increasing of the values of limits (from 0.7 to 0.35 and 7 to 28 s^{-1}), with one order on the kinetic of short duration is explained by the possibilities of the modern high advanced technologies: the registration of the processes of deformation in the fluxes of diffused light through the section of the sample of thermoplastic material of the values no greater than 0.1lx. The increasing of the range of values of the parameter is explained also by the approximation of the calculation admitted by the authors of paper [8]. This result indicates that a group of effects of deformations of the liquid surface, characterized by the values $\omega \ge 7\div28$ s^{-1} (II stage) up till now is not defined. The defined values in table Nr.1 are proposed for a separated crater in the conditions of experiment that assures: The characteristics of the field U_c= 5.5kV, the temperature of thermal treatment T= 60˚C of the sample with the thickness z_{tp}=2μm.

We will mention that for spatial parameter (kh), where $k = \frac{2\pi}{\lambda}$, in the conditions of recent experiment the range of values 1.2÷6.2 was defined that is in good accordance with the results of numerical researches (table Nr.1). The performed calculations for the conditions of regimes from the recent paper indicate that at the variation of the characteristic of the field or of the value of the temperature of thermal treatment the form of experimental shapes is saved, modifying only their shape. The peculiarities of the concreted form of one exponential dependence (see (9)) that describes the formation of one crater is proposed in fig. 4:

Table Nr. 1

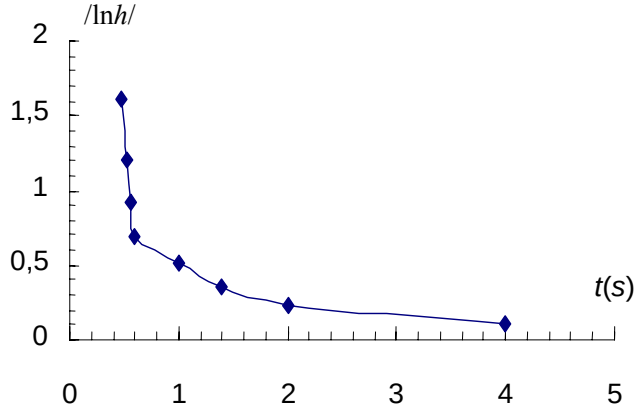

$t(s)$	h	$\|lnh\|$	$kh \equiv 2\pi(\xi/\lambda)$
0,48	0,2	1,6094	1.256
0,52	0,3	1,2039	1.884
0,56	0,4	0,9162	2.512
0,6	0,5	0,6931	3.14
1	0,6	0,5108	3.768
1,4	0,7	0,3566	4.396
2	0,8	0,2231	5.024
4	0,9	0,1053	5.652
*	1	0	6.280

Fig. 4 The logarithmical representation of pseudospatial parameter h; parameters of the curve: U_c=5.5 kV, T= 60 $^{\circ}C$, t_0=0.3 s

It is remarkable that with the increasing of sensitizing time of the liquid layers, the breaking of the straight becomes more clearly expressed. The moment of the apparition of the deformation of crater type can be determined for every characteristics of field. Using the data of the values of the pseudospatial parameter (***kh***) from table Nr.1 we can model mathematically the possible values of λ for the values ξ possible in the given experiment. The numeric model of the process of multiplication of the centers of new deformations on the different layers of viscous liquid (it was admitted $\xi_i \equiv z$), confirms the validity of the physical model proposed in [9]. The value of radial dimensions of the characteristic deformation, installed in the process of germination of the centers of new deformations of crater type is proposed in table Nr. 2:

Table Nr. 2

t^*(s)	$h(ur)$	$\lambda \geq \frac{2\pi\xi_i}{kh}$ (μm)		
		ξ_1=0.5μm	ξ_1=1μm	ξ_1=2 μm
0.48	0.2	2.5	5	10
1	0.6	0.8	1.6	3.3
2	0.8	0.6	1.2	2.5
4	0.9	0.5	1.1	2.2
**	1	0.5	1	2

Here t^* is the time of sensitizing that depends on the parameters of registration regime; $\xi_i \equiv z$ the maximal value of spatial parameter; z is the thickness of liquid layer; h is the value of pseudospatial parameter.

The values of the parameter t^* from table Nr. 2 are valid for the characteristic of the field U_c=5÷6.5 kV and T=60-80 $^{\circ}C$, on the thermoplastic layers with the thickness of $1<z\leq 2\mu$m (over the value ξ_3). The data of numerical calculation from table Nr. 2 show the dynamical parameters of periodical restructure of the deformation on the viscous liquid surface. The obtained results as the dependence of the value $t^* >> t_0$=0.3s, on the viscous layers

with z=2μm, indicate a spectrum of values of ($\boldsymbol{\lambda}$) from 10÷25μm which are included in the spectrum of values indicated in the physical model of the process of germination of the centers of spatial deformations (see [2]). Comparing the results for different maximal values $\xi_i \equiv z$ from table Nr.2 we can make the conclusion that the smallest values $\boldsymbol{\lambda}$ on the surface of PTPCI and respectively a higher resolution of registered optical images can be obtained on the layers of thicknesses of ≈0.5μm. An evident result represents the definition of the values of parameter ($\boldsymbol{\lambda}$) at the maximal value of the pseudo spatial parameter h=1 (the row marked with ** from table Nr. 2). This obtained result by numerical method thoroughly corresponds to the obtained values from the experimental researches.

The kinetic of the development of the deformation processes and germination of the centers of new deformations on the dynamical surface of the liquid (see [3]) can be followed from the dispersion shapes from the graphical representation – fig. 5. We will mention here that the function $\boldsymbol{\omega^2}$ describes the law of dispersion of the system in the absence of one interferential raster, defined from experimental measurements with the step $\boldsymbol{\Delta h}$=0.15 and the time of delay of the moment of apparition of effects of deformation in the electrostatic sample – 0.3s, the field U_c=5.5kV, according to the experimental data from table Nr. 3:

Table Nr. 3

N•0.04s	0.3+t_i(s)	$\lvert\Delta h\rvert$	h	$\lvert\omega\rvert$	kh	ω^2
1-3	0.42	0.15	0.15	15.8	0.95	249
3-12	0.78	0.15	0.3	5.2	1.9	27
12-14	0,86	0.15	0.45	23.7	2.8	529
14-22	1.18	0.15	0.6	6	3.8	36
22-100	4.3	0.15	0.45	0.4	2.8	0.16

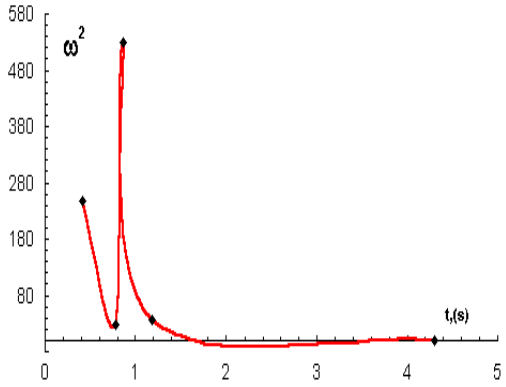

Fig. 5 The law of dispersion $\boldsymbol{\omega^2}$ during the sensitizing of the dielectric of liquid.

The numerical calculation of the spatial parameter ($\boldsymbol{kh}$) indicates that after ≈**1**$\boldsymbol{s}$ from the moment of connection of corona the dimensions of characteristic deformation $\boldsymbol{\lambda=2\pi z/kh \cong 3\mu m}$ on the layers with the thickness $\boldsymbol{z\leq 2\mu m}$. We will have to mention that for the kinetics of short duration we can establish $\boldsymbol{\lambda_{max}=2\pi z/kh \cong 13.2\mu m}$ is confirmed by direct metrical measurements performed in the real time of registration.

From the analysis of the range of values of the pseudospatial parameter ($\boldsymbol{kh}$) we can make the conclusion that for the description of the deformation phenomena of the dynamic surface of the viscous liquid we can apply the model of Newtonian liquid, for which the removing of one point of the liquid corresponds to one pixel on the matrix of numerical transformation.

The calculation of the values ($\boldsymbol{\omega}$) with relation (9) indicates the field of absolute values $|\boldsymbol{\omega}| \cong 0.5 \div 28 (s^{-1})$. The law of dispersion from relation (9) is defined graphically in fig. 2. The form of the shape $\boldsymbol{\omega^2}$ is in good concordance with the result of theoretical researches and experimental ones that indicate the possibility of the discrediting of the dispersion shapes [2]. The experimental analysis on the values of the dependence generally indicates that the shape of dispersion is determined by a certain monoparametric set of shapes (fig. 5). The evident expression of the equation $\boldsymbol{\omega^2}$ that describes the set of shapes can be represented as: $\boldsymbol{\omega^2_{(X,\,t)}}$ =0.

The form of experimental shape of the law of dispersion represents a set of kinetic parabolas of type:

$$\omega^2_+ = (\omega - X)^2 \qquad (10)$$

Here the sign + indicates that the shape of wrapping of the parabolic set is the axis of abscises (0,t); X characterizes the movement of the substance masses in the divergent fluxes on the surface of liquid.

4. The basic results, general conclusions

1. The basic results were obtained on the base of researching method elaborated by the authors that assured the storage as the form of one numerical data base in the memory of computer of the optical information obtained from the light beam diffused by the non homogeneities of the free surface of the sample of liquid dielectric – the rigid metal electrode.
2. The thermoplastic layer of PTPCI during the development of the deformations on the local micro zones $D \approx 6 \div 25 \mu m$ is similar as dielectric liquid in the interval $t \approx 0.3 \div 1 s$, $U = 5 \div 7 kV$, $T = 58 \div 80^{\circ}C$ and the values of the pseudo spatial parameter (h) enclosed in the limits 0 and 0.2.
3. The type of restructure of the surface of liquid dielectric in the range of temperatures $T = 58 \div 90^{\circ}C$ is modified as the dependence of the time of charge with the electrical charge $t = 0.3 \div 10 s$, at the constant value of the potential U of corona; the increasing of the value U from 5 till 7 kV contributes to the increasing of the speed of development of thermoplastic deformations and the increasing of the values of the pseudospatial parameter $\boldsymbol{h} > 0.2 \div 1$.
4. The increasing of the value U and the time of sensitizing assures the formation of dissipative structures both in the illuminated regions and non illuminated regions of PTPCI.
5. It was established that an optimal exposition exists for the researching in the real time of the phenomena of deformation on the surface of liquid dielectric with the values enclosed in the limits $0 \div 0.33 lx$.
6. On the base of the method of the chemical selective attack generally the dispersed model was elaborated of the deformation of the surface of liquid characterized by kinetic curves that form hysteresis loops, in the optimal regime of the registration of optical images.
7. The generalized geometrical model of the dissipative structures was realized by the identification of statistical coefficients:

a) α- the ratio between the dimensions of germination deformation and separated deformation that possesses the values enclosed between 1 and 0.5;

b) β- the ratio between the dimensions of crater from the volume of germination deformation and the mediated dimensions of one separated crater. The increasing of the value U leads to the increasing of the value in the limits 0.8 and 1;

c) γ- the most stable coefficient that characterizes the ratio of distances between the centers of deformations with the values enclosed in the limits 2 and 2.1.

8. The optical hybrid devices with big potential of application realized by PTPCI by the wrapping of the diffractive element on the refractive element of one diffractional grating, obtained by holographic method.
9. The mechanism of multiplication of the centers of new deformations on the surface of liquid is described by the relation $\boldsymbol{xC_0 \rightarrow (2x^2 + x)C_s}$, where the coefficient of multiplication (x) is functional by the increment of formation of deformations ($\boldsymbol{\omega}$).

Acknowledgements

The authors express the sincere acknowledgements to the director of Technical University College – Pendus Andrei for the financial support.

References

[1] V.A. Sibirsky, L.M. Panasiuk and B.I. Constantinov Technology of Photosensitive Layers Containing on the uses of Selenium and Tellurium, *proc. of STDA*, Scottsdale, Arizona, USA, 1998, p.271-174.
[2] B. Constantinov Possibilities of Phototermoplastic Resolving power Improvement under holographic recording procedure, *Proc. SPIE,* 09/1999, *vol.* 3378, *Gradient Index, Miniature and Diffractive Optical Systems*, p.72-77.
[3] B. Constantinov Generalized Theory of Symmetry Cluster – mode Deformation Creation Onto a Photothermoplastic Media – Free Surface, *Proc. SPIE,* 09/1999, *Vol.* 3799, Organic Photorefractive, p.186-193.
[4] B. Constantinov T. Pasechnic, S. Sircu, Diffractive optical systems adapted for outer space operation, *proc. SPIE,* 10/2000, *vol.* 4093, Current Developments in Lens Desing and Optical Systems Engineering, p. 252-260.
[5] B. Constantinov, T. Pasechnic, S. Sircu, Investigation of 2D electron systems on the charged dielectric liquid-semiconductor interface, *proc. SPIE,* 10/, 2000, *vol.* 4110, Fotorefractive Fiber and Crystal Devices, p.328-336.
[6] B. Constantinov Possibility of Fabrication and Optical Hybrid Elements on Interface of Viscous Liquid – Semiconductor Electrostatic System, *J,* Current Ukrainian Research in Optics and Photonics, Ed. SPIE Ukraine, N 2, 2002, p. 193-209.
[7] B. Constantinov, T. Pasecinic, Patent № 1909, R M.
[8] B. Constantinov, T. Pasechnic Multidifraction system for optical data recording and transmission, *proc. SPIE,* 10/2001, *vol.* 4437, Gradient index, Miniature and Diffractive Optical Systems II, p. 149-160.
[9] Constantinov B., Pasechnic T., Phase crystallization on the charged surface of viscous media, *proc. SPIE,* 10/2001, *vol.* 4440, Lithographic and Micromachining Technologies for Optical Component Fabrication, p. 309-320.
[10] B. Constantinov, S. Sircu, V. Bocan, S. Kostyukevych Industrial Product Phase Imaging: Application to Standardization and Nondestructive Testing, *proc. SPIE,* 6/2002, *vol.* 4459, Practical Holographic XVI and Holographic material III, p.291-296.
[11] B. Constantinov, S. Sircu In line methods of Optical Diagnostics in the field of Standardization and Metrology, *proc. SPIE,* 11/2001, *vol.* 4468, Engineering thin Films with Beams, Nanoscale Diagnostics, and Molecular Manufacturing, p. 408-416.